REPORT DOCUMENTATION PAGE

Form Approved
OMB No. 0704-0188

PLEASE DO NOT RETURN YOUR FORM TO THE ABOVE ADDRESS.

1. REPORT DATE *(DD-MM-YYYY)*	2. REPORT TYPE	3. DATES COVERED *(From - To)*
09-16-2010	Final Technical Report	05/31/2007 - 06/30/2010

4. TITLE AND SUBTITLE

Final Technical Report for ONR DURIP (N00014-07-1-1024):
KUPSnet: Knowledge-based Ubiquitous and Persistent Sensor Network Testbed for Threat Assessment

5a. CONTRACT NUMBER

5b. GRANT NUMBER

N00014 – 07 –1 –1024

5c. PROGRAM ELEMENT NUMBER

6. AUTHOR(S)

Liang, Qilian

5d. PROJECT NUMBER

5e. TASK NUMBER

5f. WORK UNIT NUMBER

7. PERFORMING ORGANIZATION NAME(S) AND ADDRESS(ES)

University of Texas at Arlington
Office of Sponsored Projects
PO Box 19145
Arlington, TX 76019

8. PERFORMING ORGANIZATION REPORT NUMBER

9. SPONSORING/MONITORING AGENCY NAME(S) AND ADDRESS(ES)

Office of Naval Research
875 N. Randolph St.
One Liberty Center
Arlington, VA 22203-1995

10. SPONSOR/MONITOR'S ACRONYM(S)

ONR

11. SPONSOR/MONITOR'S REPORT NUMBER(S)

12. DISTRIBUTION/AVAILABILITY STATEMENT

Approved for Public Release; Distribution is Unlimited.

13. SUPPLEMENTARY NOTES

14. ABSTRACT

This ONR award has significantly helped the PI and his research group on instrumentation. The equipment acquisition includes Agilent Spectrum Analyzer (9 KHZ to 26.5 GHZ), Agilent Arbitrary Waveform Signal Generator, 8 Time Domain's PulsON 220 (P220) UWB radars, SUN Fire X4450 Server, Sun Storage 7110 Unified Storage System, NEC projector, 12 Dell Computers, 15 licences of MATLAB with different Toolboxes, and 8 notebook computers. These equipment have provided necessary instrumentation for our research on radar sensor networks. Major achievements include students training, technology transfer to DoD product, and research accomplishments. Ten Ph.D students and ten M.S. students have been supported by this ONR project. Of these 20 Ph.D/M.S. students, 5 Ph.D students and 5 M.S. students are women.

15. SUBJECT TERMS

Radar Sensor Network, UWB Radar, Sense through foliage, Automatic Target Recognition, Waveform Design and Diversity, Compressive Sensing.

16. SECURITY CLASSIFICATION OF:			17. LIMITATION OF ABSTRACT	18. NUMBER OF PAGES	19a. NAME OF RESPONSIBLE PERSON
a. REPORT	b. ABSTRACT	c. THIS PAGE			Qilian Liang
U	U	U	UU	92	19b. TELEPHONE NUMBER *(Include area code)* 817-272-1339

Reset

Standard Form 298 (Rev. 8/98)
Prescribed by ANSI Std. Z39.18

Final Technical Report to ONR

KUPSnet: Knowledge-based Ubiquitous and Persistent Sensor Network Testbed for Threat Assessment

Division: ONR 311
Program Officer: Dr. Rabinder N. Madan
Award Number: N00014-07-1-1024
Award Amount: $192,459
Award Duration: 5/31/2007-6/30/2010

Technical Point of Contact (Principal Investigator):
Prof. Qilian Liang
Department of Electrical Engineering,
416 Yates Street, Rm 518, Box 19016
University of Texas at Arlington
Arlington, TX 76019-0016
Voice: 817-272-1339,
Fax: 817-272-2253
Email: liang@uta.edu

NAME AND ADDRESS OF UNIVERSITY OFFICIAL AUTHORIZED TO OBLIGATE CONTRACTUALLY:
Mr. Jeremy Forsberg
University of Texas at Arlington
Office of Grant & Contract Services
202 E. Border, Suite 216
Arlington, TX 76010
Phone: 817-272-2105, Fax: 817-272-5808
E-mail: ogcs@uta.edu
DUNS No (or DUNS + 4)___06-423-4610___

Final Technical Report for ONR DURIP (N00014-07-1-1024): KUPSnet: Knowledge-based Ubiquitous and Persistent Sensor Network Testbed for Threat Assessment

Qilian Liang
Department of Electrical Engineering
416 Yates Street, Room 518
University of Texas at Arlington
Arlington, TX 76019-0016
Phone: 817-272-1339; Fax: 817-272-2253
E-mail: liang@uta.edu

Abstract

This ONR award has significantly helped the PI and his research group on instrumentation. The equipment acquisition includes Agilent Spectrum Analyzer (9 KHZ to 26.5 GHZ), Agilent Arbitrary Waveform Signal Generator, 8 Time Domain's PulsON 220 (P220) UWB radars, SUN Fire X4450 Server, Sun Storage 7110 Unified Storage System, NEC projector & Installation, 12 Dell Computers, 15 licences of MATLAB with different Toolboxes, and 8 notebook computers. These equipments have provided necessary instrumentation for our research on radar sensor networks. Major achievements include students training, technology transfer to DoD product, and research accomplishments. Ten Ph.D students and ten M.S. students have been supported by this ONR project. Of these 20 Ph.D/M.S. students, 5 Ph.D students and 5 M.S. students are women.

1 Equipment Acquisition and Description

Supported by ONR DURIP (Award Number: N00014-07-1-1024), we have acquired the following equipments:

- Agilent Spectrum Analyzer (9 KHZ to 26.5 GHZ). It has been used to analyze the UWB P220 radar signals and interferences in spectrum domain. It has dual core processor with removable hard drive. The UWB P220 radar has bandwidth 6.5GHz, so the spectrum analyzer could sufficently measure the radar signals and their homonics.
- Agilent Arbitrary Waveform Signal Generator. It can generate any waveforms of our needs such as line frequency modulated (LFM) waveform, constant frequency (CF) waveform, and other waveforms. It could generate some waveforms that we designed such as ternary code waveforms, triphase coded waveforms, etc.
- 8 Time Domain's PulsON 220 (P220) UWB radars. They have been used in sense-through-wall detection to detect human, furniture, etc.
- SUN Fire X4450 Server, Sun Storage 7110 Unified Storage System. They have been used for data processing and storage.

- NEC projector & Installation. It has been used for our group seminars and meetings to exchange research ideas in our Lab.
- 12 Dell Computers. They have enabled our graduate students to perform radar sensor network simulations.
- 15 licences of MATLAB with Signal Processing Toolbox, Communications Toolbox, Image Processing Toolbox, Fuzzy Logic Toolbox, Optimization Toolbox, and Statistical Toolbox. Students have been using them for simulations in radar sensor networks.
- 8 notebook computers. They have given students mobility to perform UWB radar measurement and testing in anywhere.

These equipments have provided necessary instrumentation for our research on radar sensor networks.

2 Students Training

The PI strives to create a research-intensive educational environment and establish and maintain a strong network sensing group at UT-Arlington to develop the next generation of educators, researchers, and entrepreneurs who will drive future innovation in radars, communications, and networks.

Ten Ph.D students (Qingchun Ren, Haining Shu, Xinsheng Xia, Jing Liang, Emily Lei Xu, Ji Wu, Steve Iverson, Davis Kirachaiwanich, Ishrat Maherin and Julie Chen) and ten M.S. students (Rahul Sawant, Hung Ly, Hong-Sam Le, Mukta Athavale, Varsha Bolar, Siddhartha Mukkamala, Mamta Desai, Ashith Kumar, Urmi Desai and Sanil Fulani) have been supported by this ONR project. Of these 20 graduate students, 5 Ph.D students and 5 M.S. students are women.

2.1 Graduated PhD Students During this Project Period

Four PhD students have graduated during this project:

1. Haining Shu, PhD Dissertation: Wireless Sensor Network Lifetime Analysis and Energy Efficient Techniques, August 2007.
2. Qingchun Ren, PhD Dissertation: Medium Access Control (MAC) Layer Design and Data Query Processing for Wireless Sensor Networks, December 2007.
3. Xinsheng Xia, PhD Dissertation: Cross-Layer Design for Wireless Ad Hoc Sensor Networks, December 2007.
4. Jing Liang, Ph.D Dissertation: Radar and Non-Radar Sensor Networks, August 2009.

2.2 Graduated MS Students During this Project Period

1. Varsha Bolar, MS Thesis, Performance Analysis of Space-Time Block Coded Multiple Antenna Systems, December 2009.
2. Mukta Athavale, MS Thesis, Performance Analysis and Effect of Multiuser Interferences for Ultra-wideband Communications, August 2008.

3. Hung Ly, MS Thesis, Detection and Opportunistic Spectrum Access in Sensor Networks, August 2007.

4. Hong-Sam Le, MS Thesis, Power Control and Joint Multi-target Classification and Identification in Cognitive Wireless Networks, August 2007.

5. Rahul P. Sawant, M.S. Thesis, Wireless Sensor Network Testbed: Measurement and Analysis, August 2007.

2.3 Current Ph.D Students

With two new PhD students (Zhuo Li and Xin Wang) joining us in August 2010, we have eight PhD students and seven M.S. students in this group.

1. Emily Lei Xu, Topic: Radar Sensor Networks and MIMO Radar, starting Spring 2008.

2. Davis Kirachaiwanich, Topic: Wireless Networks and Compressive Sensing, starting Fall 2007.

3. Steve Iverson, Topic: Compressive Sensing and Signal Sparsity, starting Spring 2009.

4. Ji Wu, Topic: Compressive Sensing for Radar and Radar Sensor Networks, starting Spring 2009.

5. Ishrat Maherin, Topic: Target Detection Based on UWB Radar and Radar Sensor Networks, starting Spring 2010.

6. Julie Chen, Topic: Rate Distortion in Compressive Sensing, starting Spring 2010.

7. Xin Wang, Topic: Opportunistic and Compressive Sensing in Radar Sensor Network, starting Fall 2010.

8. Zhuo Li, Topic: Co-existence of UWB Radar Sensor Networks and Other Wireless Systems, starting Fall 2010.

2.4 Current M.S. Students

With two new MS students (Sana Agaskar and Ankit Agarwal) joining us in August 2010, we have seven M.S. students in this group.

1. Ashith Kumar, MS Thesis, Sense-through-Wall Target Detection

2. Sukhvindersingh Arora, MS Thesis, Sense-through-Wall Target Detection

3. Sanil Fulani, MS Thesis, LTE and Compressive Sensing

4. Ankit Agarwal, Measurement and Testing of Radar Sensor Networks

5. Mamta Desai, MS Thesis, UWB-Based MIMO Systems

6. Urmi Desai, MS Thesis, Compressive Sensing in MIMO Systems

7. Sana Agaskar, MS Thesis, Measurement and Testing of Radar Sensor Networks

3 Recognitions and Honors Associated with this ONR Award

During this project, the PI has received the following recognitions and honors associated with this award.

- Promoted to Associate Professor with tenure in early 2008 (Promotion and Tenure dossier submitted in Fall 2007).
- 2007 U.S. Air Force Summer Faculty Fellowship Program Award.
- 2009 U.S. Air Force Summer Faculty Fellowship Program Award.
- 2010 U.S. Air Force Summer Faculty Fellowship Program Award.
- Lead Guest Editor, Special Issue on *Radar and Sonar Sensor Networks*, *EURASIP Journal on Wireless Communications and Networking*, 2009.

4 Technology Transition to DoD Product

A technology outcome from this ONR project, sense-through-foliage target detection using UWB radar and UWB radar sensor networks, has been transferred to AFRL/RHX for the application of wideband concepts to laser cloud penetration for the purpose of airborne imaging for Air Force. This product is being implemented in Brooks City AFB in San Antonio, TX, and will be deployed in 2011-2013 for Air Force.

Forests and buildings favor asymmetric threats because the warfighter has a limited sensing capability. Forest and buildings provide excellent concealment from observation, ambush, and escape, as well as provide secure bases for enemy Command & Control (C2), weapons caches, and Improvised Explosive Device (IED)/ Weapon of Mass Destruction (WMD) assembly. These have become "the high ground" in fourth-generation warfare, providing a significant strategic advantage. We believe that solving the sense-through-foliage target detection will significantly benefit sense-through-wall and other subsurface sensing problems. In [43][32], we studied sense-through-foliage target detection using ultra-wideband (UWB) radars. We proposed a Discrete-Cosine-Transform (DCT)-based approach for sense-through-foliage target detection when the echo signal quality is good, and a Radar Sensor Network (RSN) and DCT-based approach when the echo signal quality is poor. A RAKE structure which can combine the echos from different cluster-members was proposed for clusterhead in the RSN. We compared our approach with the ideal case when both echos are available, i.e., echos with target and without target. We also compared our approach against the scheme in which 2-D image was created via adding voltages with the appropriate time offset as well as the matched filter-based approach. We observed that the matched filter-based couldn't work well because the UWB channel has memory. Simulation results show that our DCT-based scheme works much better than the existing approaches, and our RSN and DCT-based approach can be used for target detection successfully while even the ideal case fails to do it. Based on this study, AFRL/RHX has applied it to the application of wideband concepts to laser cloud penetration for the purpose of airborne imaging. According to the AFRL/RHX officer, Dr. Richard A. Albanese in USAF AFMC 711 HPW, the laser imaging through clouds will come to operational fruition in the coming three-five years.

This technology also has its Naval relevance. It will help Marine Corps and expeditionary warfighters to make the forest and wall transparent. It will directly benefit Navy's Transparent Urban Structures (TUS) program. Sense-through-foliage algorithms resulting from this research could be

integrated into emerging net-centric Navy and Marine Corps Command & Control and Intelligence, Surveillance, and Reconnaissance (C2 and ISR) acquisition programs through a Service Oriented Architecture (SOA).

5 Research Accomplishments

We have made significant contributions in the following aspects of radar sensor networks:

- sense-through-foliage target detection using UWB radar and radar sensor network [5][8][32] [37][40][43][44],
- UWB radar for Sense-through-foliage channel modeling and foliage clutter modeling [1][20][24] [41][53],
- waveform design and diversity in radar sensor networks [2][9][10][14][22][23][33][39][56][61],
- radar sensor network optimization [26][55],
- MIMO radar [23],
- multi-target detection in radar sensor networks [7][25][30][36][57][51],
- sensor network for threat assessment [4][12][29][36][38],
- virtual MIMO sensor networks [3][42][54][47],
- UWB sensor network optimization [6][50][52],
- energy efficiency in wireless sensor networks [13][15][17][21][48],
- resource allocation in wireless sensor networks [16][19][45][46][49],
- cross layer design for sensor networks [11][15],
- passive geolocation in electronic warfare [27][31],
- UWB noise radar for sense-through-wall channel modeling [34],
- Compressive sensing [58][59][60].

Appendix

In the Appendix, we attach several papers we have produced during this project period which are based on real world data from radar sensor networks.

References

[1] Jing Liang, Qilian Liang, "Outdoor Propagation Channel Modeling in Foliage Environment," *IEEE Trans on Vehicular Technology*, vol. 59, no. 5, Oct 2010.

[2] Qilian Liang, Xiuzhen Cheng, Sherwood Samn, "NEW: Network-enabled Electronic Warfare for Target Recognition," *IEEE Trans on Aerospace and Electronic Systems*, vol. 46, no. 2, April 2010.

[3] Jing Liang, Qilian Liang, "Channel Selection Algorithms in Virtual MIMO Wireless Sensor Networks," *IEEE Trans on Vehicular Technology.*, vol. 58, no. 3, pp. 2249-2257, June 2009.

[4] Qilian Liang, Xiuzhen Cheng, "KUPS: Knowledge-based Ubiquitous and Persistent Sensor networks for Threat Assessment," *IEEE Transactions on Aerospace and Electronic Systems*, vol. 44, no. 3, pp. 1060-1069, July 2008.

[5] Qilian Liang, "Biologically-Inspired Target Recognition in Radar Sensor Networks," *EURASIP Journal on Wireless Communications and Networking*, Paper ID: 523435, vol. 2010.

[6] Qingchun Ren, Qilian Liang, " Throughput and energy-efficiency Aware Ultra Wideband Communication in Wireless Sensor Networks: A Cross-Layer Approach," *IEEE Transactions on Mobile Computing*, vol. 7, no. 7, pp. 805-816, July 2008.

[7] Hung Ly, Qilian Liang, "Diversity in Radar Sensor Networks: Theoretical Analysis and Application to Target Detection," *International Journal of Wireless Information Networks*, vol. 16, no. 4, 2009.

[8] Jing Liang, Qilian Liang, "Sense-Through-Foliage Target Detection Using UWB Radar Sensor Networks," *Pattern Recognition Letter (Elsevier)*, vol. 31, 2010.

[9] Lei Xu, Qilian Liang, "Optimized Punctured ZCZ Sequence-pair Set: Design, Analysis and Application to Radar System", accepted by *EURASIP Journal on Wireless Communications and Networking,* Paper ID: 254837, vol. 2010.

[10] Qilian Liang, "Automatic Target Recognition Using Waveform Diversity in Radar Sensor Networks", *Pattern Recognition Letters (Elsevier),* vol. 29, no. 2, pp. 377-381, 2008.

[11] Xinsheng Xia, Qilian Liang, "Cross-Layer Design for Mobile Ad Hoc Networks Using Interval Type-2 Fuzzy Logic Systems", *International Journal of Uncertainty, Fuzziness and Knowledge-Based Systems*, Vol. 16, no. 3, pp. 391-407, June 2008.

[12] Qingchun Ren, Qilian Liang, Dechang Chen, "A Fuzzy Logic-Based Secure MAC Protocol Aiming at Denial of Service (DoS) Attacks in Wireless Sensor Networks", accepted by *Information Sciences (Elsevier).*

[13] Haining Shu, Qilian Liang, Jean Gao, "Wireless Sensor Network Lifetime Analysis Using Interval Type-2 Fuzzy Logic Systems", *IEEE Transactions on Fuzzy Systems*, vol. 16, no. 2, pp. 416-427, April 2008.

[14] Qilian Liang, "Radar Sensor Networks: Algorithms for Waveform Design and Diversity with Application to ATR with Delay-Doppler Uncertainty", *EURASIP Journal on Wireless Communications and Networking*, Article ID: 89103, pp. 1-9, vol. 2007.

[15] Qilian Liang, Lingming Wang, Qingchun Ren, " Fault tolerant and energy efficient cross-layer design in wireless sensor networks", *International Journal on Sensor Networks*, vol. 2, no. 3/4, pp. 248-257, 2007.

[16] Liang Zhao, Qilian Liang, "Hop-Distance Estimation in Wireless Sensor Networks with Applications to Resources Allocation," *EURASIP Journal on Wireless Communications and Networking*, Paper ID: 84256, pp. 1-8, vol. 2007.

[17] Haining Shu, Qilian Liang, Jean Gao, "Distributed sensor deployment using fuzzy logic systems," *International Journal on Wireless Information Networks*, vol. 14, no. 3, pp. 163-173, 2007.

[18] Liang Zhao, Qilian Liang, "Energy-Efficient Self-Organization for Wireless Sensor Networks: A Fully Distributed Approach", *International Journal of Distributed Sensor Networks*, vol. 3, no. 4, pp. 347-369, 2007.

[19] Qingchun Ren, Qilian Liang, "Energy and quality aware query processing in wireless sensor database systems", *Information Sciences (Elsevier)*, vol. 177, no. 10, pp. 2188-2205, May 2007.

[20] Jing Liang, Qilian Liang, Sherwood Samn, "A Propagation Environment Modeling in Foliage," accepted by *EURASIP Journal on Wireless Communications and Networking*, Paper ID: 873070, vol. 2010.

[21] Xinsheng Xia, Qilian Liang, "Latency-aware and Energy Efficiency Tradeoffs for Wireless Sensor Networks," *International Journal on Sensor Networks*, vol. 5, no. 1, 2010.

[22] Lei Xu, Qilian Liang, "Radar Sensor Network Using A New Ternary Codes: Theory and Application," submitted to *IEEE Trans on Aerospace and Electronic Systems*.

[23] Lei Xu, Qilian Liang, "Orthogonal Pulse Compression Codes for MIMO Radar System", submitted to *IEEE Trans on Aerospace and Electronic Systems*.

[24] Qilian Liang, "Wireless Channel Modeling in Foliage Environment: UWB versus Narrowband", submitted to *IEEE Trans on Vehicular Technology*.

[25] Hung Ly, Qilian Liang, "Collaborative Multi-Target Detection in Radar Sensor Networks", submitted to *International Journal of Wireless Information Networks.*

[26] Jing Liang, Qilian Liang, "Design and Analysis of Distributed Radar Sensor Networks," submitted to *IEEE Transactions on Parallel and Distributed Systems*.

[27] Jing Liang, Qilian Liang, "Passive Geolocation of RF Emitters by A Netcentric Small Unmanned Aerial System," submitted to *(Wiley) Wireless Communications and Mobile Computing*.

[28] Davis Kirachaiwanich, Qilian Liang, "Capacity of Hybrid Wireless Network," submitted to *IEEE Trans on Mobile Computing*.

[29] Qilian Liang, "Human-inspired favor weak fuzzy logic systems: theory and applications," submitted to *IEEE Trans on Systems, Man, and Cybernetics, Part b: Cybernetics*.

[30] Hong Sam Le, Qilian Liang, "Multi-target Identification and Classification in Cognitive Radar Sensor Networks," submitted to *International Journal of Wireless Information Networks*.

[31] Qilian Liang, Sherwood Samn, "Passive Geolocation Based on Wireless Channel Estimation," submitted to *IEEE Trans on Aerospace and Electronic Systems*.

[32] Qilian Liang, "UWB Radars for Sense-through-Foliage Target Detection," submitted to *IEEE Trans on Geoscience and Remote Sensing*.

[33] Lei Xu, Qilian Liang, Ting Jiang, "A ternary pulse compression code: design and application to radar system," accepted by *IEEE International Conference on Acoustic, Speech, and Signal Processing (ICASSP)*, March 2010, Dallas, TX.

[34] Jing Liang, Qilian Liang, Sherwood Samn, Ram Narayanan, "Sense-Through-Wall Channel Modeling Using UWB Noise Radar," *IEEE Globecom, International Workshop on Multi-Gigabit MM-Wave and Tera-Hz Wireless Systems*, Nov 2009, Honolulu, Hawaii.

[35] Lei Xu, Qilian Liang, "A Set of Triphase Coded Waveforms: Design and Application to Radar System," *IEEE Military Communication Conference*, Oct 2009, Boston, MA.

[36] Hong-Sam Le, Qilian Liang, "Situation Assessment via Multi-Target Identification and Classification in Radar Sensor Networks," *IEEE Military Communication Conference*, Oct 2009, Boston, MA.

[37] Qilian Liang, "Biologically-Inspired Target Recognition in Radar Sensor Networks," *IEEE International Conference on Wireless Algorithms, Systems, and Applications*, August 2009, Boston, MA.

[38] Qilian Liang, "Situation Understanding Based on Heterogeneous Sensor Networks and Human-Inspired Favor Weak Fuzzy Logic System," *IEEE International Conference on Communications*, June 2009, Dresden, Germany.

[39] Lei Xu, Qilian Liang, "Radar Sensor Network Using a New Triphase Coded Waveform: Theory and Application," *IEEE International Conference on Communications*, June 2009, Dresden, Germany.

[40] Jing Liang, Qilian Liang, "UWB Radar Sensor Networks Detection of Targets in Foliage Using Short-Time Fourier Transform," *IEEE International Conference on Communications*, June 2009, Dresden, Germany.

[41] Qilian Liang, Xiuzhen Cheng, "Wireless Channel Modeling in Foliage Environment: UWB versus Narrowband," *IEEE Military Communication Conference*, November 2008, San Diego, CA.

[42] Jing Liang, Qilian Liang, "A Graph Theoretical Algorithm for Virtual MIMO Channel Selection in Wireless Sensor Networks," *IEEE Military Communication Conference*, November 2008, San Diego, CA.

[43] Qilian Liang, Sherwood Samn, Xiuzhen Cheng, "UWB Radar Sensor Networks for Sense-through-Foliage Target Detection," *IEEE International Conference on Communications*, May 2008, Beijing, China.

[44] Jing Liang, Qilian Liang, Sherwood Samn, "A Differential Based Approach for Sense-Through-Foliage Target Detection using UWB Radar Sensor Networks," *IEEE International Conference on Communications*, May 2008, Beijing, China.

[45] Rahul Sawant, Qilian Liang, Dan Popa, Frank Lewis, "Experimental Path Loss Models for Wireless Sensor Networks," *IEEE Military Communication Conference*, Oct 2007, Orlando, FL.

[46] K. Xing, X. Cheng, L. Ma, and Q. Liang, "Superimposed Code Based Channel Assignment in Multi-Radio Multi-Channel Wireless Mesh Networkss," *ACM MobiCom 2007*, pp. 15-26, Montreal, QC, Canada, Sept 2007.

[47] Jing Liang, Qilian Liang, "SVD-QR-T Approach for Virtual MIMO Channel Selection in Wireless Sensor Networks," *IEEE International Conference on Wireless Algorithms, Systems, and Applications*, Chicago, IL, August 2007.

[48] Qingchun Ren, Qilian Liang, "Performance Analysis of Energy Detection for Cognitive Radio Wireless Networks," *IEEE International Conference on Wireless Algorithms, Systems, and Applications*, Chicago, IL, August 2007.

[49] Sejal Raje, Qilian Liang, "Time synchronization in network-centric sensor networks," *IEEE Radio and Wireless Symposium*, Long Beach, CA, 2007.

[50] Lingming Wang, Qilian Liang, "UWB Sensor Networks in Hostile Environment: Interference Analysis and Performance Study," *IEEE Radio and Wireless Symposium*, Long Beach, CA, 2007.

[51] Haining Shu, Qilian Liang, "Data Fusion in Multi-Target Radar Sensor Network," *IEEE Radio and Wireless Symposium*, Long Beach, CA, 2007.

[52] Lingming Wang, Qilian Liang, "UWB Sensor Networks in Hostile Environment: Interference Analysis and Performance Study," *Handbook of Wireless Mesh & Sensor Networking*, McGraw-Hill International, NY, 2007.

[53] Jing Liang, Qilian Liang, Sherwood Samn, "Foliage Clutter Modeling Using the UWB Radar," *IEEE International Conference on Communications*, May 2008, Beijing, China.

[54] Jing Liang, Qilian Liang, "Channel Selection Algorithms in Virtual MIMO Sensor Networks," *ACM MobiHoc 2008, First ACM Workshop on Heterogeneous Sensor and Actor Networks*, May 2008, Hong Kong.

[55] Jing Liang, Qilian Liang, "Image Fusion on Radar Sensor Networks," *International Conference on Heterogeneous Networking for Quality, Reliability, Security and Robustness (Qshine)*, Vancouver, Canada, August 2007.

[56] Qilian Liang, Sherwood Samn, "NEW-CATR: Network-enabled Electronic Warfare for Collaborative Automatic Target Recognition," *IEEE Military Communication Conference*, Oct 2007, Orlando, FL.

[57] Hung Ly, Qilian Liang, "Collaborative Multi-Target Detection in Radar Sensor Networks," *IEEE Military Communication Conference*, Oct 2007, Orlando, FL.

[58] Ji Wu, Qilian Liang, Zheng Zhou, "Compressive sensing for autoregressive hidden Markov model signal," *International Conference on Wireless Algorithms, Systems, and Applications*, August 2010, Beijing, China.

[59] Lei Xu, Qilian Liang, "Compressive sensing using singular value decomposition," *International Conference on Wireless Algorithms, Systems, and Applications*, August 2010, Beijing, China.

[60] Qilian Liang, "Compressive Sensing for Radar Sensor Networks," *IEEE Globecom*, Dec 2010, Miami, FL.

[61] Lei Xu, Q. Liang, "Radar Sensor Network Using A New Ternary Codes: Theory and Application," accepted by *IEEE Sensors Journal*.

Outdoor Propagation Channel Modeling in Foliage Environment

Jing Liang and Qilian Liang, *Senior Member, IEEE*

***Abstract*—Foliage is a rich scattering environment that is slowly time varying. Most previous investigations in foliage models center on the statistical modeling of clutters and targets. Ideally, it would be desirable to characterize the nature of the propagation channel in foliage; however, it has not been investigated in detail up until now. This paper studies the problem of nonline-of-sight (NLOS) channel modeling based on extensive data collected using both narrowband and ultrawideband (UWB) radars. The modeling adopts the CLEAN algorithm, in which the channel-impulse response (CIR) is accomplished. It is observed that the multipath contributions arriving at the receiver are grouped into clusters. The arrival of clusters can be modeled as a Poisson process, whereas within each cluster, subsequent multipath contributions or rays also arrive according to a Poisson process. However, the arrival rate is quite different, along with the carrier frequency. It is also proposed that the amplitude of multipath channels can more accurately be characterized by a log-logistic distribution (LLD) other than commonly used clutter models such as the log-normal, the Weibull, or the Rayleigh fading model. The proposed foliage channel model is extendable to other outdoor environments. This is a great advantage for the specification and development of future wireless systems.**

***Index Terms*—Channel modeling, foliage, goodness-of-fit, log-logistic, narrowband, outdoor, ultrawideband (UWB).**

I. Introduction

THE PERFORMANCE of wireless systems in foliage is confined to their propagation channels. To ensure effective sensing-through-foliage communications as well as target detection, tracking, and classification, an accurate model to characterize the wireless propagation is highly critical. Wireless channels can be categorized in a number of different ways, such as narrowband versus wideband, indoor versus outdoor, etc. In the case of narrowband, the bandwidth of signals is much smaller than the carrier frequency and the coherence bandwidth of the channel [1]; therefore, the multipath reflections are not easy to resolve in the receiving signals. On the contrary, the bandwidth of the wideband channel is on the order of or larger than the coherent bandwidth of the channel, and thus, the multipath components in the received signals are resolvable. As for an indoor or an outdoor environment, in general, the former tends to induce higher multiple scattering and diffraction due to obstacles inside the building, whereas the latter is more likely to bring on large-scale fading.

Many efforts were undertaken to investigate wireless propagation channels. In the narrowband case, Rayleigh, Rician, and Nakagami distributions were used to model the flat fading, and a narrowband model close to additive white Gaussian noise with strong specular interference was also proposed for aeronautical telemetry [2]. Particularly, narrowband radiowave propagation in foliage was studied in [3]–[5]. For wideband channels, the ultrawideband (UWB) pulse is one of the most interesting signals due to the exceptional range resolution, strong penetrating capability, and its low power. The IEEE standardized the UWB indoor multipath channel [6] on the basis of the Saleh and Valenzuela (S-V) model [7]. Compared with the indoor situation, measurements and models are inadequate for UWB outdoor propagations. Reference [8] applied a UWB radar-like test apparatus to obtain propagation delays, which serves as a preliminary investigation into UWB channel for rural terrain, but more extensive measurements and further analysis are absent for a statistical characterization. Reference [9] characterized UWB channels for an outdoor office environment by the S-V model with modifications on the ray arrival times and amplitude statistics to fit the empirical data. However, these parameters may not fit the foliage environment as trees and branches provide different scattering from that of indoor environments. Some experimental outdoor studies other than UWB are presented in [10]–[12]. Reference [10] proposes that, instead of Rayleigh, Weibull provides a better fit to spatially and temporally extended spiking data; [11] shows that the foliage is impulsively corrupted with multipath fading, which leads to an inaccuracy of the K-distribution model; and [12] models the aeronautical telemetry channel gain using a complex Gaussian random variable.

Foliage is a special environment that lies somewhere in between indoor and outdoor cases. Like an indoor environment, foliage contains a wealth of multiple scattering, owing to the rough surfaces of trunks, branches, and leaves; thus, a dominant line-of-sight (LOS) is less likely to present. Due to the climate change, the movement of trees contributes to the time-varying property, and therefore, the propagation channel cannot be as stationary as that of indoor environment. Moreover, foliage consists of intervening materials that are electromagnetically dispersive, making the propagation frequency dependent. Therefore, it is highly likely that applying both narrowband and UWB signals to model the propagation channel would have advantages over a single-type signal with limited frequency

Manuscript received June 17, 2009; revised October 15, 2009 and January 20, 2010; accepted February 5, 2010. Date of publication February 22, 2010; date of current version June 16, 2010. This work was supported in part by the U.S. Office of Naval Research under Grant N00014-07-1-0395 and Grant N00014-07-1-1024 and in part by the National Science Foundation under Grant CNS-0721515, Grant CNS-0831902, Grant CCF-0956438, and Grant CNS-0964713. The review of this paper was coordinated by Prof. T. Kuerner.

The authors are with the Department of Electrical Engineering, University of Texas at Arlington, TX 76019 USA (e-mail: jliang@wcn.uta.edu; liang@uta.edu).

Color versions of one or more of the figures in this paper are available online at http://ieeexplore.ieee.org.

Digital Object Identifier 10.1109/TVT.2010.2043697

Fig. 1. Measurement environment. Largely defoliated but dense forest.

(a) (b)

Fig. 2. Experiment. (a) Lift. (b) Equipment on top of the lift under the hut. The black weather-resistant box held the oscilloscope and Barth pulser during the testing.

content. Two radiation formats can be compared and general tendency can be concluded, and thus, a narrowband wideband study would assist with better understanding of channel characterization. The narrowband signals are tested at 200 and 400 MHz, respectively, whereas the UWB radar emissions are at a relatively low frequency that is typically between 100 MHz and 3 GHz. Each frequency component in a radar signal will sense the foliage in a slightly different manner, providing differences in multipath pulses.

The remaining part of this paper is organized as follows: Section II describes the measurement and collection of experimental data. Section III uses the CLEAN algorithm to extract the channel-impulse response (CIR) for 200-MHz, 400-MHz, and UWB signals. Section IV discusses the statistical modeling of temporal, amplitude, and phase characterizations. Section V summarizes important findings and suggests further investigation.

II. Measurement Setup

The foliage-penetration measurement effort began in August 2005 and continued through December 2005 [13]. The measurements were taken in Holliston, MA. The data used in this paper were measured in November. The foliage is made up of both deciduous and conifer trees with a higher percentage of deciduous. Generally, the height of the trees is above 25 m. Fig. 1 illustrates the largely defoliated but dense forest at that time.

The foliage experiment was constructed on a 7-t man lift, which had a total lifting capacity of 450 kg. The limit of the lifting capacity was reached during the experiment as essentially, the entire measuring apparatus was placed on the lift. Fig. 2(a) shows the lift [13]. This picture was taken in September with

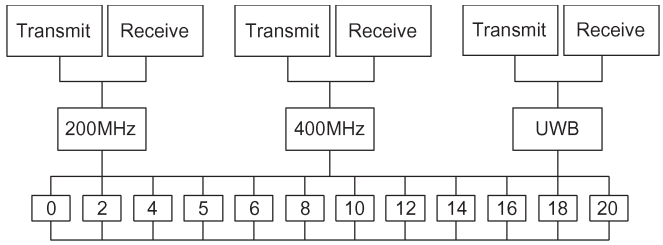

Fig. 3. Measured data file structure. “0”–“20” are 12 equally parted locations with an experimental length of 20 m. At each location, 35 pulses of 200 MHz, 400 MHz, and UWB signals are measured, respectively.

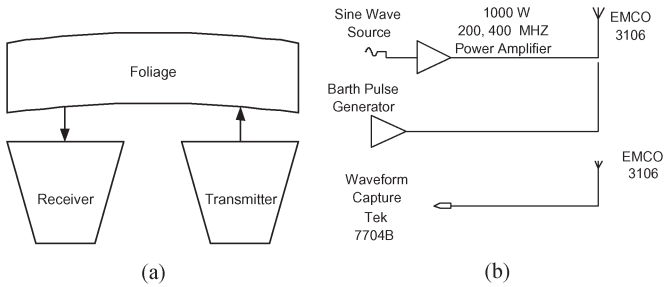

Fig. 4. Antennas. (a) Antenna layout. (b) System schematic diagram.

the foliage still largely present. A photographic side view of the equipment platform on the lift is illustrated in Fig. 2(b). The lift was a four-wheel-drive diesel platform that was driven up and down a graded track that is 25 m long with an experimental length of 20 m. This track served as a strip map synthetic aperture radar track, and the extra 5 m accommodated the length of the lift. The measurement system was moved to 12 equally parted locations named “0,” “2,” “4,” “5,” “6,” “8,” “10,” “12,” “14,” “16,” “18,” and “20” on the track. At each location along the track, 35 pulses taken 3 s apart have been obtained for the transmitted and received signals, respectively. Each sample in the pulse is spaced at a 50-ps interval, and 16 000 samples were collected for each pulse, for a total time duration of 0.8 μs. The accomplished data structure is shown in Fig. 3 [13].

The principle pieces of equipment secured on the lift under a weather shield are listed as follows [13]:

1) dual antenna mounting stand;
2) two EMCO antennas;
3) 200 MHz, 1-kW amplifier, power supply, preamp;
4) 400 MHz, 1-kW amplifier, power supply, preamp;
5) Barth pulse source (Barth Electronics, Inc. model 732 GL) for UWB;
6) Tektronix model 7704 B oscilloscope;
7) rack system;
8) HP signal generator;
9) IBM laptop;
10) custom RF switch and power supply;
11) weather shield (small hut).

The general equipment layout is shown in Fig. 4(a). Individual transmit and receive antennas have been used as it was believed that circulators did not exist for wideband signals in 2005. Antennas are EMCO ridged waveguide horns (Microwave Horn, EMCO 3106) over a frequency range of 200 MHz–2 GHz. A 5.486-m (18-ft) distance between antennas was chosen to reduce the signal coupling between the transmitter

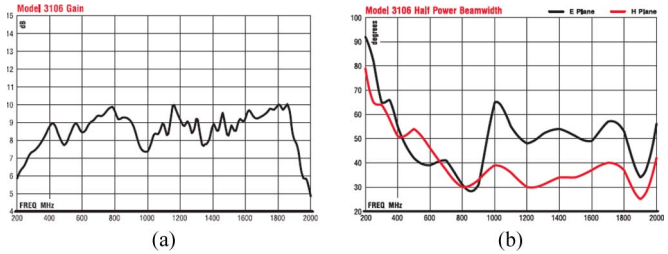

Fig. 5. EMCO 3106 technical data. (a) Gain. (b) Half power beamwidth.

and the receiver [13], [14]. The system was pointing at the specified 91.44-m (300-ft) one-way distance. Beyond 91.44 m (300 ft), the received signal disappeared into the noise. The transmit and receive antennas required two degrees of rotational freedom (azimuth and elevation). The antennas could be adjusted during the course of the experiment while having sufficient stability not to become misaligned during wind gusts in excess of 40 mi/h [13]. The position along the track was changed and the rotation angle down range adjusted at each measurement location such that the centerline of the RF beam made a series of parallel measurements along the track.

The preamplifiers were Henry Radio models 50B-200 and 50B-400 for 200 and 400 MHz, respectively. The Henry Radio power amplifiers were TEMPO-2002A and TEMPO-2400A for 1 kW pulsed at 200 and 400 MHz, respectively [13]. Each amplifier was specified at a minimum bandwidth of 2 MHz around its center frequency. The source for all of the narrowband or continuous wave signals was an Agilent 8648A signal generator. The UWB pulse generator used a coaxial reed switch to discharge a charge line for very fast rise time pulse outputs. The model 732 pulse generator provided pulses of less than 50-ps rise time, with amplitudes ranging from 150 V to more than 2 kV into any load impedance through a 50-Ω coaxial line. The generator is capable of producing pulses with a minimum width of 750 ps and a maximum of 1 μs. This output pulse width is determined by the charge line length for rectangular pulses or by capacitors for $1/e$ decay pulses.

In the hope of supporting a fairer wideband–narrowband comparison, a Yagi antenna (Antenna Research Associates LPC-2010-C), which contained the Barth pulse, was applied in transmit primarily to spread the beam of the wideband pulse [13]. Using the EMCO ridged waveguide horn, each frequency in the Barth pulse is radiated into a different beam shape. Since the Barth pulse is a high-frequency event compared with the 200- and 400-MHz narrowband frequencies employed, the overall beam shape for the Barth pulse is narrow compared with the beam for narrowband frequencies. The signal output was displayed on a computer-controlled digital storage oscilloscope (Tektronix model 7704 B). See Fig. 4(b) for the system schematic diagram and Fig. 5 for the EMCO 3106 gain and beamwidth [13], [15].

III. Channel Impulse Response Based on the Measured Data and CLEAN Algorithm

The averaged transmitted and received signals of 35 measured pulses were calculated at each location (12 locations) for 200 MHz, 400 MHz, and UWB, respectively. The transmitted

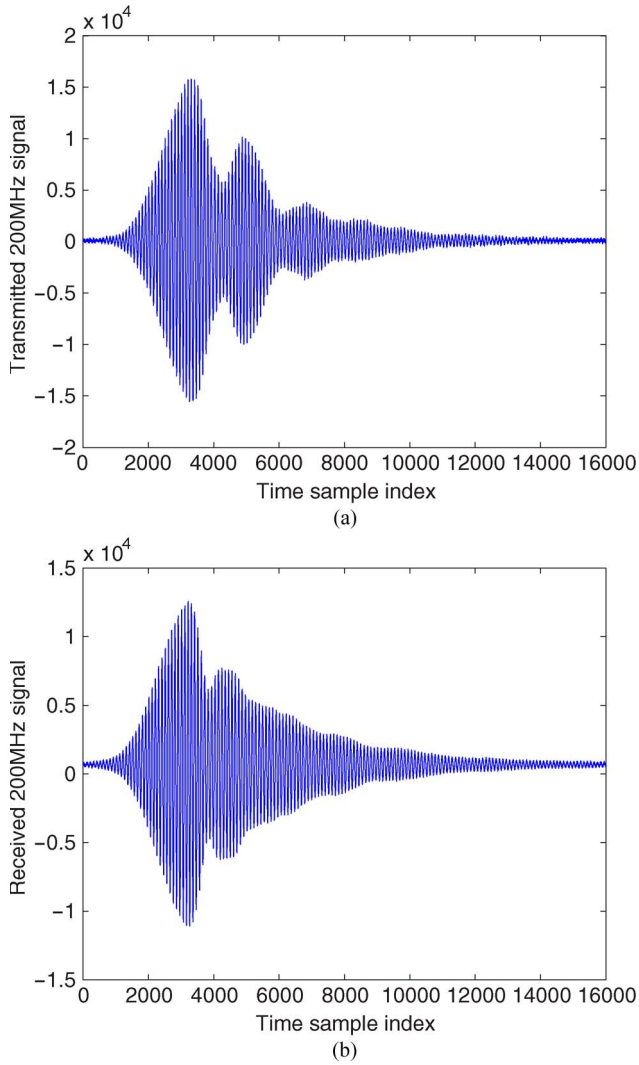

Fig. 6. Measurement of 200 MHz and 35 pulse average. (a) Transmitted pulse. (b) Received echoes.

signals and the averaged received signals at location "4" for different frequencies are shown in Figs. 6–8. According to [9], a minimum of nine samples is necessary to average out small-scale fading to permit the true shape of the power decay profile to be recovered. We believe that the average of 35 samples offers satisfactory removal of both small-scale fading and noise. Note that at a different location (e.g., "0" "2" "6"...), the result will slightly be different. However, for simplicity and conciseness, the illustration at one location is sufficient to show the essential properties.

As in foliage, the received signal is made up of distorted and time-shifted pulses, and the complex multipath CIR can be modeled as follows [16]:

$$r(t) \approx \sum_n a_n p_n(t-\tau_n) e^{j\phi_n} \tag{1}$$

where a_n, p_n, and τ_n are referred to as the amplitude (also known as path gain), unit pulse, time delay, and phase angle of the nth propagation path, respectively.

Generally, time domain, frequency domain, and sliding correlator are the three basic techniques that characterize the

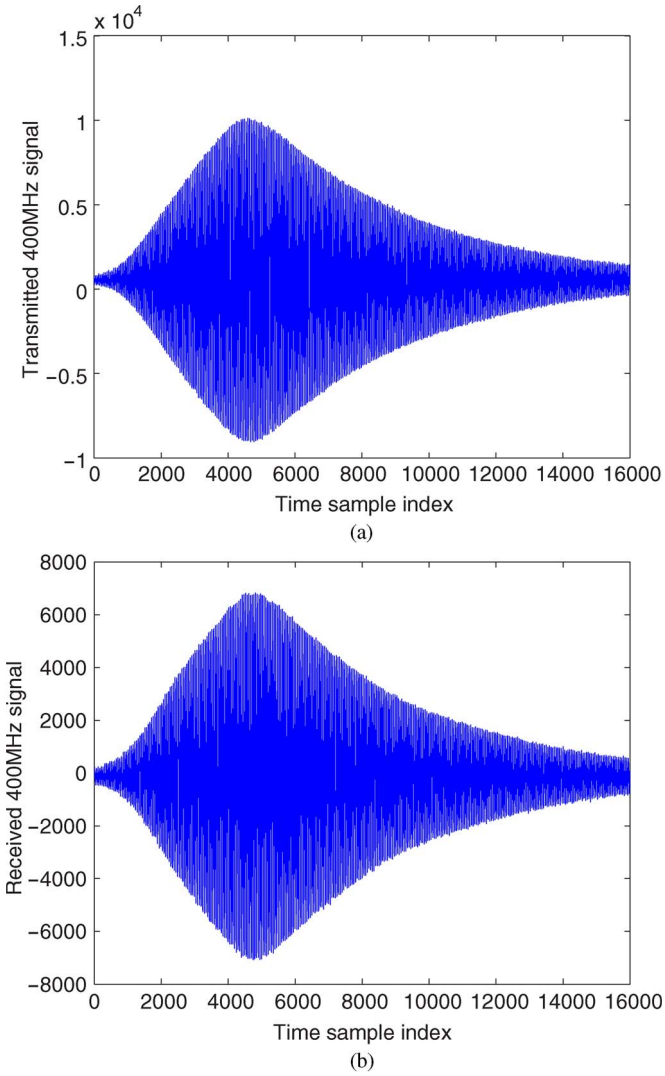

Fig. 7. Measurement of 400 MHz and 35 pulse average. (a) Transmitted pulse. (b) Received echoes.

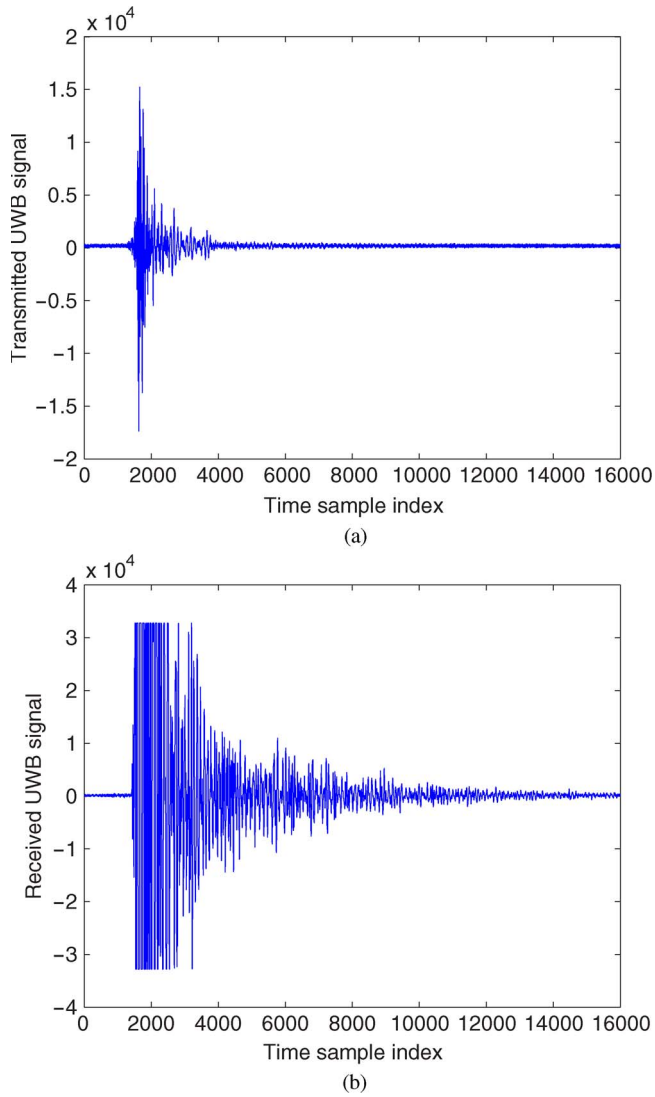

Fig. 8. Measurement of UWB and 35 pulse average. (a) Transmitted pulse. (b) Received echoes.

channel [17]. If high-resolution channel modeling is required, then a deconvolution algorithm, such as CLEAN [18], can be used to extract the CIR. It was initially introduced in [19] to enhance the radio astronomical maps of the sky and was also employed in both narrowband [18] and UWB [20]–[22].

The CLEAN algorithm is an iterative high-resolution subtractive deconvolution procedure that is capable of resolving dense multipath components, which are usually irresolvable by conventional inverse filtering [23]. It generates multiple taps by "cleaning" the similarities between the measurement and the template and thus constructs a discrete CIR in time. Recently, there have been some enhanced versions of CLEAN proposed in [16], [18], and [24]–[26].

The steps utilized in our algorithm are the following [26].

1) Calculate the autocorrelation of the transmitted signal $R_{ss}(t)$ and the cross correlation of the transmitted signal with the received waveform $R_{sy}(t)$.
2) Find the largest correlation peak in $R_{sy}(t)$, and record the normalized amplitudes α_k and the relative time delay τ_k of the correlation peak.
3) Subtract $R_{ss}(t)$ scaled by α_k from $R_{sy}(t)$ at time delay τ_k.
4) If a stopping criterion (a minimum threshold on the peak correlation) is not met, then go step 2). Otherwise, stop.

The stopping criterion should be decided on the basis of noise level. Choosing the good stopping criterion is important because the deconvolution must go deep enough to be correct, but the CLEAN algorithm starts to diverge when the noise is cleaned too deep. A good compromise is slightly below the noise level, i.e., typically 0.5σ, where σ is the standard deviation of noise. Since each CIR (12 CIR for 12 locations) obtained in this paper is based on the 35 averaged pulses (noise has been averaged out), the total number of clean components were searched.

Given the transmission, the received signals, and the CLEAN processing previously described, the obtained CIRs at location "4" are illustrated from Figs. 9–11. Note that the absolute value of the UWB channel is plotted here for comparison between the outdoor UWB channel (see Fig. 11) with the indoor S-V model [7] (see Fig. 12). These figures show the following:

1) Comparing Fig. 11 with Fig. 12, it is clear that the obtained CIR is similar to the discrete channel impulse in

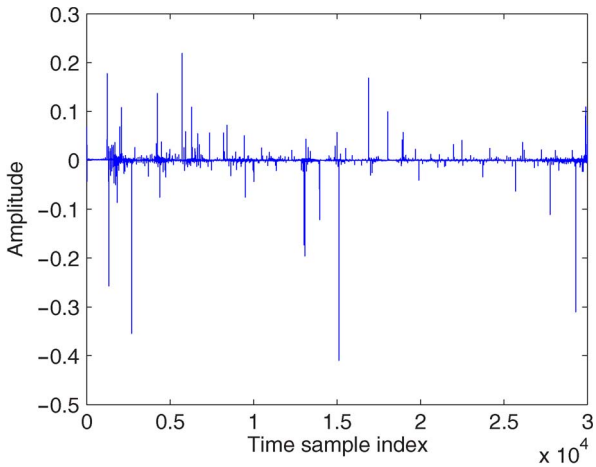

Fig. 9. CIR (200 MHz) by CLEAN from 35-pulse averaged transmitting and receiving signals.

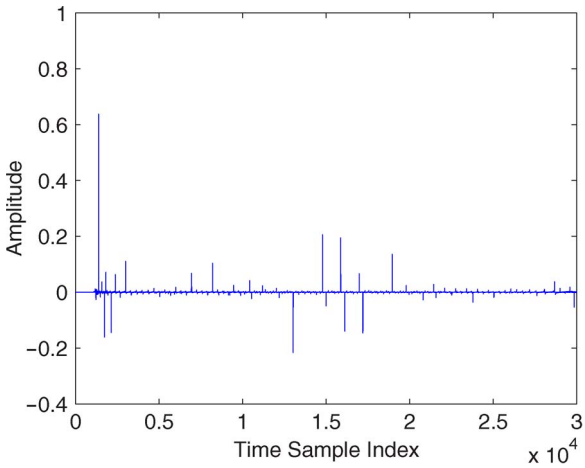

Fig. 10. CIR (400 MHz) by CLEAN from 35-pulse averaged transmitting and receiving signals.

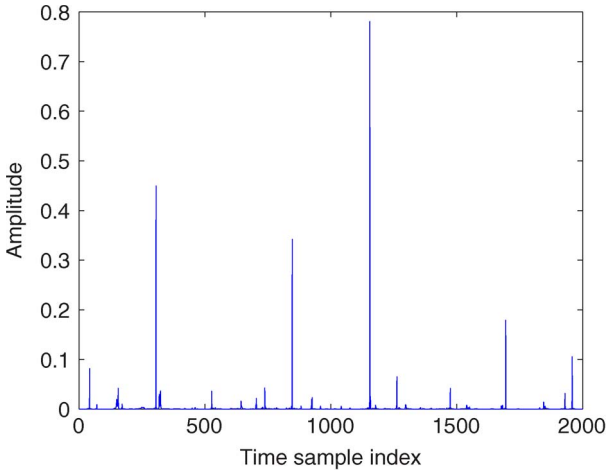

Fig. 11. UWB CIR by CLEAN from 35-pulse averaged transmitting and receiving signals.

the S-V model. The impulse responses in foliage arrive in clusters, and there are subsequent rays within each cluster. This typical phenomenon is also illustrated in Figs. 9 and 10. Due to the complex layout of trees, foliage is a rich scattering environment, which leads to multipath components in propagation channels.

2) Channels are frequency dependent. It was observed that the intervening materials, such as foliage and soil, have dielectric properties that are strongly frequency dependent. This in part explains the differences in CIR of 200 MHz, 400 MHz, and UWB.

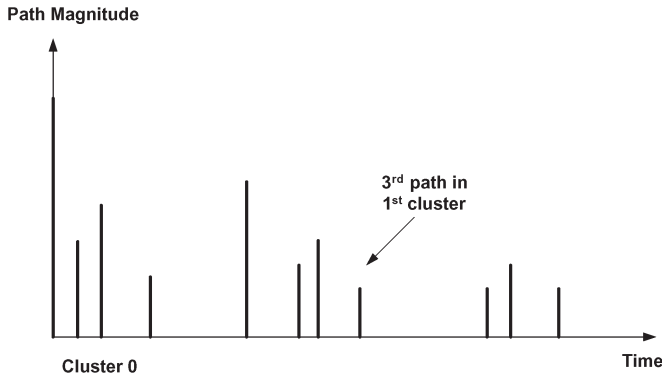

Fig. 12. Channel impulse in the S-V model.

The phase angles ϕ_n will be assumed *a priori* to be statistically independent random variable with uniform distribution over $[0, \pi)$. We believe that this is self-evident and needs no experimental justification [4].

We have experimentally derived multipath propagation channels for foliage environment using 200 MHz, 400 MHz, and UWB signals. In general, the time-varying CIR is random; therefore, we have to statistically characterize it via the measurement [27].

IV. Outdoor Channel Modeling

A. Temporal Characterization

We start with the physical realization that the rays obtained through CLEAN arrive in clusters, which is not consistent with a simple Poisson time-of-arrival model. Similar observations were found in modeling urban mobile radio channels [28]. Observing the CIR at 200 MHz, 400 MHz, and UWB for 12 locations, such as some of those given in Figs. 9–11, like in the S-V model, the time axis of multipath contributions is divided into "bins," with the probability of a ray arriving within a given "bin." In the S-V model, the arrival of clusters is modeled as a Poisson time-of-arrival process with a rate Λ, whereas within each cluster, subsequent multipath contributions or rays also arrive according to a Poisson process with a rate λ (see Fig. 13). The foliage temporal model employs the clustered "double Poisson" time-of-arrival model given the following: 1) The S-V model retains the basic features of a constant-rate Poisson arrival process and mutually independent path gain. 2) It appears to be extendable by adjusting its parameters to present different measured channel responses. 3) The parameter analysis is relatively simple. Moreover, this model can be explained from a physical viewpoint, therefore making it more readily extendable to other outdoor environments.

The time arrival of clusters in foliage can be modeled as a Poisson arrival process with a rate Λ. The first arriving ray of a cluster is formed by the transmitted signal following a

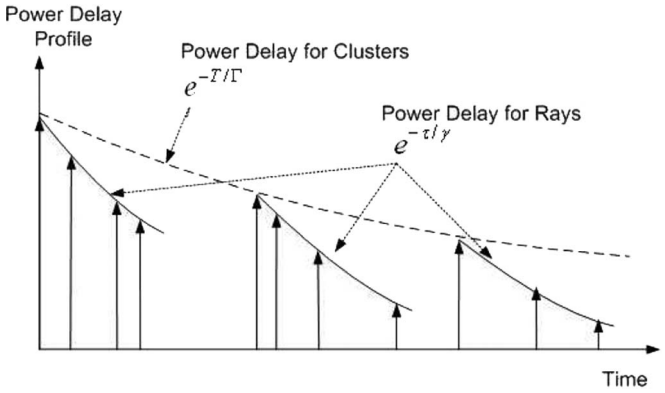

Fig. 13. Double exponential decay of the cluster power profile and the ray power profile within clusters in the S-V model.

more-or-less "direct" path to the receiver. Such a path, mostly consisting open spaces, goes through a few, but not too many, tree trunks and branches. Subsequent clusters result from reflections from farther trunks, branches, and leaves. Within each cluster, multipath contributions or rays also arrive according to a Poisson process with a rate λ. These rays within a cluster are formed by multiple "weaker" reflections from tree trunks, branches, leaves, and animals (e.g., birds and squirrels).

We define the following:

1) T_l—the arrival time of the first path of the lth cluster;
2) $\tau_{k,l}$—the delay of the kth path within the lth cluster relative to the first path arrival time T_l;
3) Λ—the cluster arrival rate;
4) λ—the ray arrival rate, i.e., the arrival rate of the paths within each cluster.

By definition, we have $\tau_{0l} = T_l$. The distributions of the cluster arrival time and the ray arrival time are given by

$$\begin{aligned} p(T_l|T_{l-1}) &= \Lambda \exp(-\Lambda(T_l - T_{l-1}), \qquad l > 0 \\ p(\tau_{k,l}|\tau_{(k-1),l}) &= \lambda \exp\left(-\lambda(\tau_{k,l} - \tau_{(k-1),l})\right), \qquad k > 0. \end{aligned} \tag{2}$$

It is worth mentioning that the clusters generally overlap. Deciding which ray belongs to a particular cluster can be difficult from time to time. Let Γ and γ denote the power delay time constants for the clusters and the rays, respectively (see Fig. 13). Typically, $\Gamma > \gamma$, and the expected power of the rays in a cluster decay faster than the expected power of the first ray of the next cluster. Note that if $T_l - T_{l-1}$ is large enough such that $e^{-(T_l - T_{l-1})/\gamma} \ll e^{-(T_l - T_{l-1})/\Gamma}$, then the lth and $(l-1)$ th cluster will appear separate. In our analysis, the cluster is determined in such a way that within each cluster, the amplitude of rays decay. Then, we observe $\bar{T}_l$, i.e., the averaged arrival time of the first path within clusters, and $\bar{\tau}_{k,l}$, i.e., the averaged arrival rate of the paths within each cluster.

Table I lists the parameters of Λ and λ, which are averaged values of 12 locations for 200 MHz, 400 MHz, and UWB impulse responses, respectively. As for indoor UWB data, see [29]. The higher Λ and λ of UWB implies its exceptional range resolution compared with narrowband signals. The lower Λ and λ of outdoor UWB than those of indoor means that the indoor environment typically has a richer multiple scattering, i.e., walls, furniture, and doors for indoor environment generally provide stronger reflections other than trunks, branches, and leaves. A higher value of Λ and λ for clusters and rays would be expected if denser trees are present. At the same time, we believe some weak rays may appear to be misdetected due to our measurement sensitivity.

TABLE I
TEMPORAL PARAMETERS FOR CHANNEL MODELS

Scenario	$\Lambda(1/ns)$	$\lambda(1/ns)$
200MHz	0.012	0.4
400MHz	0.004	0.128
Outdoor UWB	0.04	0.8
Indoor UWB Extreme NLOS	0.0667	2.1

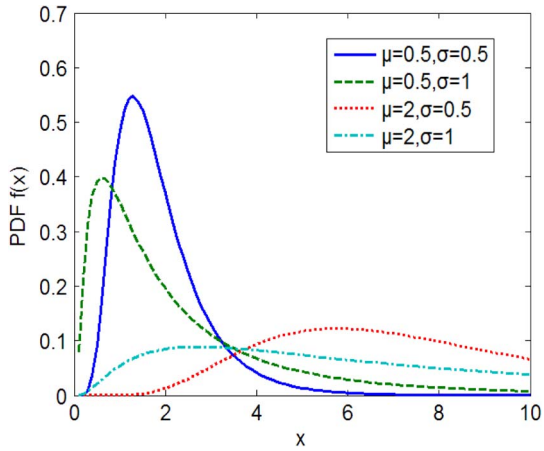

Fig. 14. Log-logistic probability density function.

B. Statistical Distribution of Channel Amplitude

In the IEEE UWB indoor channel model [6], the clutter approach was adopted (same as S-V model), but a log-normal distribution was suggested for characterizing the multipath amplitude, and an additional log-normal variable was introduced for representing the fluctuations of the total multipath gain. In this section, we propose that a log-logistic model should better characterize the multipath gain for both outdoor narrowband and UWB channels.

1) Statistic Models: Log-logistic distribution (LLD) [30] is a special case of Burr's type-XII distribution [31]. Lee *et al.* employed the LLD for the frequency analysis of multiyear drought duration [32], whereas Shoukri *et al.* adopted LLD to analyze extensive Canadian precipitation data [33], and Narda and Malik used LLD to develop a model of root growth and water uptake in wheat [34]. In spite of intensive applications in precipitation and stream-flow data, thus far, the LLD statistical model has never been applied to foliage channel modeling to the best of our knowledge.

This model is adopted due to its statistical similarity to log-normal and Weibull distributions with higher kurtosis and longer tails in probability density function (PDF), which is illustrated in Fig. 14. The expression is given by

$$f(x) = \frac{e^{\frac{\ln x - \mu}{\sigma}}}{\sigma x \left(1 + e^{\frac{\ln x - \mu}{\sigma}}\right)^2}, \qquad x > 0, \quad \sigma > 0 \tag{3}$$

where μ is the scale parameter, and σ is the shape parameter. The mean of the LLD is

$$E\{x\} = e^{\mu}\Gamma(1+\sigma)\Gamma(1-\sigma). \tag{4}$$

The variance is expressed as

$$\mathrm{Var}\{x\} = e^{2\mu}\left\{\Gamma(1+2\sigma)\Gamma(1-2\sigma) - [\Gamma(1+\sigma)\Gamma(1-\sigma)]^2\right\} \tag{5}$$

whereas the moment of order k is

$$E\{x^k\} = \sigma e^{\mu} B(k\sigma, 1-k\sigma), \qquad k < \frac{1}{\sigma} \tag{6}$$

where

$$B(m,n) = \int_0^1 x^{m-1}(1-x)^{n-1}dx. \tag{7}$$

Similarly, the PDF for log-normal distribution [35] with parameters μ and σ is

$$f(x) = \frac{1}{x\sigma\sqrt{2\pi}} e^{-\frac{(\ln x-\mu)^2}{2\sigma^2}}, \qquad x>0, \quad \sigma>0. \tag{8}$$

The Weibull distribution [36] can be made to fit measurements that lie between the Rayleigh and log-normal distributions. The PDF is represented as

$$f(x) = ba^{-b}x^{b-1}e^{-(x/a)^b}, \qquad x>0, \quad a>0, \quad b>0 \tag{9}$$

where b is the shape parameter, and a is the scale parameter.

The Rayleigh distribution, whose real and imaginary components are Gaussian variables, has the PDF as follows:

$$f(x) = \frac{x}{b^2} e^{-\frac{x^2}{2b^2}}, \qquad b>0. \tag{10}$$

If a and b are the parameters for the Weibull distribution, then the Rayleigh distribution with parameter b is equivalent to the Weibull distribution with parameters $a=\sqrt{2}b$ and $b=2$.

2) MLE: On the basis of CIR amplitude data from 12 different locations, we apply the maximum-likelihood estimation (MLE) approach to estimate the preceding parameters for log-logistic, log-normal, Weibull, and Rayleigh models, respectively. MLE is often used when the sample data are known and the parameters of the underlying probability distribution are to be estimated [37], [38]. It is generalized as follows.

Letting $y_1, y_2, \ldots, y_N$ be N independent samples drawn from a random variable $\mathbf{Y}$ with m parameters $\theta_1, \theta_2, \ldots, \theta_m$, where $\theta_i \in \theta$, then the joint PDF of $y_1, y_2, \ldots, y_N$ is

$$L_N(\mathbf{Y}|\theta) = f_{Y|\theta}(y_1|\theta_1, \ldots, \theta_m), \ldots, f_{Y|\theta}(y_n|\theta_1, \ldots, \theta_m). \tag{11}$$

When expressed as the conditional function of $\mathbf{Y}$ depends on the parameter θ, the likelihood function is

$$L_n(\mathbf{Y}|\theta) = \prod_{k=1}^{N} f_{Y|\theta}(y_k|\theta_1, \theta_2, \ldots, \theta_m). \tag{12}$$

The MLE of $\theta_1, \theta_2, \ldots, \theta_m$ is the set of values $\hat{\theta}_1, \hat{\theta}_2, \ldots, \hat{\theta}_m$ that maximize the likelihood function $L_N(\mathbf{Y}|\theta)$.

TABLE II
ESTIMATED PARAMETERS FOR STATISTIC MODEL

PDF	Log-Logistic	Log-normal
200MHz	$\hat{\mu} = -3.79907$ $\hat{\sigma} = 0.43948$ $\varepsilon_\mu = 0.0517626$ $\varepsilon_\sigma = 0.0250518$	$\hat{\mu} = -3.69473$ $\hat{\sigma} = 0.811659$ $\varepsilon_\mu = 0.0550099$ $\varepsilon_\sigma = 0.0390963$
400MHz	$\hat{\mu} = -3.75666$ $\hat{\sigma} = 0.482505$ $\varepsilon_\mu = 0.071783$ $\varepsilon_\sigma = 0.035901$	$\hat{\mu} = -3.61265$ $\hat{\sigma} = 0.917049$ $\varepsilon_\mu = 0.0795182$ $\varepsilon_\sigma = 0.0565477$
Outdoor UWB	$\hat{\mu} = -3.30616$ $\hat{\sigma} = 0.590192$ $\varepsilon_\mu = 0.202988$ $\varepsilon_\sigma = 0.101636$	$\hat{\mu} = -3.13344$ $\hat{\sigma} = 1.12623$ $\varepsilon_\mu = 0.225245$ $\varepsilon_\sigma = 0.164277$
PDF	Weibull	Rayleigh
200MHz	$\hat{a} = 0.0388139$ $\hat{b} = 1.00543$ $\varepsilon_a = 0.0027934$ $\varepsilon_b = 0.00456447$	$\hat{b}$=0.0474046
400MHz	$\hat{a} = 0.0447926$ $\hat{b} = 0.903163$ $\varepsilon_a = 0.00458706$ $\varepsilon_b = 0.0536079$	$\hat{b}$=0.0609159
Outdoor UWB	$\hat{a} = 0.080002$ $\hat{b} = 0.765597$ $\varepsilon_a = 0.0222858$ $\varepsilon_b = 0.106023$	$\hat{b}$=0.141188

TABLE III
RMSE COMPARISON BETWEEN STATISTIC MODELS

PDF	Log-Logistic	Log-normal	Weibull	Rayleigh
200MHz	5.7016	6.2850	8.8810	9.7562
400MHz	5.9023	6.5635	9.7056	10.3359
UWB	2.1867	2.4756	3.0136	4.8975

As the logarithmic function is monotonically increasing, maximizing $L_N(\mathbf{Y}|\theta)$ is equivalent to maximizing $\ln(L_N(\mathbf{Y}|\theta))$. Hence, it can be shown that a necessary but not sufficient condition to obtain the MLE $\hat{\theta}$ is to solve the likelihood equation

$$\frac{\partial}{\partial\theta}\ln\left(L_n(\mathbf{Y}|\theta)\right) = 0. \tag{13}$$

We obtain $\hat{\mu}$ and $\hat{\sigma}$ for log-logistic, $\hat{\mu}$ and $\hat{\sigma}$ for log-normal, $\hat{a}$ and $\hat{b}$ for Weibull, and $\hat{b}$ for Rayleigh, respectively, which are shown in Table II. We also explore the standard deviation (STD) errors of each parameter, which are also shown in Table II in the form of ε_x, where x denotes a different parameter for each model. From Table II, it is obvious that the log-logistic model provides smaller STD errors than those of log-normal.

3) Goodness-of-Fit in Curve and RMSE: We may also observe to what extent does the PDF curve of the statistic model match that of the CIR amplitude data by means of root mean square error (RMSE). Letting i $(i = 1, 2, \ldots, n)$ be the sample index of the CIR amplitude, c_i is the corresponding density value, whereas $\hat{c}_i$ is the density value of the statistical model with estimated parameters by means of MLE. RMSE is obtained through

$$\mathrm{RMSE} = \sqrt{\frac{1}{n}\sum_{i=1}^{n}(c_i - \hat{c}_i)^2} \tag{14}$$

where n is the sample index. The RMSEs for 200 MHz, 400 Hz, and UWB are listed in Table III. It demonstrates that LLD is the model that fits the channel amplitude data best.

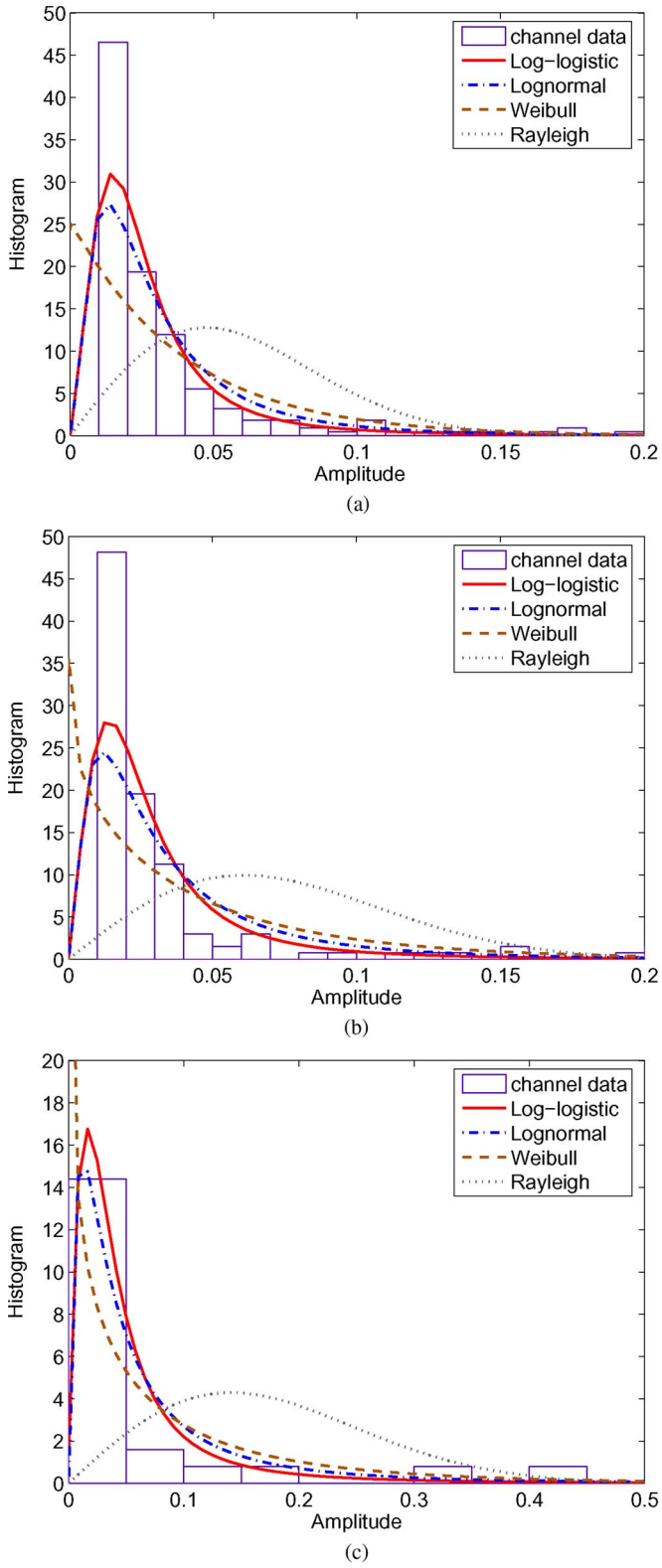

Fig. 15. Goodness-of-fit illustration by density. (a) CIR for 200 MHz. (b) CIR for 400 MHz. (c) CIR for UWB.

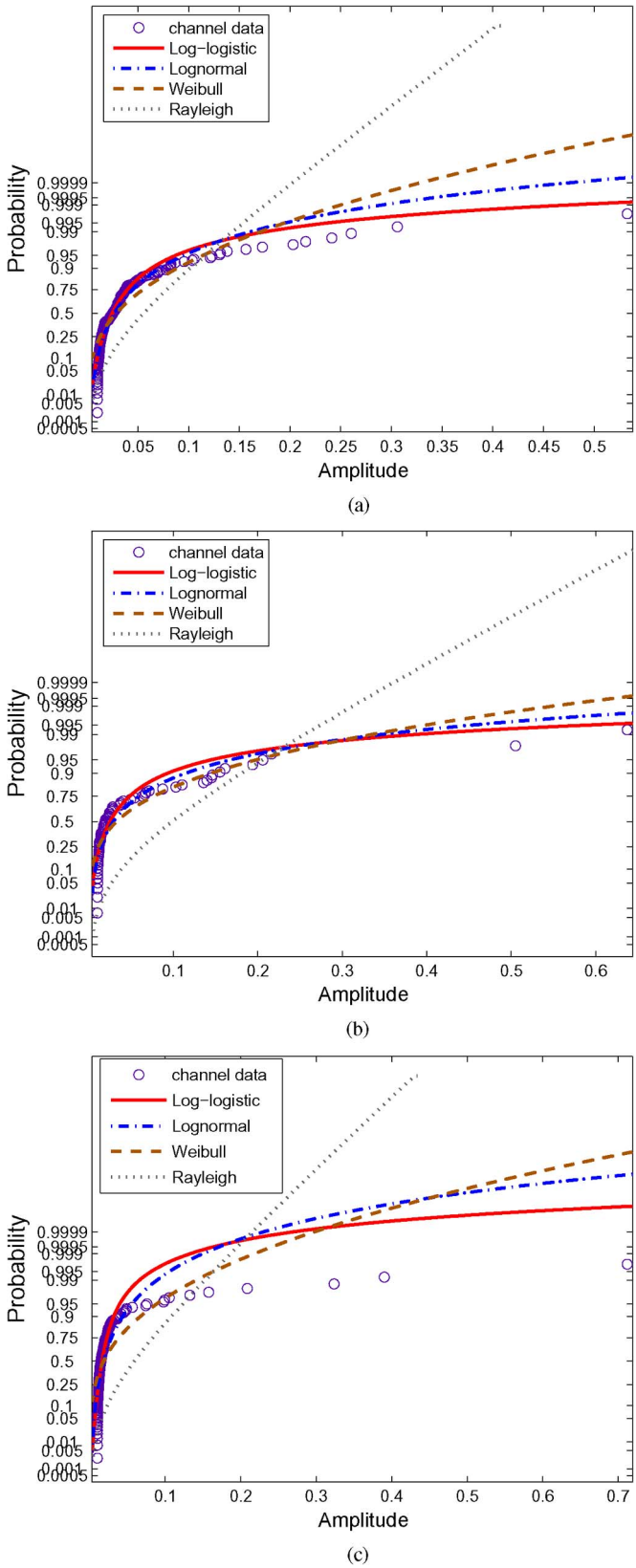

Fig. 16. Goodness-of-fit illustration by cumulated probability. (a) CIR for 200 MHz. (b) CIR for 400 MHz. (c) CIR for UWB.

One may also draw the foregoing conclusion from Figs. 15 and 16, which describe the goodness-of-fit by curves. In Fig. 15, the absolute gains of all our resolved paths are plotted in terms of histogram. It can easily be seen that the Rayleigh model provides the worst goodness-of-fit compared with LLD, log-normal, and Weibull. In addition, Weibull is not a good choice due to the inaccurate kurtosis and high tails. Comparing LLD with log-normal, it is obvious that LLD is able to provide

higher kurtosis, sharper slope, and lower tail. In other words, LLD provides generally better goodness-of-fit than that of log-normal. Fig. 16 uses cumulated statistical methodology to compare the goodness-of-fit for LLD, log-normal, Weibull, and Rayleigh models. It shows that LLD offers a general better fit compared with other models.

The foregoing investigations show that in foliage environment, LLD can better characterize the amplitude of multipath impulse responses other than commonly used log-normal, Weibull, and Rayleigh models for both narrowband and UWB signals.

V. Conclusions and Future Work

This paper has presented the propagation measurement results of 200 MHz, 400 MHz, and UWB signals in Holliston foliage in November with a largely defoliated but dense forest. Like an indoor environment, foliage contains a wealth of multiple scattering owing to the rough surfaces of trunks, branches, and leaves. The CLEAN algorithm was used to resolve dense multipath components, which were usually unresolvable by conventional inverse filtering.

We came to the following conclusions: 1) Foliage non-LOS (NLOS) channels are generally frequency dependent, which is illustrated by the different temporal and amplitude properties of CIR based on three measurement frequencies. This is due to the fact that foliage is made up of intervening materials that have dielectric properties associated with frequencies. 2) The temporal characterizations of CIR for both narrowband and UWB are similar to those of the S-V model for an indoor environment. Therefore, we model the time arrival of clusters as a Poisson process with a rate Λ and the subsequent multipath contributions using another Poisson process with a rate λ. The analysis results of Λ and λ are shown in Table I. The capability of multipath resolution (from high to low) is that UWB $>$ 200 MHz $>$ 400 MHz, and the indoor environment typically has a richer multiple scattering than that of the outdoors. 3) The amplitude of multipath channels can more accurately be characterized by LLD other than log-normal, Weibull, or Rayleigh. We apply the MLE approach to estimate the parameters for those models based on CIR amplitude data. Tables II and III show that LLD provides smaller STD errors than those of log-normal, as well as the smallest RMSE. Additionally, the better fit provided by LLD is visually shown in Figs. 15 and 16. Our model is extendable by adjusting the temporal and LLD parameters to represent the channels within the same foliage at different season or other foliage environment. This model can easily be used in simulation and analysis for the planning of wireless networks and designing fixed terrestrial and satellite communication services.

The channels discussed in this paper are slowly time varying. At each location, 35 pulses were taken 3 s apart, having a roughly 0.9 correlation coefficient at each location. Generally, foliage is time varying from time to time because of changes along with the seasons or due to the movement of branches and leaves on windy days. For future work, we may collect extensive data to explore the time-varying nature of wireless propagation channels in foliage.

Acknowledgment

The authors would like to thank Dr. S. W. Samn of the Air Force Research Laboratory/RHX for providing the radar data.

References

[1] J. G. Proakis, *Digital Communications*, 4th ed. New York: McGraw-Hill, 2001.
[2] M. Rice, R. Dye, and K. Welling, "Narrowband channel model for aeronautical telemetry," *IEEE Trans. Aerosp. Electron. Syst.*, vol. 36, no. 4, pp. 1371–1377, Oct. 2000.
[3] T. Fernandes, R. F. S. Caldeirinha, M. Al-Nuaimi, and J. Richter, "A discrete RET model for millimeter-wave propagation in isolated tree formations," *IEICE Trans. Commun.*, vol. E88-B, no. 6, pp. 2411–2418, Jun. 2005.
[4] R. F. S. Caldeirinha, "Radio characterization of single trees at micro- and millimetre wave frequencies," Ph.D. dissertation, Univ. Glamorgan, Pontypridd, U.K., Apr. 2001.
[5] N. C. Rogers, A. Seville, J. Richter, D. Ndzi, R. F. S. Caldeirinha, A. Shukla, M. Al-Nuaimi, K. Craig, and J. Austin, "A generic model of 1–60 GHz radio propagation trough vegetation—Final report," Radiocommun., Agency, London, U.K., May 2002.
[6] J. R. Foerster, "Channel modeling sub-committee report final," IEEE P802.15-02/490r1-SG3a, IEEE 802.15.SG3a, Feb. 2003.
[7] A. A. Saleh and R. A. Valenzuela, "A statistical model for indoor multipath propagation," *IEEE J. Sel. Areas Commun.*, vol. SAC-5, no. 2, pp. 128–137, Feb. 1987.
[8] M. Z. Win, F. Ramírez-Mireles, R. A. Scholtz, and M. A. Barnes, "Ultra-wide bandwidth (UWB) signal propagation for outdoor wireless communications," in *Proc. IEEE Veh. Technol. Conf.*, May 1997, vol. 1, pp. 251–255.
[9] C. W. Kim, X. Sun, L. C. Chiam, B. Kannan, F. P. S. Chin, and H. K. Garg, "Characterization of ultra-wideband channels for outdoor office environment," in *Proc. IEEE Wireless Commun. Netw. Conf.*, Mar. 2005, vol. 2, pp. 950–955.
[10] F. L. Posner, "Spiky sea clutter at high range resolutions and very low grazing angles," *IEEE Trans. Aerosp. Electron. Syst.*, vol. 38, no. 1, pp. 58–73, Jan. 2002.
[11] S. Watts, "Radar detection prediction in K-distribution sea clutter and thermal noise," *IEEE Trans. Aerosp. Electron. Syst.*, vol. AES-23, no. 1, pp. 40–45, Jan. 1987.
[12] M. Rice, A. Davis, and C. Bettweiser, "Wideband channel model for aeronautical telemetry," *IEEE Trans. Aerosp. Electron. Syst.*, vol. 40, no. 1, pp. 57–69, Jan. 2004.
[13] C. Dill, "Foliage penetration (Phase II) field test: Narrowband versus wideband foliage penetration," Final Rep. of Contract No. F41624-03-D-7001/04, Jul. 2005–Feb. 2006.
[14] J. A. Henning, "Design and performance of an ultra-wideband foliage penetrating noise radar," M.S. thesis, Univ. Nebraska, Lincoln, NE, May 2001.
[15] [Online]. Available: www.ets-lindgren.com/pdf/ant4.pdf
[16] R. J.-M. Cramer, R. A. Scholtz, and M. Z. Win, "Evaluation of an ultra-wide-band propagation channel," *IEEE Trans. Antennas Propag.*, vol. 50, no. 5, pp. 561–570, May 2002.
[17] T. S. Rappaport, *Wireless Communications: Principles and Practice*, 2nd ed. Upper Saddle River, NJ: Prentice-Hall, 2002.
[18] R. G. Vaughan and N. L. Scott, "Super-resolution of pulsed multipath channels for delay spread characterization," *IEEE Trans. Commun.*, vol. 47, no. 3, pp. 343–347, Mar. 1999.
[19] J. A. Högbom, "Aperture synthesis with a non-regular distribution of interferometer baselines," *Astron. Astrophys. Suppl. Ser.*, vol. 15, pp. 417–426, 1974.
[20] P. C. Richardson, W. Xiang, and W. Stark, "Modeling of ultra-wideband channels within vehicles," *IEEE J. Sel. Areas Commun.*, vol. 24, no. 4, pp. 906–912, Apr. 2006.
[21] B. M. Donlan, D. R. McKinstry, and R. M. Buehrer, "The UWB indoor channel: Large and small scale modeling," *IEEE Trans. Wireless Commun.*, vol. 5, no. 10, pp. 2863–2873, Oct. 2006.
[22] W. Yang and Z. Naitong, "A new multi-template CLEAN algorithm for UWB channel impulse response characterization," in *Proc. Int. Conf. Commun. Technol.*, Nov. 2006, pp. 1–4.
[23] A. F. Molisch, "Ultrawideband propagation channels: Theory, measurement and modeling," *IEEE Trans. Veh. Technol.*, vol. 54, no. 5, pp. 1528–1545, Sep. 2005.

[24] S. M. Yano, "Investigating the ultra-wideband indoor wireless channel," in *Proc. IEEE Veh. Technol. Spring Conf.*, May 2002, vol. 3, pp. 1200–1204.
[25] Z. Irahhauten, G. J. M. Janssen, H. Nikookar, A. Yarovoy, and L. P. Ligthart, "UWB channel measurements and results for office and industrial environments," in *Proc. IEEE Int. Conf. Ultra-Wideband*, Sep. 2006, pp. 225–230.
[26] J. H. Reed, *An Introduction to Ultra Wideband Communication Systems*. Upper Saddle River, NJ: Prentice-Hall, 2005.
[27] M. Pätzold, A. Szczepanski, and N. Youssef, "Methods for modeling of specified and measured multipath power-delay profiles," *IEEE Trans. Veh. Technol.*, vol. 51, no. 5, pp. 978–988, Sep. 2002.
[28] G. L. Turin, F. D. Clapp, T. L. Johnston, S. B. Fine, and D. Lavry, "A statistical model of urban multipath propagation," *IEEE Trans. Veh. Technol.*, vol. VT-21, no. 1, pp. 1–9, Feb. 1972.
[29] M.-G. Di Benedetto and G. Giancola, *Understanding Ultra Wideband Radio Fundamentals*. Upper Saddle River, NJ: Prentice-Hall, 2004.
[30] R. C. Gupta, O. Akman, and S. Lvin, "A study of log-logistic model in survival analysis," *Biometrical J.*, vol. 41, no. 4, pp. 431–443, Jul. 1999.
[31] I. W. Burr, "Cumulative frequency functions," *Ann. Math. Statist.*, vol. 13, no. 2, pp. 215–232, Jun. 1942.
[32] K. S. Lee, J. Sadeghipour, and J. A. Dracup, "An approach for frequency analysis of multiyear drought duration," *Water Resour. Res.*, vol. 22, no. 5, pp. 655–662, 1986.
[33] M. M. Shoukri, I. U. M. Mian, and D. S. Tracy, "Sampling properties of estimators of the log-logistic distribution with application to Canadian precipitation data," *Can. J. Statist.*, vol. 16, no. 3, pp. 223–236, Sep. 1988.
[34] N. K. Narda and R. K. Malik, "Dynamic model of root growth and water uptake in wheat," *Indian J. Agric. Eng.*, vol. 3, pp. 147–155, 1993.
[35] E. Limpert, W. Stahel, and M. Abbt, "Log-normal distributions across the sciences: Keys and clues," *BioScience*, vol. 51, no. 5, pp. 341–352, May 2001.
[36] W. Weibull, "A statistical distribution function of wide applicability," *Trans. ASME, J. Appl. Mech.*, vol. 18, no. 3, pp. 293–297, 1951.
[37] J. L. Devore, *Probability and Statistics for Engineering and the Sciences*. Monterey, CA: Brooks/Cole, 1982.
[38] M. Barkat, *Signal Detection and Estimation*, 2nd ed. London, U.K.: Artech House, 2005.

Jing Liang received the B.S. and M.S. degrees in electrical engineering from Beijing University of Posts and Telecommunications, Beijing, China, in 2003 and 2006, respectively, and the Ph.D. degree in electrical engineering from the University of Texas at Arlington, in August 2009.

She is currently a Research Assistant Professor with the Department of Electrical Engineering, University of Texas at Arlington. Her current research interests include radar sensor networks, collaborative and distributed signal processing, wireless communications, wireless networks, and fuzzy logic systems.

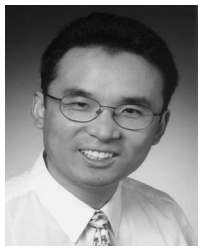

Qilian Liang (M'01–SM'05) received the B.S. degree in electrical engineering from Wuhan University, Wuhan, China, in 1993, the M.S. degree in electrical engineering from Beijing University of Posts and Telecommunications, Beijing, China, in 1996, and the Ph.D. degree in electrical engineering from the University of Southern California, Los Angeles, in May 2000.

He was a Member of Technical Staff with Hughes Network Systems Inc., San Diego, CA. Since August 2002, he has been with the Department of Electrical Engineering, University of Texas at Arlington (UTA), where he is currently an Associate Professor. He has published more than 170 journal and conference papers and six book chapters and has six U.S. patents pending. His research interests include radar and sonar sensor networks, wireless communications, compressive sensing, wireless networks, signal processing for communications, fuzzy logic systems and applications, and collaborative and distributed signal processing.

Dr. Liang received the 2002 IEEE TRANSACTIONS ON FUZZY SYSTEMS Outstanding Paper Award, the 2003 U.S. Office of Naval Research Young Investigator Award, the 2005 UTA College of Engineering Outstanding Young Faculty Award, and the 2007 and 2009 U.S. Air Force Summer Faculty Fellowship Program Award.

Sense-Through-Wall Channel Modeling Using UWB Noise Radar

Jing Liang, Qilian Liang
Department of Electrical Engineering
University of Texas at Arlington
Arlington, TX 76019-0016, USA
Email: jliang@wcn.uta.edu, liang@uta.edu

Sherwood W. Samn
Air Force Research Laboratory/HEX
Brooks City Base
San Antonio, TX 78235, USA
Email: Sherwood.samn@brooks.af.mil

Ram M. Narayanan
Department of Electrical Engineering
The Pennsylvania State University
University Park, PA 16802, USA
Email: ram@engr.psu.edu

***Abstract*— Sensing-through-wall will benefit various applications such as emergence rescues and military operations. In order to add more signal processing functionality, it is vital to understand the characterization of sense-through-wall channel. In this paper, we propose a statistical channel model on a basis of real experimental data using UWB noise radar. We employ CLEAN algorithm to obtain the multipath channel impulse response (CIR) and observe that the channel amplitude at each path can be accurately characterized as T location-scale distribution. We also analyze that the multipath contributions arrive at the receiver are grouped into clusters. The time of arrival of clusters can be modeled as a Poisson arrival process, while within each cluster, subsequent multipath contributions or rays also arrive according to a Poisson process. However, these arrival rates are much smaller than those of indoor UWB channels.**

I. Introduction

Sensing-through-wall techniques have attracted great interest due to a broad range of military and civilian applications. During detection, it is more likely that signal processing occurs at one side of the wall and the interior space to be exploited is on the other and it can not be seen through conventional measures. Therefore it is desirable that the wall penetration sensing provide following information: building layouts like rooms and inner objects; identification of humans and their positions; the composition and structure of the wall. These characterizations will be of great use in locating weapon caches during military operations, searching and rescuing people from natural diasters such as earthquakes and providing sustainability assessment of bridges and buildings.

In recent years UWB waveforms are frequently employed for indoor wireless propagation systems due to the exceptional range resolution and strong penetrating capability. There has been a great amount of research on statistical modeling of UWB indoor multipath channels [1]-[3] and IEEE [4] has standardized it on a basis of Saleh and Valenzuela (S-V) channel model [5]. There have been some efforts investigating sensing-through-wall using UWB waveforms. [6] uses finite difference time-domain (FDTD) method to simulate reflected UWB pulses for three different types of walls. [7] proposes UWB transmission pulses for walls with different thickness and conductivity. However, these reports only describe about transmitted or reflected waveforms based on simulation, sense-through-wall channel has not yet been touched on. Imaging techniques have also been employed to show objects behind the wall in [8] and [9]. [8] uses wideband synthetic aperture radar and incorporates wall thickness and dielectric constant to generate the indoor scene through image fusion. [9] discusses the advantages of using thermally generated noise as a probing signal and analyzes the basic concepts of synthetic aperture radar image formation using noise waveforms. Nevertheless these studies haven't provide any insight into any property of through-wall radio channel.

In this paper, we propose a statistical multipath model of through-wall radio channel based on real measurement. The UWB noise waveform presented in [9] has been adopted in our work. This is due to the inherently low probability of intercept (LPI) and low probability of detection (LPD). These characterizations provide immunity from detection, jamming, and interference. We investigate the model based on channel impulse response (CIR) obtained through CLEAN processing method. It is observed that the amplitude of channel coefficient at each path can be accurately characterized by T location-scale distribution. It is also observed that the multipath contributions arrive at the receiver are grouped into clusters. The time of arrival of clusters can be modeled as a Poisson arrival process, while within each cluster, subsequent multipath contributions or rays also arrive according to a Poisson process.

The rest of this paper is organized as follows. In Section II, we summarize the measurement and collection of the data. In Section III, we apply CLEAN algorithm to extract CIR. Section IV presents the channel model in terms of amplitude and temporal parameters. Conclusion and future work is given in Section V.

II. Measurement Setup

A UWB noise radar system was set up in the Radar Imaging Lab at Villanova University. Fig. 1 illustrates the layout of the experiment room. The wall segment, constructed utilizing solid concrete blocks with a dielectric constant of 7.66, is 0.14m thick 2.8m long and 2.3m high. The room behind this wall is empty.

A horn antenna, model ETS-Lindgren 3164-04, with an operational bandwidth from 0.7 to 6 GHz, was used as the transceiver. The antenna was placed only 1cm to the front

978-1-4244-5626-0/09/$26.00 ©2009 IEEE

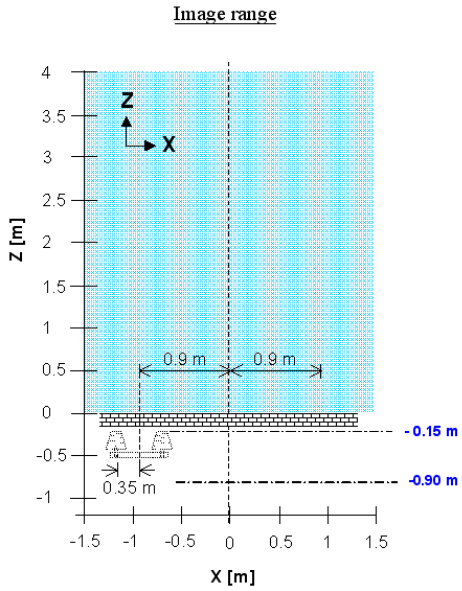

Fig. 1. Experiment Setup

wall, which is illustrated in Fig. 2. Therefore the propagation length from antenna front edge to the backside of the wall is 15cm. 37 times of measurements are collected at different but equally spaced positions along the wall with step size 5cm. An Agilent network analyzer, model ENA 5071B, was used for signal synthesis and data collection.

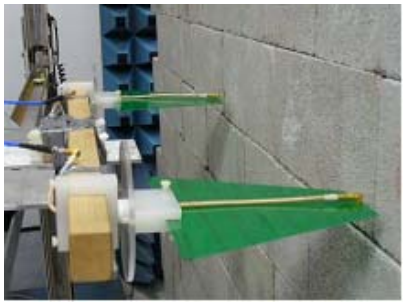

Fig. 2. Radar antenna and wall in the experiment

III. Channel Impulse Response Based on the Measured Data and CLEAN Algorithm

The transmitted noise waveform and received echoes of one measurement are plotted in Fig. 3. It shows that UWB noise waveform has a very good sensing-through-wall capability. During 37 experiments, the frequency of the transmitted signal is $400 - 720$ MHz and sampling rate is 1.5GHz/s. The tremendously large amplitude at around sample 100 is due to the antenna coupling [10]. Note that at a different position the measurement result will be slightly different but the characterization of the signals are quite similar. Thus the illustration of pulses collected at one position is sufficient to describe the property.

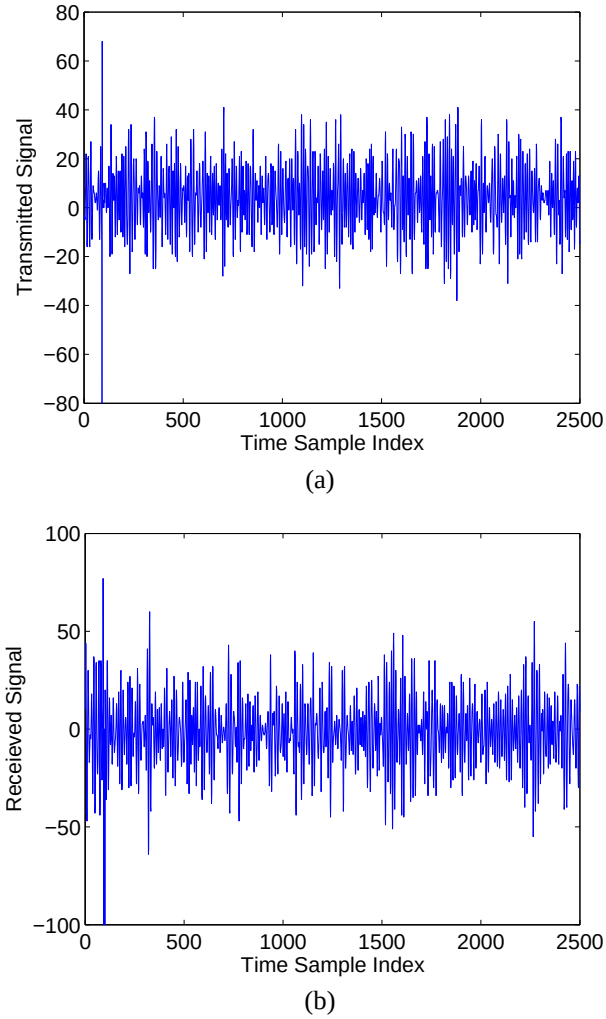

Fig. 3. UWB noise waveforms: (a) transmitted pulse (b) received echoes

Fig. 4 shows the histogram of transmitted and received waveform amplitude. It is very interesting to see that after sensing-through-the wall, the back scattered signal still roughly follows Gaussian distribution. This conclusion applies to all other 36 measurements. Assume the Gaussian mean and variance are μ and σ^2 respectively, Table I shows the detail of these parameters.

Since the transmitted and received signals have been known, the CLEAN algorithm can be used to extract channel impulse response (CIR). This method was initially introduced in [11] to enhance radio astronomical maps of the sky, and has been frequently employed in UWB channel characterization problems [12]-[14]. The CLEAN algorithm is an iterative, high-resolution, subtractive deconvolution procedure that is capable resolving dense multipath components which are usually irresolvable by conventional inverse filtering [16].

Our steps involved [15] are:

1) Calculate the autocorrelation of the transmitted signal $R_{ss}(t)$ and the cross-correlation of the transmitted with the received waveform $R_{sy}(t)$.

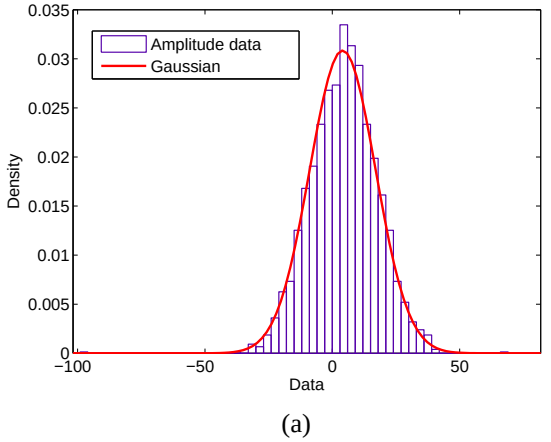

(a)

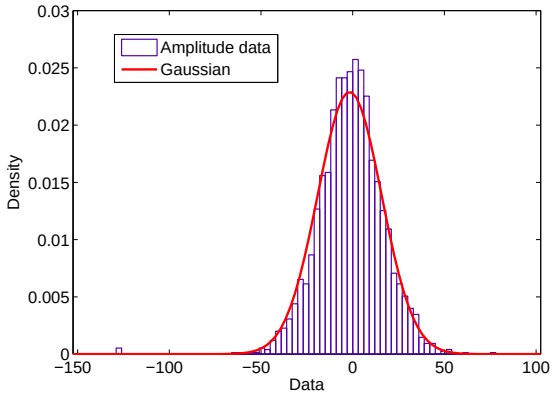

(b)

Fig. 4. Amplitude density: (a) transmitted pulse (b) received echoes

TABLE I

ESTIMATED STATISTICAL PARAMETERS OF TRANSMITTED AND RECEIVED SIGNALS

parameter	transmitted signal	received signal
μ	4.0512	-1.6756
STD Error of μ	0.258655	0.348318
σ	12.9328	17.4159
STD Error of σ	0.182952	0.246372

2) Find the largest correlation peak in $R_{sy}(t)$, record the normalized amplitudes α_k and the relative time delay τ_k of the correlation peak.
3) Subtract $R_{ss}(t)$ scaled by α_k from $R_{sy}(t)$ at the time delay τ_k.
4) If a stopping criterion (a minimum threshold) on the peak correlation is not met, go step 2. otherwise stop.

Fig. 5 illustrated the absolute value of through-wall CIR at one measurement position by CLEAN algorithm. We can see that the channel consists of multipaths that arrive in clusters. Each cluster is made up of subsequent rays. This is very similar to the multipath rays in S-V channel model. However, in S-V model, the largest scattering, i.e., the highest magnitude always appears at the first path. It is obvious to see this is not

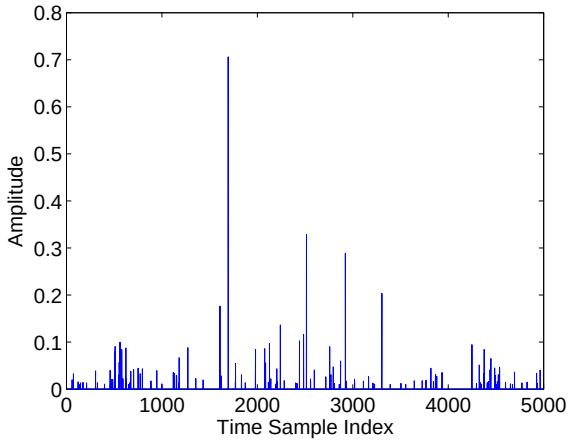

Fig. 5. Normalized CIR by CLEAN algorithm

the general case in the through-wall channel. On a basis of CIR, the channel can be represented as

$$r(t) \approx \sum_n a_n p_n(t - \tau_n) \tag{1}$$

where a_n and τ_n is referred to as the amplitude and delay of the n^{th} propagation path. In the next Section we shall analyze them in detail.

IV. SENSE-THROUGH-WALL CHANNEL MODELING

A. Temporal Characterization

Like in S-V model, multipath contributions arrive at the receiver grouped into clusters and therefore similar methodology used in S-V model studies may be also applied to sensing-through-wall CIR. The time of arrival of clusters can be modeled as a Poisson arrival process with a rate Λ, while within each cluster, subsequent multipath contributions or rays also arrive according to a Poisson process with a rate λ.

We define:

- T_l : the arrival time of the first path of the l-th cluster;
- $\tau_{k,l}$: the delay of the k-th path within the l-th cluster relative to the first path arrival time T_l;
- Λ : the cluster arrival rate;
- λ : the ray arrival rate, i.e., the arrival rate of the paths within each cluster;
- $\bar{\tau}$: the mean excess delay;
- σ_τ : the rms delay spread

By definition, we have $\tau_{0l} = T_l$. The distributions of the cluster arrival time and the ray arrival time are given by

$$\begin{aligned} p(T_l|T_{l-1}) &= \Lambda \exp\left(-\Lambda(T_l - T_{l-1}), l > 0\right) \\ p(\tau_{k,l}|\tau_{(k-1),l}) &= \lambda \exp\left(-\lambda(\tau_{k,l} - \tau_{(k-1),l})\right), k > 0 \end{aligned} \tag{2}$$

$\bar{\tau}$, σ_τ are defined by

$$\bar{\tau} \equiv \frac{\sum_n a_n^2 \tau_n}{\sum_n a_n^2} \tag{3}$$

$$\sigma_\tau \equiv \sqrt{\bar{\tau^2} - \bar{\tau}^2} \tag{4}$$

where

$$\bar{\tau^2} \equiv \frac{\sum_n a_n^2 \tau_n^2}{\sum_n a_n^2} \tag{5}$$

We analyze these parameters based on 37 experiments and show the result in Table II.

TABLE II
TEMPORAL PARAMETERS FOR SENSE-THROUGH-WALL CHANNEL MODEL

parameter	$\Lambda(1/ns)$	$\lambda(1/ns)$	$\bar{\tau}(\mu s)$	σ_τ
value	0.002	0.0224	1.8153	0.0827

We may compare the Λ and λ in Table II with the same parameters for indoor UWB, which are 0.0667 and 2.1 respectively with unit $1/ns$ [17]. The parameters for through-wall channel is much smaller due to the resistance of wireless propagation in wall.

B. Statistical Distribution of Channel Amplitude

In the S-V model, the amplitude follows rayleigh distribution. In the IEEE UWB indoor channel model [4], log-normal distribution was introduced for representing the fluctuations of the total multipath gain. In this Section we propose that the amplitude of sensing-through-wall channel follows T location-scale distribution. Its probability density function (PDF) is

$$f(x) = \frac{\Gamma(\frac{\nu+1}{2})}{\phi\sqrt{\nu\pi}\cdot\Gamma(\frac{\nu}{2})}[\frac{\nu + (\frac{x-\delta}{\phi})^2}{\nu}]^{-(\frac{\nu+1}{2})}, \phi > 0, \nu > 0 \tag{6}$$

where δ is the location parameter, ϕ is scale parameter, ν is shape parameter and $\Gamma(\cdot)$ denotes gamma function. Note that if define $y \equiv \frac{x-\delta}{\phi}$, then y follows student's T distribution with ν degrees of freedom. As v goes to infinity, the T location-scale distribution approaches the standard Gaussian distribution.

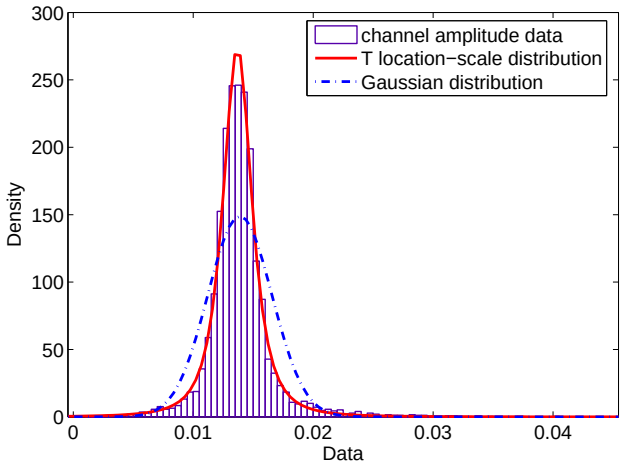

Fig. 6. Goodness-of-fit

Fig. 6 clearly illustrates to what extend does the CIR amplitude match the PDF curve of the statistic model. The absolute amplitude values of CIR have been plotted in terms of histogram. We compare T location-scale distribution with Gaussian distribution. Although the transmitted and received signal amplitude follows Gaussian model, this is not the case for the channel. It can be easily seen that T location-scale model provides perfect goodness-of-fit.

On a basis of CIR amplitudes from 37 different positions, we apply Maximum Likelihood Estimation (MLE) approach to estimate the parameters [18] [19]. It is generalized as follows:

Let $y_1, y_2, \cdots, y_N$ be N independent samples drawn from a random variable $\mathbf{Y}$ with m parameters $\theta_1, \theta_2, \cdots, \theta_m$, where $\theta_i \in \theta$, then the joint PDF of $y_1, y_2, \cdots, y_N$ is

$$L_N(\mathbf{Y}|\theta) = f_{Y|\theta}(y_1|\theta_1, \cdots, \theta_m) \ldots f_{Y|\theta}(y_n|\theta_1, \cdots, \theta_m) \tag{7}$$

When expressed as the conditional function of $\mathbf{Y}$ depends on the parameter θ, the likelihood function is

$$L_N(\mathbf{Y}|\theta) = \prod_{k=1}^{N} f_{Y|\theta}(y_k|\theta_1, \theta_2, \cdots, \theta_m) \tag{8}$$

The maximum likelihood estimate of $\theta_1, \theta_2, \cdots, \theta_m$ is the set of values $\hat{\theta}_1, \hat{\theta}_2, \cdots, \hat{\theta}_m$ that maximize the likelihood function $L_N(\mathbf{Y}|\theta)$.

As the logarithmic function is monotonically increasing, maximizing $L_N(\mathbf{Y}|\theta)$ is equivalent to maximizing $\ln(L_N(\mathbf{Y}|\theta))$. Hence, it can be shown that a necessary but not sufficient condition to obtain the ML estimate $\hat{\theta}$ is to solve the likelihood equation

$$\frac{\partial}{\partial\theta} \ln(L_N(\mathbf{Y}|\theta)) = 0 \tag{9}$$

We obtain $\hat{\delta}$, $\hat{\phi}$ and $\hat{\nu}$ for T location-scale distribution, $\hat{\mu}$ and $\hat{\sigma}$ for Gaussian distribution. These are shown in table III. We also explore the standard deviation (STD) error of each parameter. These descriptions are also shown in table III in the form of ε_x, where x denotes different parameter for each model. It can be seen that T location-scale provides smaller STD errors than those of Gaussian distribution.

TABLE III
STATISTICAL AMPLITUDE PARAMETERS FOR SENSE-THROUGH-WALL CHANNEL MODEL

PDF	T location-scale	Gaussian
Parameters	$\hat{\delta} = 0.0136836$ $\hat{\phi} = 0.00129967$ $\hat{\nu} = 2.18286$ $\varepsilon_\delta = 2.35418e^{-005}$ $\varepsilon_\phi = 2.50893e^{-005}$ $\varepsilon_\nu = 0.0821753$	$\hat{\mu} = -0.0138875$ $\hat{\sigma} = 0.00267908$ $\varepsilon_\mu = 3.78917e^{-005}$ $\varepsilon_\sigma = 2.67975e^{-005}$
RMSE	9.8983	25.5854

We may also observe the goodness-of-fit by root mean square error (RMSE). Let i (i=$1, 2, \cdots, n$) be the sample index of CIR amplitude in Fig. 6. c_i is the corresponding density value of CIR amplitude and $\hat{c}_i$ is the density value of the statistical model with estimated parameters by means of MLE. RMSE is obtained through

$$\mathsf{RMSE} = \sqrt{\frac{1}{n}\sum_{i=1}^{n}(c_i - \hat{c}_i)^2} \tag{10}$$

where n is the total amount of sample index. The RMSE for T location-scale and Gaussian distributions have been listed in Table III also. It demonstrates that T location-scale is the model that fits the channel amplitude data very well.

V. Conclusion

From our investigation, we would draw following conclusions: 1)UWB noise waveform may have a very good sensing-through-wall capability for walls composed of solid concrete blocks. 2)Sense-through-wall channels are made up of multipath components and the highest magnitude does not always appear at the first path. 3)The multipath contributions arrive at the receiver are grouped into clusters. The time of arrival of clusters can be modeled as a Poisson arrival process, while within each cluster, subsequent multipath contributions or rays also arrive according to a Poisson process. However, these arrival rates are much smaller than those of indoor UWB channels. 4) The amplitude of channel coefficient at each path can be more accurately characterized as T location-scale distribution other than Gaussian distribution due to better goodness-of-fit and smaller root-mean-square-error (RMSE).

Acknowledgement

This work was supported in part by Office of Naval Research (ONR) under Grant N00014-07-1-0395 and N00014-07-1-1024, and National Science Foundation (NSF) under Grant CNS-0721515 and CNS-0831902.

References

[1] D. Cassioli, M. Z. Win, and A. F. Molisch, "The ultra-wide bandwidth indoor channel: From statistical study to simulations", *IEEE J. Select. Areas Commun.*, vol. 20, pp. 1247-1257, Aug. 2002.

[2] S. S. Ghassemzadeh, R. Jana, C. W. Rice, W. Turin, and V. Tarokh, "Measurement and modeling of an ultra-wide bandwidth indoor channel", *IEEE Trans. Commun.*, vol. 52, pp. 1786-1796, Oct. 2004.

[3] B. M. Donlan, D. R. McKinstry and R. M. Buehrer, "The UWB Indoor Channel: Large and Small Scale Modeling", *IEEE Trans. on Wireless Commun.*, vol. 5, pp. 2863-2873, Oct. 2006.

[4] IEEE 802.15.SG3a, "Channel modeling sub-committee report final", *IEEE P802.15-02/490r1-SG3a*, Feb. 2003.

[5] A. A. Saleh and R. A. Valenzuela, "A statistical model for indoor multipath propagation", *IEEE Journal on Selected Areas in Communications*, vol. 5, no.2, pp. 128-137, Feb. 1987.

[6] Z. Yun and M. F. Iskander, "UWB Pulse Propagation through Complex Walls in Indoor Wireless Communications Environments", *International Conference on Wireless Networks, Communications and Mobile Computing, 2005*, vol.2, pp. 1358-1361, June 2005.

[7] N. Noori, A. Abolghasemi and M. Fardis, "Modeling of ultra wideband transmission through building walls", *International Conference on Microwave and Millimeter Wave Technology, 2008, ICMMT 2008*, vol.2, pp. 982-985.

[8] F. Ahmad and M.G.Amin, "Multi-location wideband synthetic aperture imaging for urban sensing applications", *Journal of the Franklin Institute*, 345 (6), pp.618-639, Sep 2008.

[9] R. M. Narayanan, "Through-wall radar imaging using UWB noise waveforms", *Journal of the Franklin Institute*, 345 (6), pp.659-678, Sep 2008.

[10] J. A. Henning, "Design and Performance of An Ultra-Wideband Foliage Penetrating Noise Radar", Masters Thesis, University of Nebraska, May 2001.

[11] J. A. Högbom, "Aperture Synthesis with a non-regular distribution of interferometer baselines", *Astronomy and Astrophysics Supplement Ser.*, vol. 15, pp. 417-426, 1974.

[12] R. J. -M. Cramer, R. A. Scholtz and M. Z. Win, "Evaluation of an ultra-wide-band propagation channel", *IEEE Transactions on Antennas and Propagation*, vol. 50, pp. 561-570, May 2002.

[13] P. C. Richardson, W. Xiang and W. Stark, "Modeling of ultra-wideband channels within vehicles", *IEEE Journal on selected areas in communications*, vol. 24, pp. 906-912, Apr. 2006.

[14] W. Yang and Z. Naitong, "A new multi-template CLEAN algorithm for UWB channel impulse response characterization", in *Proc. Int. Conf. Coommun. Technol.*, Nov. 2006, pp. 1-4.

[15] J. H. Reed, *An introduction to Ultra Wideband Communication Systems*, Prentice Hall, 2005.

[16] A. F. Molisch, "Ultrawideband propagtion channels: Theory, measurement and modeling", *IEEE Transactions on Vehicular Technology*, vol. 54, Sept. 2005, pp. 1528-1545.

[17] M. -G. Di Benedetto and G. Giancola, *Understanding ultra wideband Radio Fundamentals*, Prentice Hall, 2004.

[18] Devore, *Probability and Statistics for Engineering and the Sciences*, Monterey, CA: BrooksiCole, 1982.

[19] M. Barkat, *Signal deteciton and estimation*, 2nd, London: Artech house, 2005.

NEW: Network-Enabled Electronic Warfare for Target Recognition

QILIAN LIANG
University of Texas at Arlington

XIUZHEN CHENG
George Washington University

SHERWOOD W. SAMN
Air Force Research Laboratory

Network-enabled electronic warfare (NEW) is the development of modeling and simulation efforts that explore the advantages and limitations of NEW concepts. The advantages of linking multiple electronic support measures (ESM) and electronic attack (EA) assets to achieve improved capabilities across a networked battle force have yet to be quantified. In this paper, we utilize radar sensors as ESM and EA assets to demonstrate the advantages of NEW in collaborative automatic target recognition (CATR). Signal (waveform) design for radar sensor networks (RSN) in NEW is studied theoretically. The conditions for waveform coexistence and the interferences among waveforms in RSN are analyzed. We apply the NEW to CATR via waveform diversity combining and propose maximum-likelihood (ML)-ATR algorithms for nonfluctuating targets as well as fluctuating targets. Simulation results indicate that our NEW-CATR performs much better than the single sensor-based ATR algorithm for nonfluctuating and fluctuating targets.

Manuscript received November 9, 2007; revised August 13, November 3, 2008; released for publication November 14, 2008.

IEEE Log No. T-AES/46/2/936798.

Refereeing of this contribution was handled by J. Lee.

The research of Q. Liang was supported in part by the U.S. Office of Naval Research (ONR) under Grant N00014-07-1-0395, N00014-07-1-1024, N00014-03-1-0466, and the National Science Foundation (NSF) under Grant CNS-0721515, CNS-0831902 and CCF-0956438. The research of X. Cheng was supported in part by the NSF CAREER award CNS-0347674 and NSF under Grant CNS-0721699 and CNS-0831852.

Authors' addresses: Q. Liang, Dept. of Electrical Engineering, University of Texas at Arlington, Arlington, TX 76019-0016, E-mail: (liang@uta.edu); X. Cheng, Dept. of Computer Science, George Washington University, Washington, DC 20052; S. W. Samn, Air Force Research Laboratory/RHX, Brooks City Base, San Antonio, TX 78235.

I. INTRODUCTION AND MOTIVATION

In current and future military operational environments such as the Global War on Terrorism (GWOT) and Maritime Domain Awareness (MDA), war fighters require technology that can support their information needs in a manner that is independent of their location and consistent with their level of command or responsibility and operational situation. To support this need, the U.S. Department of Defense (DoD) has developed the concept of network centric warfare (NCW) defined as "*military operations that exploit state-of-the-art information and networking technology to integrate widely dispersed human decision makers, situational and targeting sensors, and forces and weapons into a highly adaptive, comprehensive system to achieve unprecedented mission effectiveness*" [1]. Network-enabled electronic warfare (NEW) is the form of electronic combat used in NCW. Focus is placed on a network of interconnected, adapting systems that are capable of making choices about how to survive and achieve their design goals in a dynamic environment. The goal of NEW is to develop modeling and simulation efforts that explore the advantages and limitations of NEW concepts. The advantages of linking multiple electronic support measures (ESM) and electronic attack (EA) assets to achieve improved capabilities across a networked battle force have yet to be quantified [2]. In this paper we utilize radar sensors as ESM and EA assets to demonstrate the advantages of NEW in collaborative automatic target recognition (CATR). The network of radar sensors should operate with multiple goals managed by an intelligent platform network that can manage the dynamics of each radar to meet the common goals of the platform rather than each radar operating as an independent system. Therefore, it is significant to perform signal design and processing and networking cooperatively within and between platforms of radar sensors and their communication modules. This need is also apparent in the recent solicitations from the U.S. Office of Naval Research [2, 3]. For example, in [3] it is stated, "Algorithms are sought for fused and/or coherent cross-platform RF sensing. The focus of this effort is to improve surveillance utilizing a network, not fusion of disparate sensor products. The algorithms should be capable of utilizing RF returns from multiple aspects in a time-coordinated sensor network."

In this paper, we study waveform design and diversity algorithms for radar sensor networks. Waveform diversity is the technology that allows one or more sensors onboard a platform to automatically change operating parameters, e.g., frequency, gain pattern, and pulse repetition frequency (PRF), to meet the varying environments. It has long been recognized that judicious use of properly designed waveforms, coupled with advanced receiver strategies,

is fundamental to fully utilizing the capacity of the electromagnetic spectrum. However, it is the relatively recent advances in hardware technology that are enabling a much wider range of design freedoms to be explored. As a result there are emerging and compelling changes in system requirements such as more efficient spectrum usage, higher sensitivities, greater information content, improved robustness to errors, reduced interference emissions, etc. The combination of these changes is fueling a worldwide interest in the subject of waveform design and the use of waveform diversity techniques.

Most existing works on waveform design and selection are focused on the single radar or sonar system. In 1974 Fitzgerald [8] demonstrated the inappropriateness of selection of waveforms based on measurement quality alone: the interaction between the measurement and the track can be indirect, but must be accounted for. Since then, extensive works on waveform design have been reported. Bell [6] used information theory to design radar waveforms for the measurement of extended radar targets exhibiting resonance phenomena. In [5], the singularity expansion method was used to design discriminant waveforms such as K-pulse, E-pulse, and S-pulse. Sowelam and Tewfik [23] developed a signal selection strategy for radar target classification, and a sequential classification procedure was proposed to minimize the average number of necessary signal transmissions. Intelligent waveform selection was studied in [4, 12], but the effect of Doppler shift was not considered. In [16], time-frequency–based generalized chirps were used as waveform for detection and estimation. In [15], the performance of constant frequency (CF) and linear frequency modulated (LFM) waveform fusion from the standpoint of the whole system was studied, but the effect of clutter was not considered. In [24], a new time-frequency signal decomposition algorithm based on the S-method was proposed and evaluated on the high-frequency surface-wave radar (HFSWR) data; it demonstrated that it provided an effective way for analyzing and detecting maneuvering air targets with significant velocity changes, including target signal separation from the heavy clutter. In [25], CF and LFM waveforms were studied for a sonar system, but it was assumed that the sensor was nonintelligent (i.e., the waveform cannot be selected adaptively). All the above studies and design methods focused on the waveform design or selection for a single active radar or sonar system. In [21], cross-correlation properties of two radars are briefly mentioned, and the binary coded pulses using simulated annealing [7] are highlighted. However, the cross-correlation of two binary sequences such as binary coded pulses (e.g., Barker sequence) is much easier to study than that of two analog radar waveforms.

In this paper, we focus on the waveform diversity and design for radar sensor networks using the CF pulse waveform. Compared with previous works, this paper has the following novelties.

1) Our focus is placed on a network of interconnected, adapting radar systems that are capable of making choices about how to survive and achieve their design goals in a dynamic environment.

2) We study waveform design and diversity for radar sensors networks. In space-time adaptive processing (STAP) [18], the waveform (pulse) design is essentially for a single radar system. The pulse is sent repeatedly at different times, and the echos are received and processed by an antenna array, and no interference exists among pulses if the pulse repetition interval is large enough.

3) We investigate CATR using radar sensor networks and compare it against the single-radar system in CATR.

4) Simulations are performed for nonfluctuating targets as well as fluctuating targets, and a real-world application example, sense-through-foliage target detection, is presented.

The rest of this paper is organized as follows: In Section II, we study the coexistence of radar waveforms. In Section III, we analyze the interferences among radar waveforms. In Section IV, we propose a RAKE structure for waveform diversity combining and present a maximum-likelihood (ML) algorithm for CATR. In Section V, we provide simulation results on ML-CATR. In Section VI, we conclude this paper and discuss future research.

II. COEXISTENCE OF RADAR WAVEFORMS

In radar sensor networks (RSN), radar sensors interfere with each other, and the signal-to-interference-ratio may be very low if the waveforms are not properly designed. In this paper, we introduce orthogonality as one criterion for waveform design in RSN to make radars coexist. In addition, since the radar channel is narrowband, we also consider the bandwidth constraint.

In our RSNs, we choose the CF pulse waveform, which can be defined as

$$x(t) = \sqrt{\frac{E}{T}} \exp(j2\pi\beta t), \qquad -T/2 \le t \le T/2 \quad (1)$$

where β is the RF carrier frequency in rad/s. In radar, ambiguity function (AF) is an analytical tool for waveform design and analysis, which succinctly characterizes the behavior of a waveform paired with its matched filter. The AF is useful for examining resolution, side lobe behavior, and ambiguities in both range and Doppler for a given waveform [18]. For a single radar, the matched filter for waveform $x(t)$ is

$x^*(-t)$ and the AF of CF pulse waveform is

$$A(\tau,F_D)=\left|\int_{-T/2+\tau}^{T/2}x(t)\exp(j2\pi F_D s)x^*(t-\tau)dt\right| =\left|\frac{E\sin[\pi F_D(T-|\tau|)]}{T\pi F_D}\right|,\qquad -T\le\tau\le T. \tag{2}$$

We can simplify this AF in the following three special cases:

1) When $\tau=0$,

$$A(0,F_D)=\left|\frac{E\sin(\pi F_D T)}{T\pi(F_D)}\right|. \tag{3}$$

2) When $F_D=0$,

$$A(\tau,0)=\left|\frac{E(T-|\tau|)}{T}\right|. \tag{4}$$

3) When $\tau=F_D=0$,

$$A(0,0)=E. \tag{5}$$

Note that the above ambiguity is for one radar only (no coexisting radar).

For RSNs the waveforms from different radars interfere with each other. We choose the waveform for radar i as

$$x_i(t)=\sqrt{\frac{E}{T}}\exp[j2\pi(\beta+\delta_i)t],\qquad -T/2\le t\le T/2 \tag{6}$$

which means that there is a frequency shift δ_i for radar i. To minimize the interference from one waveform to another, optimal values for δ_i should be determined to make the waveforms orthogonal to each other, i.e., let the cross-correlation between $x_i(t)$ and $x_n(t)$ be 0,

$$\int_{-T/2}^{T/2}x_i(t)x_n^*(t)dt =\frac{E}{T}\int_{-T/2}^{T/2}\exp[j2\pi(\beta+\delta_i)t]\exp[-j2\pi(\beta+\delta_n)t]dt \tag{7}$$

$$=E\,\mathrm{sinc}[\pi(\delta_i-\delta_n)T]. \tag{8}$$

If we choose

$$\delta_i=\frac{i}{T} \tag{9}$$

where i is a dummy index, (8) can be written as

$$\int_{-T/2}^{T/2}x_i(t)x_n^*(t)dt=\begin{cases}E & i=n\\ 0 & i\ne n\end{cases}. \tag{10}$$

Therefore choosing $\delta_i=i/T$ in (6) yields orthogonal waveforms, i.e., the waveforms can coexist if the carrier spacing is a multiple of $1/T$ between two radar waveforms. In other words, orthogonality amongst carriers can be achieved by separating the carriers by a multiple of the inverse of waveform pulse duration. With this design, all the orthogonal waveforms can work simultaneously. However, there may exist time-delay and Doppler-shift ambiguity which may interfere with other waveforms in RSN.

III. INTERFERENCES OF WAVEFORMS IN RADAR SENSOR NETWORKS

A. RSN with Two Radar Sensors

We are interested in analyzing the interference from one radar to another if a time delay and Doppler shift are present. For a simple case where there are two radar sensors (i and n), the AF of radar i (considering the interference from radar n) is

$$A_i(t_i,t_n,F_{D_i},F_{D_n}) =\left|\int_{-\infty}^{\infty}[x_i(t)\exp(j2\pi F_{D_i}t)+x_n(t-t_n)\times\exp(j2\pi F_{D_n}t)]x_i^*(t-t_i)dt\right| \tag{11}$$

$$\le\left|\int_{-T/2+\max(t_i,t_n)}^{T/2+\min(t_i,t_n)}x_n(t-t_n)\exp(j2\pi F_{D_n}t)x_i^*(t-t_i)dt\right| +\left|\int_{-T/2+t_i}^{T/2}x_i(t)\exp(j2\pi F_{D_i}t)x_i^*(t-t_i)dt\right| \tag{12}$$

$$=\left|\int_{-T/2+\max(t_i,t_n)}^{T/2+\min(t_i,t_n)}x_n(t-t_n)\exp(j2\pi F_{D_n}t)x_i^*(t-t_i)dt\right| +\left|\frac{E\sin[\pi F_{D_i}(T-|t_i|)]}{T\pi F_{D_i}}\right|. \tag{13}$$

To make the analysis easier, it is generally assumed that the radar sensor platform has access to the Global Positioning System (GPS) and the inertial navigation unit (INU) timing and navigation data [3]. In this paper, we assume that the radar sensors are synchronized and that $t_i=t_n=\tau$. Then (13) can be simplified as

$$A_i(\tau,F_{D_i},F_{D_n})\approx|E\,\mathrm{sinc}[\pi(n-i+F_{D_n}T)]| +\left|\frac{E\sin[\pi F_{D_i}(T-|\tau|)]}{T\pi F_{D_i}}\right|. \tag{14}$$

We have the following three special cases:

1) If $F_{D_i}=F_{D_n}=0$, and δ_i and δ_n follow (9), (14) becomes

$$A_i(\tau,0,0)\approx\left|\frac{E(T-|\tau|)]}{T}\right|. \tag{15}$$

2) If $\tau=0$, (14) becomes

$$A_i(0,F_{D_i},F_{D_n})\approx|E\,\mathrm{sinc}[\pi(n-i+F_{D_n}T)]| +\left|\frac{E\sin(\pi F_{D_i}T)}{T\pi F_{D_i}}\right|. \tag{16}$$

3) If $F_{D_i} = F_{D_n} = 0$, $\tau = 0$, and δ_i and δ_n follow (9), (14) becomes

$$A_i(0,0,0) \approx E. \tag{17}$$

B. RSN with M Radar Sensors

Our analysis on an RSN with two radar sensors can be extended to the case of M radars. Assuming that the time delay τ for each radar is the same, then the AF of radar 1 (considering interferences from all the other $M-1$ radars with CF pulse waveforms) can be expressed as

$$A_1(\tau,F_{D_1},\ldots,F_{D_M}) \approx \sum_{i=2}^{M} |E\,\mathrm{sinc}[\pi(i-1+F_{D_i}T)]| + \left|\frac{E\sin[\pi F_{D_1}(T-|\tau|)]}{T\pi F_{D_1}}\right|. \tag{18}$$

Similarly, we have the following three special cases:

1) $F_{D_1} = F_{D_2} = \cdots = F_{D_M} = 0$ and the frequency shift δ_i in (6) for each radar follows (9); then (18) becomes

$$A_1(\tau,0,0,\ldots,0) \approx \left|\frac{E(T-|\tau|)]}{T}\right|. \tag{19}$$

Comparing it against (4), we notice that a radar may exist that can get the same signal strength as that of the single radar in a single radar system (no coexisting radar) when the Doppler shift is 0.

2) If $\tau = 0$, then (18) becomes

$$A_1(0,F_{D_1},F_{D_2},\ldots,F_{D_M}) \approx \sum_{i=2}^{M} |E\,\mathrm{sinc}[\pi(i-1+F_{D_i}T)]| + \left|\frac{E\sin(\pi F_{D_1}T)}{T\pi F_{D_1}}\right|. \tag{20}$$

Compared with (3), a radar in RSN has higher interferences when unknown Doppler shifts exist.

3) $F_{D_1} = F_{D_2} = \cdots = F_{D_M} = 0$, $\tau = 0$ and δ_i in (6) follows (9); then (18) becomes

$$A_1(0,0,0,\ldots,0) \approx E. \tag{21}$$

IV. NEW FOR COLLABORATIVE AUTOMATIC TARGET RECOGNITION

In NEW, the radar sensors are networked together in an ad hoc fashion. They do not rely on a preexisting fixed infrastructure, such as a wireless backbone network or a base station. They are self-organizing entities that are deployed on demand in support of various events, surveillance, battlefield, disaster relief, search and rescue, etc. Scalability concern suggests a hierarchical organization of radar sensor networks with the lowest level in the hierarchy being a cluster. As argued in [9, 10, 13, 17], in addition to helping with scalability and robustness, aggregating sensor nodes into clusters has additional benefits:

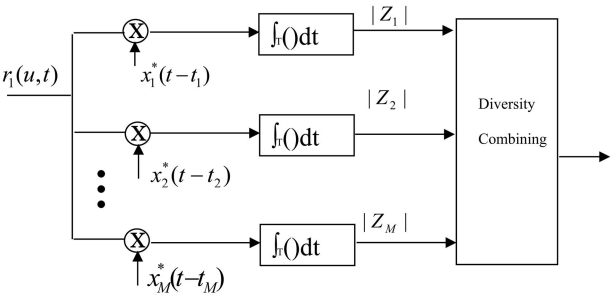

Fig. 1. Waveform diversity combining by clusterhead in RSN.

1) conserving radio resources such as bandwidth,
2) promoting spatial code reuse and frequency reuse,
3) simplifying the topology, e.g., when a mobile radar changes its location, it is sufficient for the nodes in the attended clusters to update their topology information,
4) reducing the generation and propagation of routing information, and
5) concealing the details of global network topology from individual nodes.

In RSN, each radar can provide its waveform parameters such as δ_i to its clusterhead radar, and the clusterhead radar can combine the waveforms from its cluster members.

In RSN with M radars, the received signal for clusterhead (assume it's radar 1) is

$$r_1(u,t) = \sum_{i=1}^{M} \alpha(u)x_i(t-t_i)\exp(j2\pi F_{D_i}t) + n(u,t) \tag{22}$$

where $\alpha(u)$ stands for radar cross section (RCS), which can be modeled using non-zero constants for nonfluctuating targets and four Swerling target models for fluctuating targets [18]; F_{D_i} is the Doppler shift of the target relative to waveform i; t_i is the delay of waveform i; and $n(u,t)$ is the additive white Gaussian noise (AWGN). In this paper, we propose a RAKE structure for waveform diversity combining, as illustrated by Fig. 1. The RAKE structure is so named because it reminds one of a garden rake, each branch collecting echo energy in a way similar to how tines on a rake collect leaves. This figure summarizes how the clusterhead works. The received signal $r_1(u,t)$ consists of echoes triggered by the waveforms from each radar sensor, $x_i^*(t-t_i)$ is used to retrieve the amplified waveform from radar i (amplified by the target RCS) based on the orthogonal property presented in Sections II and III, and then this information is time-averaged for diversity combining.

According to this structure, the received $r_1(u,t)$ is processed by a bank of matched filters, then the output of branch 1 (after integration) is

$$Z_1(u;t_1,\ldots,t_M,F_{D_1},\ldots,F_{D_M}) = \int_{-T/2}^{T/2} r_1(u,t)x_1^*(t-t_1)ds \tag{23}$$

$$= \int_{-T/2}^{T/2}\left[\sum_{i=1}^{M}\alpha_i(u)x_i(t-t_i)\exp(j2\pi F_{D_i}t)+n(u,t)\right] \times x_1^*(t-t_1)dt. \tag{24}$$

Assuming $t_1 = t_2 = \cdots = t_M = \tau$, then based on (18),

$$Z_1(u;\tau,F_{D_1},\ldots,F_{D_M}) \approx \sum_{i=2}^{M}\alpha(u)E\,\mathrm{sinc}[\pi(i-1+F_{D_i}T)] + \frac{\alpha(u)E\sin[\pi F_{D_1}(T-|\tau|)]}{T\pi F_{D_1}} + n(u,\tau). \tag{25}$$

Similarly, we can get the output for any branch m ($m = 1,2,\ldots,M$);

$$Z_m(u;\tau,F_{D_1},\ldots,F_{D_M}) \approx \sum_{i=1,i\neq m}^{M}\alpha(u)E\,\mathrm{sinc}[\pi(i-m+F_{D_i}T)] + \frac{\alpha(u)E\sin[\pi F_{D_m}(T-|\tau|)]}{T\pi F_{D_m}} + n(u,\tau). \tag{26}$$

Therefore $Z_m(u;\tau,F_{D_1},\ldots,F_{D_M})$ consists of three parts, namely, signal (reflected signal from radar m waveform) $\alpha(u)E\sin[\pi F_{D_m}(T-|\tau|)]/T\pi F_{D_m}$, interferences from other waveforms $\sum_{i=1,i\neq m}^{M}\alpha(u)\cdot E\ \mathrm{sinc}[\pi(i-m+F_{D_i}T)]$, and noise $n(u,\tau)$.

We can also have the following three special cases for $|Z_m(u;\tau,F_{D_1},\ldots,F_{D_M})|$:

1) When $F_{D_1} = \cdots = F_{D_M} = 0$,

$$Z_m(u;\tau,0,0,\ldots,0) \approx \frac{E\alpha(u)(T-|\tau|)]}{T} + n(u,\tau) \tag{27}$$

which means that if there is no Doppler mismatch, there is no interference from other waveforms.

2) If $\tau = 0$, (26) becomes

$$Z_m(u;0,F_{D_1},\ldots,F_{D_M}) \approx \sum_{i=1,i\neq m}^{M}\alpha(u)E\,\mathrm{sinc}[\pi(i-m+F_{D_i}T)] + \frac{\alpha(u)E\sin[\pi F_{D_m}T]}{T\pi F_{D_m}} + n(u). \tag{28}$$

3) If $\tau = 0$, and $F_{D_1} = \cdots = F_{D_M} = 0$, (26) becomes

$$Z_m(u;0,0,0,\ldots,0) \approx E\alpha(u) + n(u). \tag{29}$$

Doppler mismatch happens quite often in a target search where the target velocity is not yet known. However, in target recognition, generally high-resolution measurements of targets in range ($\tau = 0$) and Doppler are available; therefore, (29) will be used for CATR.

The process of combining all the Z_ms ($m = 1,2,\ldots,M$) is very similar to the diversity combining in wireless communications that combats channel fading, and the combination schemes may be different for different applications. In this paper, we are interested in applying the RSN waveform diversity to CATR, e.g., recognizing that the echo on a radar display is that of an aircraft, ship, motor vehicle, bird, person, rain, chaff, clear-air turbulence, land clutter, sea clutter, bare mountains, forested areas, meteors, aurora, ionized media, or other natural phenomena via collaborations among different radars. Early radars were "blob" detectors in that they detected the presence of a target and gave its location in range and angle; then, radar began to be more than a blob detector and could provide recognition of one type of target from another [21]. It is known that small changes in the aspect angle of complex (multiple scatter) targets can cause major changes in the RCS. This has been considered in the past as a means of target recognition, and is called RCS, but it has not had much success [21]. In [19], a parametric filtering approach was proposed for target detection using airborne radar. In [14], knowledge-based sensor networks were applied to threat assessment. In this paper, we propose ML-CATR algorithms for nonfluctuating targets as well as fluctuating targets.

A. ML-CATR for Nonfluctuating Targets

In some sources, the nonfluctuating target is identified as a "Swerling 0" or "Swerling 5" model [22]. For nonfluctuating targets, the RCS $\alpha_m(u)$ is just a constant α for a given target. In (29), $n(u,\tau)$ is a zero-mean Gaussian random variable for a given τ, so $|Z_m(u;0,0,\ldots,0)|$ follows a Rician distribution because signal $E\alpha(u)$ is a positive constant, $E\alpha$, for a nonfluctuating target. Let $y_m \triangleq |Z_m(u;0,0,\ldots,0)|$; then the probability density function (pdf) of y_m is

$$f(y_m) = \frac{2y_m}{\sigma^2}\exp\left[-\frac{(y_m^2+\lambda^2)}{\sigma^2}\right]I_0\left(\frac{2\lambda y_m}{\sigma^2}\right) \tag{30}$$

where

$$\lambda = E\alpha \tag{31}$$

σ^2 is the noise power (with I and Q subchannel power $\sigma^2/2$), and $I_0(\cdot)$ is the zero-order modified Bessel function of the first kind. Let $\mathbf{y} \triangleq [y_1,y_2,\ldots,y_M]$; then the pdf of $\mathbf{y}$ is

$$f(\mathbf{y}) = \prod_{m=1}^{M} f(y_m). \tag{32}$$

Our CATR is a multiple-category hypothesis testing problem, i.e., it decides a target category (e.g., aircraft, ship, motor vehicle, bird, etc.) based on $r_1(u,t)$. Assume there are a total of N categories, and a category n target has RCS α_n; therefore the ML-CATR algorithm to decide a target category C can be expressed as

$$C = \arg\max_{n=1}^{N} f(\mathbf{y} \mid \lambda = E\alpha_n) \tag{33}$$

$$= \arg\max_{n=1}^{N} \prod_{m=1}^{M} \frac{2y_m}{\sigma^2} \exp\left[-\frac{(y_m^2 + E^2\alpha_n^2)}{\sigma^2}\right] I_0\left(\frac{2E\alpha_n y_m}{\sigma^2}\right). \tag{34}$$

B. ML-CATR for Fluctuating Targets

Fluctuating target modeling is more realistic when the target RCS is drawn from either the Rayleigh or chi-square of a deg four pdf. The Rayleigh model describes the behavior of a complex target consisting of many scatters, none of which is dominant. The fourth-degree chi-square model targets have many scatters of similar strength with one dominant scatter. Based on different combinations of pdf and decorrelation characteristics (scan-to-scan or pulse-to-pulse decorrelation), four Swerling models are used [18]. In this paper we focus on the "Swerling 2" model, which is a Rayleigh distribution with pulse-to-pulse decorrelation. The pulse-to-pulse decorrelation implies that each individual pulse results in an independent value for RCS α.

For the Swerling 2 model, the RCS $|\alpha(u)|$ follows a Rayleigh distribution, and its I and Q subchannels follow zero-mean Gaussian distributions with a variance γ^2. Assume

$$\alpha(u) = \alpha_I(u) + j\alpha_Q(u) \tag{35}$$

and $n(u) = n_I(u) + jn_Q(u)$ follows a zero-mean complex Gaussian distribution with a variance σ^2 for the I and Q subchannels. Therefore, according to (29), $Z_m(u;0,0,0,\ldots,0)$ is a zero-mean Gaussian random variable with a variance $E^2\gamma^2 + \sigma^2$ for the I and Q subchannels, which means $y_m \triangleq |Z_m(u;0,0,\ldots,0)|$ follows a Rayleigh distribution with a parameter $\sqrt{E^2\gamma^2 + \sigma^2}$:

$$f(y_m) = \frac{y_m}{E^2\gamma^2 + \sigma^2} \exp\left(-\frac{y_m^2}{E^2\gamma^2 + \sigma^2}\right). \tag{36}$$

The mean value of y_m is $\sqrt{\pi(E^2\gamma^2 + \sigma^2)/2}$, and the variance is $(4-\pi)(E^2\gamma^2 + \sigma^2)/2$. The variance of signal is $(4-\pi)E^2\gamma^2/2$, and the variance of noise is $(4-\pi)\sigma^2/2$.

Let $\mathbf{y} \triangleq [y_1, y_2, \ldots, y_M]$; then the pdf of $\mathbf{y}$ is

$$f(\mathbf{y}) = \prod_{m=1}^{M} f(y_m). \tag{37}$$

Assume there are a total of N categories, and a category n target has a RCS $\alpha_n(u)$ (with a variance γ_n^2), so the ML-ATR algorithm to decide a target category C can be expressed as

$$C = \arg\max_{n=1}^{N} f(\mathbf{y} \mid \gamma = \gamma_n) \tag{38}$$

$$= \arg\max_{n=1}^{N} \prod_{m=1}^{M} \frac{y_m}{E^2\gamma_n^2 + \sigma^2} \exp\left(-\frac{y_m^2}{E^2\gamma_n^2 + \sigma^2}\right). \tag{39}$$

V. SIMULATIONS AND REAL-WORLD APPLICATION EXAMPLE

A. Computer Simulations

RSNs will be required to detect a broad range of target classes. Too often, the characteristics of objects that are not of interest (e.g., bird) are similar to those of threat objects (e.g., missile). Therefore, new techniques to distinguish threats from undesired detections (e.g., birds, etc.) are needed. We applied our ML-CATR to this important application to recognize a target from many target classes. We assume that the domain of target classes is known a priori (N in Sections IVA and IVB), and that the RSN is confined to work only on the known domain.

For nonfluctuating target recognition, our targets have 5 classes with different RCS values, which are summarized in Table I [21]. We applied the ML-CATR algorithms in Section IVA (for the nonfluctuating target case) to classify an unknown target as one of these 5 target classes. At each average signal-to-noise ratio (SNR) value, we ran Monte-Carlo simulations for 10^5 times for each target. The average SNR value is based on the average power from all targets (signal variance), so the actual SNRs for bird and missile are much lower than the average SNR value, for example, at the average SNR = 16 dB, the bird target SNR = −33.1646 dB, and the missile target SNR = 0.8149 dB; and at average SNR = 20 dB, the bird target SNR = −29.1646 dB, and the missile target SNR = 4.8149 dB. In Figs. 2(a), 2(b), we plotted the probability of the automatic target recognition (ATR) error in bird and missile recognition when they are assumed to be nonfluctuating targets. These figures indicate that a single radar system can't perform well in both recognitions, because the probability of the ATR error is above 10%, which cannot be used for real-world ATR. However, the 5-radar RSN and 10-radar RSN can maintain very low ATR errors. In Fig. 2(c), we plotted the average probability of the ATR error for all 5 targets. Since the other 3 targets (different aircrafts) have much higher SNRs, their ATR error is lower, which makes the average probability of ATR error lower.

TABLE I
RCS Values at Microwave Frequency for 5 Targets

Index n	Target	RCS
1	Bird	0.01
2	Conventional unmanned winged missile	0.5
3	Small single-engine aircraft	1
4	Small fighter aircraft or 4 passenger jet	2
5	Large fighter aircraft	6

For fluctuating target recognition, we assume the fluctuating targets follow the Swerling 2 model (Rayleigh distribution with pulse-to-pulse decorrelation), and assume the RCS value listed in Table I to be the standard deviation (std) γ_n of RCS $\alpha_n(u)$ for target n. We applied the ML-CATR algorithm in Section IVB (for the fluctuating target case) for target recognition within the 5-targets domain. Similarly we ran Monte-Carlo simulations at each SNR value. In Figs. 3(a), 3(b), 3(c), we plotted the ATR performance for fluctuating targets and compared the performances of a single-radar system, a 5-radar RSN, and a 10-radar RSN. Observe that the two RSNs perform much better than the single-radar system. The ATR error for the missile is higher than that for the bird because the Rayleigh distribution of the missile has a lot of overlap with its neighbor targets (aircrafts). Comparing Figs. 2(a), 2(b), 2(c) to Figs. 3(a), 3(b), 3(c), it is clear that higher SNRs are needed for the fluctuating target recognition as compared with the nonfluctuating target recognition. According to Skolnik [21], the radar performance with a probability of recognition error (p_e) less than 10% is good enough. Our RSN with waveform-diversity can achieve a probability of ATR error much less than 10% for each target ATR as well as the average ATR for all targets. However, the single-radar system has a probability of ATR error much higher than 10%. Fig. 3(c) also tells us that it is impossible for the average probability of ATR error of a single-radar system to be less than 10%, even at an extremely high SNR. Our RSN with waveform diversity is very promising for real-world ATR.

B. Real-World Application Example

We verified our approach based on a real-world application example, sense-through-foliage target detection from the U.S. Air Force Research Laboratory. The target is a trihedral reflector (as shown in Fig. 4) in a forest. We plot two collections using ultra wideband (UWB) radars in Figs. 5(a) and 5(b). Fig. 5(a) has no target in range, and Fig. 5(b) has a target at samples around 13,900. We plot the echo differences between Figs. 5(a) and 5(b) in Fig. 5(c). However, it is impossible to identify whether there is any target or where that target is, based on Fig. 5(c), which means single radar doesn't work even in the ideal case. Since significant pulse-to-pulse variability exists in the echoes, this motivates us to explore the spatial and time diversity using the radar sensor networks approach. The echoes, i.e., RF responses by the pulse of each cluster-member

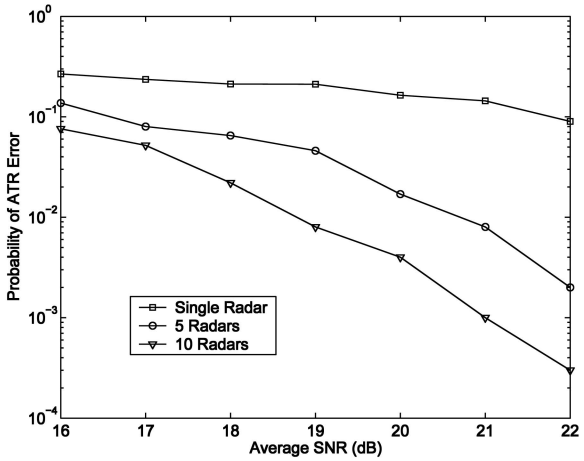

(a)

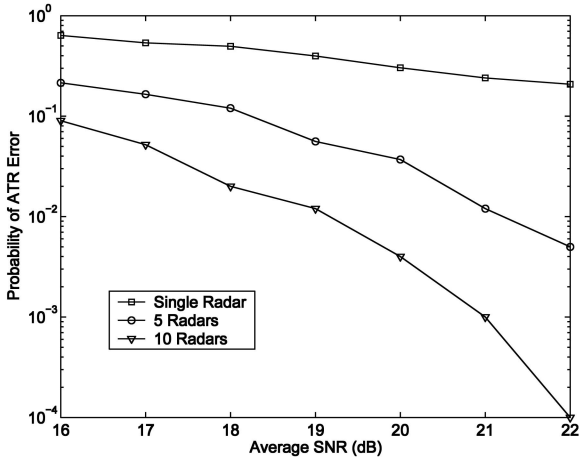

(b)

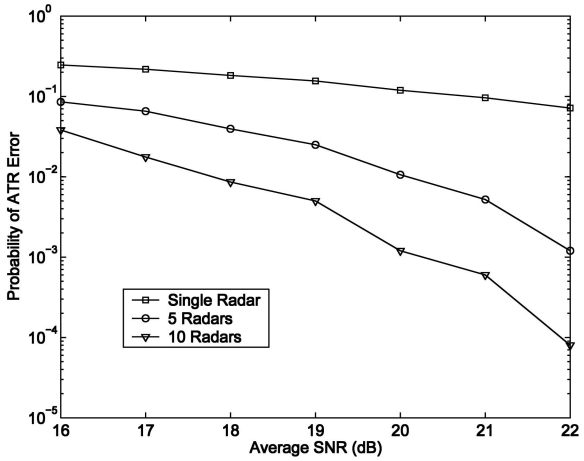

(c)

Fig. 2. Probability of ATR error for nonfluctuating targets at different average SNR (dB) values. (a) Bird. (b) Missile. (c) Average probability of ATR error for 5 targets.

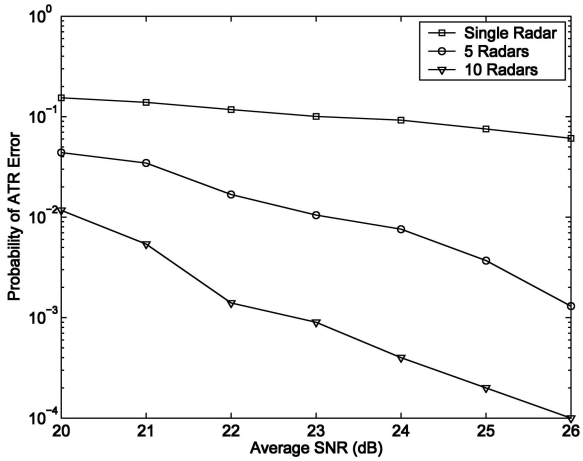

(a)

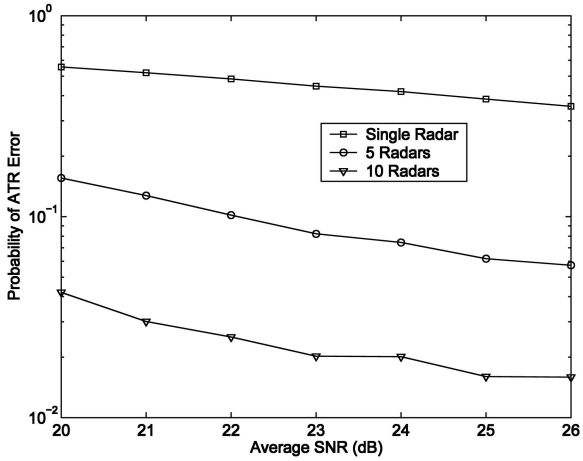

(b)

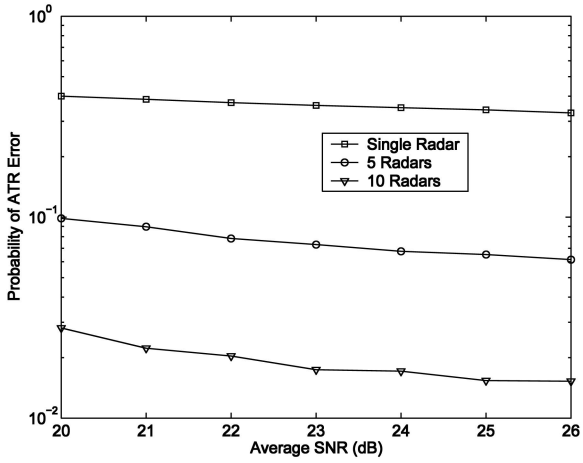

(c)

Fig. 3. Probability of ATR error for fluctuating targets at different average SNR (dB) values. (a) Bird. (b) Missile. (c) Average probability of ATR error for 5 targets.

radar, are combined by the clusterhead using the RAKE structure in Fig. 1.

We ran simulations for an RSN with 30 radar sensors, and plotted the power of ac values in Figs. 6(a) and 6(b) for the two cases (with target and without target, respectively). Observe that in Fig. 6(b), the power of ac values (around sample 13,900) where the target is located is nonfluctuating (monotonically increasing, then decreasing). Although some other samples also have very high ac power values, it is very clear that they are fluctuating, and the power of ac values behaves like random noise because, generally, the clutter has Gaussian distribution in the frequency domain.

Fig. 4. Target (a trihedral reflector) shown on stand at 300 ft from measurement lift.

VI. CONCLUSIONS AND FUTURE WORKS

We have studied the CF pulse waveform design and diversity in RSNs. We showed that the waveforms can coexist if the carrier frequency spacing is a multiple of $1/T$ between two radar waveforms. We made analysis on interferences among waveforms in RSN and proposed a RAKE structure for waveform diversity combining in RSN. As an application example, we applied the waveform design and diversity to CATR in RSN and proposed ML-CATR algorithms for nonfluctuating targets as well as fluctuating targets. Simulation results show that an RSN using our waveform diversity-based ML-ATR algorithms performs much better than a single-radar system for nonfluctuating targets and fluctuating targets recognition. We also validated our RSN approach via a real-world sense-through-foliage target detection example.

In our future research, we will investigate the CATR when multiple targets coexist in RSN and when the number of targets are time varying. In this paper, we used spatial diversity combining. For multitarget ATR, we will further investigate spatial-temporal-frequency combining for waveform diversity in RSN.

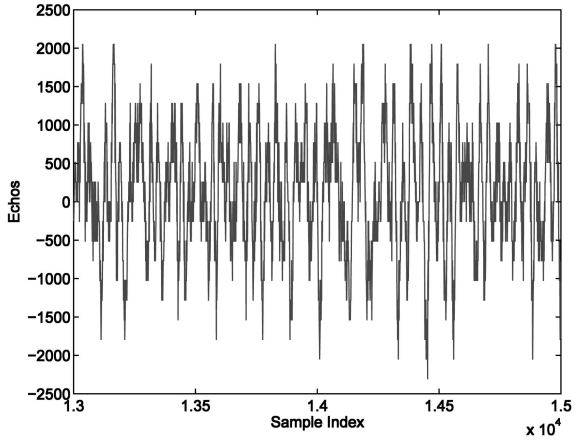

(a)

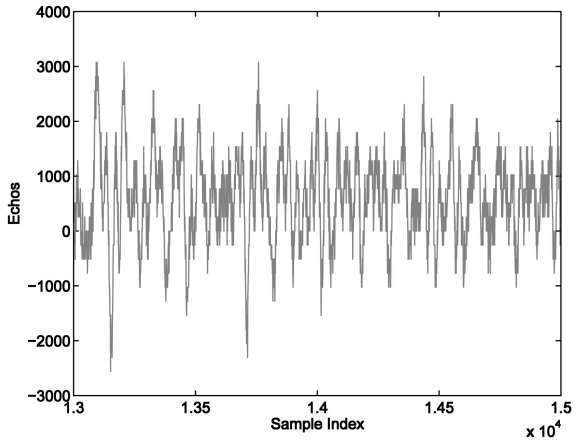

(b)

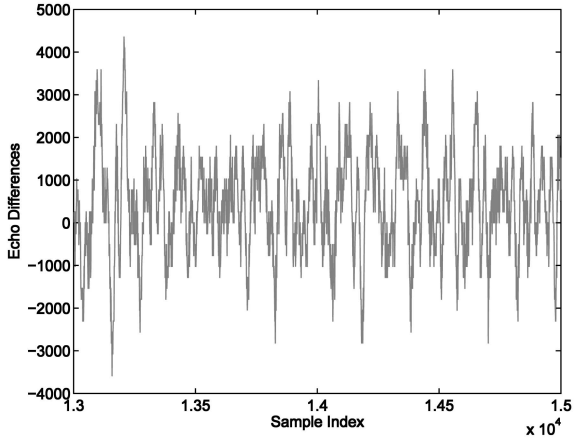

(c)

Fig. 5. Measurement of UWB radar. (a) Expanded view of traces (no target) from sample 13,001 to 15,000. (b) Expanded view of traces (with target) from sample 13,001 to 15,000. (c) Differences between (a) and (b).

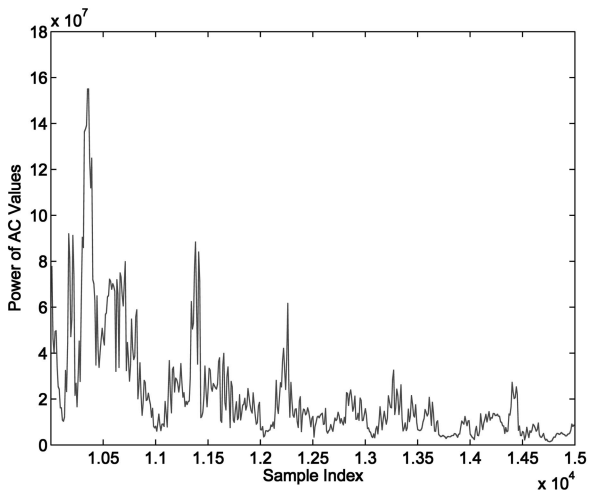

(a)

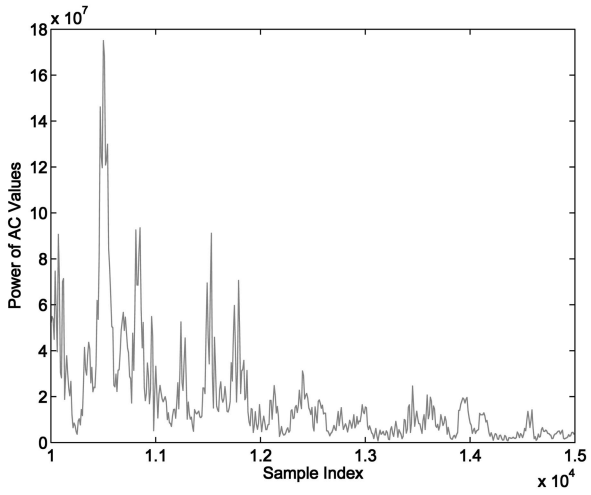

(b)

Fig. 6. Power of ac values based on RSNs approach. (a) No target. (b) With target in field (in samples around 13,900).

REFERENCES

[1] ONR BAA 06-016
Command and Control and Combat Systems (C2 and CS).
Online: available http://www.onr.navy.mil/02/baa/expired.asp.

[2] ONR BAA 07-009
Electronic Warfare Discovery and Invention (D&I).
Online: available http://www.onr.navy.mil/02/baa/.

[3] ONR BAA 07-017
NET-SENTRIC Surveillance.
Online: available http://www.onr.navy.mil/02/baa/.

[4] Baggenstoss, P.
Adaptive pulse length correction (APLECORR): A strategy for waveform optimization in ultrawideband active sonar.
IEEE Transactions on Oceanic Engineering, **23**, 1 (1998), 1–11.

[5] Baum, C. E., et al.
The singularity expansion method and its application to target identification.
Proceedings of the IEEE, **79**, 10 (Oct. 1991).

[6] Bell, M. R.
Information theory and radar waveform design.
IEEE Transactions on Information Theory, **39**, 5 (Sept. 1993), 1578–1597.

[7] Deng, H.
Synthesis of binary sequences with good correlation and cross-correlation properties by simulated annealing.
IEEE Transactions on Aerospace and Electronic Systems, **32**, 1 (Jan. 1996).

[8] Fitzgerald, R.
Effects of range-Doppler coupling on chirp radar tracking accuracy.
IEEE Transactions on Aerospace and Electronic Systems, **10** (July 1974), 528–532.

[9] Hou, T-C., and Tsai, T-J.
An access-based clustering protocol for multihop wireless ad hoc networks.
IEEE Journal of Selected Areas in Communications, **19**, 7 (July 2001), 1201–1210.

[10] Iwata, A., Chiang, C. C., Pei, G., Gerla, M., and Chen, T. W.
Scalable routing strategies for ad hoc networks.
IEEE Journal of Selected Areas in Communications, **17** (1999), 1369–1379.

[11] Johnson, R. A., and Titlebaum, E. L.
Range Doppler uncoupling in the Doppler tolerant bat signal.
In *Proceedings of IEEE Ultrasonics Symposium*, New York, 1972, 64–67.

[12] Kershaw, D., and Evans, R.
Optimal waveform selection for tracking system.
IEEE Transactions on Information Theory, **40**, 5 (1994), 1536–1550.

[13] Lin, C. R., and Gerla, M.
Adaptive clustering in mobile wireless networks.
IEEE Journal of Selected Areas in Communications, **16** (1997), 1265–1275.

[14] Liang, Q., and Cheng, X.
KUPS: Knowledge-based ubiquitous and persistent sensor networks for threat assessment.
IEEE Transactions on Aerospace and Electronic Systems, **44**, 3 (July 2008).

[15] Niu, R., Willett, P., and Bar-Shalom, Y.
Tracking consideration in selection of radar waveform for range and range-rate measurements.
IEEE Transactions on Aerospace and Electronic Systems, **38**, 2 (2002).

[16] Papandreou, A., Boudreaux-Bartels, G. F., and Kay, S. M.
Detection and estimation of generalized chirps using time-frequency representation.
In *Twenty-Eighth Asilomar Conference on Signals, Systems and Computers*, vol. 1, Oct. 1994, 50–54.

[17] Perkins, C. E.
Cluster-Based Networks.
In C. E. Perkins (Ed.), *Ad Hoc Networking*, Boston: Addison-Wesley, 2001, ch. 4, 75–138.

[18] Richards, M. A.
Fundamentals of Radar Signal Processing.
New York: McGraw-Hill, 2005.

[19] Roman, J., Rangaswamy, M., Davis, D., Zhang, Q., Himed, B., and Michels, J.
Parametric adaptive matched filter for airborne radar applications.
IEEE Transactions on Aerospace and Electronic Systems, **36**, 2 (2000), 677–692.

[20] Sarkar, T. K., and Sangruji, N.
An adaptive nulling system for a narrow-band signal with a look-direction constraint utilizing the conjugate gradient method.
IEEE Transactions on Antennas and Propagation, **37**, 7 (July 1989), 940–944.

[21] Skolnik, M. I.
Introduction to Radar Systems (3rd ed.).
New York: McGraw-Hill, 2001.

[22] Swerling, P.
Probability of detection for fluctuating targets.
IRE Transactions on Information Theory, **6** (Apr. 1960), 269–308.

[23] Sowelam, S., and Tewfik, A.
Waveform selection in radar target classification.
IEEE Transactions on Information Theory, **46**, 3 (2000), 1014–1029.

[24] Stankovic, L., Thayaparan, T., and Dakovic, M.
Signal decomposition by using the S-method with application to the analysis of HF radar signals in sea-clutter.
IEEE Transactions on Signal Processing, **54**, 11 (Nov. 2006), 4332–4342.

[25] Sun, Y., Willett, P., and Lynch, R.
Waveform fusion in sonar signal processing.
IEEE Transactions on Aerospace and Electronic Systems, **40**, 2 (2004).

Qilian Liang is an associate professor in the Department of Electrical Engineering, University of Texas at Arlington. He received the B.S. degree from Wuhan University in 1993, M.S. degree from Beijing University of Posts and Telecommunications in 1996, and Ph.D. from University of Southern California (USC) in May 2000, all in electrical engineering.

Prior to joining the faculty of the University of Texas at Arlington in August 2002, he was a member of the technical staff in Hughes Network Systems, Inc. in San Diego, CA. His research interests include radar sensor networks, wireless sensor networks, wireless communications, communication system and communication theory, signal processing for communications, fuzzy logic systems and applications, collaborative and distributed signal processing, etc.

Dr. Liang has published more than 160 journal and conference papers, 7 book chapters, and has 6 U.S. patents pending. He received the 2002 IEEE Transactions on Fuzzy Systems Outstanding Paper Award, 2003 U.S. Office of Naval Research (ONR) Young Investigator Award, 2005 UTA College of Engineering Outstanding Young Faculty Award, and 2007 U.S. Air Force Summer Faculty Fellowship Program Award.

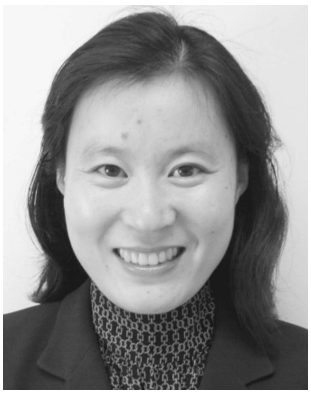

Xiuzhen (Susan) Cheng is an associate professor in the Department of Computer Science, The George Washington University. She received her M.S. degree and Ph.D. in computer science from the University of Minnesota, Twin Cities in 2000 and 2002, respectively.

Her current research interests include wireless and mobile computing, sensor networking, wireless and mobile security, and algorithm design and analysis.

Dr. Cheng has served on the editorial boards of several technical journals and in the technical program committees of various professional conferences/workshops. She is a program cochair or vice cochair for several conferences such as WASA'06, ICPP'09, and MASS'09. Dr. Cheng worked as a program director in the National Science Foundation (NSF) for 6 months in 2006 and joined NSF again as a part-time program director in April 2008. She received the NSF CAREER Award in 2004.

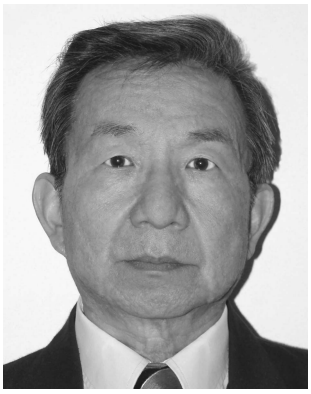

Sherwood W. Samn was born in Los Angeles, CA, in 1941. He received his B.A. degree in physics and mathematics and Ph.D. in applied mathematics from the University of California, Berkeley, in 1963 and 1968, respectively.

From 1968 to 1974 he taught at the Indiana University–Purdue University at Indianapolis. Since then he has joined the Mathematics Group at the Air Force Research Laboratory at Brooks City-Base in San Antonio, TX. He has published in functional analysis, optimal control, statistics, operations research, integral equations, and FDTD modeling. His current interests are electromagnetic propagation, signal processing, and antenna design with emphasis on their applications to detection problems.

Pattern Recognition Letters 31 (2010) 1412–1421

Contents lists available at ScienceDirect

Pattern Recognition Letters

journal homepage: www.elsevier.com/locate/patrec

Sense-Through-Foliage target detection using UWB radar sensor networks

Jing Liang *, Qilian Liang

Department of Electrical Engineering, University of Texas at Arlington, Arlington, TX 76019-0016, USA

ARTICLE INFO

Article history:
Received 13 January 2009
Received in revised form 17 December 2009
Available online 10 March 2010
Communicated by J.A. Robinson

Keywords:
Target detection
Radar sensor networks
Foliage
Short-time Fourier transform (STFT)
Differential-based approach

ABSTRACT

In this paper, we propose two signal processing approaches to detect the target obscured by foliage based on real data collected by an Ultra-wide band (UWB) radar sensor. One is a differential-based four-step signal processing approach that estimates and offsets the impulsive clutter; the other approach employs short-time Fourier transform (STFT) to distinguish the target from foliage clutter. Both of these approaches provide better detection performance compared to the common 2-D image algorithm used for UWB radar. From time to time, due to the significant pulse-to-pulse variability of the foliage clutter, neither differential-based nor STFT approach can detect the target. In this case, we propose radar sensor network (RSN) and a RAKE structure in addition to the previous signal processing approaches for data fusion. The result shows that accurate detection can be achieved. Numerical performances have been analyzed for both cases in terms of probability of detection and probability of false alarm.

1. Introduction

Detection and identification of objects that are embedded in a strong clutter (e.g., foliage, soil cover and buildings) is of interest to both military and civilian research. The efficient and accurate detection provides a broad range of applications, such as locating weapon caches during military operations and rescuing people from natural diasters. Currently the detection of targets, such as human, vehicles and weapons that are hidden in foliage is still a challenging issue due to the low detection and high false alarm rate. This is mainly due to the following facts:

1. Given multipath propagation effects of rough surfaces, scattering from trees and ground tend to overwhelm the weak backscattering of targets.
2. Target is an object, so are trees. When both of them appear to have similar dielectric and frequency properties, it's hard to make a clear distinction between foliage clutter and desired targets.
3. Due to the changes in atmosphere and ground conditions, foliage is more likely to be a time-variant channel environment. For example, wind results in moving branches and leaves, therefore the foliage clutter is quite impulsive in nature.

There have been many efforts undertaken to investigate foliage penetration (FOPEN). They can be categorized into two groups. One direction is to pursue the foliage clutter modeling and analysis in order to gain better understanding of the clutter and improve the detection performance. Sheen et al. (1994) measured one-way transmission properties of foliage using a bistatic and coherent wide-band system over the band from 300 to 1300 MHz. Fleischman et al. (1996) made measurements of two-way foliage attenuation by synthetic aperture radar (SAR) and discussed probability dependency for frequency, polarization and depression angle. Other than SAR, Millimeter-Wave (MMW) radars also have been applied in measurements of foliage attenuation and ground reflectivity (Schwering et al., 1988; Ulaby et al., 1988; Nashashibi et al., 2004). These studies have showed the strong spatial and angular fluctuations of foliage. The clutter contains many spikes and is very "impulsive", therefore it's difficult to achieve effective and accurate target detection. Although K-distribution has been favored for statistic model of radar clutter (Nohara and Haykin, 1991; Watts, 1987) demonstrated that in very spiky and impulsive foliage clutter, K-distribution is inaccurate. Based on an Ultra-wide band (UWB) radar, (Kapoor et al., 1996) proposed an alpha-stable model while (Liang et al., 2008) presented a log-logistic model for foliage clutter. However, to what extent can the detection performance be improved has not been further analyzed in these studies.

The second group centers on advanced signal processing approaches to support better image formation for target detection. (MacDonald et al., 1997) described the on-going development of a test bed system including real-time UHF FOPEN SAR image formation and Automatic Target Detection and Cueing (ATD/C) processing that was based on Bayesian neural network (BNN) algorithm. However, the BNN discriminator requires an elaborate and extensive training process. Alternative approaches, based on the application of a set of filters, have been proposed. As nonlinear filters have demonstrated good noise suppression characteristics in

* Corresponding author. Tel.: +1 8172723488; fax: +1 8172722253.
E-mail addresses: jliang@wcn.uta.edu (J. Liang), liang@uta.edu (Q. Liang).

0167-8655/$ - see front matter © 2010 Elsevier B.V. All rights reserved.
doi:10.1016/j.patrec.2010.03.005

many environments with "spiky noise characteristics, (Mitra et al., 2004) presented a number of simple rank-order filters (Alpha-Trimmed, Modified Nearest Neighbor, Inner-Sigma Filter etc.) for UWB SAR image processing. This work has analyzed that the inner-sigma filter can generate good target detection performance with respect to many of the other filters. Nevertheless, this is very preliminary investigation and further performance estimation is needed. Other interesting filter schemes include adaptive Windrow Least Mean Squares (LMS) filter design (Nanis et al., 1995) and a sequence of directional filters using a hidden Markov model (HMM) (Runkle et al., 2001). Notice that all these approaches are employed for SAR image. Other than SAR, a whitening/dewhitening (WD) transform has been proposed in (Mayer et al., 2003) to help correct target spectral signatures under varying conditions for general multispectral image, but this transform can not be directly applied to colored noise, which also occurs in foliage detection.

Three types of waveforms are commonly seen in the literature dealing with the practical FOPEN measurements. The first type is multiwavelengths. Tan et al. (2007) used multiwavelength Light Detection and Ranging (lidar) to detect a vehicle hidden inside a vegetated area. Due to the fact that a laser beam is generally considered not being able to penetrating vegetation foliage, when the vegetation is dense and the target is completely covered, it is not possible to detect the hidden targets using a lidar sensor. The second type is Millimeter-Wave (MMW) (Nashashibi and Ulaby, 2005), that falls in the class of microwave. Compared to the lidar, the wavelength of microwave is much longer. Microwave and millimeter-wave (MMW) frequencies penetrate through foliage with higher attenuations, and thus this type of radar requires numbers of openings through most foliage covers. Relatively low frequency UWB signals between 100 MHZ and 3 GHz are frequently employed in recent years owning to the following characteristics: (1) high resolutions (2) very good ability of penetration, such as penetrating walls and ground (Ferrell, 1994; Xu and Narayanan, 2001; Withington et al., 2003) 3) low power cost. Despite comparatively short detection range, UWB signal would have advantages over a narrowband signal with limited frequency content.

In this paper, we propose two approaches to detect the target obscured by foliage based on the "good" data (the detail will be provided in Section 2) collected by a UWB radar. One is a differential-based four-step signal processing approach: estimate the clutter decay profile, offset the impulsive clutter, compute the derivative power and finally make a detection decision according to the threshold. The other approach employs short-time Fourier transform (STFT) to distinguish the target from foliage clutter. Both of these approaches provide better detection performance compared to the 2D image algorithm employed in (Withington et al., 2003). As far as "poor" data is concerned, neither differential-based nor STFT approach can detect the target due to the significant pulse-to-pulse variability. In this case, we propose radar sensor network (RSN) and a RAKE structure in addition to the previous signal schemes for data fusion. The numerical performances have been analyzed for both "good" and "poor" data in terms of probability of detection (P_d) and probability of false alarm (P_{fa}).

The remainder of this paper is organized as follows. Section 2 summarizes the measurement of data used in this work. Section 3 proposes differential-based approach and STFT for target detection when the signal quality is "good". Section 4 proposes RSN and RAKE structure when the signal quality is "poor". Section 5 concludes our work and discusses future research.

2. Sense-Through-Foliage data measurement and collection

The sense-through-foliage measurement effort began in August 2005 and continued through December 2005. The data used in this paper were measured in November, involved largely defoliated but dense forest.

The principle pieces of equipment are:

- dual antenna mounting stand,
- two antennas,
- a trihedral reflector target mounted on an artist easel stand,
- Barth pulse source (Barth Electronics, Inc. model 732 GL) for UWB,
- Tektronix model 7704 B oscilloscope,
- rack system,
- HP signal generator,
- IBM laptop,
- Custom RF switch and power supply,
- weather shield (small hut).

A bistatic system (individual transmit and receive antennas) has been used as it was believed that circulators did not exist for wideband signals in 2005. An 18 ft distance between antennas was chosen to reduce the signal coupling between transmitter and the receiver (Henning, 2001). The triangular-shaped target, which was shown in Fig. 1, was a round trip distance of 600 ft from the bistatic antennas (300 ft one way). The UWB pulse generator uses a coaxial reed switch to discharge a charge line for a very fast rise time pulse outputs. The model 732 pulse generator provides pulses of less than 50 picoseconds (ps) rise time, with amplitude from 150 V to greater than 2 kV into any load impedance through a 50 ohm coaxial line. The generator is capable of producing pulses with a minimum width of 750 ps and a maximum of 1×10^{-6} s. This output pulse width is determined by charge line length for rectangular pulses, or by capacitors for 1/e decay pulses.

The radar experiment was constructed on a seven-ton man lift, which had a total lifting capacity of 450 kg. The limit of the lifting capacity was reached during the experiment as essentially the entire measuring apparatus was placed on the lift. It was a 4-wheel drive diesel platform that was driven up and down a graded track 25 m long. The measurement system was moved to different positions on the track. The illustration of the lift was shown in Fig. 2. This picture was taken in September with the foliage largely still present.

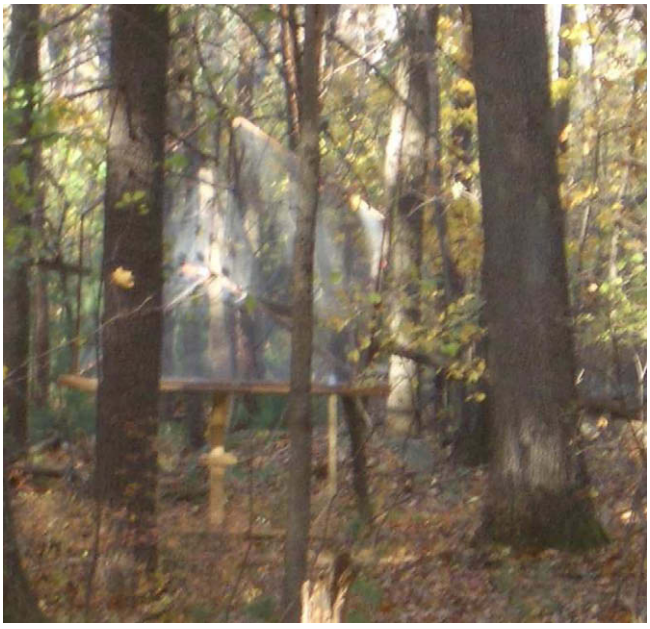

Fig. 1. The target (a trihedral reflector) is shown on the stand at 300 ft from the lift.

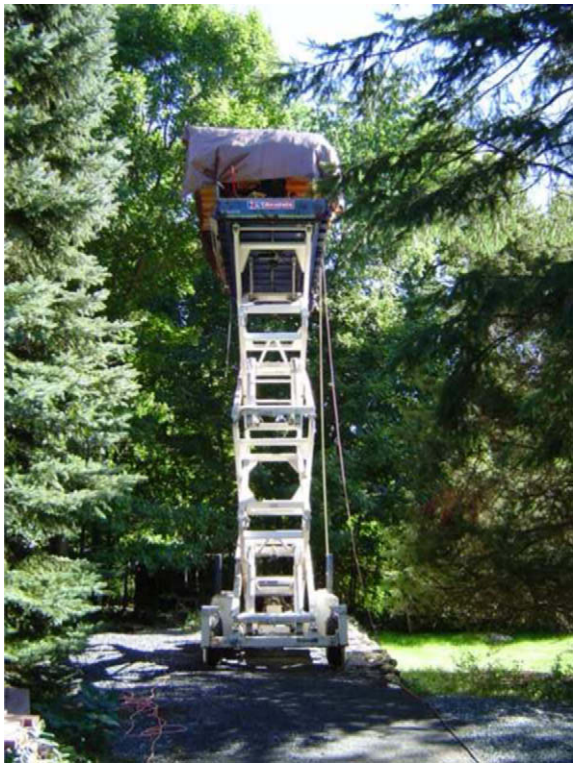

Fig. 2. This figure shows the lift with the experiment. The antennas are at the far end of the lift from the viewer under the roof that was built to shield the equipment from the elements. This picture was taken in September with the foliage largely still present. The cables coming from the lift are a ground cable to an earth ground and one of 4 tethers used in windy conditions.

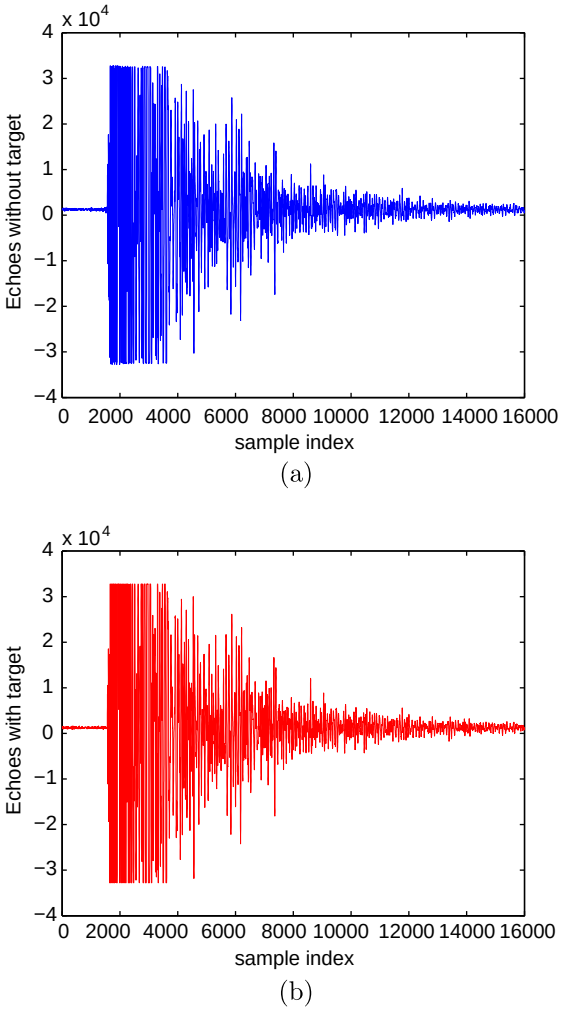

Fig. 3. Measurement with very good signal quality and 100 pulses integration. (a) No target on range, (b) with target on range (target appears at around sample 13900–14000).

For the data we used in this paper, each sample is spaced at 50 ps interval, and 16,000 samples were collected for each collection for a total time duration of 0.8×10^{-6} s at a rate of approximately 20 Hz. There are two sets of data. Initially, the Barth pulse source was operated at lower amplitude and 35 pulses of signals were obtained. The unit of amplitude is "V". This collection is referred to as "poor" data, which means signal quality is poor. Later, additional improvements were made in the measurement procedure, including the improved isolation of transmit and receive antennas, the addition of a log-periodic antenna (Antenna Research Associates LPC-2010-C) as a transmit antenna, and the EMCO ridged waveguide horn (Microwave horn, EMCO 3106). 100 pulses at different sites were collected using the new transmitted signal with higher amplitude. The integration of these 100 pulses is referred to as "good" data.

3. Target detection for good data: a differential-based approach and short-time Fourier transform

3.1. Target detection problem

In Fig. 3, we plot two received collections for "good" data. Fig. 3a shows the situation that there is not a target on range and Fig. 3b shows the opposite case. The target appears around samples from 13,900 to 14,000. In order to further analyze the discrepancy between these two collections, we provide expanded views of traces from sample 13,001 to 15,000 in Fig. 4a and b. Since there is no target in Fig. 4a, it can be considered that this collection represents the backscattering of foliage clutter. Therefore, it's quite straightforward that the target response will be the difference between Fig. 4b and a, which is plotted in Fig. 4c. Nevertheless, in practice we either obtain Fig. 4a (clutter echoes without target) or Fig. 4b (combined echoes of both target and clutter) without the priori knowledge about the presence of a target. The challenge is how can we make target detection simply based on Fig. 4a (with target) or Fig. 4b (no target)?

To solve this problem, we applied the algorithm proposed in (Withington et al., 2003), where 2D image (range and azimuth) was created via adding voltages with the appropriate time offset. In Fig. 5a and b, we plot the 2D image created based on the above two data sets (from samples 13,800 to 14,200). Since the measurement was made with one radar, the bright spot should represent reflections from an object or objects. Unfortunately, from these two figures, we may declare there are several targets in each image. Therefore, the simple 2D image algorithm provided very high false alarm rate for current radar data.

3.2. A differential-based approach

In order to improve the detection performance, we consider removing the clutter signal first (Liang et al., 2008). Of course, since the foliage is very impulsive and time-variant in nature, it is very challenging to generate real-time clutter data. Also, notice that in Fig. 4b, for samples where target appears (around sample from 13900 to 14,000), the waveform changes much abruptly than that

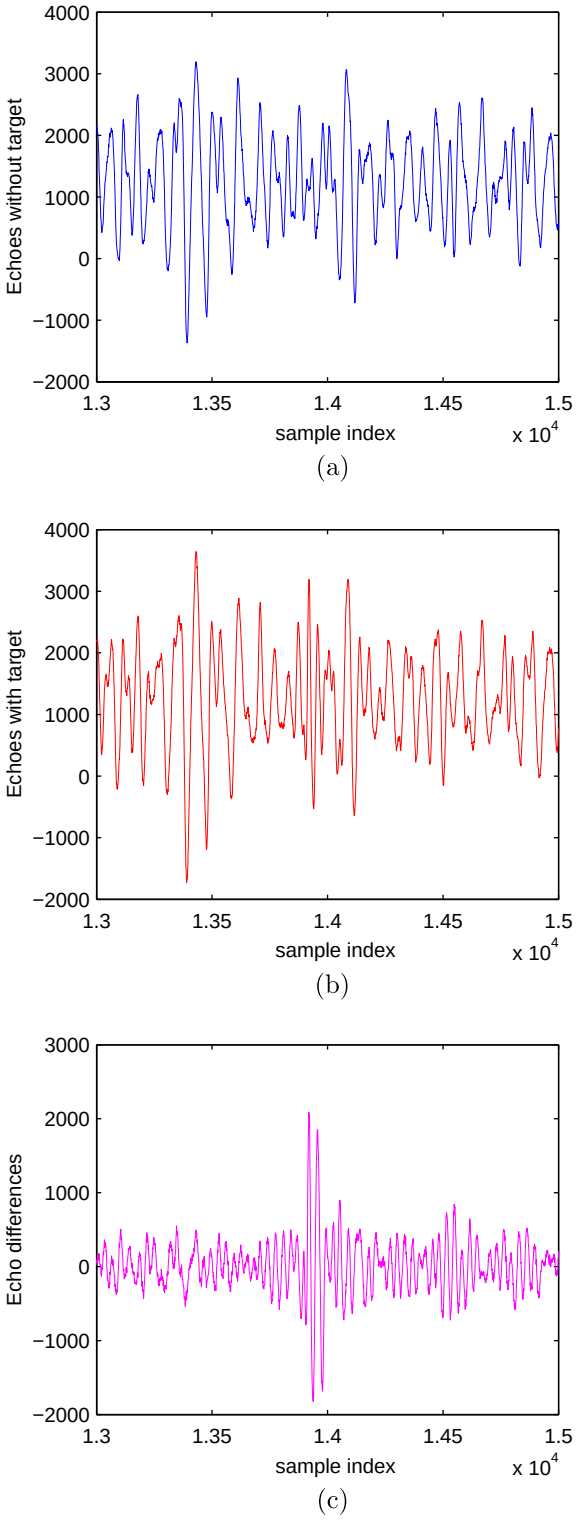

Fig. 4. Measurement with good signal quality and 100 pulses integration. (a) Expanded view of traces (no target) from samples 13001 to 15000. (b) Expanded view of traces (with target) from samples 13001 to 15000. (c) Expanded view of traces difference between with and without target.

in Fig. 4a. As derivative represents the changing rate of a function, it is quite intuitively that the derivatives of amplitude value at around samples 13900–14,000 should be larger than those without target. Therefore, we decide to combine the clutter offset with the differentiation computation to test the detection performance. The block diagram of this approach is illustrated in Fig. 6.

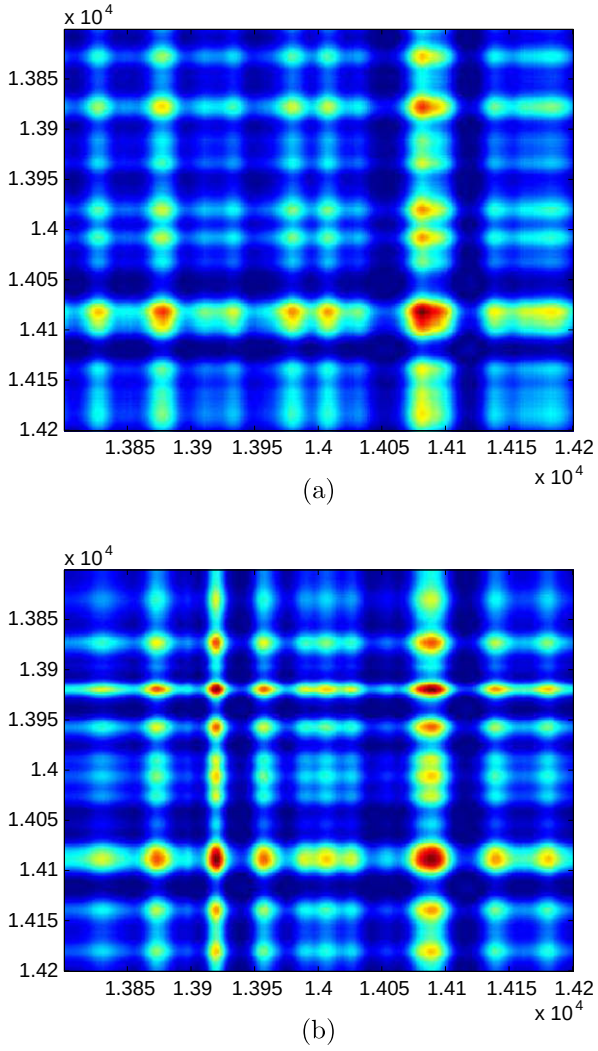

Fig. 5. 2D image created via adding voltages with the appropriate time offset. (a) No target, (b) with target in the field.

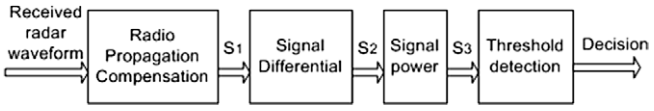

Fig. 6. Block diagram of differential-based approach for single radar.

1. *Step 1.* According to UWB indoor multi-path channel model (Foerster, 2003), the average power decay profile (PDP) is characterized by an exponential decay of the amplitude of the clusters (Benedetto and Giancola, 2004). Therefore, we may roughly consider the foliage decay profile as

$$\hat{y} = \begin{cases} Ae^{-Bx} & y > 0 \\ -Ae^{-Bx} & \text{otherwise} \end{cases} \quad (1)$$

where $\hat{y}$ is the amplitude of estimated clutter echo, x is sample index and y is the amplitude of original measured data. A and B are constants. These two parameters should be carefully chosen so that $\hat{y}$ is as close to y as possible. We apply trust-region algorithm (Liu and Chen, 2004; Xiao and Li, 2008) and robust least-squares fitting by minimizing the least absolute residuals

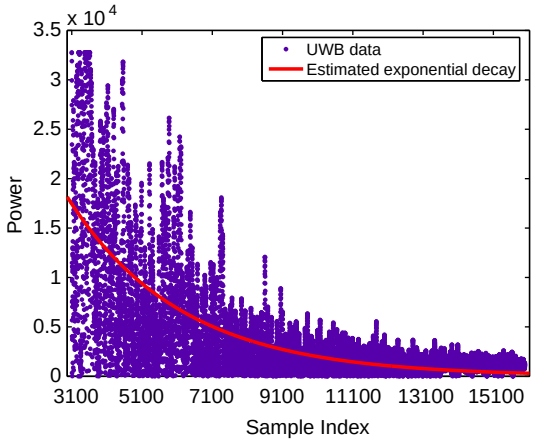

Fig. 7. Curve fit for foliage clutter decay profile.

Table 1
Estimated clutter decay parameters.

Data set	A (with 95% confidence bounds)	B (with 95% confidence bounds)
Good data	1.317×10^4 $(1.301 \times 10^4, 1.332 \times 10^4)$	0.0002628 (0.0002664, 0.0002592)
Poor data	6881 (6779, 6983)	0.0002506 (0.0002549, 0.0002463)

(LAR). We use LAR criteria instead of the commonly used least-squares fitting because the LAR is more robust than least squares in cases where the statistical properties and distribution of the noise are unknown (Ke et al., 2007. (Fig. 7 illustrates the goodness-of-fit for foliage clutter decay profile for "good" data. Although the figure for "poor" data is not provided due to the similarity and conciseness, Table 1 shows the estimated parameters A and B for both "good" and "poor" data.

2. *Step 2.* By offsetting the clutter signal, we get

$$S_1 = y - \hat{y} \tag{2}$$

3. *Step 3.* Apply derivation and compute power

$$S_2 = \frac{dS_1}{dx} \tag{3}$$

$$S_3 = S_2^2 \tag{4}$$

4. *Step 4.* Finally apply threshold detection to conclude whether there is a target or not.

We plot the power of clutter-accounted and differentiated echoes in Fig. 8. It is quite straightforward to see there is no target in Fig. 8a and there is target in Fig. 8b at samples from 13,900 to 14,000.

3.3. Short-time Fourier transform approach

Another way to understand the abrupt change where target appears is that the signal contains more AC values when there is target. Therefore we also consider employing the short-time Fourier transform (STFT) approach, which uses a slide window to determine the sinusoidal frequency and phase content of a signal as it changes over time (Gabor, 1946). This form of the Fourier transform, also known as time-dependent Fourier transform, has numbers of applications in sonar and radar processing.

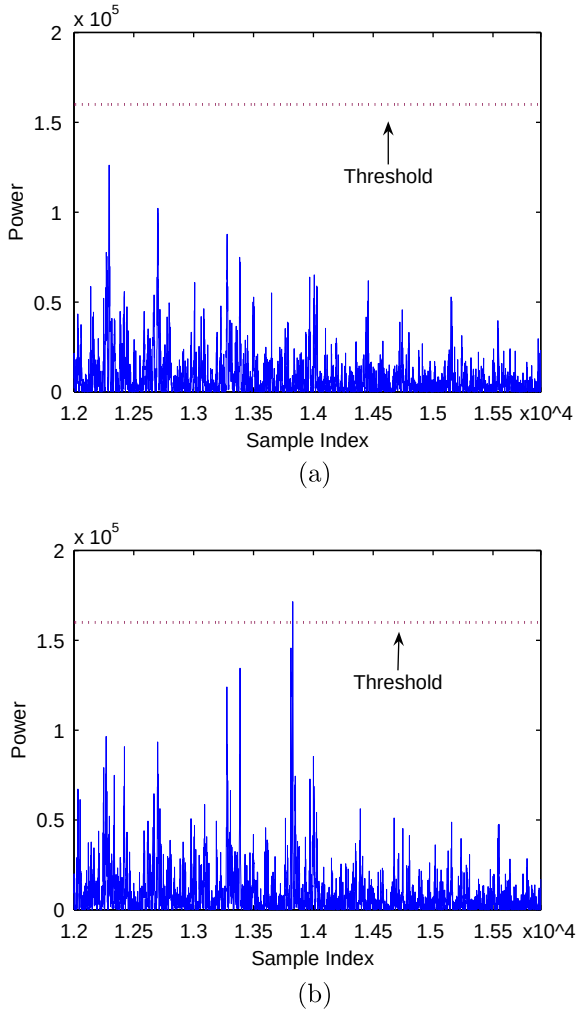

Fig. 8. The power of processed waveforms with differential-based approach for good data. (a) No target, (b) with target in the field.

For the continuous-time signal, the function to be transformed is multiplied by a nonzero window sliding along the time axis, therefore a two-dimensional expression can be defined as:

$$F(m,w) = \int_{-\infty}^{\infty} x(t)w(t-m)e^{-jwt}dt \tag{5}$$

where $x(t)$ is the function to be transformed and $w(t)$ is the window function. $F(m,w)$ represents sinusoidal values at the center of the window. m is the starting time position of window $w(t)$.

The discrete STFT can be expressed as

$$F(m,w) = \sum_{n=0}^{N-1} r(n)w(n-m)e^{-jwn} \tag{6}$$

where $r(n)$ is UWB radar measurement and $w(n)$ is the window function.

We apply a rectangular window, with its length $L = 30$ and step size $M = 16$.

$$w(n) = \begin{cases} 1 & \text{if } 0 \leqslant n \leqslant 29 \\ 0 & \text{otherwise} \end{cases} \tag{7}$$

Then the cumulated power of AC values ($m \geqslant 4$) can be obtained by

$$P(m) = \sum_{w=4}^{L-1} |F(m,w)|^2 \tag{8}$$

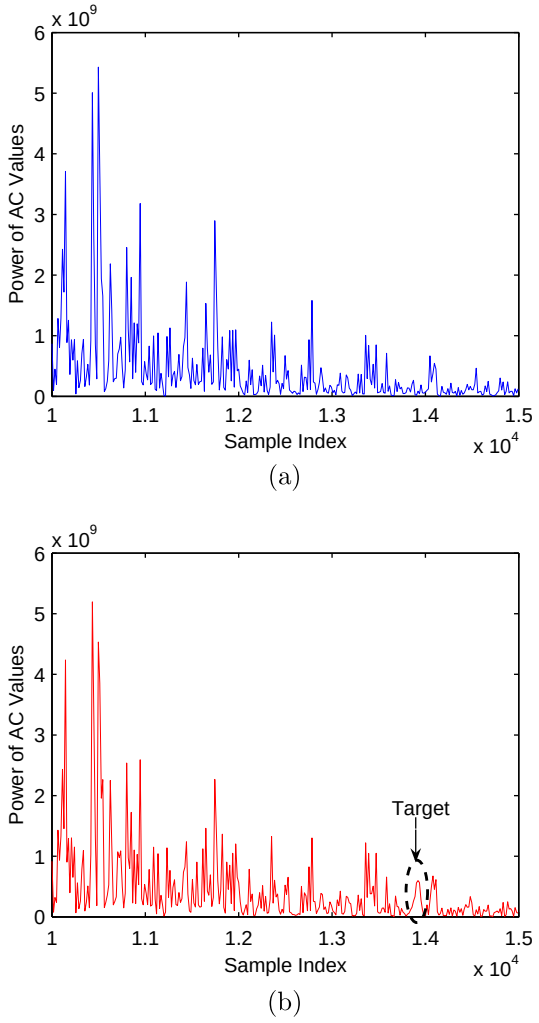

Fig. 9. The power of AC values versus sample index using STFT for good data. (a) No target, (b) with target in the field.

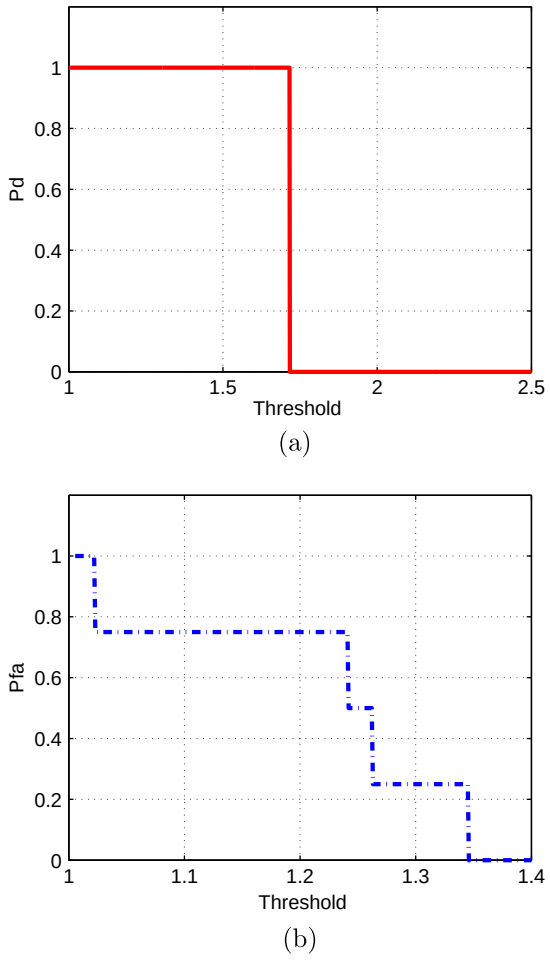

Fig. 10. Performance of differential-based approach based on good data. (a) Probability of detection. (b) Probability of false alarm.

We plot the power of AC values $P(m)$ versus time domain sample index in Fig. 9a and b for the data collection in Fig. 3a and b respectively. We can see that at the samples where there is a target, the curve of the power signal looks like a Gaussian probability density function (PDF) other than chaotic impulses. And thus it is quite straightforward to see that there is no target on range in Fig. 9a.

It's worth mentioning that for better visual inspection, window length and step size may change for radar data collected in a different environment.

3.4. Performance analysis

We analyzed the detection performance in terms of probability of detection (P_d) and probability of false alarm (P_{fa}) for both differential-based approach and STFT approach. Fig. 10 shows the relationship between the performance and the threshold for differential-based approach. The unit of the threshold illustrated by X axis is "10^5 W". The decision of the threshold has been intensively studied (Skolnik, 2001) therefore it's out of the scope of this paper. It can be clearly seen that the higher the threshold, the higher the P_{fa}, but the lower the P_d. In order to achieve accurate target detection ($100\%P_d$ and $0\%P_{fa}$), the threshold should be set in the range of $[1.346 \times 10^5, 1.716 \times 10^5]$.

As for STFT approach, since the Gaussian curves are not as numerically intuitive as the threshold detection, we first analyze all the segments of curves that are similar to Gaussian PDF, then design the decision criteria. The general Gaussian model for these curves is defined as

$$f(x) = \sum_{i=1}^{n} a \times e^{-\left(\frac{x-b}{c}\right)^2} \tag{9}$$

where a is the amplitude, b is the centroid (location), c is related to the peak width and n is the number of peaks to fit. For simplicity we choose $n = 1$, therefore c is the standard deviation (STD). Notice that the detection decision is determined by the shape of the Gaussian curve, i.e., related with factors a and c, not decided by b. The larger a and c, the higher probability that the target exists. Since the detection depends on both a and c, we normalize them respectively

Table 2
Gaussian parameters and normalized product for good data using STFT.

Data	Gaussian parameter a	Gaussian parameter c	Product of the normalized factors
Target	6.02×10^8	2.82	0.8876
False alarm 1	4.071×10^8	1.615	0.3438
False alarm 2	1.353×10^8	0.9674	0.0684
False alarm 3	3.563×10^8	1.52	0.2832
False alarm 4	2.904×10^8	1.091	0.1657

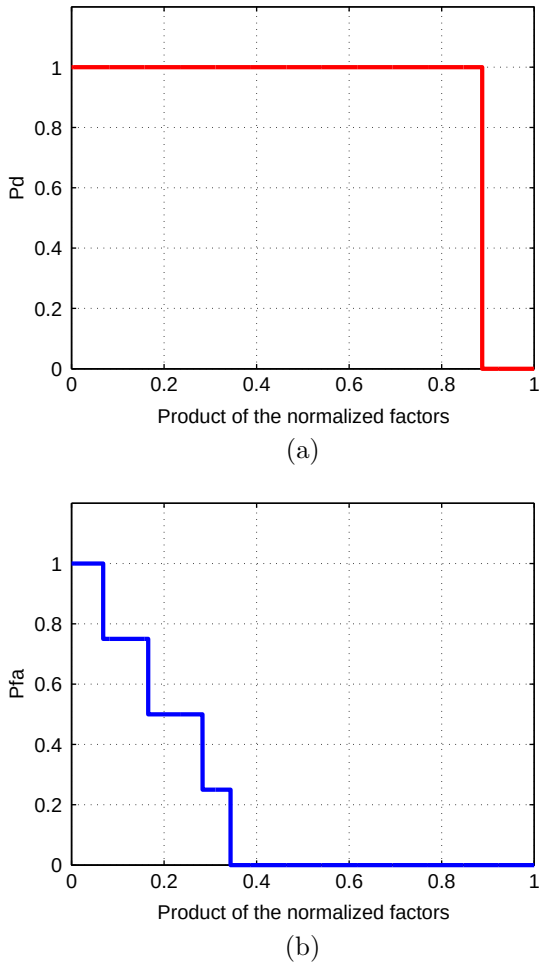

Fig. 11. Performance of STFT approach based on good data. (a) Probability of detection. (b) Probability of false alarm.

and set the product of these normalized factors as a decision criteria. These parameters are shown in Table 2. Fig. 11 illustrates the performance for STFT. When the product of normalized factor is in the range [0.3439,0.8876] the accurate target detection ($100\%P_d$ and $0\%P_{fa}$) can be achieved.

Compare STFT approach with differential-based approach, both of them are able to detect target effectively. Meanwhile, each of them has inherited defects. For differential-based approach, the major disadvantage is that it requires clutter estimation. If the clutter signal is not removed, the performance of detection is not acceptable. Therefore when the Target-to-Clutter ratio (TCR) is weak, this approach may not work well, which is exactly the case for "poor" data. The drawback of STFT approach is that the detection is not numerically intuitive, therefore it requires extra training and computing for setting up the decision boundary.

4. Target detection for poor data: radar sensor networks and RAKE structure

As mentioned in Section 2, when the Barth pulse source was operated at low amplitude, significant pulse-to-pulse variability was noted and the return signal quality is poor. Fig. 12 illustrate the received echoes in this situation. Even with the application of our proposed differential-based scheme or STFT approach, it is difficult to detect the target. Since pulse-to-pulse variability exists in the echoes at different time or different site, the spatial and time diversity can be explored by using Radar Sensor Networks (RSN).

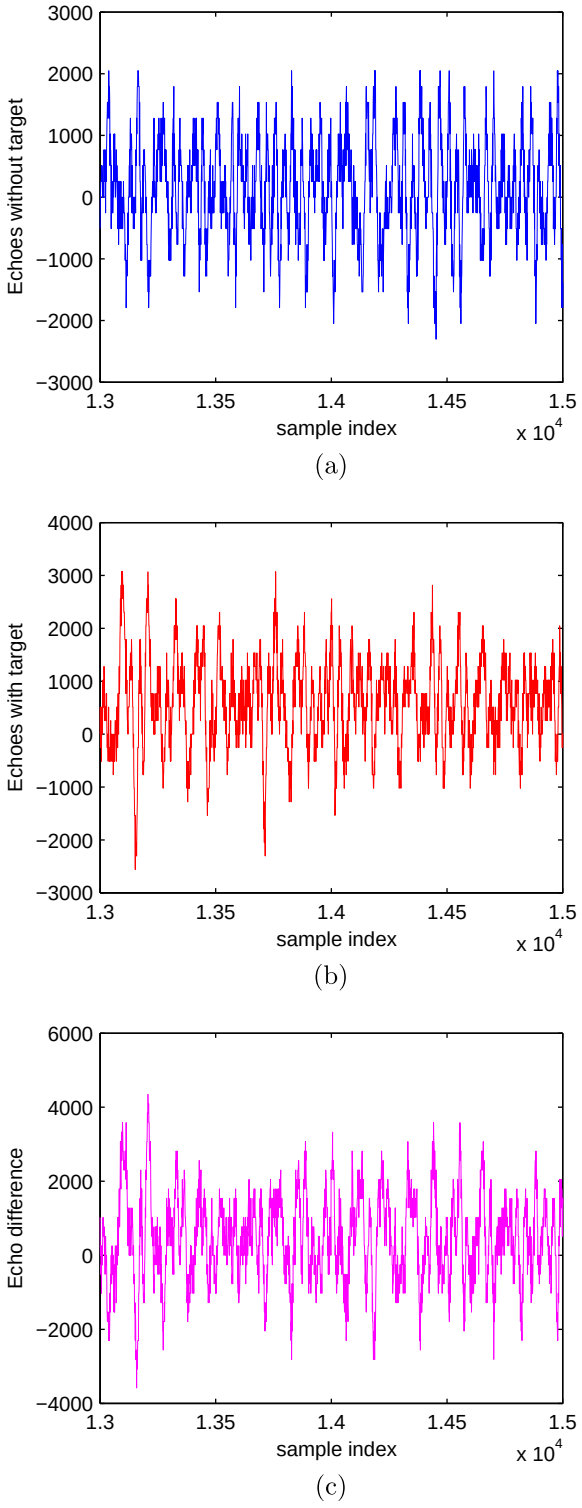

Fig. 12. Measurement with poor signal quality. (a) Expanded view of traces (no target) from samples 13001 to 15000. (b) Expanded view of traces (with target) from samples 13001 to 15000. (c) Expanded view of traces difference between with and without target.

In nature, a network of multiple radar sensors can be utilized to combat performance degradation of single radar (Haykin, 2005). These radar sensors are managed by an intelligent clusterhead that combines waveform diversity in order to satisfy the common goals of the network other than each radar operate substantively. As

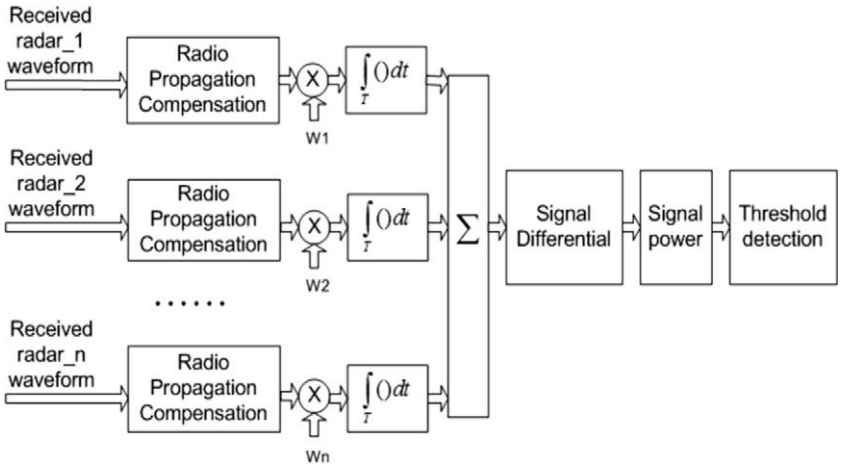

Fig. 13. Block diagram of differential-based approach and diversity combination in RSN.

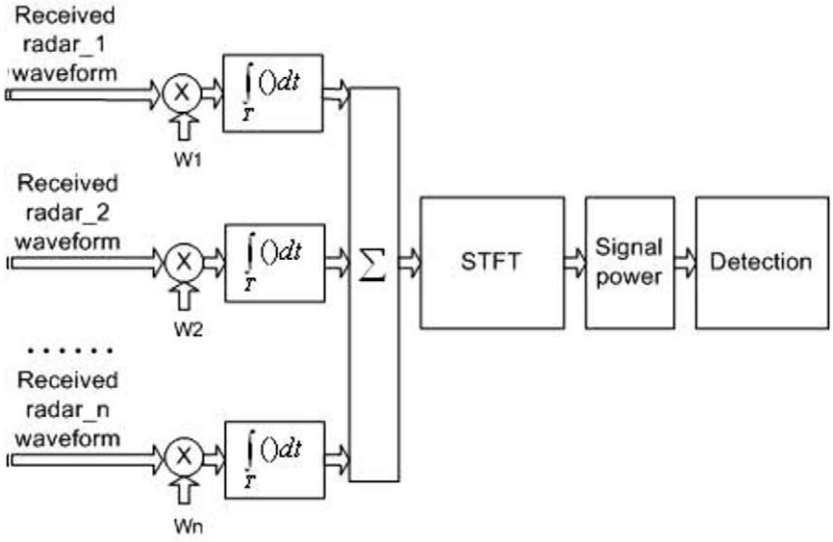

Fig. 14. Block diagram of STFT based approach and diversity combination in RSN.

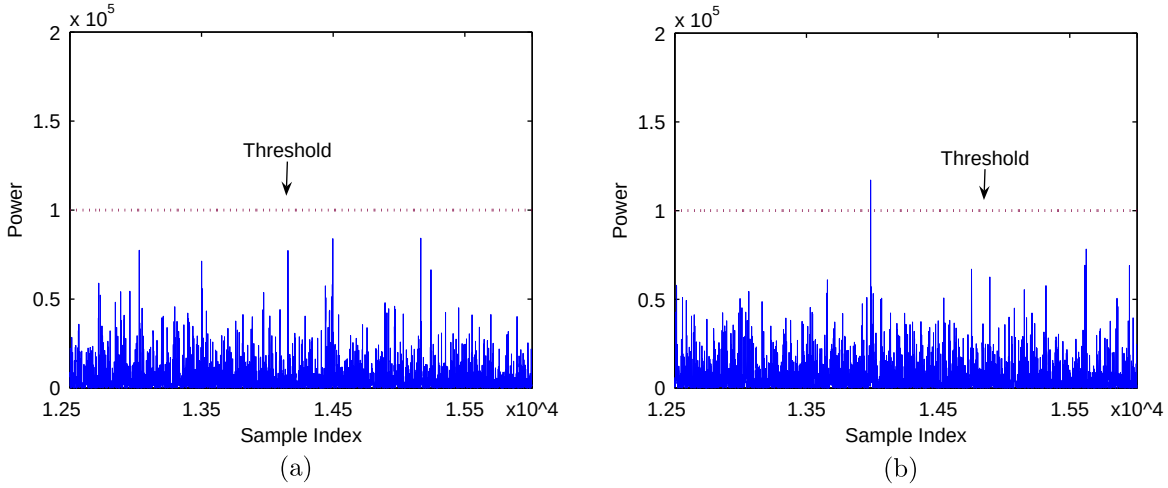

Fig. 15. The power of processed waveforms with differential-based approach and RSN for poor data. (a) No target, (b) with target in the field.

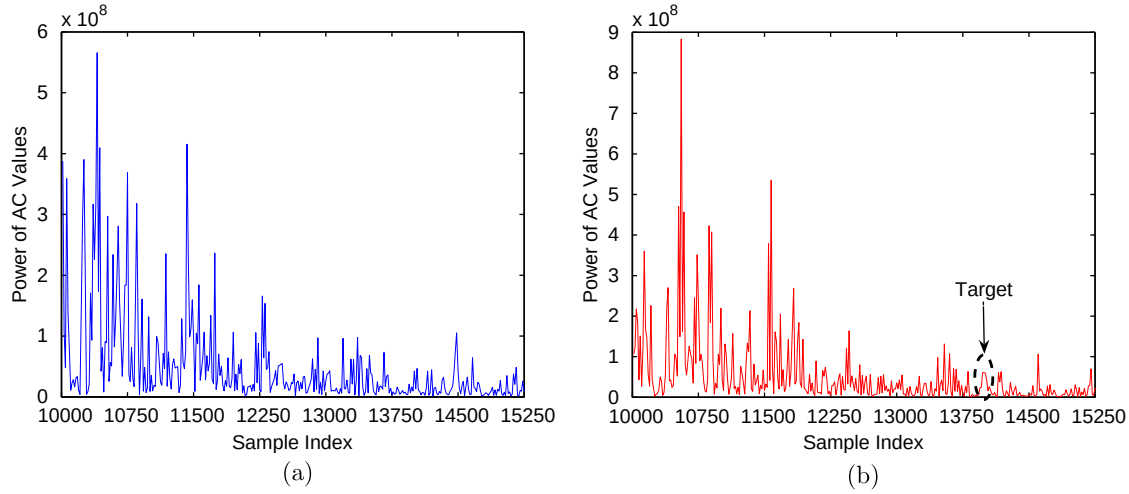

Fig. 16. The power of AC values versus sample index using STFT and RSN for poor data. (a) No target, (b) with target in the field.

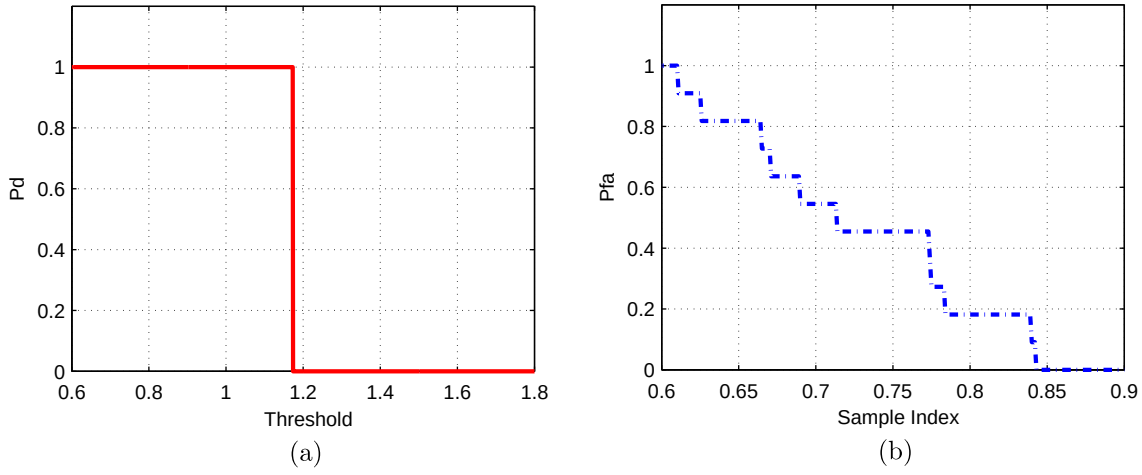

Fig. 17. Performance of differential-based approach based on poor data. (a) Probability of detection (b) Probability of false alarm.

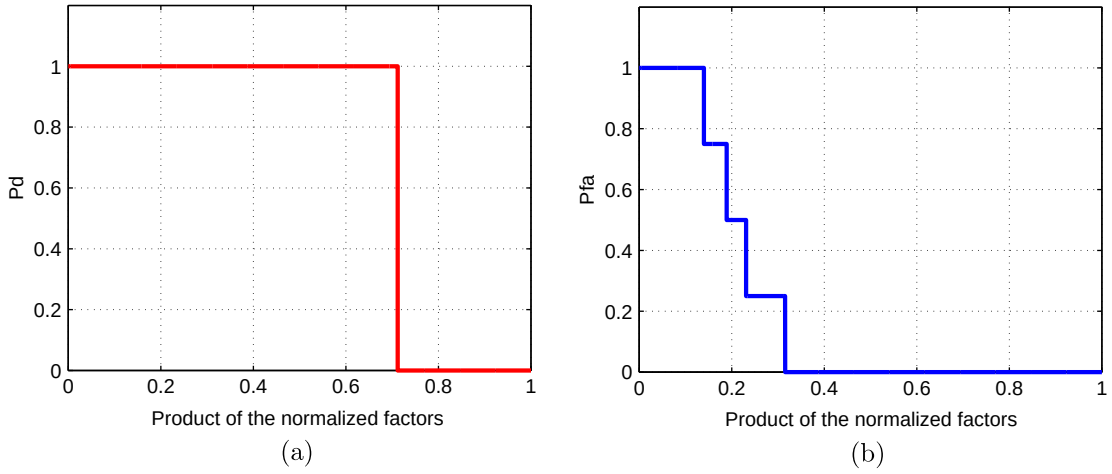

Fig. 18. Performance of STFT approach based on poor data. (a) Probability of detection. (b) Probability of false alarm.

radar sensors are environment dependent (Johnson and Titlebaum, 1972), it may provide better signal quality if uncorrelated radars work collaboratively to perform data fusion. For example, consider a system of two radars. If they are spaced sufficiently far apart, it is not likely that both of them experience deep fading at the same time. By selecting better waveform from the two candidates, the more accurate detection will be achieved compared to using single radar.

Table 3
Gaussian parameters and normalized product for poor data using STFT.

Data	Gaussian parameter a	Gaussian parameter c	Product of the normalized factors
Target	6.068×10^7	3.177	0.7120
False alarm 1	3.795×10^7	1.649	0.2311
False alarm 2	3.267×10^7	1.567	0.1891
False alarm 3	8.523×10^7	1.002	0.3154
False alarm 4	2.511×10^7	1.509	0.1399

In our work, we assume the radar sensors are synchronized and RAKE structure is employed to combine the diversity of received signals. The detailed processing diagrams are illustrated in Figs. 13 and 14 for differential-based approach and STFT approach respectively. The echo, i.e., the backscattering received by each radar sensor, is combined by the clusterhead using a weighted average, and the weight w_i is determined by the power of each echo $x_i(m)$ (m is the sample index),

$$w_i = \frac{E_i}{\sum_{i=1}^{n} E_i} \tag{10}$$

and

$$E_i = \mathrm{var}(x_i(m)) + [\mathrm{mean}(x_i(m))]^2 \tag{11}$$

As for STFT, we apply window length $L = 25$ and step size $M = 15$. We ran simulations for $n = 35$. Figs. 15 and 16 show the results. For RSN with differential-based approach, it is obvious that there is a target around sample 13,950 in Fig. 15b and no target appears in Fig. 15a. Also, for RSN with STFT approach, around samples 13,900–14,000, Gaussian curve appears. The related parameters for "poor" data are shown in Tables 1 and 3 respectively. Figs. 17 and 18 illustrate the analyzed detection performance. For differential-based approach, accurate detection is obtained when the threshold lies in [0.843, 1.173]. For STFT, the decision boundary should be within [0.3155, 0.7120].

5. Conclusion and future works

In this paper, we propose two signal processing approaches to improve sense-through-foliage target detection. Additionally, we employ Radar Sensor Networks (RSN) and RAKE structure to improve the robustness of the detection performance. However, as each approach has its own advantage and drawback, it's hard to conclude which is superior. Detecting targets obscured by foliage will be an on-going research that may include future works listed as follows:

1. Investigate the time-variant properties of foliage clutter. The foliage is not a static environment due to the changes in temperature and ground conditions. Although many previous studies have assumed the clutter to be time-invariant, the future analysis on the noncoherent and variant properties will help better understand the impulsiveness nature of the foliage.
2. As more sensing-through-foliage data will be collected, we may optimize the proposed approaches and improve their robustness.
3. Apply proposed approaches and structures to targets obscured by other clutters, such as walls, soil cover, etc.

Acknowledgement

The authors would like to thanks Dr. Sherwood W. Samn in AFRL/RHX for providing the radar data. This work was supported in part by Office of Naval Research (ONR) under Grants N00014–07-1–0395 and N00014–07-1–1024, and National Science Foundation (NSF) under Grants CNS-0721515, CNS-0831902, CCF-0956438, and CNS-0964713.

References

Benedetto, M.D., Giancola, G., 2004. Understanding Ultra Wide Band Radio Fundamentals. Person Education.
Ferrell, B., 1994. Ultrawideband foliage penetration measurement. In: Proc. IEEE Nation Radar Conf. 1994, pp. 80–84.
Fleischman, J.G., Ayasli, S., Adams, E.M., Gosselin, D.R., 1996. Foliage penetration experiment. Part I: Foliage attenuation and backscatter analysis of SAR imagery. IEEE Trans. Aerosp. Electron. Systems 32 (January), 135–144.
Foerster, J.R., 2003. Channel modeling sub-committee report final, IEEE P802.15-02/490r1-SG3a, IEEE 802.15.SG3a.
Gabor, D., 1946. Theory of communication. J. IEE 93 (3), 429–457.
Haykin, S., 2005. Cognitive radar networks. 1st IEEE International Workshop on Computational Advances in Multi-Sensor Adaptive Processing, December, pp. 1–3.
Henning, J.A., 2001. Design and Performance of An Ultra-Wideband Foliage Penetrating Noise Radar. Master's Thesis, University of Nebraska, May 2001.
Johnson, R.A., Titlebaum, E.L., 1972. Range Doppler Uncoupling in the Doppler Tolerant Bat Signal. In: Proc. of IEEE Ultrasonics Symposium, New York, pp. 64–67.
Kapoor, R., Tsihrintzis, G.A., Nandhakumar, N., 1996. Detection of obscured targets in heavy-tailed radar clutter usingan ultra-wideband (UWB) radar and alpha-stable clutter models. In: Proc. 30th Asilomar Conf. on Signals, Systems and Computers, November, vol. 2, pp. 863–867.
Ke, J., Zhang, C., Qiao, Y., 2007. Modified evolution strategy based identification of multi-input single-output Wiener–Hammerstein model. In: 3rd Internat. Conf. on Natural Computation 2007 (ICNC'07), pp. 251–255.
Liang, J., Liang, Q., Samn, S.W., 2008. A differential based approach for sense-through-foliage target detection using UWB radar sensor networks. In: IEEE Internat. Conf. on Communications 2008 (ICC'08) Rec., pp. 1952–1956.
Liang, J., Liang, Q., Samn, S.W., 2008. Foliage clutter modeling using the UWB radar. In: IEEE Internat. Conf. on Communications 2008 (ICC'08) Rec., pp. 1937–1941.
Liu, T., Chen, H., 2004. Real-time tracking using trust-region methods. IEEE Trans. Pattern Anal. Machine Intell. 26, 397C402.
MacDonald, D., Isenman, J., Roman, J., 1997. Radar detection of hidden targets. In: Aerospace and Electronics Conf. 1997 (NAECON'97), vol. 2, pp. 846–855.
Mayer, R., Bucholtz, F., Scribner, D., 2003. Object detection by using whitening/dewhitening to transform target signatures in multitemporal hyperspectral and multispectral imagery. IEEE Trans. Geosci. Remote Sensing 41 (Part 2), 1136–1142.
Mitra, A.K., Lewis, T.L., Shaw, A.K., 2004. Rank-order filters for FOPEN target detection. IEEE Signal Process. Lett. 11 (Part 1), 93–96.
Nanis, J.G., Halversen, S.D., Owirka, G.J., Novak, L.M., 1995. Adaptive filters for detection of targets in foliage. IEEE Aerosp. Electron. Systems Mag. 10 (August), 34–36.
Nashashibi, A.Y., Ulaby, F.T., 2005. Detection of stationary foliage-obscured targets by polarimetric millimeter-wave radar. IEEE Trans. Geosci. Remote Sensing 43 (January), 13–23.
Nashashibi, A.Y., Sarabandi, K., Oveisgharan, S., et al., 2004. Millimeter-wave measurement of foliage attenuation and ground reflectivity of tree stands at Nadir incidence. IEEE Trans. Antennas Propagat. 52 (May), 1211–2004.
Nohara, T., Haykin, S., 1991. Canadian east coast radar trials and the K-distribution. IEE Proc. – F 138 (April), 80–88.
Runkle, P., Nguyen, L.H., McClellan, J.H., Carin, L., 2001. Multi-aspect target detection for SAR imagery using hidden Markov models. IEEE Trans. Geosci. Remote Sensing 39 (January), 46–55.
Schwering, F.K., Violette, E.J., Espeland, R.H., 1988. Millimeter-wave propagation in vegetation: Experiments and theory. IEEE Trans. Geosci. Remote Sensing 26 (May), 355–367.
Sheen, D.R., Malinas, N.P., Kletzli, D.W., Lewis, T.B., Roman, J.F., 1994. Foliage transmission measurements using a ground-based ultrawideband (UWB) (3001300 Mhz) SAR system. IEEE Trans. Geosci. Remote Sensing 32 (January), 118–130.
Skolnik, M.I., 2001. Introduction to Radar Systems, 3rd ed. McGraw Hill, New York.
Tan, S., Greenlee, S., Stoker, J., 2007. Detection of foliage-obscured vehicle using a multiwavelength polarimetric lidar. In: IEEE Internat. Geoscience and Remote Sensing Symposium 2007 (IGARSS'07), pp. 2503–2506.
Ulaby, F.T., Van Deventer, T.E., East, J.R., Haddock, T.F., Coluzzi, M.E., 1988. Millimeter-wave bistatic scattering from ground and vegetation targets. IEEE Trans. Geosci. Remote Sensing 26 (May), 229–243.
Watts, S., 1987. Radar detection prediction in K-distribution sea clutter and thermal noise. IEEE Trans. Aerosp. Electron. Systems 23 (January), 40–45.
Withington, P., Fluhler, H., Nag, S., 2003. Enhancing homeland security with advanced UWB sensors. IEEE Microwave Mag. (September).
Xiao, L., Li, P., 2008. Improvement on mean shift based tracking using second-order information. In: 19th Internat. Conf. on Pattern Recognition 2008 (ICPR'08), pp. 1–4.
Xu, X., Narayanan, R.M., 2001. FOPEN SAR imaging using UWB step-frequency and random noise waveforms. IEEE Trans. Aerosp. Electron. Systems 37 (October), 1287–1300.

Hindawi Publishing Corporation
EURASIP Journal on Wireless Communications and Networking
Volume 2010, Article ID 873070, 12 pages
doi:10.1155/2010/873070

Research Article

A Propagation Environment Modeling in Foliage

Jing Liang,[1] Qilian Liang,[1] and Sherwood W. Samn[2]

[1] *Department of Electrical Engineering, University of Texas at Arlington, Arlington, TX 76019-0016, USA*
[2] *Air Force Research Laboratory/HEX, Brooks City Base, San Antonio, TX 78235, USA*

Correspondence should be addressed to Jing Liang, jliang@wcn.uta.edu

Received 16 September 2009; Accepted 22 January 2010

Academic Editor: Xiuzhen (Susan) Cheng

Foliage clutter, which can be very large and mask targets in backscattered signals, is a crucial factor that degrades the performance of target detection, tracking, and recognition. Previous literature has intensively investigated land clutter and sea clutter, whereas foliage clutter is still an open-research area. In this paper, we propose that foliage clutter should be more accurately described by a log-logistic model. On a basis of pragmatic data collected by ultra-wideband (UWB) radars, we analyze two different datasets by means of maximum likelihood (ML) parameter estimation as well as the root mean square error (RMSE) performance. We not only investigate log-logistic model, but also compare it with other popular clutter models, namely, log-normal, Weibull, and Nakagami. It shows that the log-logistic model achieves the smallest standard deviation (STD) error in parameter estimation, as well as the best goodness-of-fit and smallest RMSE for both poor and good foliage clutter signals.

1. Introduction and Motivation

Detection and identification of military equipment in a strong clutter background, such as foliage, soil cover, or building has been a long-standing subject of intensive study. It is believed that solving the target detection through foliage environment will significantly benefit sense-through-wall and many other subsurface sensing problems. However, to this date, the detection of foliage-covered targets with satisfied performances is still a challenging issue. Recent investigations in environment behavior of tree canopies have shown that both signal backscattering and attenuation are significantly influenced by tree architecture [1]. Therefore using the return signal from foliage to establish the clutter model that accounts for environment effects is of great importance for the sensing-through-foliage radar detection.

Clutter is a term used to define all unwanted echoes from natural environment [2]. The nature of clutter may necessarily vary on a basis of different applications and radar parameters. Most previous studies have investigated land clutter or sea clutter, and some conclusions have been reached. For example, log-normal, Weibull, and K-distributions have been proven to be better suited for the clutter description other than Rayleigh and Rician models in high-resolution radar systems. Fred did statistical comparisons and found that sea clutter at low-grazing angles and high range resolution is spiky based on the data measured from various sites in Kauai and Hawaii [3]. David generalized radar clutter models using noncentral chi-square density by allowing the noncentrality parameter to fluctuate according to the gamma distribution [4]. Furthermore, Leung et al. used a Neural-Network-based approach to predict the sea clutter model [5, 6].

However, as far as clutter modeling in forest is concerned, it is still of great interest and will be likely to take some time to reach any agreement. A team of researchers from MIT [7] and U. S. Army Research Laboratory (ARL) [8, 9] have measured ultra-wideband (UWB) backscatter signals in foliage for different polarizations and frequency ranges. The measurements show that the foliage clutter is impulsively corrupted with multipath fading, which leads to inaccuracy of the K-distributions description [10]. The US Air Force Office of Scientific Research (AFOSR) has conducted field measurement experiment concerning foliage penetration radar since 2004 and noted that metallic targets may be more easily identified with wideband than with narrowband signals.

In this investigation, we will apply ultra-wideband (UWB) radar to model the foliage clutter. UWB radar

emissions are at a relatively low frequency typically between 100 MHz and 3 GHz. Additionally, the fractional bandwidth of the signal is very large (greater than 0.2). Such a radar sensor has exceptional range resolution, as well as the ability to penetrate many common materials (e.g., walls). Law enforcement personnel have used UWB ground-penetrating radars (GPRs) for at least a decade. Like the GPR, sensing-through-foliage radar takes advantage of UWB's very fine resolution (time gating) and the low frequency of operation.

In our work, we investigate the log-logistic distribution (LLD) to model foliage clutter and illustrate the goodness-of-fit to real UWB clutter data. Additionally, we compare the goodness-of-fit of LLD with existing popular models, namely, log-normal, Weibull, and Nakagami by means of maximum likelihood estimation (MLE) and the root mean square error (RMSE). The result shows that log-logistic model provides the best fit to the foliage clutter. Our contribution is not only the new proposal on the foliage clutter model with detailed parameter estimation, but also providing the criteria and approaches based on which the statistical analysis is obtained. Further, based on LLD the theoretical study about the probability of detection as well as the probability of false alarm are discussed.

The rest of this paper is organized as follows. Section 2 provides a review on statistical models of log-logistic, log-normal, Weibull, and Nakagami, and discusses their applicability for foliage clutter modeling. Section 3 summarizes the measurement and the two sets of clutter data that are used in this paper. Section 4 discusses estimation on parameters and the goodness-of-fit for log-logistic, log-normal, Weibull and Nakagami models, respectively. Section 5 analyzes the performance of radar detection in the presence of foliage clutter. Finally, Section 6 concludes this paper and describes some future research topics.

2. Clutter Models

Many radar clutter models have been proposed in terms of distinct statistical distributions; most of which describe the characteristics of clutter amplitude or power. Before detailed analysis on our measurement, we would like to discuss the properties and applicability of log-logistic, log-normal, Weibull, and Nakagami statistic distributions, which are designated as "curve-fit" models in Section 4, since they are more likely to provide good fit to our collections of pragmatic clutter data. Detailed explanations would be given in the following subsections.

2.1. Log-Logistic Model. Recently Log-logistic model has been applied in hydrological analysis. This distribution is a special case of Burr's type-XII distribution [11] as well as a special case of the kappa distribution proposed by Mielke andJohnson [12]. Lee et al. employed the log-logistic distribution (LLD) for frequency analysis of multiyear drought durations [13], whereas Shoukri et al. employed LLD to analyze extensive Canadian precipitation data [14], and Narda and Malik used LLD to develop a model of root growth and water uptake in wheat [15]. In spite of its intensive application in precipitation and stream-flow data, the log-logistic distribution (LLD) [16] statistical model, to the best of our knowledge, has never been applied to radar foliage clutter. The motivation for considering log-logistic model is based on its higher kurtosis and longer tails, as well as its probability density function (PDF) similarity to log-normal and Weibull distributions. It is intended to be employed to estimate how well the model matches our collected foliage clutter statistics.

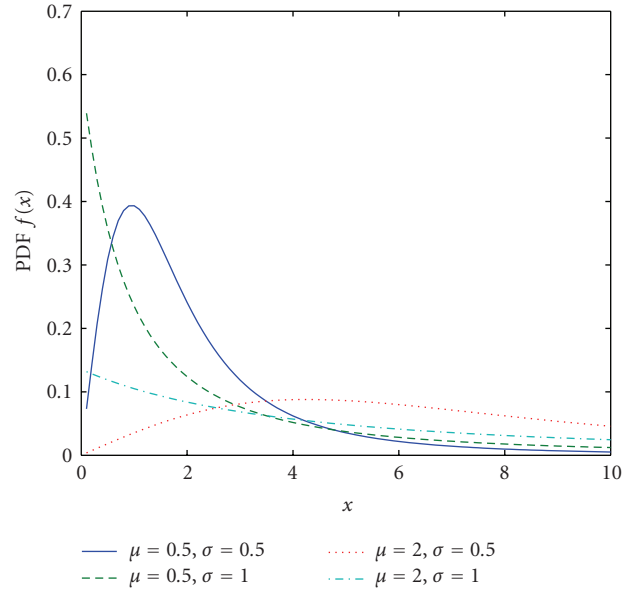

Figure 1: Log-logistic distribution PDF for $\mu = 0.5$ and $\sigma = 0.5$, $\mu = 0.5$ and $\sigma = 1$, $\mu = 2$ and $\sigma = 0.5$, $\mu = 2$ and $\sigma = 1$.

Here we apply the two-parameter distribution with parameters μ and σ. The PDF for this distribution is given by

$$f(x) = \frac{e^{((\ln x-\mu)/\sigma)}}{\sigma x\left(1+e^{((\ln x-\mu)/\sigma)}\right)^2}, \quad x > 0,\ \sigma > 0, \tag{1}$$

where μ is a scale parameter and σ is a shape parameter. The mean of the LLD is

$$E\{x\} = e^{\mu}\Gamma(1+\sigma)\Gamma(1-\sigma). \tag{2}$$

The variance is given by

$$\mathrm{Var}\{x\} = e^{2\mu}\left\{\Gamma(1+2\sigma)\Gamma(1-2\sigma) - [\Gamma(1+\sigma)\Gamma(1-\sigma)]^2\right\}, \tag{3}$$

while the moment of order k is

$$E\left\{x^k\right\} = \sigma e^{\mu}B(k\sigma, 1-k\sigma), \quad k < \frac{1}{\sigma}, \tag{4}$$

where

$$B(m,n) = \int_0^1 x^{m-1}(1-x)^{n-1}dx. \tag{5}$$

The PDFs for LLD for selected μ's and σ's are illustrated in Figure 1.

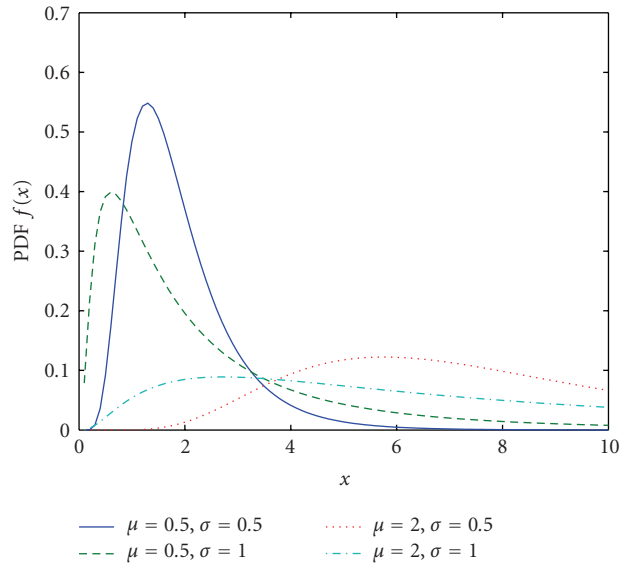

Figure 2: Log-normal distribution PDF for $\mu = 0.5$ and $\sigma = 0.5$, $\mu = 0.5$ and $\sigma = 1$, $\mu = 2$ and $\sigma = 0.5$, $\mu = 2$ and $\sigma = 1$.

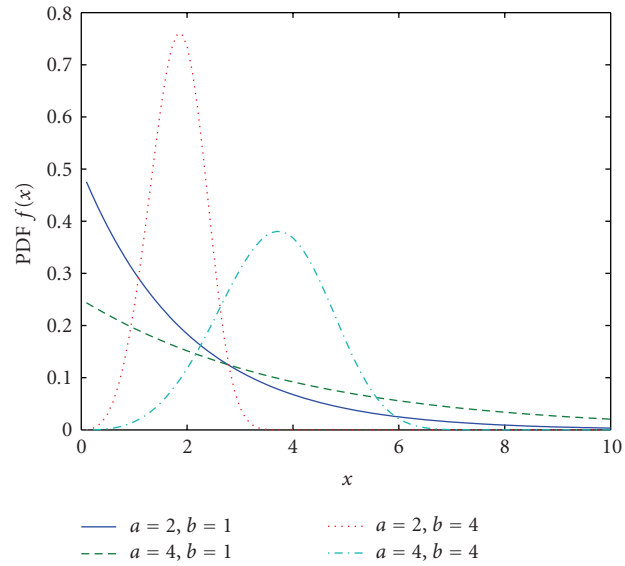

Figure 3: Weibull distribution PDF for $a = 2$ and $b = 1$, $a = 4$ and $b = 1$, $a = 2$ and $b = 4$, $a = 4$ and $b = 4$.

2.2. Log-Normal Model. The log-normal distribution is most frequently used when the radar sees land clutter [17] or sea clutter [18] at low-grazing angles (≤5 degrees) since log-normal has a long tail. However, it has been reported that the log-normal model tends to overestimate the dynamic range of the real clutter distribution [19]. Furthermore, whether it is applicable to model foliage clutter still requires detailed analysis.

The log-normal distribution [20] is also a two-parameter distribution with parameters μ and σ. The PDF for this distribution is given by

$$f(x) = \frac{1}{x\sigma\sqrt{2\pi}} e^{-(\ln x - \mu)^2/2\sigma^2}, \quad x > 0, \sigma > 0, \tag{6}$$

where μ is a scale parameter and σ is a shape parameter. The mean, variance, and the moment of order k are given, respectively, by

$$\begin{aligned} E\{x\} &= e^{\mu+(\sigma^2/2)}, \\ \mathrm{Var}\{x\} &= \left(e^{\sigma^2} - 1\right) e^{2\mu+\sigma^2}, \\ E\left\{x^k\right\} &= e^{k\mu+((k^2\sigma^2)/2)}. \end{aligned} \tag{7}$$

The PDFs for selected μ's and σ's for log-normal distribution are shown in Figure 2.

2.3. Weibull Model. The Weibull distribution, which is named after Waloddi Weibull, can be made to fit clutter measurements that lie between the Rayleigh and log-normal distribution [21]. It has been applied to land clutter [22, 23], sea clutter [24, 25] and weather clutter [26]. However, in very spiky sea and foliage clutter, the description of the clutter statistics provided by Weibull distributions may not always be sufficiently accurate [27].

The Weibull distribution is also a two-parameter distribution with parameters a and b. The PDF for this distribution is given by

$$f(x) = ba^{-b}x^{b-1}e^{-(x/a)^b}, \quad x > 0, a > 0, b > 0, \tag{8}$$

where b is the shape parameter and a is the scale parameter. The mean, variance, and the moment of order k are given, respectively, by

$$\begin{aligned} E\{x\} &= a\Gamma\left(1 + \frac{1}{b}\right), \\ \mathrm{Var}\{x\} &= a^2\left\{\Gamma\left(1 + \frac{2}{b}\right) - \left[\Gamma\left(1 + \frac{1}{b}\right)\right]^2\right\}, \\ E\left\{x^k\right\} &= a^k\Gamma\left(1 + \frac{k}{b}\right). \end{aligned} \tag{9}$$

The PDFs for selected a's and b's for Weibull distribution are shown in Figure 3.

2.4. Nakagami Model. In the foliage penetration setting, the target returns suffer from multipath effects corrupted with fading. As Nakagami distribution is used to model scattered fading signals that reach a receiver by multiple paths, it is natural to investigate how well it fits the foliage clutter statistics.

The PDF for Nakagami distribution is given by

$$f(x) = 2\left(\frac{\mu}{\omega}\right)^{\mu} \frac{1}{\Gamma(\mu)} x^{(2\mu-1)} e^{-(\mu/\omega)x^2}, \quad x > 0, \omega > 0, \tag{10}$$

where μ is the shape parameter and ω is the scale parameter.

The mean, variance, and the moment of order k of Nakagami distribution are given, respectively by

$$E\{x\} = \frac{\Gamma(\mu + (1/2))}{\Gamma(\mu)}\left(\frac{\omega}{\mu}\right)^{1/2},$$
$$\mathrm{Var}\{x\} = \omega\left[1 - \frac{1}{\mu}\left(\frac{\Gamma(\mu + (1/2))}{\Gamma(\mu)}\right)^{2}\right], \quad (11)$$
$$E\left\{x^{k}\right\} = \frac{\Gamma(\mu + (k/2))}{\Gamma(\mu)}\left(\frac{\omega}{\mu}\right)^{k/2}.$$

The PDFs for selected μ's and ω's for the Nakagami distribution are illustrated in Figure 4.

3. Experiment Setup and Data Collection

The foliage penetration measurement effort began in August 2005 and continued through December 2005. Working in August through the fall of 2005, the foliage measured included late summer foliage and fall and early winter foliage. Late summer foliage, because of the limited rainfall, involved foliage with decreased water content. Late fall and winter measurements involved largely defoliated but dense forest. A picture of experiment site is shown in Figure 5.

The principle pieces of equipment are

(i) Dual antenna mounting stand,

(ii) Two antennas,

(iii) A trihedral reflector target,

(iv) Barth pulse source (Barth Electronics, Inc. model 732 GL) for UWB,

(v) Tektronix model 7704 B oscilloscope,

(vi) Rack system,

(vii) HP signal Generator,

(viii) IBM laptop,

(ix) Custom RF switch and power supply,

(x) Weather shield (small hut).

A bistatic UWB radar (individual transmit and receive antennas) was used (see Figure 6) as it was believed that circulators did not exist for wideband signals at that time. The foliage clutter was a round trip distance of 600 feet from the bistatic antennas (300 feet one way).

An 18-foot distance between antennas was chosen to reduce the signal coupling between transmitter and the receiver [28]. The radar was constructed on a seven-ton man lift, which had a total lifting capacity of 450 kG. The limit of the lifting capacity was reached during the experiment as essentially the entire measuring apparatus was placed on the lift (as shown in Figure 7). Throughout this work, a Barth pulse source (Barth Electronics, Inc., model 732 GL) was used. The pulse generator uses a coaxial reed switch to discharge a charge line for a very fast rise-time pulse outputs. The model 732 pulse generator provides pulses of less than 50 picoseconds (ps) rise time, with amplitude from 150 V to greater than 2 kV into any load impedance through a 50 ohm coaxial line. The generator is capable of producing pulses with a minimum width of 750 ps and a maximum of 1 microsecond. This output pulse width is determined by charge line length for rectangular pulses, or by capacitors for 1/e decay pulses.

For the return data we used in this paper, each sample is spaced at 50 picoseconds interval, and 16.000 samples were collected for each collection for a total time duration

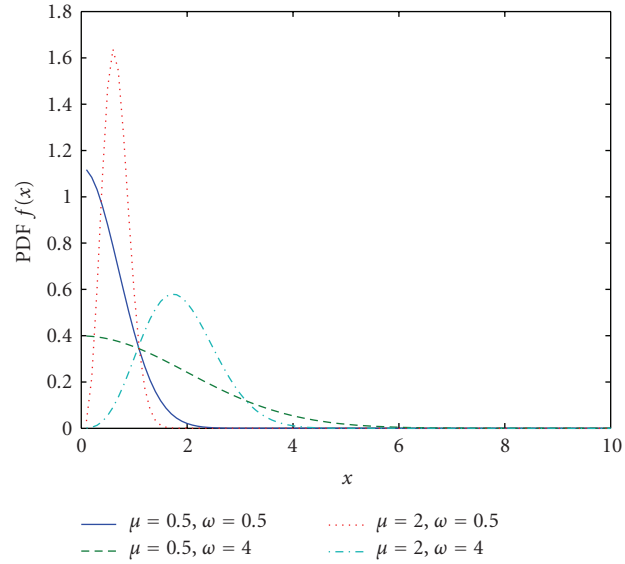

Figure 4: Nakagami distribution PDF for $\mu = 0.5$ and $\omega = 0.5$, $\mu = 0.5$ and $\omega = 4$, $\mu = 2$ and $\omega = 0.5$, $\mu = 2$ and $\omega = 4$.

Figure 5: A picture of foliage.

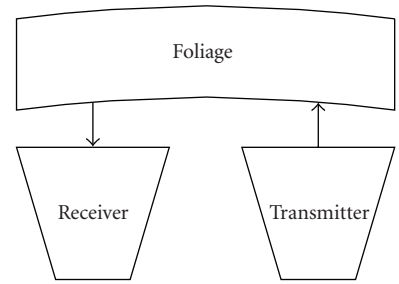

Figure 6: Illustration for the experimental radar antennas.

Figure 7: This figure shows the lift with the experiment. The antennas are at the far end of the lift from the viewer under the roof that was built to shield the equipment from the elements. This picture was taken in September with the foliage largely still present. The cables coming from the lift are a ground cable to an earth ground and one of 4 tethers used in windy conditions.

of 0.8 microseconds at a rate of approximately 20 Hz. We considered two sets of data from this experiment. Initially, the Barth pulse source was operated at lower amplitude and 35 pulses of clutter signals were obtained at each site but different time. These pulses have been averaged to remove the random noise. Data have been collected from 10 different sites. one collection of transmitted pulse and received backscattering are shown in Figures 8(a) and 8(b), respectively. The unit of clutter amplitude in this paper is "V". Although pulse-to-pulse variability was noted for collections of received echoes, the decay profiles of returned signals are quite similar. These data are referred to as dataset I.

Later, additional improvements were made in the measurement procedure, including the improved isolation of transmit and receive antennas, the addition of a log-periodic antenna (Antenna Research Associates LPC-2010-C) as a transmit antenna, and the EMCO ridged waveguide horn (Microwave horn, EMCO 3106). Echoes for dataset II were collected using this higher-amplitude transmitted pulses. Two collections at different site with 100 pulses average have been obtained; one of which is shown in Figure 8(c). To make them clearer to readers, we provide expanded views of received traces from samples 10.000 to 12.000 in Figure 9.

4. Statistical Analysis of the Foliage Clutter

4.1. Maximum Likelihood Estimation. Using the collected clutter data mentioned above, we apply Maximum Likelihood Estimation (MLE) approach to estimate the parameters of the log-logistic, log-normal, Weibull, and Nakagami models. MLE is often used when the sample data are known and parameters of the underlying probability distribution are to be estimated [29, 30]. It is generalized as follows.

Let $y_1, y_2, \ldots, y_N$ be N independent samples drawn from a random variable $\mathbf{Y}$ with m parameters $\theta_1, \theta_2, \ldots, \theta_m$, where $\theta_i \in \theta$, then the likelihood function expressed as a function of θ conditional on $\mathbf{Y}$ is

$$L_N(\mathbf{Y} \mid \theta) = \prod_{k=1}^{N} f_{Y|\theta}(y_k \mid \theta_1, \theta_2, \ldots, \theta_m). \tag{12}$$

The maximum likelihood estimate of θ_1, θ_2,..., θ_m is the set of values $\hat{\theta}_1, \hat{\theta}_2, \ldots, \hat{\theta}_m$ that maximize the likelihood function $L_N(\mathbf{Y} \mid \theta)$.

As the logarithmic function is monotonically increasing, maximizing $L_N(\mathbf{Y} \mid \theta)$ is equivalent to maximizing $\ln(L_N(\mathbf{Y} \mid \theta))$. Hence, it can be shown that a necessary but not sufficient condition to obtain the ML estimate $\hat{\theta}$ is to solve the likelihood equation

$$\frac{\partial}{\partial \theta} \ln(L_N(\mathbf{Y} \mid \theta)) = 0. \tag{13}$$

Note that the amplitude of foliage clutter faded with the increase of sample time. Even at the same sample, it varies for different collections. In order to better analyze its randomness, we studied each collection. Using the collected clutter radar mentioned above, we apply MLE to obtain $\hat{\mu}$ and $\hat{\sigma}$ for log-logistic, $\hat{\mu}$ and $\hat{\sigma}$ for the log-normal, $\hat{a}$ and $\hat{b}$ for the Weibull, and $\hat{\mu}$ and $\hat{\omega}$ for the Nakagami. The estimation results for dataset I are listed in Table 1. We also explore the standard deviation (STD) error of each parameter. These descriptions are shown in Table 1 in the form of ε_x, where x denotes different parameter for each model. We also calculate the average values of estimated parameters and their STD errors in Table 2.

From Tables 1 and 2, it can be easily seen that STD errors for log-logistic and log-normal parameters are less than 0.02 and the estimated parameters for these two models vary little from data to data compared to parameters of Weibull and Nakagami. It is obvious that log-logistic model provides the smallest STD error for all the 10 collections compared to log-normal. Although accurate shape parameter estimation can be achieved by both Weibull and Nakagami models, their scale parameters are not acceptable.

The estimation results for dataset II are shown in Table 3. Due to the improvement on this set of signal, STD error for log-logistic and log-normal parameters have been reduced compared to those in dataset I. However, for Weibull and Nakagami, it is a different case, which implies that log-logistic and log-normal are much more accurate to model foliage clutter.

In view of smaller error in parameter estimation, log-logistic model fits the collected data best compared to log-normal, Weibull, and Nakagami. Log-normal model is also acceptable.

Table 1: Estimated parameters for dataset I.

PDF	Log-Logistic	Log-normal	Weibull	Nakagami
Data 1	$\hat{\mu} = 7.24161$	$\hat{\mu} = 7.0455$	$\hat{a} = 2975.33$	$\hat{\mu} = 0.177062$
	$\hat{\sigma} = 1.06483$	$\hat{\sigma} = 2.20761$	$\hat{b} = 0.594979$	$\hat{\omega} = 9.09663e+007$
	$\varepsilon_\mu = 0.0141212$	$\varepsilon_\mu = 0.0174527$	$\varepsilon_a = 41.6157$	$\varepsilon_\mu = 0.00150615$
	$\varepsilon_\sigma = 0.00724181$	$\varepsilon_\sigma = 0.0123415$	$\varepsilon_b = 0.00356925$	$\varepsilon_\omega = 1.70907e+006$
Data 2	$\hat{\mu} = 6.9716$	$\hat{\mu} = 6.72573$	$\hat{a} = 2285.13$	$\hat{\mu} = 0.162375$
	$\hat{\sigma} = 1.2126$	$\hat{\sigma} = 2.33617$	$\hat{b} = 0.563747$	$\hat{\omega} = 7.4776e+007$
	$\varepsilon_\mu = 0.014747$	$\varepsilon_\mu = 0.0184691$	$\varepsilon_a = 33.7127$	$\varepsilon_\mu = 0.00137422$
	$\varepsilon_\sigma = 0.00773723$	$\varepsilon_\sigma = 0.0130602$	$\varepsilon_b = 0.00337485$	$\varepsilon_\omega = 1.46679e+006$
Data 3	$\hat{\mu} = 7.00554$	$\hat{\mu} = 6.76262$	$\hat{a} = 2341.52$	$\hat{\mu} = 0.164695$
	$\hat{\sigma} = 1.10741$	$\hat{\sigma} = 2.31258$	$\hat{b} = 0.57073$	$\hat{\omega} = 7.46366e+007$
	$\varepsilon_\mu = 0.0145728$	$\varepsilon_\mu = 0.0182825$	$\varepsilon_a = 34.1207$	$\varepsilon_\mu = 0.001395$
	$\varepsilon_\sigma = 0.0076303$	$\varepsilon_\sigma = 0.0129283$	$\varepsilon_b = 0.00341448$	$\varepsilon_\omega = 1.45459e+006$
Data 4	$\hat{\mu} = 7.03055$	$\hat{\mu} = 6.80711$	$\hat{a} = 2395.85$	$\hat{\mu} = 0.167391$
	$\hat{\sigma} = 1.07858$	$\hat{\sigma} = 2.25973$	$\hat{b} = 0.579381$	$\hat{\omega} = 7.4926e+007$
	$\varepsilon_\mu = 0.0142027$	$\varepsilon_\mu = 0.0178647$	$\varepsilon_a = 34.4066$	$\varepsilon_\mu = 0.0014916$
	$\varepsilon_\sigma = 0.00741556$	$\varepsilon_\sigma = 0.0126329$	$\varepsilon_b = 0.00345156$	$\varepsilon_\omega = 1.44727e+006$
Data 5	$\hat{\mu} = 7.16226$	$\hat{\mu} = 6.95712$	$\hat{a} = 2806.76$	$\hat{\mu} = 0.17112$
	$\hat{\sigma} = 1.10132$	$\hat{\sigma} = 2.26592$	$\hat{b} = 0.577823$	$\hat{\omega} = 9.03298e+007$
	$\varepsilon_\mu = 0.014605$	$\varepsilon_\mu = 0.0179137$	$\varepsilon_a = 40.4226$	$\varepsilon_\mu = 0.00145265$
	$\varepsilon_\sigma = 0.00750067$	$\varepsilon_\sigma = 0.0126675$	$\varepsilon_b = 0.00347389$	$\varepsilon_\omega = 1.72749e+006$
Data 6	$\hat{\mu} = 7.01527$	$\hat{\mu} = 6.77515$	$\hat{a} = 2360.33$	$\hat{\mu} = 0.165292$
	$\hat{\sigma} = 1.10123$	$\hat{\sigma} = 2.30286$	$\hat{b} = 0.572749$	$\hat{\omega} = 7.50824e+007$
	$\varepsilon_\mu = 0.0144902$	$\varepsilon_\mu = 0.0182057$	$\varepsilon_a = 34.2753$	$\varepsilon_\mu = 0.00140035$
	$\varepsilon_\sigma = 0.00758568$	$\varepsilon_\sigma = 0.012874$	$\varepsilon_b = 0.00342376$	$\varepsilon_\omega = 1.46145e+006$
Data 7	$\hat{\mu} = 7.14523$	$\hat{\mu} = 6.94201$	$\hat{a} = 2753.69$	$\hat{\mu} = 0.170964$
	$\hat{\sigma} = 1.09486$	$\hat{\sigma} = 2.25621$	$\hat{b} = 0.578948$	$\hat{\omega} = 8.80474e+007$
	$\varepsilon_\mu = 0.0145132$	$\varepsilon_\mu = 0.0178369$	$\varepsilon_a = 39.585$	$\varepsilon_\mu = 0.00145125$
	$\varepsilon_\sigma = 0.00745994$	$\varepsilon_\sigma = 0.0126132$	$\varepsilon_b = 0.00347442$	$\varepsilon_\omega = 1.68382e+006$
Data 8	$\hat{\mu} = 6.95411$	$\hat{\mu} = 6.71591$	$\hat{a} = 2250.66$	$\hat{\mu} = 0.162448$
	$\hat{\sigma} = 1.11486$	$\hat{\sigma} = 2.31898$	$\hat{b} = 0.564989$	$\hat{\omega} = 7.31436e+007$
	$\varepsilon_\mu = 0.0146774$	$\varepsilon_\mu = 0.0183331$	$\varepsilon_a = 33.1387$	$\varepsilon_\mu = 0.00137488$
	$\varepsilon_\sigma = 0.00768003$	$\varepsilon_\sigma = 0.0129641$	$\varepsilon_b = 0.0033763$	$\varepsilon_\omega = 1.4338e+006$
Data 9	$\hat{\mu} = 7.18561$	$\hat{\mu} = 6.9715$	$\hat{a} = 2840.72$	$\hat{\mu} = 0.172324$
	$\hat{\sigma} = 1.09854$	$\hat{\sigma} = 2.27088$	$\hat{b} = 0.581219$	$\hat{\omega} = 8.97304e+007$
	$\varepsilon_\mu = 0.0145483$	$\varepsilon_\mu = 0.0179529$	$\varepsilon_a = 40.6593$	$\varepsilon_\mu = 0.00146348$
	$\varepsilon_\sigma = 0.00749265$	$\varepsilon_\sigma = 0.0126952$	$\varepsilon_b = 0.0034984$	$\varepsilon_\omega = 1.70923e+006$
Data 10	$\hat{\mu} = 7.192$	$\hat{\mu} = 6.99196$	$\hat{a} = 2869.65$	$\hat{\mu} = 0.173572$
	$\hat{\sigma} = 1.0866$	$\hat{\sigma} = 2.23975$	$\hat{b} = 0.584803$	$\hat{\omega} = 9.01631e+007$
	$\varepsilon_\mu = 0.0144166$	$\varepsilon_\mu = 0.0177067$	$\varepsilon_a = 40.837$	$\varepsilon_\mu = 0.0014747$
	$\varepsilon_\sigma = 0.0073916$	$\varepsilon_\sigma = 0.0125211$	$\varepsilon_b = 0.00351294$	$\varepsilon_\omega = 1.71142e+006$

Table 2: Averaged estimated parameters for dataset I.

PDF	Log-Logistic	Log-normal	Weibull	Nakagami
Average	$\hat{\mu} = 7.0904$	$\hat{\mu} = 6.8695$	$\hat{a} = 2588$	$\hat{\mu} = 0.1687$
	$\hat{\sigma} = 1.1061$	$\hat{\sigma} = 2.2771$	$\hat{b} = 0.5769$	$\hat{\omega} = 8.218e+007$
	$\varepsilon_\mu = 0.0145$	$\varepsilon_\mu = 0.0180$	$\varepsilon_a = 37.4316$	$\varepsilon_\mu = 0.0014$
	$\varepsilon_\sigma = 0.0075$	$\varepsilon_\sigma = 0.0127$	$\varepsilon_b = 0.0035$	$\varepsilon_\omega = 1.4905e+006$

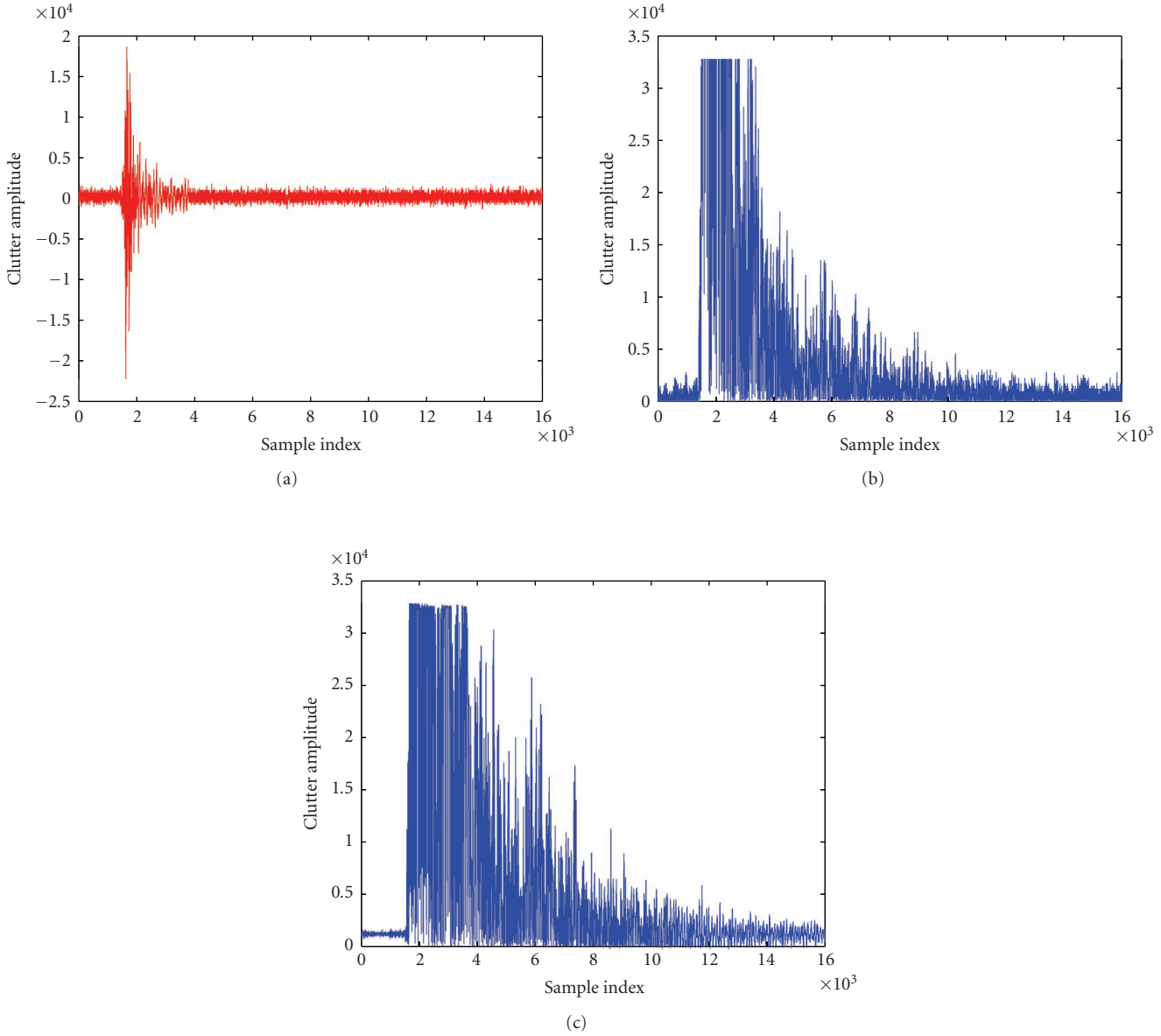

Figure 8: Clutter data: (a) transmitted pulse before antenna amplification, (b) an example of received echoes from dataset I, and (c) an example of received echoes from dataset II.

4.2. Goodness-of-Fit in Curve and RMSE. We may also observe the extent to which the PDF curve of the statistic model matches that of clutter data by calculating the averaged root mean square error (RMSE) for each dataset. Let i (i=1, 2, ..., n) be the sample index of clutter amplitude; c_i is the corresponding PDF value whereas $\hat{c}_i$ is the PDF value of the statistical model with estimated parameters by means of MLE. The RMSE is obtained by

$$\text{RMSE} = \frac{1}{k}\sum_{k}\sqrt{\frac{1}{n}\sum_{i=1}^{n}(c_i - \hat{c}_i)^2}. \tag{14}$$

Here we apply n =100 for each model and k is the number of data collections for each set.

In Figures 10 and 11, we use one collection from dataset I and II, respectively to illustrate the goodness-of-fit in curve. Also, we calculate the averaged RMSE of each model for both collected dataset I and II. The PDF of absolute amplitude of one collection of clutter data is presented by means of histogram bars. In Figure 10, it can be seen obviously that log-logistic model with MLE parameters provides the best goodness-of-fit compared to other models, since it provides the most suitable kurtosis, slope and tail. As for the maximum PDF value, the log-logistic is about 1×10^{-3}, while those of other models are over 1.2×10^{-3}. For the slope part, which connects the kurtosis and the tail, and is in the range from 0.1×10^4 to 0.5×10^4 by x axes, the log-logistic model provides the smallest skewness whereas Nakagami

Table 3: Estimated and averaged parameters for dataset ii.

PDF	Log-Logistic	Log-normal	Weibull	Nakagami
Data 1	$\hat{\mu} = 7.76868$	$\hat{\mu} = 7.79566$	$\hat{a} = 4901.07$	$\hat{\mu} = 0.239587$
	$\hat{\sigma} = 0.786511$	$\hat{\sigma} = 1.41771$	$\hat{b} = 0.743223$	$\hat{\omega} = 1.16839e+008$
	$\varepsilon_\mu = 0.0107792$	$\varepsilon_\mu = 0.011208$	$\varepsilon_a = 55.3011$	$\varepsilon_\mu = 0.00207912$
	$\varepsilon_\sigma = 0.00521601$	$\varepsilon_\sigma = 0.00792559$	$\varepsilon_b = 0.00434465$	$\varepsilon_\omega = 1.88719e+006$
Data 2	$\hat{\mu} = 7.78096$	$\hat{\mu} = 7.8046$	$\hat{a} = 4942.48$	$\hat{\mu} = 0.240593$
	$\hat{\sigma} = 0.787426$	$\hat{\sigma} = 1.41855$	$\hat{b} = 0.745233$	$\hat{\omega} = 1.17237e+008$
	$\varepsilon_\mu = 0.0107917$	$\varepsilon_\mu = 0.0112147$	$\varepsilon_a = 55.6114$	$\varepsilon_\mu = 0.00208848$
	$\varepsilon_\sigma = 0.0052213$	$\varepsilon_\sigma = 0.00793033$	$\varepsilon_b = 0.0043612$	$\varepsilon_\omega = 1.88953e+006$
Average	$\hat{\mu} = 7.7748$	$\hat{\mu} = 7.7881$	$\hat{a} = 4921.8$	$\hat{\mu} = 0.2401$
	$\hat{\sigma} = 0.7870$	$\hat{\sigma} = 1.4181$	$\hat{b} = 0.7442$	$\hat{\omega} = 1.1704+008$
	$\varepsilon_\mu = 0.0108$	$\varepsilon_\mu = 0.0112$	$\varepsilon_a = 55.4565$	$\varepsilon_\mu = 0.0021$
	$\varepsilon_\sigma = 0.0052$	$\varepsilon_\sigma = 0.0079$	$\varepsilon_b = 0.0044$	$\varepsilon_\omega = 1.8884+006$

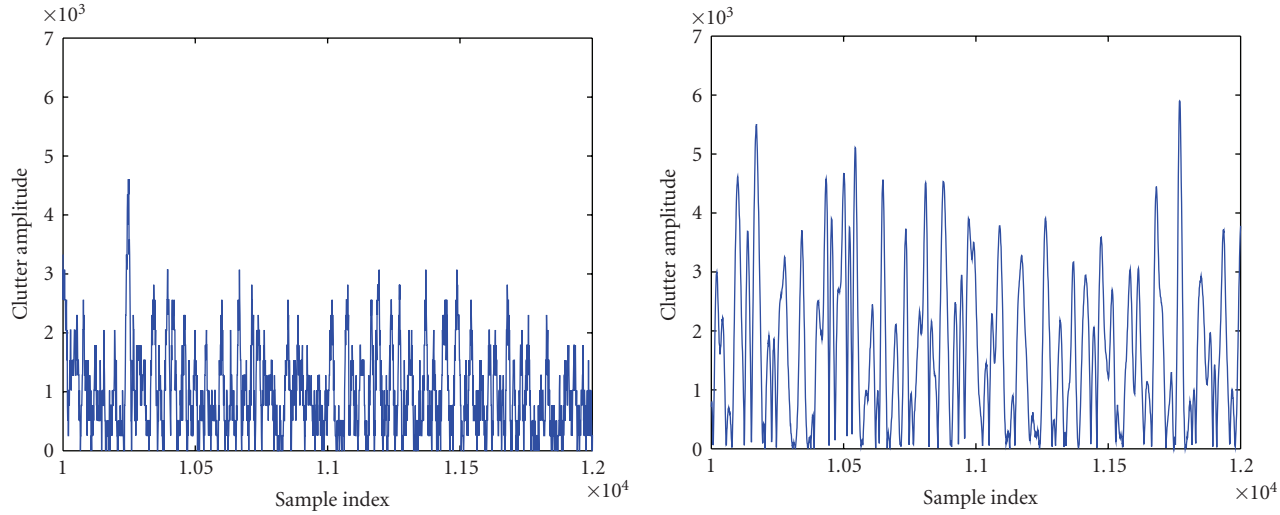

Figure 9: Expanded view from clutter samples 10.000 to 12.000 (a) from dataset I, and (b) from dataset II.

provides the largest. Examination of these tails shows that log-logistic and log-normal provide very similar-valued tails, while tails of the Weibull and the Nakagami are lager than the collected data. Meanwhile, we obtain that $\text{RMSE}_{\text{log-logistic}} = 2.5425\times10^{-5}$, $\text{RMSE}_{\text{log-normal}} = 3.2704\times10^{-5}$, $\text{RMSE}_{\text{Weibull}} = 3.7234 \times 10^{-5}$, and $\text{RMSE}_{\text{Nakagami}} = 5.4326 \times 10^{-5}$. This also illustrates that the log-logistic model is more accurate than the other three models.

Similarly, in Figure 11 histogram bars denote the PDF of the absolute amplitude of one collection of clutter data from set II. Compared to Figure 10, the log-logistic and the log-normal provide similar extent of goodness-of-fit. Weibull is worse since it cannot fit well in either kurtosis or tail, while Nakagami is the worst and unacceptable. Also, we obtain $\text{RMSE}_{\text{log-logistic}} = 2.739 \times 10^{-5}$, $\text{RMSE}_{\text{log-normal}} = 3.1866 \times 10^{-5}$, $\text{RMSE}_{\text{Weibull}} = 3.6361 \times 10^{-5}$, and $\text{RMSE}_{\text{Nakagami}} = 4.4045 \times 10^{-5}$. This illustrates that for clutter backscattering dataset II, the log-logistic model still fits the best.

5. Target Detection Performance

One of the primary goals for a radar is target detection; therefore based on clutter models that have been investigated in the previous sections, we apply a special case of the Bayesian criterion named Neyman-Parson criterion to analyze the target detection performance in the foliage environment.

If the received sample signal is R, then the two hypotheses are shown as follows.

$$H_0 : R = C + n,$$
$$H_1 : R = S + C + n, \tag{15}$$

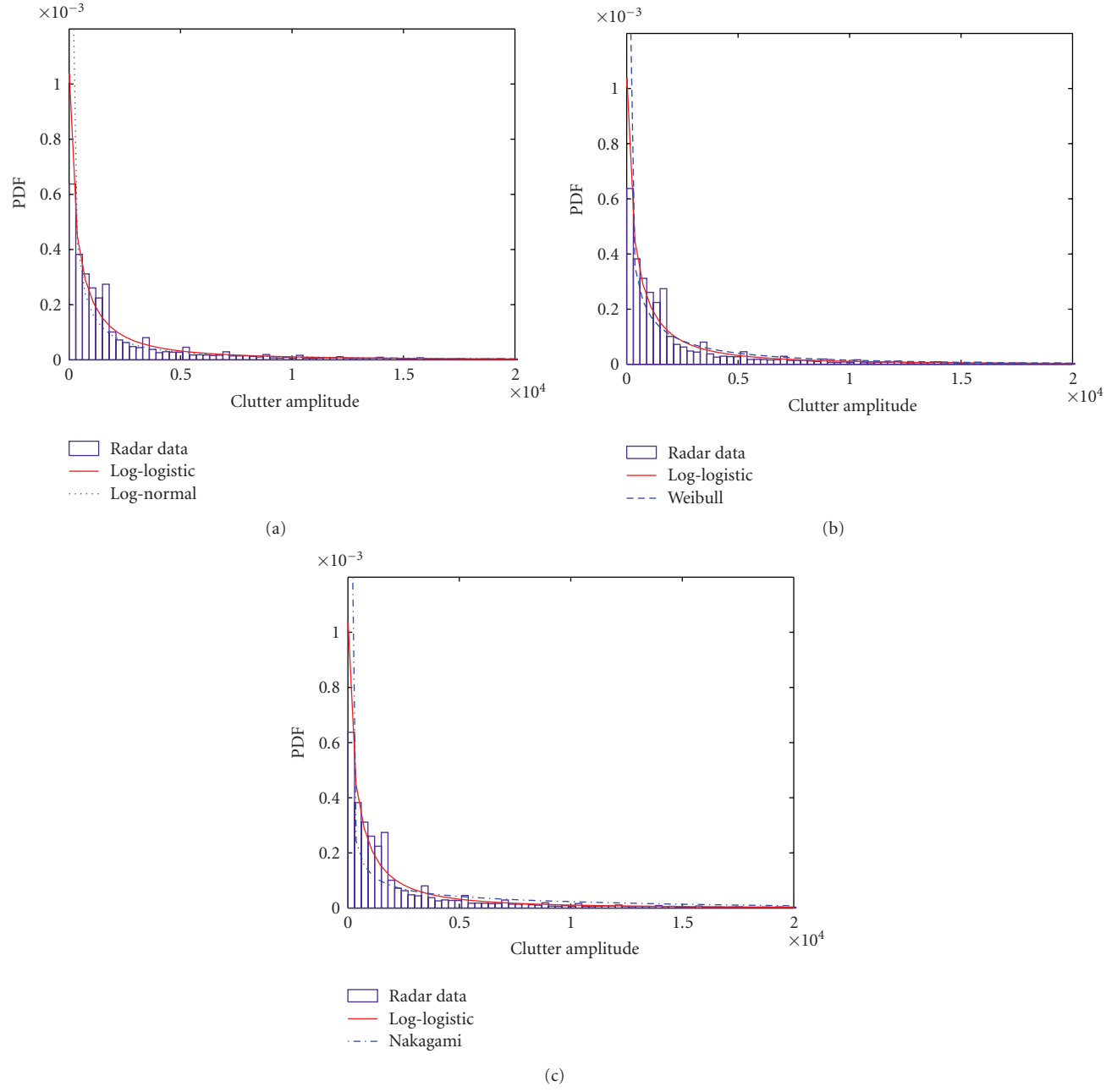

FIGURE 10: Clutter model comparison from dataset I: (a) log-logistic versus log-normal, (b) log-logistic versus Weibull, and (c) log-logistic versus Nakagami. $\text{RMSE}_{\text{log-logistic}} = 2.5425 \times 10^{-5}$, $\text{RMSE}_{\text{log-normal}} = 3.2704 \times 10^{-5}$, $\text{RMSE}_{\text{Weibull}} = 3.7234 \times 10^{-5}$, and $\text{RMSE}_{\text{Nakagami}} = 5.4326 \times 10^{-5}$.

where C and n represent the random variable of clutter and noise, respectively. C follows log-logistic model with both parameters μ and σ, and n is Gaussian noise with zero mean and variance ν^2. S is the target signal, which assumes to be a constant for simplicity.

Therefore $f(R \mid H_0)$ and $f(R \mid H_1)$ mean that

(i) $f(R \mid H_0)$ = PDF of R given that a target was not present,

(ii) $f(R \mid H_1)$ = PDF of R given that a target was present.

They can be denoted as follows.

$$f(R \mid H_0) = \int_0^\infty \frac{e^{(\ln r-\mu)/\sigma}}{\sigma r\left(1+e^{(\ln r-\mu)/\sigma}\right)^2} \times \frac{1}{\sqrt{2\pi}\nu} e^{-(R-r)^2/2\nu^2} dr, \tag{16}$$

$$f(R \mid H_1) = \int_0^\infty \frac{e^{((\ln(r-s)-\mu)/\sigma)}}{\sigma(r-s)\left(1+e^{((\ln(r-s)-\mu)/\sigma)}\right)^2} \times \frac{1}{\sqrt{2\pi}\nu} e^{-(R-s-r)^2/2\nu^2} dr. \tag{17}$$

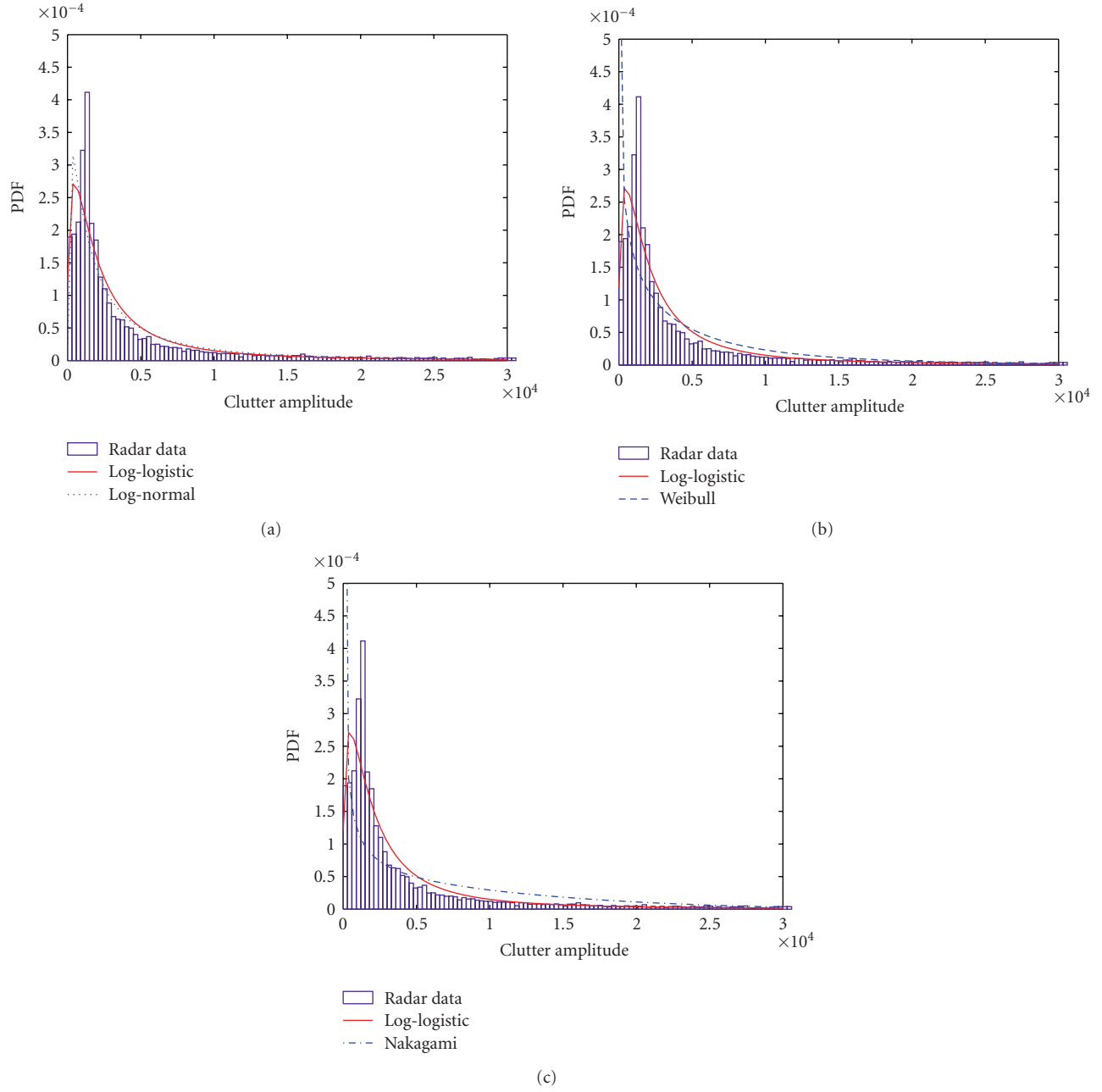

FIGURE 11: Clutter model comparison from dataset II: (a) log-Logistic versus log-normal, (b) log-logistic versus Weibull (c), and log-logistic versus Nakagami. $\text{RMSE}_{\text{log-logistic}} = 2.739 \times 10^{-5}$, $\text{RMSE}_{\text{log-normal}} = 3.1866 \times 10^{-5}$, $\text{RMSE}_{\text{Weibull}} = 3.6361 \times 10^{-5}$, and $\text{RMSE}_{\text{Nakagami}} = 4.4045 \times 10^{-5}$.

If the probability that a target was not present is $P(H_0)$ whereas the probability that a target was present is $P(H_1)$, then PDF of R is

$$f(R) = P(H_0)f(R \mid H_0) + P(H_1)f(R \mid H_1). \tag{18}$$

To decide whether there is a target or not, Neyman-Pearson detection rule is shown as

$$\frac{f(R \mid H_0)}{f(R \mid H_1)} \underset{H_1}{\overset{H_0}{\gtrless}} \frac{P(H_1)}{P(H_0)}. \tag{19}$$

In case of $P(H_1) = P(H_0)$, (20) is simplified as

$$f(R \mid H_0) \underset{H_1}{\overset{H_0}{\gtrless}} f(R \mid H_1), \tag{20}$$

which actually is

$$\frac{e^{[((s^2-2s(R-r))/2\gamma^2)+(\ln((r/r-s))/\sigma)]}}{(r/(r-s))\left[\left(1+e^{((\ln r-\mu)/\sigma)}\right)/\left(1+e^{((\ln(r-s)-\mu)/\sigma)}\right)\right]^2} \underset{H_1}{\overset{H_0}{\gtrless}} 1. \tag{21}$$

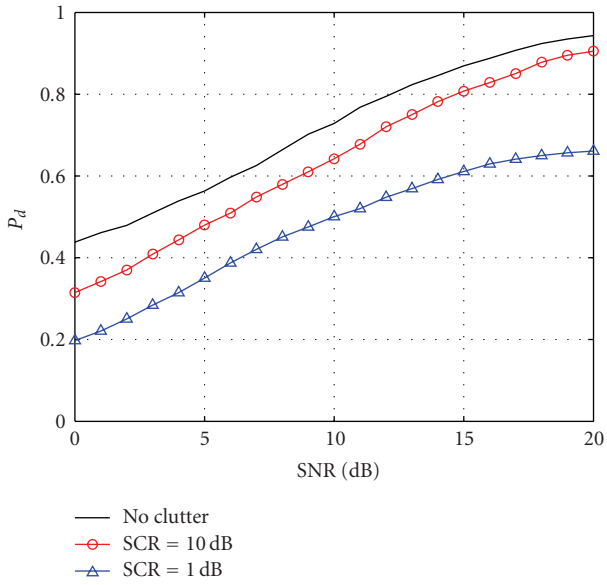

Figure 12: Probability of detection.

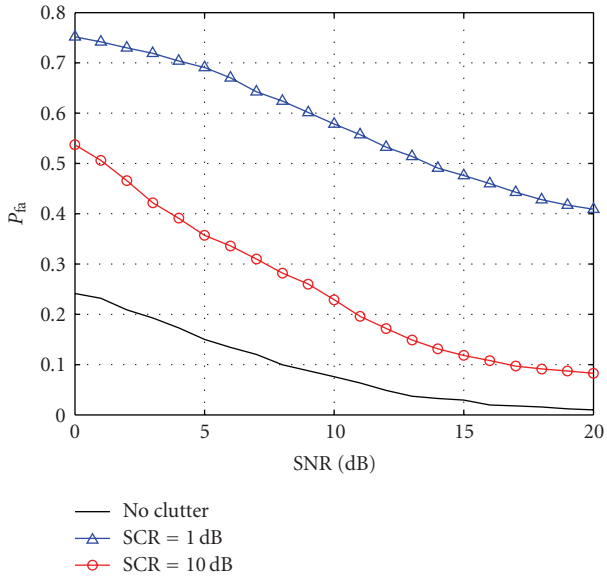

Figure 13: Probability of false alarm.

It is easy to obtain the decision threshold T in terms of the above function:

$$T = -\frac{\nu^2}{s}\ln\left[\frac{1+e^{((\ln r-\mu)/\sigma)}}{1+e^{((\ln(r-s)-\mu)/\sigma)}}\right]^2 + \frac{\nu^2[\ln(r/(r-s))-\sigma]}{s\sigma} + \frac{s}{2} + r. \tag{22}$$

Under hypothesis H_0, a false alarm occurs anytime $R > T$, therefore the probability of false alarm is

$$\begin{aligned} P_{\mathrm{FA}} &= \int_T^\infty f(R \mid H_0)dR \\ &= \frac{1}{\sqrt{2\pi}\sigma\nu}\int_T^\infty\int_0^\infty \frac{e^{[-((R-r)^2/2\nu^2)+((\ln r-\mu)/\sigma)]}}{\left(1+e^{((\ln r-\mu)/\sigma)}\right)^2 r}dr\,dR. \end{aligned} \tag{23}$$

Similarly, under hypothesis H_1, when $R > T$, the target is detectable. Therefore the probability of detection is

$$\begin{aligned} P_D &= \int_T^\infty f(R \mid H_1)dR, \\ &= \frac{1}{\sqrt{2\pi}\sigma\nu}\int_T^\infty\int_0^\infty \frac{e^{[-((R-r-s)^2/2\nu^2)+(\ln(r-s)-\mu)/\sigma]}}{\left(1+e^{((\ln(r-s)-\mu)/\sigma)}\right)^2 (r-s)}dr\,dR. \end{aligned} \tag{24}$$

Figure 12 shows the probability of detection for a fluctuating radar target using Monte Carlo simulation. The "no clutter" curve describes the situation when there are only radar echoes and noise. Swerling II model is applied for the detection [31]. "SCR" stands for signal-to-clutter ratio, where log-logistic clutter model is used, and "SNR" is the signal to noise ratio. These curves show that, no matter what SCR is, the clutter generally reduces the probability of detection. When SCR increases, the probability of detection will become more close to the value of "no clutter" case along with the increase of SNR. Similarly, Figure 13 illustrates the probability of false alarm, which shows that the clutter tremendously increase the probability of false alarm.

6. Conclusion

On a basis of two sets of foliage clutter data collected by a UWB radar, we show that it is more accurate to describe the amplitude of foliage clutter using log-logistic statistic model rather than log-normal, Weibull, or Nakagami. Log-normal is also acceptable. The goodness-of-fit for Weibull is worse whereas that of Nakagami is the worst. Our contribution is not only the new proposal on the foliage clutter model with detailed parameters, but also providing the criteria and approaches based on which the statistical analysis is obtained. Further, the theoretical study on the probability of detection and the probability of false alarm in the presence of log-logistic foliage clutter are discussed. Future research will investigate the characteristics of targets and the design of radar receivers for the log-logistic clutter so as to improve the performance of target detection, tracking and identification in foliage.

Acknowledgments

This work was supported in part by the U.S. Office of Naval Research under Grant N00014-07-1-0395 and Grant 00014-07-1-1024 and in part by the National Science Foundation under Grant CNS-0721515, Grant CNS-0831902, Grant CCF-0956438, and Grant CNS-0964713.

References

[1] M. L. Imhoff, "A theoretical analysis of the effect of forest structure on synthetic aperture radar backscatter and the remote sensing of biomass," *IEEE Transactions on Geoscience and Remote Sensing*, vol. 33, no. 2, pp. 341–352, 1995.

[2] M. I. Skolnik, *Introduction to Radar Systems*, McGraw-Hill, New York, NY, USA, 3rd edition, 2001.

[3] F. L. Posner, "Spiky sea clutter at high range resolutions and very low grazing angles," *IEEE Transactions on Aerospace and Electronic Systems*, vol. 38, no. 1, pp. 58–73, 2002.

[4] D. A. Shnidman, "Generalized radar clutter model," *IEEE Transactions on Aerospace and Electronic Systems*, vol. 35, no. 3, pp. 857–865, 1999.

[5] G. Hennessey, H. Leung, A. Drosopoulos, and P. C. Yip, "Sea-clutter modeling using a radial-basis-function neural network," *IEEE Journal of Oceanic Engineering*, vol. 26, no. 3, pp. 358–372, 2001.

[6] N. Xie, H. Leung, and H. Chan, "A multiple-model prediction approach for sea clutter modeling," *IEEE Transactions on Geoscience and Remote Sensing*, vol. 41, no. 6, pp. 1491–1502, 2003.

[7] J. G. Fleischman, S. Ayasli, E. M. Adams, and D. R. Gosselin, "Foliage attenuation and backscatter analysis of SAR imagery," *IEEE Transactions on Aerospace and Electronic Systems*, vol. 32, no. 1, part 3, pp. 135–144, 1996.

[8] J. W. Mccorkle, "Early results from the Army Research Laboratory ultrawide-bandwidth foliage penetration SAR," in *Underground and Obscured Object Imaging and Detection*, vol. 1942 of *Proceedings of SPIE*, Orlando, Fla, USA, April 1993.

[9] D. R. Sheen, N. P. Malinas, D. W. Kletzli, T. B. Lewis, and J. F. Roman, " Foliage transmission measurements using a ground-based ultrawide band (300–1300 MHz) SAR system," *IEEE Transactions on Geoscience and Remote Sensing*, vol. 32, no. 1, pp. 118–130, 1994.

[10] S. Watts, "Radar detection prediction in K-distributed sea clutter and thermal noise," *IEEE Transactions on Aerospace and Electronic Systems*, vol. 23, no. 1, pp. 40–45, 1987.

[11] I. W. Burr, "Cumulative frequency functions," *Annals of Mathematical Statistics*, vol. 13, pp. 215–232, 1942.

[12] P. W. Mielke and E. S. Johnson, "Three-parameter kappa distribution maximum likelihood estimates and likelihood ratio tests," *Monthly Weather Review*, vol. 101, pp. 701–709, 1973.

[13] K. S. Lee, J. Sadeghipour, and J. A. Dracup, "An approach for frequency analysis of multiyear dought duration," *Water Resources Research*, vol. 22, no. 5, pp. 655–662, 1986.

[14] M. M. Shoukri, I. U. H. Mian, and D. S. Tracy, "Sampling properties of estimators of the log-logistic distribution with application to Canadian precipitation data," *The Canadian Journal of Statistics*, vol. 16, no. 3, pp. 223–236, 1988.

[15] N. K. Narda and R. K. Malik, "Dynamic model of root growth and water uptake in wheat," *Journal of Agricultural Engineering*, vol. 3, no. 3-4, pp. 147–155, 1993.

[16] R. C. Gupta, O. Akman, and S. Lvin, "A study of log-logistic model in survival analysis," *Biometrical Journal*, vol. 41, no. 4, pp. 431–443, 1999.

[17] M. Warden, "An experimental study of some clutter characteristics," in *Proceedings of AGARD Conference on Advanced Radar Systems*, May 1970.

[18] G. V. Trunk and S. F. George, "Detection of targets in non-Gaussian sea clutter," *IEEE Transactions on Aerospace and Electronic Systems*, vol. 6, no. 5, pp. 620–628, 1970.

[19] D. C. Schleher, "Radar detection in Weibull clutter," *IEEE Transactions on Aerospace and Electronic Systems*, vol. 12, no. 6, pp. 735–743, 1976.

[20] E. Limpert, W. A. Stahel, and M. Abbt, "Log-normal distributions across the sciences: keys and clues," *BioScience*, vol. 51, no. 5, pp. 341–352, 2001.

[21] W. Weibull, "A statistical distribution function of wide applicability," *Journal of Applied Mechanics*, vol. 18, no. 3, pp. 293–297, 1951.

[22] R. R. Boothe, "The Weibull distribution applied to the ground clutter backscatter coefficient," Tech. Rep. RE-TR-69-15, U.S. Army Missile Command, 1969.

[23] M. Sekine, S. Ohtani, T. Musha, et al., "Weibull-distributed ground clutter," *IEEE Transactions on Aerospace and Electronic Systems*, vol. 17, no. 4, pp. 596–598, 1981.

[24] F. A. Fay, J. Clarke, and R. S. Peters, "Weibull distributed applied to sea clutter," in *Proceedings of the International Radar Conference (Radar '77)*, vol. 155, pp. 101–104, October 1977.

[25] M. Sekine, T. Musha, Y. Tomita, T. Hagisawa, T. Irabu, and E. Kiuchi, "Weibull-distributed sea clutter," *IEE Proceedings F*, vol. 130, no. 5, p. 476, 1983.

[26] M. Sekine, T. Musha, Y. Tomita, T. Hagisawa, T. Irabu, and E. Kiuchi, "On Weibull-distributed weather clutter," *IEEE Transactions on Aerospace and Electronic Systems*, vol. 15, no. 6, pp. 824–830, 1979.

[27] G. A. Tsihrintzis and C. L. Nikias, "Evaluation of fractional, lower-order statistics-based detection algorithms on real radar sea-clutter data," *IEE Proceedings: Radar, Sonar and Navigation*, vol. 144, no. 1, pp. 29–37, 1997.

[28] J. A. Henning, *Design and performance of an ultra-wideband foliage penetrating noise radar*, M.S. thesis, University of Nebraska, May 2001.

[29] J. L. Devore, *Probability and Statistics for Engineering and the Sciences*, BrooksiCole, Monterey, Calif, USA, 1982.

[30] M. Barkat, *Signal Deteciton and Estimation*, Artech House, London, UK, 2nd edition, 2005.

[31] M. A. Richards, *Fundamentals of Radar Signal Processing*, McGraw-Hill, New York, NY, USA, 2005.

NEW-CATR: Network-enabled Electronic Warfare for Collaborative Automatic Target Recognition

Qilian Liang
Department of Electrical Engineering
University of Texas at Arlington
Arlington, TX 76019-0016, USA
E-mail: liang@uta.edu

Sherwood W. Samn
Air Force Research Laboratory/HEX
Brooks City Base
San Antonio, TX 78235, USA
E-mail: Sherwood.samn@brooks.af.mil

***Abstract*— Network-enabled Electronic Warfare (NEW) is to develop modeling and simulation efforts to explore the advantages and limitations of network-enabled electronic warfare concepts. The advantages of linking multiple electronic support measures (ESM) and electronic attack (EA) assets to achieve improved capabilities across a networked battleforce have yet to be quantified. In this paper, we will use radar sensors as ESM and EA assets to demonstrate the advantages of NEW in Collaborative Automatic Target Recognition (CATR). We apply the NEW to CATR via waveform diversity combining and and propose maximum-likehood (ML)-ATR algorithms for nonfluctuating target as well as fluctuating target. Simulation results show that our NEW-CATR performs much better than single sensor-based ATR algorithm for nonfluctuating targets or fluctuating targets. Conclusions are drawn based on our analysis and simulations and future research works on this research topic are discussed.**[1]

Index Terms : Network-enabled electronic warfare, radar sensor networks, waveform diversity, collaborative automatic target recognition, maximum-likelihood, interferences.

I. Introduction and Motivation

In current and future military operational environments, such as Global War on Terrorism (GWOT) and Maritime Domain Awareness (MDA), warfighters require technologies evolved to support information needs regardless of location and consistent with the users level of command or responsibility and operational situation. To support this need, the U.S. Department of Defense (DoD) has developed the concept of Network Centric Warfare (NCW), defined as "*military operations that exploit state-of-the-art information and networking technology to integrate widely dispersed human decision makers, situational and targeting sensors, and forces and weapons into a highly adaptive, comprehensive system to achieve unprecedented mission effectiveness*" [1]. The goal of electronic warfare is to control the electromagnetic (EM) spectrum by exploiting, disrupting, or denying enemy use of the spectrum while ensuring its use by friendly forces [2].

[1]1-4244-1513-06/07/$25.00 ©2007 IEEE

Network-enabled Electronic Warfare (NEW) is to develop modeling and simulation efforts to explore the advantages and limitations of network-enabled electronic warfare concepts. The advantages of linking multiple electronic support measures (ESM) and electronic attack (EA) assets to achieve improved capabilities across a networked battleforce have yet to be quantified [2]. In this paper, we will use radar sensors as ESM and EA assets to demonstrate the advantages of NEW in Collaborative Automatic Target Recognition (CATR). The network of radar sensors should operate with multiple goals managed by an intelligent platform network that can manage the dynamics of each radar to meet the common goals of the platform, rather than each radar to operate as an independent system. Therefore, it is significant to perform signal design and processing and networking cooperatively within and between platforms of radar sensors and their communication modules. This need is also testified by recent solicitations from U.S. Office of Naval Research [2][3]. For example, in [3], it is stated that "Algorithms are sought for fused, and or, coherent cross-platform Radio Frequency (RF) sensing. The focus of this effort is to improve surveillance utilizing a network, not fusion of disparate sensor products. The algorithms should be capable of utilizing RF returns from multiple aspects in a time-coordinated sensor network." In this paper, we will study waveform design and diversity algorithms for radar sensor networks. Waveform diversity is the technology that will allow one or more sensors on board a platform to automatically change operating parameters, e.g., frequency, gain pattern, and pulse repetition frequency (PRF) to meet the varying environments. It has long been recognized that judicious use of properly designed waveforms, coupled with advanced receiver strategies, is fundamental to fully utilizing the capacity of the electromagnetic spectrum. However, it is only relatively recent advances in hardware technology that are enabling a much wider range of design freedoms to be explored. As a result, there are emerging and compelling changes in system requirements such as more efficient spectrum usage, higher sensitivities, greater information content, improved robustness to errors,

reduced interference emissions, etc. The combination of these is fuelling a worldwide interest in the subject of waveform design and the use of waveform diversity techniques.

In the existing works on waveform design and selection, Fitzgerald [8] demonstrated the inappropriateness of selection of waveform based on measurement quality alone: the interaction between the measurement and the track can be indirect, but must be accounted for. Bell [6] used information theory to design radar waveform for the measurement of extended radar targets exhibiting resonance phenomena. In [5], singularity expansion method was used to design some discriminant waveforms such as K-pulse, E-pulse, and S-pulse. Sowelam and Tewfik [24] developed a signal selection strategy for radar target classification, and a sequential classification procedure was proposed to minimize the average number of necessary signal transmissions. Intelligent waveform selection was studied in [4][12], but the effect of doppler shift was not considered. In [15], the performance of constant frequency (CF) and linear frequency modulated (LFM) waveform fusion from the standpoint of the whole system was studied, but the effects of clutter was not considered. In [23], CF and LFM waveforms were studied for sonar system, but it was assumed that the sensor is nonintelligent (i.e., waveform can't be selected adaptively). All the above studies and design methods were focused on the waveform design or selection for a single active radar or sensor. In [21], cross-correlation properties of two radars are briefly mentioned and the binary coded pulses using simulated annealing [7] are highlighted. However, the cross-correlation of two binary sequences such as binary coded pulses (e.g. Barker sequence) are much easier to study than that of two analog radar waveforms. In this paper, we will focus on the waveform diversity and design for radar sensor networks using constant frequency (CF) pulse waveform.

The rest of this paper is organized as follows. In Section II we propose a RAKE structure for waveform diversity combining and propose maximum-likelihood (ML) algorithms for CATR. In Section II we propose another RAKE structure for UWB radar diversity combining. In Section IV, we conclude this paper and provide some future works.

II. NEW for Collaborative Automatic Target Recognition

In NEW, the radar sensors are networked together in an ad hoc fashion. They do not rely on a preexisting fixed infrastructure, such as a wireline backbone network or a base station. They are self-organizing entities that are deployed on demand in support of various events surveillance, battlefield, disaster relief, search and rescue, etc. Scalability concern suggests a hierarchical organization of radar sensor networks with the lowest level in the hierarchy being a cluster. As argued in [14] [10] [9] [17], in addition to helping with scalability and robustness, aggregating sensor nodes into clusters has additional benefits:

1) conserving radio resources such as bandwidth;
2) promoting spatial code reuse and frequency reuse;
3) simplifying the topology, e.g., when a mobile radar changes its location, it is sufficient for only the nodes in attended clusters to update their topology information;
4) reducing the generation and propagation of routing information; and,
5) concealing the details of global network topology from individual nodes.

In Radar Sensor Network (RSN), each radar can provide their waveform parameters such as δ_i to their clusterhead radar, and the clusterhead radar can combine the waveforms from its cluster members. In this paper, we propose a RAKE structure for waveform diversity combining, as illustrated by Fig. 1. According to this structure, the received $r_1(u,t)$ is processed by a bank of matched filters.

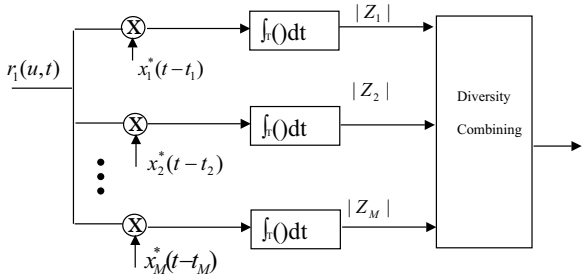

Fig. 1. Waveform diversity combining by clusterhead in RSN.

How to combine all the Z_m's ($m = 1, 2, \cdots, M$) are very similar to the diversity combining in communations to combat channel fading, and the combination schemes may be different for different applications. In this paper, we are interested in applying RSN waveform diversity to CATR, e.g., recognition that the echo on a radar display is that of an aircraft, ship, motor vehicle, bird, person, rain, chaff, clear-air turbulence, land clutter, sea clutter, bare montains, forested areas, meteors, aurora, ionized media, or other natural phenomena via collaborations among different radars. Early radars were "blob" detectors in that they detected the presence of a target and gave its location in range and angle, and radar began to be more than a blob detector and could provide recognition of one type of target from another[21]. It is known that small changes in the aspect angle of complex (multiple scatter) targets can cause major changes in the radar cross section (RCS). This has been considered in the past as a means of target recognition,

and is called *fluctuation of radar cross section with aspect angle*, but it has not had much success[21]. In this paper, we propose a maximum likelihood collaborative automatic target recognition (ML-CATR) algorithm for RSN. We will study non-fluctuating target as well as fluctuating target.

A. ML-CATR for Non-fluctuating Targets

In some sources, the non-fluctuating target is identified as "Swerling 0" or "Swerling 5" model [22]. For non-fluctuating target, the RCS $\alpha_m(u)$ is just a constant α for a given target. Noise $n(u,\tau)$ is a zero-mean Gaussian random variable for given τ, so $|Z_m|$ follows Rician distribution because signal $E\alpha(u)$ is a positive constant $E\alpha$ for non-fluctuating target. Let $y_m \stackrel{\triangle}{=} |Z_m|$, then the probability density function (pdf) of y_m is

$$f(y_m) = \frac{2y_m}{\sigma^2}\exp[-\frac{(y_m^2+\lambda^2)}{\sigma^2}]I_0(\frac{2\lambda y_m}{\sigma^2}) \quad (1)$$

where

$$\lambda = E\alpha, \quad (2)$$

σ^2 is the noise power (with I and Q sub-channel power $\sigma^2/2$), and $I_0(\cdot)$ is the zero-order modified Bessel function of the first kind. Let $\mathbf{y} \stackrel{\triangle}{=} [y_1, y_2, \cdots, y_M]$, then the pdf of $\mathbf{y}$ is

$$f(\mathbf{y}) = \prod_{m=1}^{M} f(y_m) \quad (3)$$

Our CATR is a multiple-category hypothesis testing problem, i.e., to decide a target category (e.g. aircraft, ship, motor vehicle, bird, etc) based on $r_1(u,t)$. Assume there are totally N categories and category n target has RCS α_n, so the ML-CATR algorithm to decide a target category C can be expressed as,

$$\begin{aligned} C &= \arg\max_{n=1}^{N} f(\mathbf{y}|\lambda = E\alpha_n) \quad (4)\\ &= \arg\max_{n=1}^{N} \prod_{m=1}^{M} \frac{2y_m}{\sigma^2}\exp[-\frac{(y_m^2+E^2\alpha_n^2)}{\sigma^2}] \\ &\quad I_0(\frac{2E\alpha_n y_m}{\sigma^2}) \quad (5)\end{aligned}$$

B. ML-CATR for Fluctuating Targets

Fluctuating target modeling is more realistic in which the target RCS is drawn from either the Rayleigh or chi-square of degree four pdf. The Rayleigh model describes the behavior of a complex target consisting of many scatters, none of which is dominant. The fourth-degree chi-square models targets having many scatters of similar strength with one dominant scatter. Based on different combinations of pdf and decorrelation characteristics (scan-to-scan or pulse-to-pulse decorrelation), four Swerling models are used[19]. In this paper, we will focus on "Swerling 2" model which is Rayleigh distribution with pulse-to-pulse decorrelation. The pulse-to-pulse decorrelation implies that each individual pulse results in an independent value for RCS α.

For Swerling 2 model, the RCS $|\alpha(u)|$ follows Rayleigh distribution and its I and Q subchannels follow zero-mean Gaussian distributions with variance γ^2. Assume

$$\alpha(u) = \alpha_I(u) + j\alpha_Q(u) \quad (6)$$

and $n(u) = n_I(u) + jn_Q(u)$ follows zero-mean complex Gausian distribution with variance σ^2 for the I and Q subchannels. Z_m is a zero-mean Gaussian random variable with variance $E^2\gamma^2 + \sigma^2$ for the I and Q subchannels, which means $y_m \stackrel{\triangle}{=} |Z_m|$ follows Rayleigh distribution with parameter $\sqrt{E^2\gamma^2+\sigma^2}$,

$$f(y_m) = \frac{y_m}{E^2\gamma^2+\sigma^2}\exp(-\frac{y_m^2}{E^2\gamma^2+\sigma^2}) \quad (7)$$

The mean value of y_m is $\sqrt{\frac{\pi(E^2\gamma^2+\sigma^2)}{2}}$, and variance is $\frac{(4-\pi)(E^2\gamma^2+\sigma^2)}{2}$. The variance of signal is $\frac{(4-\pi)E^2\gamma^2}{2}$ and the variance of noise is $\frac{(4-\pi)\sigma^2}{2}$.

Let $\mathbf{y} \stackrel{\triangle}{=} [y_1, y_2, \cdots, y_M]$, then the pdf of $\mathbf{y}$ is

$$f(\mathbf{y}) = \prod_{m=1}^{M} f(y_m) \quad (8)$$

Assume there are totally N categories and category n target has RCS $\alpha_n(u)$ (with variance γ_n^2), so the ML-ATR algorithm to decide a target category C can be expressed as,

$$\begin{aligned} C &= \arg\max_{n=1}^{N} f(\mathbf{y}|\gamma = \gamma_n) \quad (9)\\ &= \arg\max_{n=1}^{N} \prod_{m=1}^{M} \frac{y_m}{E^2\gamma_n^2+\sigma^2}\exp(-\frac{y_m^2}{E^2\gamma_n^2+\sigma^2})\end{aligned}$$

C. Simulations

Radar sensor networks will be required to detect a broad range of target classes. Too often, the characteristics of objects that are not of interest (e.g., bird) will be similar to those of threat objects (e.g., missile). Therefore, new techniques to discriminate threat against undesired detections (e.g. birds, etc.) are needed. We applied our ML-CATR to this important application, to recognize a target from many target classes. We assume that the domain of target classes is known a priori (N in Sections II-A and II-B), and that the RSN is confined to work only on the known domain.

For non-fluctuating target recognition, our targets have 5 classes with different RCS values, which are summarized in Table I[21]. We applied the ML-CATR algorithms in Section II-A (for nonfluctuating target case) to classify an unknown target as one of these 5 target classes. At each average SNR value, we ran Monte-Carlo simulations

for 10^5 times for each target. The average SNR value is based on the average power from all targets (signal variance), so the actual SNRs for bird and missile are much lower than the average SNR value. For example, at the average SNR=16dB, the bird target SNR=-33.1646dB, and missile target SNR=0.8149dB; and at average SNR=20dB, the bird target SNR=-29.1646dB, and missile target SNR=4.8149dB. In Fig. 2(a)(b), we plotted the probability of ATR error in bird and missile recognition when they are assumed as nonfluctuating targets. Observe both figures, single radar system can't perform well in both recognitions, and their probability of ATR error is above 10%, which can't be used for real-world ATR. However, the 5-radar RSN and 10-radar RSN can maintain very low ATR errors. In Fig. 2(c), we plotted the average probability of ATR error for all 5 targets recognition. Since the other 3 targets (different aircrafts) have much higher SNRs, so their ATR error is lower, which makes the average probability of ATR error lower.

For fluctuating target recognition, we assume the fluctuating targets follow "Swerling 2" model (Rayleigh with pulse-to-pulse decorrelation), and assume the RCS value listed in Table I to be the standard deviation (std) γ_n of RCS $\alpha_n(u)$ for target n. We applied the ML-CATR algorithm in Section II-B (for fluctuating target case) for target recognition within the 5 targets domain. Similarly we ran Monte-Carlo simulations at each SNR value. In Fig. 3(a)(b)(c), we plot the ATR performance for fluctuating targets and compared the performances of single radar system, 5-radar RSN, and 10-radar RSN. Observe that the two RSNs perform much better than the single radar system. The ATR error for missile is higher than that of bird because Rayleigh distribution of missile has lots of overlap with its neighbor targets (aircrafts). Comparing Fig. 2(a)(b)(c) to Fig. 3(a)(b)(c), it is clear that higher SNRs are needed for fluctuating target recognition comparing to nonfluctuating target recognition. According to Skolnik[21], radar performance with probability of recognition error (p_e) less than 10% is good enough. Our RSN with waveform-diversity can have probability of ATR error much less than 10% for each target ATR as well as the average ATR for all targets. However, the single radar system has probability of ATR error much higher than 10%. Observe Fig. 3(c), the average probability of ATR error of single-radar is impossible to be less than 10% even at extreme high SNR. Our RSN with waveform diversity is very promising to be used for real-world ATR.

III. Sense-through-Foliage Target Detection Using Radar Sensor Network

In Figs. 4a and 4b, we plot two collections using UWB radars. Fig. 4a has no target on range, and Fig. 4b has target at samples around 14,000. We plot the echo differences between Figs. 4a and 4b in Fig. 4c. However, it is impossible to identify whether there is any target and where there is target based on Fig. 4c. Since significant pulse-to-pulse variability exists in the echos, this motivate us to explore the spatial and time diversity using Radar Sensor Networks (RSN).

TABLE I

RCS values at microwave frequency for 5 targets.

Index n	Target	RCS
1	Bird	0.01
2	Conventional unmanned winged missile	0.5
3	Small single-engine aircraft	1
4	Small flighter aircraft or 4 passenger jet	2
5	Large flighter aircraft	6

In Fig. 5, the echo, i.e., RF response by the pulse of each cluster-member sensor, will be combined by the clusterhead using a weighted average, and the weight w_i is determined by the power of each echo $x_i(n)$ (n is the sample index),

$$w_i = \frac{E_i}{\sum_{i=1}^{M} E_i} \tag{10}$$

and

$$E_i = \text{var}(x_i(n)) + [\text{mean}(x_i(n))]^2 \tag{11}$$

We ran simulations for $M = 30$, and plot the power of AC values in Figs. 6a and 6b for the two cases (with target and without target) respectively. Observe that in Fig. 6b, the power of AC values (around sample 14,000) where the target is located is non-fluctuating (monotonically increase then decrease). Although some other samples also have very high AC power values, it is very clear that they are quite fluctuating and the power of AC values behaves like random noise because generally the clutter has Gaussian distribution in the frequency domain.

IV. Conclusions and Future Works

We have studied constant frequency pulse waveform design and diversity in radar sensor networks. We proposed a RAKE structure for waveform diversity combining in RSN. As an application example, we applied the waveform design and diversity to CATR in RSN and proposed ML-CATR algorithms for nonfluctuating target as well as fluctuating target. Simulation results show that RSN using our waveform diversity-based ML-ATR algorithm performs much better than single radar system for nonfluctuating targets and fluctuating targets recognition.

In our future works, we will investigate the CATR when multiple targets co-exist in RSN, and the number of targets are time-varying. In this paper, we used spatial diversity combining. For multi-target ATR, we will further investigate spatial-temporal-frequency combining for waveform diversity in RSN.

ACKNOWLEDGEMENT

This work was supported in part by ONR under Grant N00014-07-1-0395, N00014-03-1-0466, N00014-07-1-1024, NSF under Grant CNS-0721515, and AFOSR Summer Faculty Fellowship Program Award.

REFERENCES

[1] ONR BAA 06-016, "Command and Control and Combat Systems (C2 and CS)", http://www.onr.navy.mil/02/baa/expired.asp.

[2] ONR BAA 07-009, "Electronic Warfare Discovery and Invention (D&I)," http://www.onr.navy.mil/02/baa/.

[3] ONR BAA 07-017, "NET-SENTRIC Surveillance," http://www.onr.navy.mil/02/baa/.

[4] P. Baggenstoss, "Adaptive pulselength correction (APLECORR): a strategy for waveform optimization in ultrawideband active sonar," *IEEE Trans on Oceanic Engineering*, vol. 23, no. 1, pp. 1-11, 1998.

[5] C. E. Baum, et al, "The singularity expansion method and its application to target identification", *Proc. of the IEEE*, vol 79, no. 10, Oct 1991.

[6] M. R. Bell, "Information theory and radar waveform design", *IEEE Trans on Information Theory*, vol. 39, no. 5, pp. 1578-1597, Sept 1993.

[7] H. Deng, "Synthesis of binary sequences with good correlation and cross-correlation properties by simulated annealing," *IEEE Trans on Aerospace and Electronic Systems*, vol. 32, no. 1, Jan 1996.

[8] R. Fitzgerald, "Effects of range-doppler coupling on chirp radar tracking acuracy," *IEEE Trans on Aerospace and Eletronic Systems*, vol. 10, pp. 528-532, July 1974.

[9] T.-C. Hou and T-J. Tsai, " An access-based clustering protocol for multihop wireless ad hoc networks," *IEEE J. Selected Areas in Communications*, vol. 19, no. 7, pp. 1201-1210, July 2001.

[10] A. Iwata, C. C. Chiang, G. Pei, M. Gerla, and T. W. Chen, " Scalable routing strategies for ad hoc networks," *IEEE J. Selected Areas in Communications*, vol. 17, pp. 1369-1379, 1999.

[11] R. A. Johnson and E. L. Titlebaum, "Range Doppler Uncoupling in the Doppler Tolerant Bat Signal", *Proc. of IEEE Ultrasonics Symposium*, New York, pp. 64-67, 1972.

[12] D. Kershaw and R. Evans, "Optimal waveform selection for tracking system", *IEEE Trans on Information Theory*, vol. 40, no. 5, pp. 1536-1550, 1994.

[13] Q. Liang, X. Cheng, " KUPS: Knowledge-based Ubiquitous and Persistent Sensor Networks for Threat Assessment", submitted to *IEEE Trans on Aerospace and Electronic Systems*.

[14] C. R. Lin and M. Gerla, "Adaptive clustering in mobile wireless networks," *IEEE J. Selected Areas in Communications*, vol. 16, pp. 1265-1275, 1997.

[15] R. Niu, P. Willett, and Y. Bar-Shalom, "Tracking consideration in selection of radar waveform for range and range-rate measurements", *IEEE Transactions on Aerospace and Electronic Systems*, Vol. 38, No. 2, 2002.

[16] A. Papandreou, G. F. Boudreaux-Bartels, and S. M. Kay, "Detection and estimation of generalized chirps using time-frequency representations", *Twenty-Eighth Asilomar Conference on Signals, Systems and Computers*, vol. 1, pp. 50-54, Oct. 1994.

[17] C. E. Perkins, "Chapter 4, Cluster-Based Networks," *Ad Hoc Networking*, Edited by C. E. Perkins, pp. 75-138, Addison-Wesley, 2001.

[18] J. Roman, M. Rangaswamy, D. Davis, Q. Zhang, B. Himed, and J. Michels, "Parametric adaptive matched filter for airborne radar applications," *IEEE Trans. Aerosp. Electron. Syst.*, vol. 36, no. 2, pp. 677-692, 2000.

[19] M. A. Richards, *Fundamentals of Radar Signal Processing*, McGraw-Hill Companies, New York, 2005.

[20] T.K. Sarkar and N. Sangruji, "An adaptive nulling system for a narrow-band signal with a look-direction constraint utilizing the conjugate gradient method," *IEEE Trans. Antennas Propagat.*, vol. 37, no. 7, pp. 940-944, July 1989.

[21] M. I. Skolnik, *Introduction to Radar Systems*, 3rd ed, New York, McGraw Hill, 2001.

[22] P. Swerling, "Probability of detection for fluctuating targets", *IRE Trans on Information Theory*, vol. 6, pp. 269-308, April 1960.

[23] Y. Sun, P. Willett, and R. Lynch, "Waveform fusion in sonar signal processing", *IEEE Transactions on Aerospace and Electronic Systems*, Vol. 40, No. 2, 2004

[24] S. Sowelam and A. Tewfik, "Waveform selection in radar target classification," *IEEE Trans on Information Theory*, vol. 46, no. 3, pp. 1014-1029, 2000.

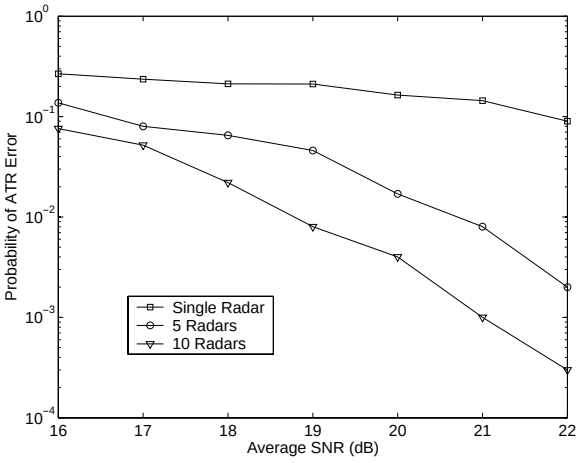

(a)

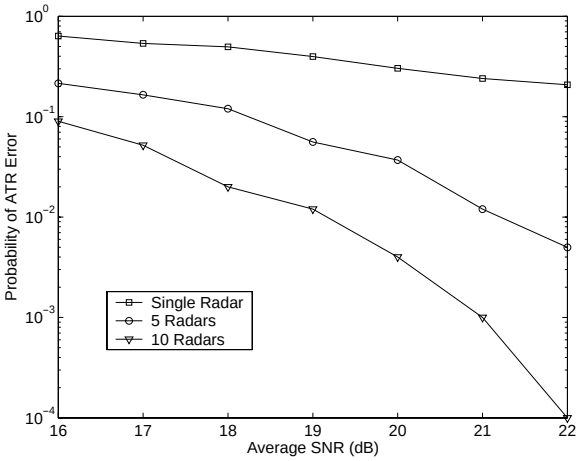

(b)

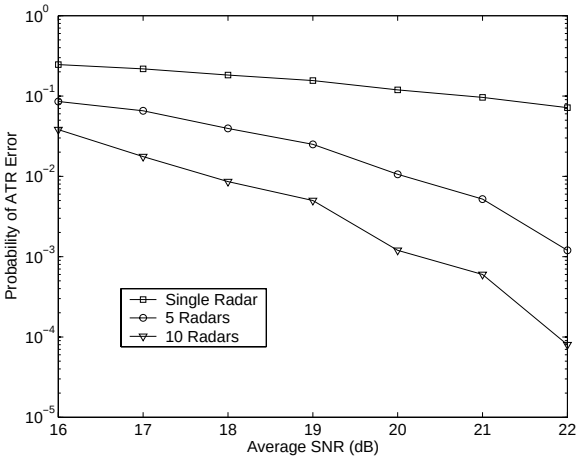

(c)

Fig. 2. Probability of ATR error for *nonfluctuating* targets at different average SNR (dB) values. (a) bird, (b) missile, (c) the average probability of ATR error for 5 targets.

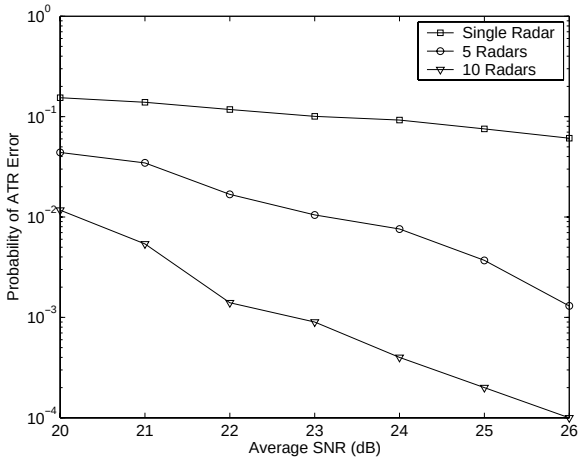

(a)

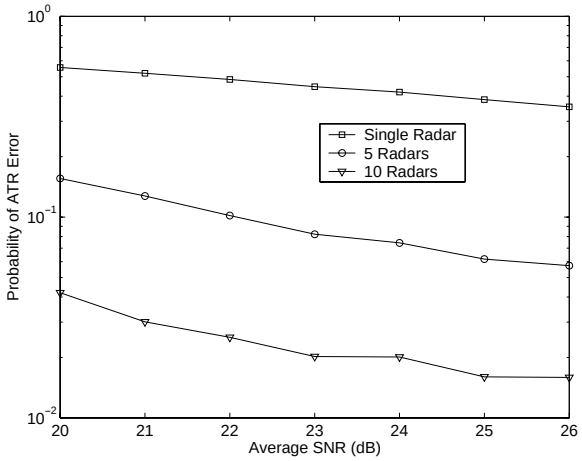

(b)

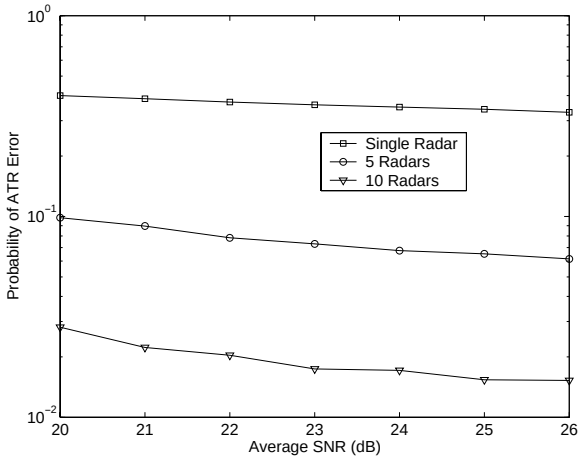

(c)

Fig. 3. Probability of ATR error for *fluctuating* targets at different average SNR (dB) values. (a) bird, (b) missile, (c) the average probability of ATR error for 5 targets.

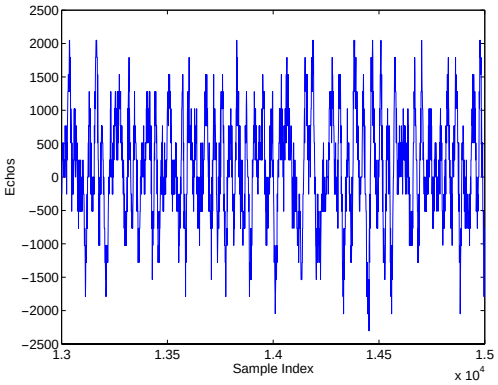

(a)

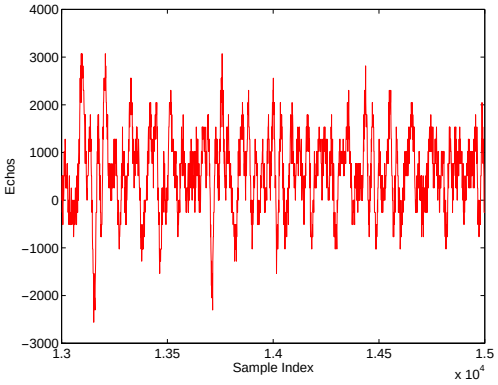

(b)

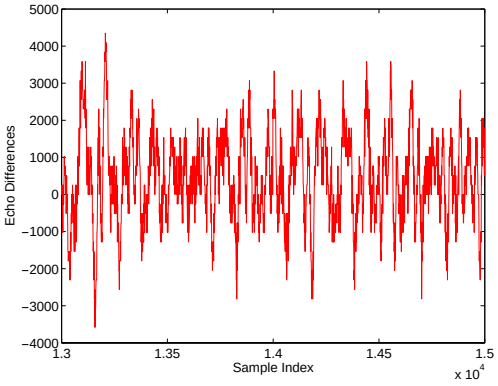

(c)

Fig. 4. Measurement with poor signal quality and 35 pulses average. (a) Expanded view of traces (no target) from sample 13,001 to 15,000. (b) Expanded view of traces (with target) from sample 13,001 to 15,000. (c) The differences between (a) and (b).

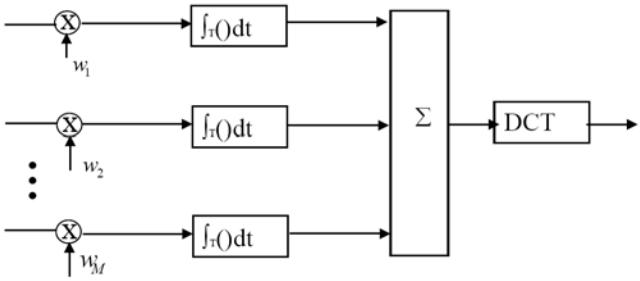

Fig. 5. Echo combining by clusterhead in RSN.

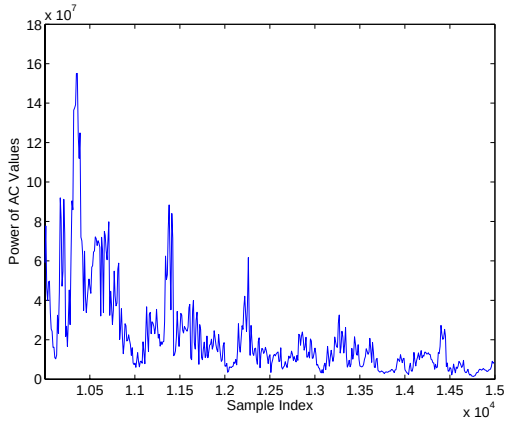

(a)

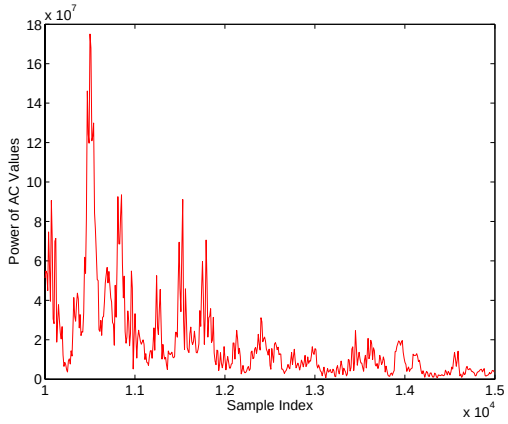

(b)

Fig. 6. Power of AC values based on UWB radar sensor networks and DCT based approach. (a) No target (b) With target in the field.

Wireless Channel Modeling in Foliage Environment: UWB versus Narrowband

Qilian Liang
Department of Electrical Engineering
University of Texas at Arlington
Arlington, TX 76019-0016, USA
E-mail: liang@uta.edu

Xiuzhen Cheng
Dept of Computer Science
George Washington University
Washington, DC 20052
E-mail: cheng@gwu.edu

***Abstract*— In this paper, we study the wireless channel modeling in foliage environment, a rich scattering and time-varying environment, based on extensive data collected using UWB and narrowband (200MHz and 400MHz) radars. We apply two approaches to the wireless channel modeling: Saleh and Valenzuela (S-V) method for UWB channel modeling and CLEAN method for narrowband and UWB channel modeling. We validated that UWB echo signals (within a burst) don't hold self-similarity, which means the future signals can't be forecasted based on the received signals and channel modeling is necessary from statistical point of view. Based on the S-V method for UWB channel modeling, in foliage UWB channel, the multi-path contributions arrive at the receiver are grouped into clusters. The time of arrival of clusters can be modeled as a Poisson arrival process, while within each cluster, subsequent multipath contributions or rays also arrive according to a Poisson process. At different field (near field, medium field, and far field), we observe that the Poisson process parameters are quite different. We also observe that the amplitude of channel coefficient at each path follows Rician distribution for medium and far field, and it's non-stationary for paths from near field (one of two Rician distributions), and these observations are quite different with the IEEE indoor UWB channel model and S-V indoor channel model. Based on the CLEAN method, the narrowband (200MHz and 400MHz) and UWB channel impulse responses have many similarities: both can be modeled as linear time-variant filter channel.**

I. Introduction and Motivation

In July 2003, the Channel Modeling sub-committee of study group IEEE 802.15.SG3a published the final report regarding the UWB indoor multipath channel model [4]. It is a modified version of the indoor Saleh and Valenzuela (S-V) channel model [6]. The S-V model was developped for NLOS channel, and it has also been applied to LOS channels where it is perhaps less valid, unless LOS components are specifically added [5] The IEEE suggested an initial set of values for the indoor UWB channel model which has range less than 10 meters. However, lots of applications of UWB are for outdoor activities such as sense-through-foliage target detection. Forests favor asymmetric threats because the warfighter has a limited sensing capability. Forests provide excellent concealment from observation, ambush, and escape, as well as provide secure bases for enemy Command & Control (C2), weapons caches, and Improvised Explosive Device (IED)/ Weapon of Mass Destruction (WMD) assembly. These have become "the high ground" in fourth-generation warfare, providing a significant strategic advantage. Unfortunately, no work has been done on the outdoor UWB channel modeling.

In this paper, we will model the UWB and narrowband channels using UWB and narrowband radars in foliage environment which is a rich scattering and time-varying environment. UWB radar emissions are at a relatively low frequency-typically between 100 MHz and 3 GHz. Additionally, the fractional bandwidth of the signal is very large (greater than 0.2). Such radar sensor has exceptional range resolution that also has an ability to penetrate many common materials (e.g., walls). Law enforcement personnel have used UWB ground penetrating radars (GPRs) for at least a decade. Like the GPR, sense-through-foliage radar takes advantage of UWB's very fine resolution (time gating) and low frequency of operation.

The rest of this paper is organized as follows. In Section II, we summarize the measurement and collection of data we used in this paper. In Section III, we present our outdoor UWB channel model in rich scattering and time-varying environment. In Section IV, we study the channel impulse response based on CLEAN method for narrowband and UWB channels. We conclude this paper in Section V.

II. Experiment Setup and Data Collection

Our work is based on the data collected in UWB radar-based sense-through-foliage experiment in late summer and fall. Late summer foliage, because of the limited rainfall, involved foliage with decreased water content. Late fall and winter measurements involved largely defoliated but dense forest, so it's a rich scattering environment. Because of wind or different temperature in dense forest, it's also a time-varying environment. The UWB radar-based

978-1-4244-2677-5/08/$25.00 ©2008 IEEE

experiment was constructed on a seven-ton man lift, which had a total lifting capacity of 450 kg. The limit of the lifting capacity was reached during the experiment as essentially the entire measuring apparatus was placed on the lift (as shown in Fig. 1). For the UWB data we used in this paper, each sample is spaced at 50 picosecond interval, and 16,000 samples were collected for each collection for a total time duration of 0.8 microseconds at a rate of approximately 20 Hz. The Barth pulse source was operated at low amplitude and 35 pulses reflected signal were averaged for each collection. Significant pulse-to-pulse variability was noted for these collections. We plot the transmitted pulse (one realization) in Fig. 2a) and the received echos in one collection in Fig. 2b (averaged over 35 pulses).

Fig. 1. This figure shows the lift with the experiment. The antennas are at the far end of the lift from the viewer under the roof that was built to shield the equipment from the elements. This picture was taken in September with the foliage largely still present. The cables coming from the lift are a ground cable to an earth ground and one of 4 tethers used in windy conditions.

For comparison, we also studied narrowband (200MHz and 400MHz) radar signal propagation. For the data we used in this paper, each sample is spaced at 50 picosecond interval, and 16,000 samples were collected for each collection for a total time duration of 0.8 microseconds at a rate of approximately 20 Hz. Fig. 3a shows the transmitted signal and Fig. 3b shows the received echos (averaged over 35 pulses) for 200MHz narrowband radar. Fig. 4a shows the transmitted signal and Fig. 4b shows the received echos (averaged over 35 pulses) for 400MHz narrowband radar. The data collections were extensive. 20 different positions were used, and 35 collections were performed at each position for UWB, 200MHZ, and 400MHz radars.

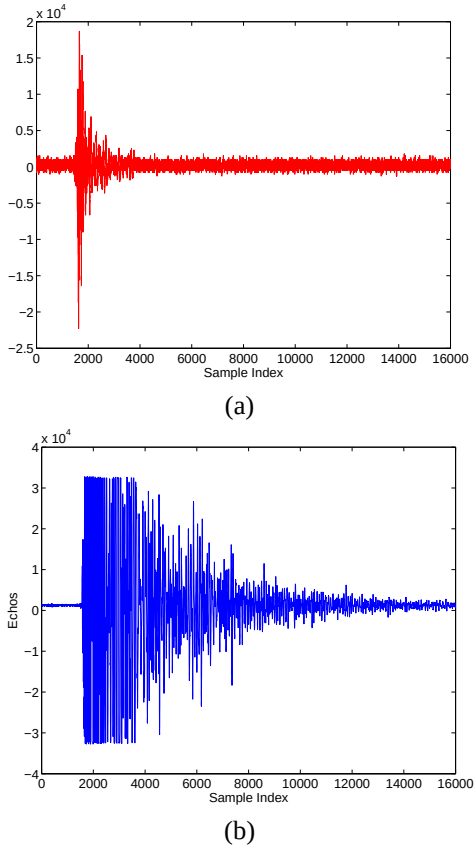

Fig. 2. UWB radar transmitted pulse and received echos in one experiment. (a) Transmitted pulse. (b) Received echos.

III. UWB Channel Modeling Based on S-V Approaches

A. Introduction to Channel Modeling for Indoor UWB Channel

In the S-V model [6], the arrival of clusters is modelled as a Poisson arrival process with a rate Λ, while within each cluster, subsequent multipath contributions or rays also arrive according to a Poisson process with a rate λ (see Fig. 5). In the S-V model, the magnitude of the k-th path within the l-th cluster follows a Rayleigh distribution, and the phase of each path is assumed to be a statistically independent random variable over $[0, 2\pi)$. Besides, the average Power Decay Profile (PDP) is characterized by an exponential decay of the amplitude of the clusters, and a different exponential decay for the amplitude of the received pulses within each cluster, as shown in Fig. 6. In the IEEE UWB indoor channel model [4], the cluster approach was adopted (same as S-V model), but a log-normal distribution was suggested for characterizing the multi-path gain amplitude, and an additional log-normal variable was introbuced for representing the fluctuations of the total multipath gain. Besides, the phase of each path is

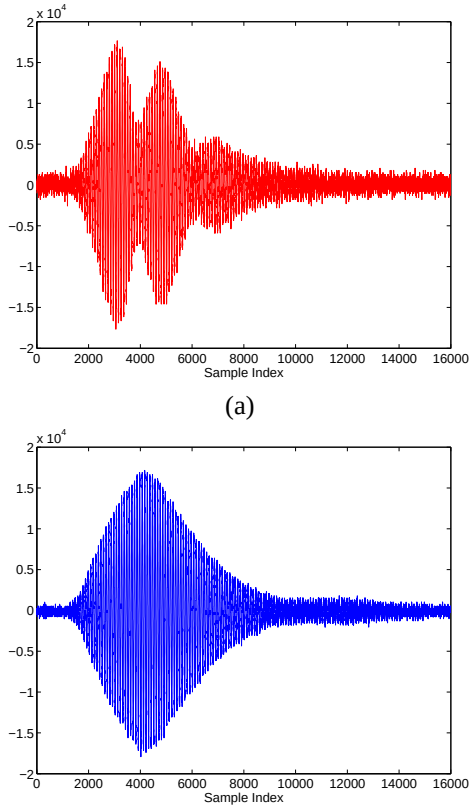

Fig. 3. Narrowband radar (200MHz) transmitted pulse and received echos in one experiment. (a) Transmitted pulse. (b) Received echos.

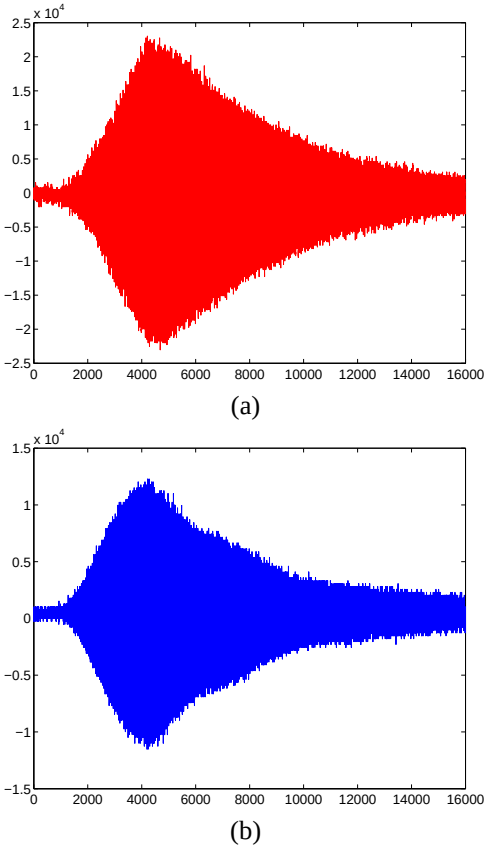

Fig. 4. Narrowband radar (400MHz) transmitted pulse and received echos in one experiment. (a) Transmitted pulse. (b) Received echos.

assumed to be either 0 or π with equal probability.

B. Outdoor UWB Channel Modeling

1) Cluster Arrival and Power Decay Profile: We study the outdoor UWB signal propagation in three cases: near field (less than $55m$), medium field ($55m$–$85m$), and far field (above $85m$ and up to $120m$ in this study). In the data collection, each sample is spaced at 50 picosecond interval, so these cases are corresponding to samples 1–7333 for near field, samples 7333–11333 for medium field, and samples 11334–16000 for far field. In Fig. 7, we plot the power profile of the received echos (averaged over 30 collections to eliminate the effect of random noise and each collection was averaged based on 35 pulses) for the three different cases. Since the transmitted pulse (as plotted in Fig. 2a) is a very narrow impulse pulse (like a delta function in time domain), we analyzed the channel property based on the received echos power profile plotted in Fig. 7, and similar methodology was also used in S-V model studies [6].

Observe Fig. 7, multi-path contributions arrive at the receiver grouped into clusters. The time of arrival of

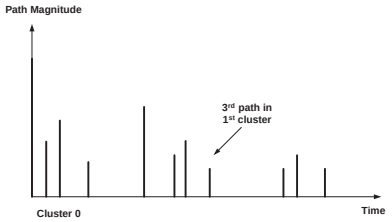

Fig. 5. An illustration of the channel impulse response in S-V model.

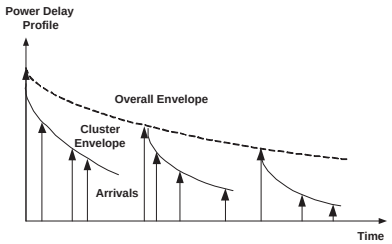

Fig. 6. An illustration of the double exponential decay of the mean cluster power and the ray power within clusters in S-V model.

clusters can be modeled as a Poisson arrival process with a rate Λ, while within each cluster, subsequent multipath

contributions or rays also arrive according to a Poisson process with a rate λ (see Fig. 5). We define:

- T_l = the arrival time of the first path of the l-th cluster;
- $\tau_{k,l}$ = the delay of the k-th path within the l-th cluster relative to the first path arrival time T_l;
- Λ = the cluster arrival rate;
- λ = the ray arrival rate, i.e., the arrival rate of the paths within each cluster.

By definition, we have $\tau_{0l} = T_l$. The distributions of the cluster arrival time and the ray arrival time are given by

$$p(T_l|T_{l-1}) = \Lambda \exp\left(-\Lambda(T_l - T_{l-1}), l > 0\right)$$
$$p(\tau_{k,l}|\tau_{(k-1),l}) = \lambda \exp\left(-\lambda(\tau_{k,l} - \tau_{(k-1),l})\right), k > 0 \quad (1)$$

The above observations are very similar as that for the indoor UWB channel. Specifically, we also observed the Λ and λ are quite different for three different cases.

- Observe Fig. 7a for near field, Λ (1/ns) is around 0.02 (one cluster in every $50ns$ or 1000 samples), and λ (1/ns) is around 0.4 (one path in every $2.5ns$ or 50 samples). Perhaps it's because some major scatters in near field (such as tree stems) reflected signals, so some paths are quite dominant.
- Observe Fig. 7b for medium field, clusters arrive quite often. Λ (1/ns) is around 0.05 (one cluster in every $20ns$ or 400 samples), and λ (1/ns) is around 1 (one path in every $1ns$ or 20 samples).
- Observe Fig. 7c for far field, clusters almost always arrive (because of rich scattering), so Λ (1/ns) is around 0.5 (one cluster in every $2ns$ or 20 samples), and λ (1/ns) is around 4 (one path in every $250ps$ or 5 samples). Perhaps it's because of rich scattering, every path has very similar power level.

Besides, the average PDP can be represented by an exponential decay of the amplitude of the clusters, and a different exponential decay for the amplitude of the received pulses within each cluster, as shown in Fig. 6.

2) Statistical Distribution of Channel Coefficients: We also study the statistical distributions of each given path. We plot the histogram for some sample values of the above three cases based on 30 collections and each collection is averaged over 35 pulses. Near field samples are based on samples 5001–6000; medium field samples are based on samples 8001–9000; and far field samples are based on samples 12001–13000. Since the samples are very close (within 7.5m distance), so their path-loss effect can be ignored. For each case, we have 30000 samples, and we plot their histogram in Fig. 8.

First, observe Fig. 8c for far field, the histogram can be almost perfectly modelled by a non-zero-mean Gaussian distribution, which means the amplitude of the channel

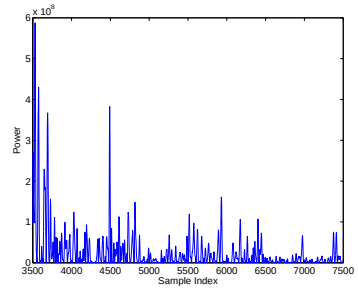

(a)

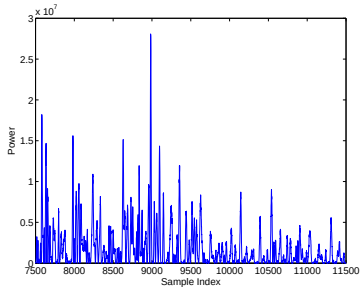

(b)

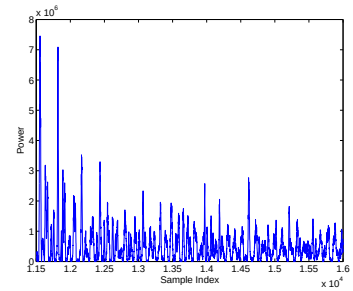

(c)

Fig. 7. The power profile for three different cases: (a) near field, (b) medium field, and (c) far field.

coefficient follows a Rician distribution,

$$p_\alpha(x) = \frac{x}{\sigma^2} \exp\{-\frac{x^2 + s^2}{2\sigma^2}\} I_0(\frac{xs}{\sigma^2}) \quad x \geq 0 \quad (2)$$

where s is the mean value of Gaussian and $I_0(\cdot)$ is the zero order modified Bessel function. This kind of channel is known as Rician fading channel. A Rician channel is characterized by two parameters, Rician factor K which is the ratio of the direct path power to that of the multipath, i.e., $K = s^2/2\sigma^2$, and the Doppler spread (or single-sided fading bandwidth) f_d. Similarly, Fig. 8b for medium field, the histogram can be approximately modelled by a non-zero-mean Gaussian distribution, which means the amplitude of the channel coefficient follows a Rician distribution. Observe Fig. 8a for near field, the histogram can be approximately modelled by two non-zero-mean Gaussian distributions, which means it's non-stationary, and the amplitude of the channel coefficient follows one of two Rician distributions. **The above observations are**

quite different with the indoor UWB channel model (log-normal distribution) and S-V model (Rayleigh distribution). The sign of channel coefficient is either +1 or -1, i.e., its phase is either 0 or π, which matches the IEEE indoor UWB channel model.

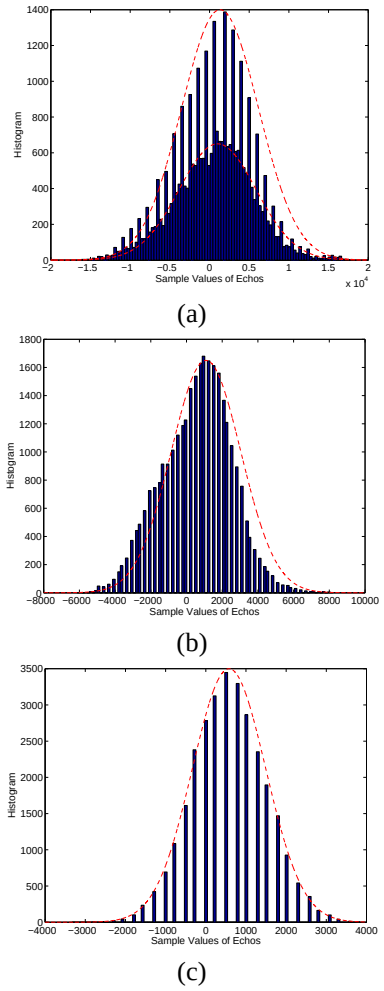

Fig. 8. The histograms and their approximation using Gaussian distributions (dashed lines). The histograms are based on 30 collections and each collection is averaged over 35 pulses. (a) near field samples, (b) medium field samples, and (c) far field samples.

IV. Wireless Channel Modeling Based on CLEAN Method

We apply the CLEAN algorithm to obtain the UWB channel model based on the transmitted pulses and received echos. The CLEAN algorithm was first introduced in [3] and has been applied to UWB measurements [2][7] and it assumes that the channel is a series of impulses which is consistent with the tapped-delay line channel model. This algorithm searches the received echos iteratively with the template to find the maximum correlation [1]. The steps are [5]:

1) Calculate the autocorrelation of the template $r_{ss}(t)$ and the cross-correlation of the template with the received waveform $r_{sy}(t)$.
2) Find the largest correlation peak in $r_{sy}(t)$, record the normalized amplitudes α_k and relative time delay τ_k of the correlation peak.
3) Subtract $r_{ss}(t)$ scaled by α_k from $r_{sy}(t)$ at the time delay τ_k.
4) If a stopping criterion (e.g., a minimum threshold on the peak correlation) is not met, go to step 2. Otherwise stop.

Based on the CLEAN method, we successfully obtained the channel impulse responses for all transmit waveforms and receive echoes. For illustration purposes, in Figs. 9, 10, and 11, we plot the channel impulse responses for 200MHz, 400MHz, and UWB channels using CLEAN method in two experiments. Observe that for all channels, channel impulse responses have many similarities: all can be modeled as linear time-variant filter channel, which is a more general case of the S-V model.

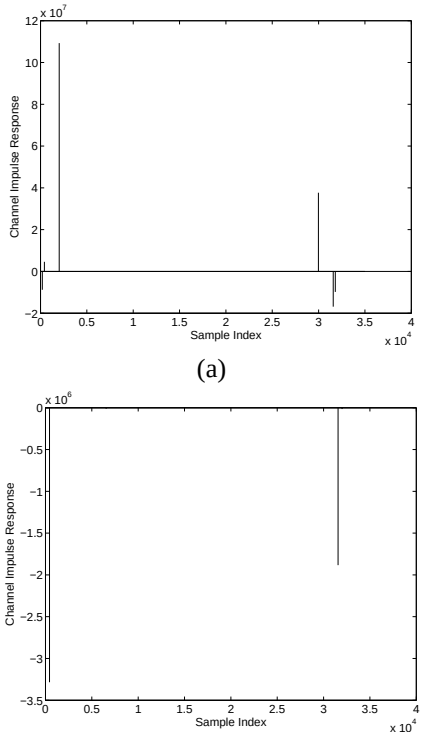

Fig. 9. The channel impulse responses for 200MHz channel using CLEAN method in two experiments.

V. Conclusions

In this paper, we studied the statistical modeling for outdoor wireless channels (200MHz, 400MHz, and UWB) in

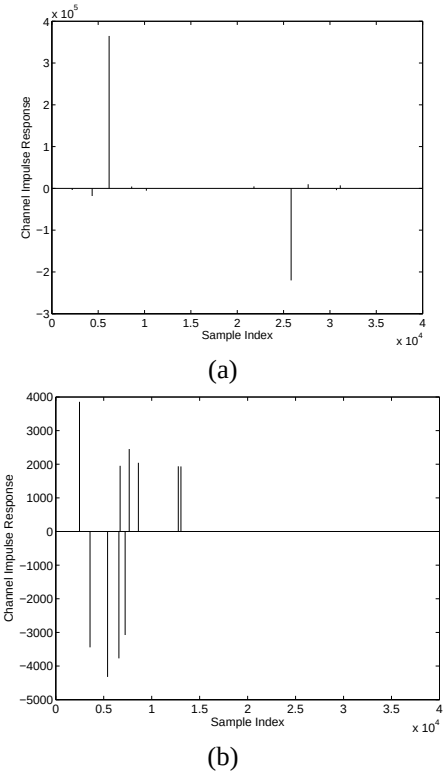

Fig. 10. The channel impulse responses for 400MHz channels using CLEAN method in two experiments.

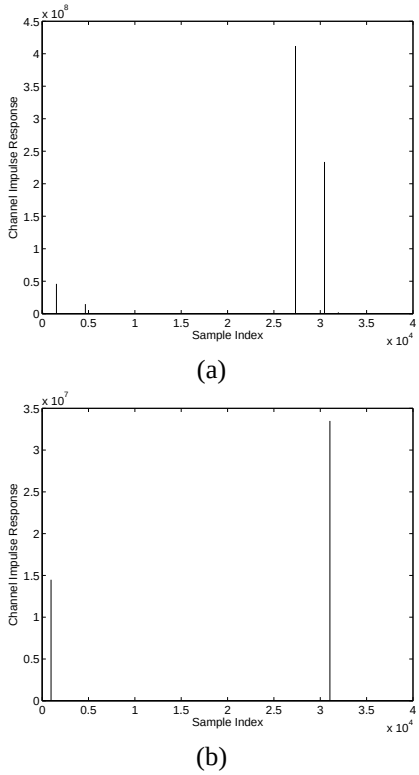

Fig. 11. The channel impulse responses for UWB channels using CLEAN method in two experiments.

rich scattering and time-varying environment based on extensive data collected using narrowband and UWB radars. We validated that UWB echo signals (within a burst) don't hold self-similarity, which means the future signals can't be forecasted based on the received signals and channel modeling is necessary from statistical point of view. In outdoor UWB channel, the multi-path contributions arrive at the receiver are grouped into clusters. The time of arrival of clusters can be modeled as a Poisson arrival process, while within each cluster, subsequent multipath contributions or rays also arrive according to a Poisson process. At different field (near field, medium field, and far field), we observed that the Poisson process parameters are quite different. We also observed that the amplitude of channel coefficient at each path follows Rician distribution for medium and far field, and it's non-stationary for paths from near field (one of two Rician distributions), and these observations are quite different with the IEEE indoor UWB channel model and S-V model. Using CLEAN method, we observed that for all channels, channel impulse responses have many similarities: all can be modeled as linear time-variant filter channel, which is a more general case of the S-V model.

ACKNOWLEDGEMENT

The authors would like to thank Dr. Sherwood Samn in AFRL/RHX for providing the radar data.

The research of Liang was supported in part by Office of Naval Research (ONR) under Grant N00014-07-1-0395 and N00014-07-1-1024, and National Science Foundation (NSF) under Grant CNS-0721515 and CNS-0831902. The research of Cheng was supported in part by NSF under Grant CNS-0721669 and CNS-0831852.

REFERENCES

[1] R. M. Buehrer, et al, "Characterization of the UWB channel," *IEEE Conf on Ultra Wideband Systems and Technologies*, pp. 26-31, Reston, VA, Nov 2003.

[2] R. J.-M. Cramer, *An Evaluation of Ultrawideband Propagation Channels*, Ph.D Dissertation, USC, 2000.

[3] J. A. Hogbom, "Aperture synthesis with a non-regular distribution of interferometer baseline," *Atronomy and Astrophysics Supplement Ser.*, vol. 15, 1974.

[4] IEEE 802.15.SG3a, "Channel modeling sub-committee report final," *IEEE P802.15-02/490r1-SG3a*, Feb 2003.

[5] J. H. Reed, *An Introduction to Ultra Wideband Communication Systems*, Prentice Hall, Upper Saddler River, NJ, 2005.

[6] A. A. Saleh and R. A. Valenzuela, "A statistical model for indoor multipath propagation," *IEEE J. on Selected Areas in Communications*, vol. 5, no. 2, pp. 128-137, Feb 1987.

[7] R. A. Scholtz, M. Z. Win, and J. M. Cramer, "Evaluation of the Characteristics of the ultra-wideband propagation channel," *Proc of Antenna and Propagation Symposium*, vol. 2, no. 626-630, 1998.

This full text paper was peer reviewed at the direction of IEEE Communications Society subject matter experts for publication in the ICC 2008 proceedings.

UWB Radar Sensor Networks for Sense-through-Foliage Target Detection

Qilian Liang
Department of Electrical Engineering
University of Texas at Arlington
Arlington, TX 76019-0016, USA
E-mail: liang@uta.edu

Sherwood W. Samn
Air Force Research Laboratory/HEX
Brooks City Base
San Antonio, TX 78235, USA
E-mail: Sherwood.samn@brooks.af.mil

Xiuzhen Cheng
Dept of Computer Science
George Washington University
Washington, DC 20052
E-mail: cheng@gwu.edu

***Abstract*— In this paper, we propose a Discrete-Cosine-Transform (DCT)-based approach for sense-through-foliage target detection when the echo signal quality is good, and a Radar Sensor Network (RSN) and DCT-based approach when the echo signal quality is poor. A RAKE structure which can combine the echos from different cluster-members is proposed for clusterhead in the RSN. We compared our approach with the ideal case when both echos are available, i.e., echos with target and without target. We also compared our approach against the scheme in which 2-D image was created via adding voltages with the appropriate time offset. Simulation results show that our DCT-based scheme works much better than the existing approach, and our RSN and DCT-based approach can be used for target detection successfully while even the ideal case fails to do it.**

I. Introduction and Motivation

Forests and buildings favor asymmetric threats because the warfighter has a limited sensing capability. Forest and buildings provide excellent concealment from observation, ambush, and escape, as well as provide secure bases for enemy Command & Control (C2), weapons caches, and Improvised Explosive Device (IED)/ Weapon of Mass Destruction (WMD) assembly. These have become "the high ground" in fourth-generation warfare, providing a significant strategic advantage. We believe that solving the sense-through-foliage target detection will significantly benefit sense-through-wall and other subsurface sensing problems. The objective of this paper is to develop measurable advances in improving the understanding of intelligence for the forest conflict using UWB radar. The key focus of this study is to develop advanced technologies that make foliage transparent, thereby eliminating the safe harbor that forest provides to hostile forces and their malicious activities. Sense-through-foliage target detection resulting from this research will benefit emerging Department of Defense (DoD) net-centric warfare programs.

In this paper, we will apply our expertise in signal processing, data fusion, sensor networks, etc to achieve effective sense-through-foliage technology using ultra-wideband (UWB) radar. UWB radar emissions are at a relatively low frequency-typically between 100 MHz and 3 GHz. Additionally, the fractional bandwidth of the signal is very large (greater than 0.2). Such radar sensor has exceptional range resolution that also has an ability to penetrate many common materials (e.g., walls). Law enforcement personnel have used UWB ground penetrating radars (GPRs) for at least a decade. Like the GPR, sense-through-foliage radar takes advantage of UWB's very fine resolution (time gating) and low frequency of operation. In the existing works on UWB radar/sensor based target detection, Time Domain Inc has invented UWB radars, and some algorithms for target detection were overviewed in [5]; these are mainly based on target response signal strength (1-D) and different copies of signals to construct 2-D features. The Adaptive Polarization-Difference Imaging (APDI) algorithm and PDI technique [3][4] were originally developed for optical imaging and in many situations can provide significant enhancements in target detection and feature extraction over conventional methods. The rest of this paper is organized as follows. In Section II, we summarize the measurement and collection of data we used in this paper. In Section III, we propose a discrete-cosine-transform (DCT) based approach for sense-through-foliage target detection with good signal quality. In Section IV, we propose a radar sensor network (RSN) and DCT-based approach for sense-through-foliage target detection when the signal quality is poor. We conclude this paper and discuss some future research topics in Section V.

II. Sense-through-Foliage Data Measurement and Collection

Our work is based on the sense-through-foliage data from Air Force Research Lab. The foliage penetration measurement effort began in August 2005 and continued through December 2005. Working in August through the fall of 2005, the foliage measured included late summer foliage and fall and early winter foliage. Late summer foliage, because of the limited rainfall, involved foliage with decreased water content. Late fall and winter measurements involved largely defoliated but dense forest.

The foliage experiment was constructed on a seven-ton man lift, which had a total lifting capacity of 450 kg. The limit of the lifting capacity was reached during the experiment as essentially the entire measuring apparatus

was placed on the lift. The principle pieces of equipment secured on the lift are: Barth pulser, Tektronix model 7704 B oscilloscope, dual antenna mounting stand, two antennas, rack system, IBM laptop, HP signal Generator, Custom RF switch and power supply and Weather shield (small hut). The target is a trihedral reflector (as shown in Fig. 1). Throughout this work, a Barth pulse source (Barth Electronics, Inc. model 732 GL) was used. The pulse generator uses a coaxial reed switch to discharge a charge line for a very fast rise time pulse outputs. The model 732 pulse generator provides pulses of less than 50 picoseconds (ps) rise time, with amplitude from 150 V to greater than 2 KV into any load impedance through a 50 ohm coaxial line. The generator is capable of producing pulses with a minimum width of 750 ps and a maximum of 1 microsecond. This output pulse width is determined by charge line length for rectangular pulses, or by capacitors for 1/e decay pulses.

Fig. 1. The target (a trihedral reflector) is shown on the stand at 300 feet from the lift.

For the data we used in this paper, each sample is spaced at 50 picosecond interval, and 16,000 samples were collected for each collection for a total time duration of 0.8 microseconds at a rate of approximately 20 Hz. We considered two sets of data from this experiment. Initially, the Barth pulse source was operated at low amplitude and 35 pulses reflected signal were averaged for each collection. Significant pulse-to-pulse variability was noted for these collections. The scheme for the sense-through-foliage target detection with "poor" signal quality will be presented in Section IV. Later, good signal quality data were collected using higher amplitude pulses and 100 pulses reflected signals were averaged for each collection. The scheme for target detection with "good" signal quality will be presented in Section III.

III. Sense-through-Foliage Target Detection with Good Signal Quality: A DCT-based Approach

In Fig. 2, we plot two collections with good signal quality, one without target on range (Fig. 2a) and the other one

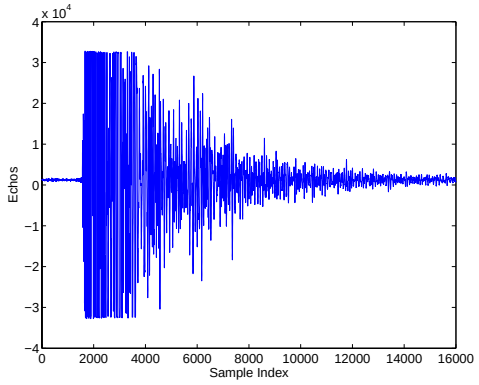

(a)

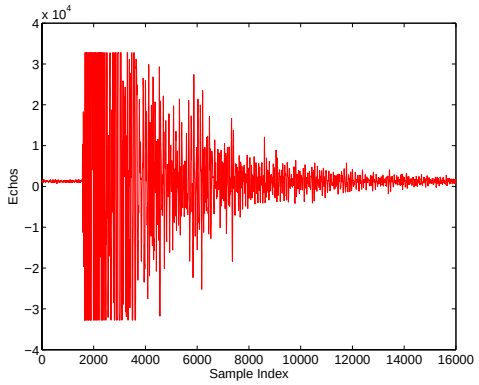

(b)

Fig. 2. Measurement with very good signal quality and 100 pulses average. (a) No target on range, (b) with target on range (target appears at around sample 14,000).

with target on range (Fig. 2b and target appears at around sample 14,000). To make it more clear to the readers, we provide expanded views of traces (with target) from sample 13,001 to 15,000 for the above two collections in Figs. 3a and 3b. Since there is no target in Fig. 3a, it can be treated as the response of foliage clutter. It's quite straightfoward that the target response will be the echo difference between Fig. 3b and Fig. 3a, which is plotted in Fig. 3c. However, it's impossible to obtain Fig. 3a (clutter echo) in practical situation if there is target on range. The challenge is how to make target detection based on Fig. 3b (with target) or Fig. 3a (no target) only?

Observe Fig. 3b, for samples where target appears (around sample 14,000), the sample strength changes much abruptly than that in Fig. 3a, which means echo from target contains more AC values than that without target. Motivated by this, we applied Discrete Cosine Transform (DCT) to the echos $x(iM+n)$ $(n = 0, 1, 2, \cdots, N-1)$ where N is the DCT window length, M is the step size of each DCT window, and i is the window index. Let $x(n,i) \triangleq x(iM+n)$

$$X(K,i) = \sum_{n=0}^{N-1} x(n,i)\cos(\frac{2\pi}{N}nK) \qquad (1)$$

then we cumulate the power of AC values (for $K > 2$)

$$P(i) = \sum_{K=3}^{N-1} X(K,i)^2 \quad (2)$$

For $N = 100$ and $M = 10$, we plot the power of AC values $P(i)$ versus iM (time domain sample index) in Figs. 4a and 4b for the above data sets in Figs. 3a and 3b respectively. Observe that in Fig. 4b, the power of AC values (around sample 14,000) where the target is located is non-fluctuating (monotonically increase then decrease). Although some other samples also have very high AC power values, it is very clear that they are quite fluctuating and the power of AC values behave like random noise because generally the clutter has Gaussian distribution in the frequency domain [2].

We compared our DCT-based approach to the scheme proposed in [5]. In [5], 2-D image was created via adding voltages with the appropriate time offset. In Figs. 5a and 5b, we plot the 2-D image created based on the above two data sets (from samples 13,800 to 14,200). However, it's not clear which image shows there is target on range.

IV. Sense-through-Foliage Target Detection with Poor Signal Quality: A Sensor Network and DCT-based Approach

As mentioned in Section II, when the Barth pulse source was operated at low amplitude and the sample values are not obtained based on sufficient pulse response averaging (averaged over 35 pulses for each collection), significant pulse-to-pulse variability was noted and the return signal quality is poor. In Figs. 6a and 6b, we plot two collections with poor signal quality. Fig. 6a has no target on range, and Fig. 6b has target at samples around 14,000. We plot the echo differences between Figs. 6a and 6b in Fig. 6c. However, it is impossible to identify whether there is any target and where there is target based on Fig. 6c. We observed the DCT-based approach failed to detect target based on one collection. Since significant pulse-to-pulse variability exists in the echos, this motivate us to explore the spatial and time diversity using Radar Sensor Networks (RSN).

In RSN, each radar can provide their pulse parameters such as timing to their clusterhead radar, and the clusterhead radar can combine the echos (RF returns) from the target and clutter. In this paper, we propose a RAKE structure for combining echos, as illustrated by Fig. 7. The integration means time-average for a sample duration T and it's for general case when the echos are not in discrete values. It is quite often assumed that the radar sensor platform will have access to Global Positioning Service (GPS) and Inertial Navigation Unit (INU) timing and navigation data [1]. In this paper, we assume the radar sensors are synchronized in RSN. In Fig. 7, the echo, i.e., RF response by the pulse of each cluster-member sensor, will be combined by the clusterhead using a weighted average, and the weight w_i is determined by the power of each echo $x_i(n)$ (n is the sample index),

$$w_i = \frac{E_i}{\sum_{i=1}^{M} E_i} \quad (3)$$

and

$$E_i = \text{var}(x_i(n)) + [\text{mean}(x_i(n))]^2 \quad (4)$$

We ran simulations for $M = 30$, and plot the power of AC values in Figs. 8a and 8b for the two cases (with target and without target) respectively. Observe that in Fig. 4b, the power of AC values (around sample 14,000) where the target is located is non-fluctuating (monotonically increase then decrease). Although some other samples also have very high AC power values, it is very clear that they are quite fluctuating and the power of AC values behaves like random noise because generally the clutter has Gaussian distribution in the frequency domain.

V. Conclusions and Future Works

In this paper, we proposed a DCT-based approach for sense-through-foliage target detection when the echo signal quality is good, and a sensor network and DCT-based approach when the echo signal quality is poor. A RAKE structure which can combine the echos from different cluster-members is proposed for clusterhead in the RSN. We compared our approach with ideal case when both echos are available, i.e., echos with target and without target. We also compared our approach against the scheme in which 2-D image was created via adding voltages with the appropriate time offset. Simulation results show that our DCT-based scheme works much better than the existing approach, and our RSN and DCT-based approach can be used for target detection successfully while the ideal case fails to do it. For future works, we will collect more data with different targets and perform automatic target recognition besides target detection.

Acknowledgement

This work was supported in part by ONR under Grant N00014-07-1-0395, N00014-03-1-0466, N00014-07-1-1024, NSF under Grant CNS-0721515, and AFOSR Summer Faculty Fellowship Program Award.

References

[1] ONR BAA 07-017, "NET-SENTRIC Surveillance," http://www.onr.navy.mil/02/baa/.

[2] D. K. Barton, *Radar System Analysis and Modeling*, Artech House, Boston, MA, 2006.

[3] M. P. Rowe, E. N. Pugh, Jr., J. S. Tyo, and N. Engheta, "Polarization-difference imaging: a biologically inspired technique for observation through scattering media," *Optics Letters*, Vol. 20, pp. 608-610, 1995.

[4] J. S. Tyo, M. P. Rowe, E. N. Pugh, Jr., N. Engheta, "Target detection in optically scattering media by polarization difference imaging," *Applied Optics*, Vol. 35, pp. 1855-1870, 1996.

[5] P. Withington , H. Fluhler, and S. Nag , "Enhancing homeland security with advanced UWB sensors," *IEEE Microwave Magazine*, Sept 2003.

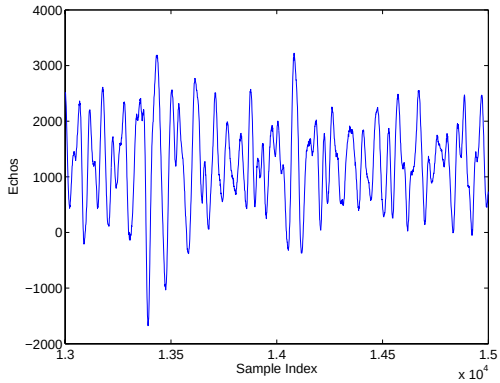

(a)

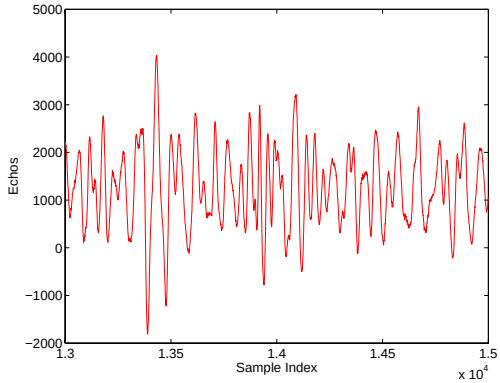

(b)

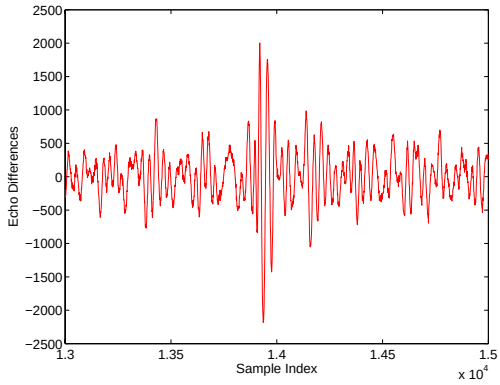

(c)

Fig. 3. Measurement with very good signal quality and 100 pulses average. (a) Expanded view of traces (with target) from samples 13,001 to 15,000. (b) Expanded view of traces (without target) from samples 13,001 to 15,000. (c) The differences between (a) and (b).

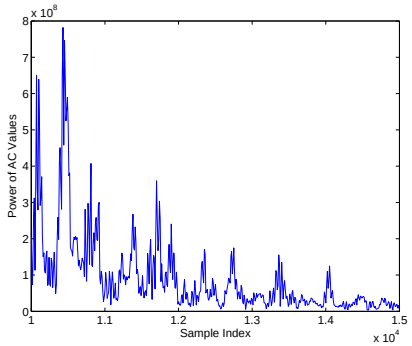

(a)

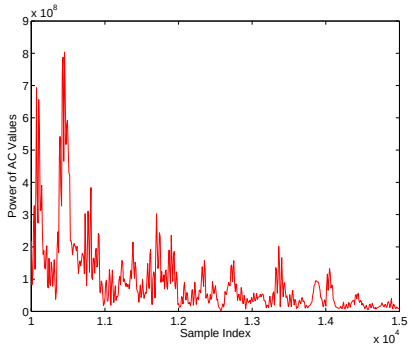

(b)

Fig. 4. The power of AC values versus sample index. (a) No target (b) With target in the field.

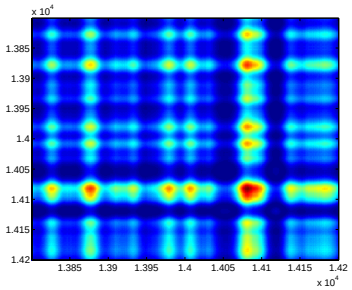

(a)

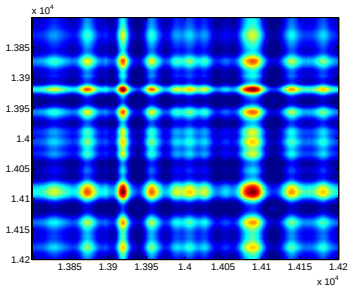

(b)

Fig. 5. 2-D image created via adding voltages with the appropriate time offset. (a) No target (b) With target in the field.

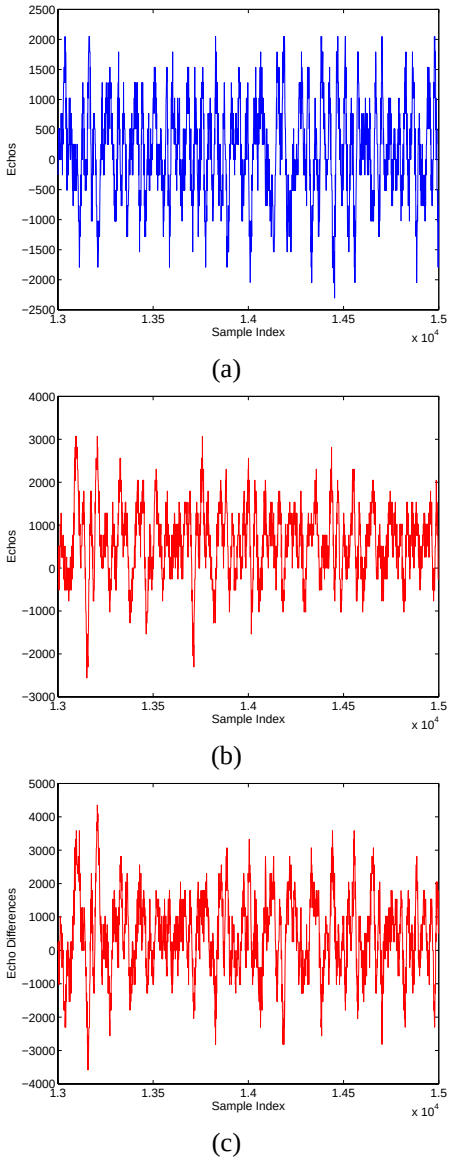

Fig. 6. Measurement with poor signal quality and 35 pulses average. (a) Expanded view of traces (no target) from sample 13,001 to 15,000. (b) Expanded view of traces (with target) from sample 13,001 to 15,000. (c) The differences between (a) and (b).

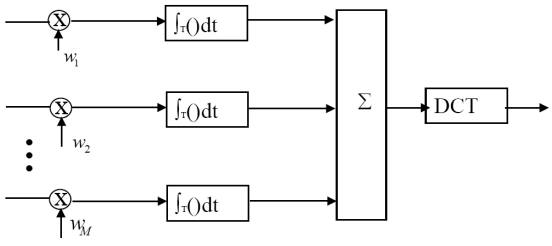

Fig. 7. Echo combining by clusterhead in RSN.

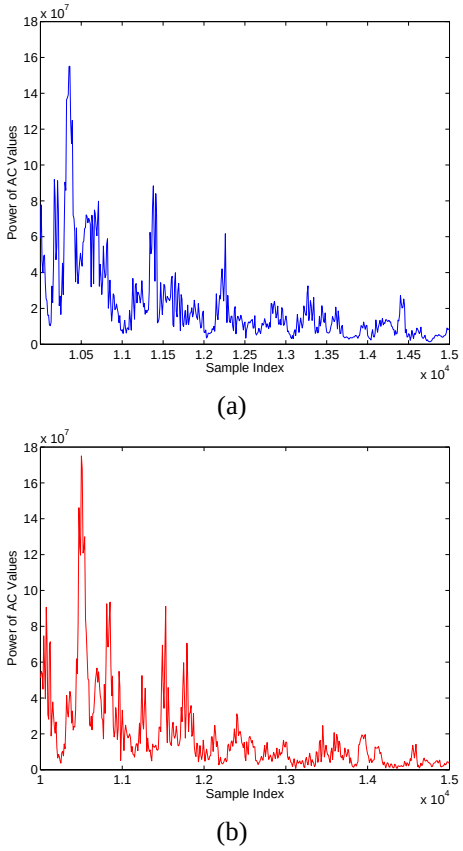

Fig. 8. Power of AC values based on UWB radar sensor networks and DCT based approach. (a) No target (b) With target in the field.

This full text paper was peer reviewed at the direction of IEEE Communications Society subject matter experts for publication in the ICC 2008 proceedings.

Foliage Clutter modeling Using the UWB Radar

Jing Liang, Qilian Liang
Department of Electrical Engineering
University of Texas at Arlington
Arlington, TX 76019-0016, USA
Email: jliang@wcn.uta.edu, liang@uta.edu

Sherwood W. Samn
Air Force Research Laboratory/HEX
Brooks City Base
San Antonio, TX 78235, USA
Email: Sherwood.samn@brooks.af.mil

***Abstract*— In this paper, we propose that the foliage clutter follows log-logistic model using maximum likelihood (ML) parameter estimation as well as the root mean square error (RMSE) on PDF curves between original clutter and statistical model data. The measured clutter data is provided by Air Force Office of Scientific Research (AFOSR). In addition to investigating the log-logistic model, we also compare it with other popular clutter models, namely log-normal, Weibull and Nakagami. We show that the log-logistic model not only achieves the smallest standard deviation (STD) error on estimated model parameters, but also has the best goodness-of-fit and smallest RMSE. Further, the performance of detection at presence of foliage clutter is theoretically analyzed.**

I. Introduction and Motivation

Clutter is a term used to define all unwanted echoes from natural environment [1]. The nature of clutter may necessarily vary on a basis of different applications and radar parameters. Most previous studies have investigated land clutter and sea clutter. As far as clutter modeling in forest is concerned, it is still of great interest and is likely to take some time to reach any agreement. A team of researchers from MIT [2] and U. S. Army Research Laboratory (ARL) [3] [4] have measured ultra-wideband (UWB) backscatter signals in foliage for different polarizations and frequency ranges. The measurements show that the foliage clutter is impulsively corrupted with multipath fading, which leads to inaccuracy of the K-distributions description [5]. The Air Force Office of Scientific Research (AFOSR) has conducted field measurement experiment concerning foliage penetration radar since 2004 and noted that metallic targets may be more easily identified with wideband than with narrowband signals [6].

In this investigation, we will apply ultra-wide band (UWB) radar to model the foliage clutter. UWB radar emissions are at a relatively low frequency-typically between 100 MHz and 3 GHz. Additionally, the fractional bandwidth of the signal is very large (greater than 0.2). Such radar sensors have exceptional range resolution that also has an ability to penetrate many common materials (e.g., walls). Law enforcement personnel have used UWB ground penetrating radars (GPRs) for at least a decade. Like the GPR, sense-through-foliage radar takes advantage of UWB's very fine resolution (time gating) as well as low frequency of operation.

In our present work, we investigate the use of the log-logistic distribution to model foliage clutter and illustrate the goodness-of-fit to real UWB clutter data conducted by AFOSR. Additionally, we compare the goodness-of-fit with existing popular models namely log-normal, Weibull, and Nakagami by means of maximum likelihood estimation (MLE) and the root mean square error (RMSE). The result shows that log-logistic model provides the best fit to the foliage clutter.

The rest of this paper is organized as follows. In Section II we discuss the properties and applicability of log-logistic as a statistical model for foliage clutter. The measurement and collection of clutter data we used in this paper are summarized in Section III. Section IV discusses the estimation of model parameters and the goodness-of-fit. section V analyzes the performance of radar detection at presence of foliage clutter. Finally, section VI concludes this paper and describes some future work.

II. Log-logistic Model

Log-logistic has been applied recently in hydrological analysis. In spite of its intensive application in precipitation and stream-flow data, the log-logistic distribution (LLD) [7] statistical model, to the best of our knowledge, has never been applied to radar foliage clutter. The motivation for considering log-logistic model is based on its higher kurtosis and longer tails, as well as its shape similarity to log-normal and Weibull distributions. Thus it is intended to be employed to estimate how well the model matches our collected foliage clutter statistics.

Here we employ the two-parameter distribution with parameters μ and σ. The PDF for this distribution is given by

$$f(x) = \frac{e^{\frac{\ln x-\mu}{\sigma}}}{\sigma x(1+e^{\frac{\ln x-\mu}{\sigma}})^2}, \quad x>0,\ \sigma>0 \qquad (1)$$

where μ is scale parameter and σ is shape parameter.

III. Experiment Setup and Data Collection

Our work is based on the sense-through-foliage data from Air Force Research Lab [6]. The foliage penetration measurement effort began in August 2005 and continued through December 2005. Working in August through the fall of 2005, the foliage measured included late summer foliage and fall and early winter foliage. Late summer foliage, because of the limited rainfall, involved foliage with decreased water content. Late fall and winter measurements involved largely defoliated but dense forest.

Fig. 1. This figure shows the lift with the experiment. The antennas are at the far end of the lift from the viewer under the roof that was built to shield the equipment from the elements. This picture was taken in September with the foliage largely still present. The cables coming from the lift are a ground cable to an earth ground and one of 4 tethers used in windy conditions.

The UWB radar-based experiment was constructed on a seven-ton man lift, which had a total lifting capacity of 450 kg. The limit of the lifting capacity was reached during the experiment as essentially the entire measuring apparatus was placed on the lift (as shown in Fig. 1). The principle pieces of equipment secured on the lift are: Barth pulser, Tektronix model 7704 B oscilloscope, dual antenna mounting stand, two antennas, rack system, IBM laptop, HP signal Generator, Custom RF switch and power supply and Weather shield (small hut). Throughout this work, a Barth pulse source (Barth Electronics, Inc. model 732 GL) was used. The pulse generator uses a coaxial reed switch to discharge a charge line for a very fast rise time pulse outputs. The model 732 pulse generator provides pulses of less than 50 picoseconds (ps) rise time, with amplitude from 150 V to greater than 2 KV into any load impedance through a 50 ohm coaxial line. The generator is capable of producing pulses with a minimum width of 750 ps and a maximum of 1 microsecond. This output pulse width is determined by charge line length for rectangular pulses, or by capacitors for 1/e decay pulses.

For the data we used in this paper, each sample is spaced at 50 picoseconds interval, and 16,000 samples were collected for each collection for a total time duration of 0.8 microseconds at a rate of approximately 20 Hz. The Barth pulse source was operated at low amplitude and 10 pulses reflected clutter signal were obtained for each collection at the same site but different time, one example of transmitted pulse and received backscattering are shown in Fig. 2(a) and (b) respectively. To make them clearer to readers, we provide expanded views of received traces from sample 10,000 to 12,000 in (c).

IV. Statistical Analysis of the Foliage Clutter Data

A. Maximum Likelihood Estimation

Using the collected clutter data mentioned above, we apply Maximum Likelihood Estimation (MLE) approach to estimate the parameters of the log-logistic, log-normal, Weibull, and

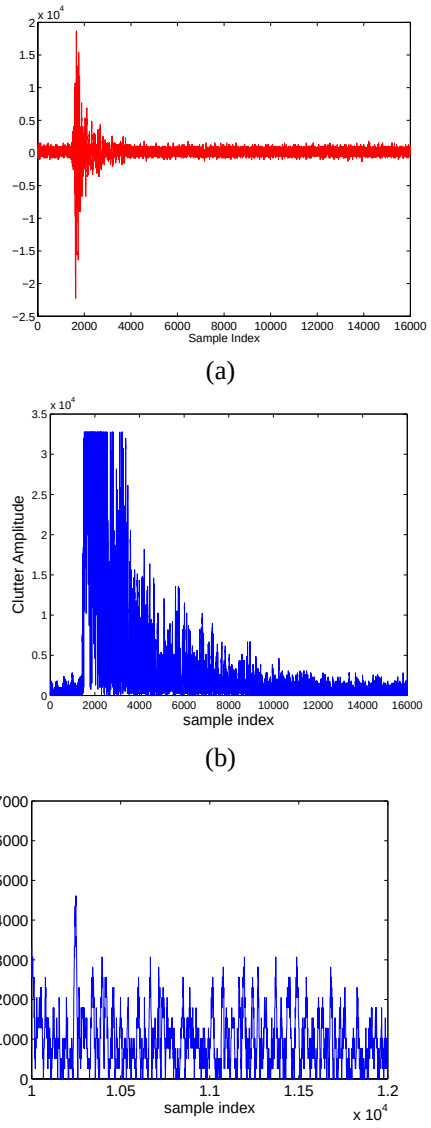

Fig. 2. Clutter data (a)transmitted pulse before antenna amplification (b)received echoes (c) Expanded view from clutter samples 10,000 to 12,000

Nakagami models. MLE is often used when the sample data are known and parameters of the underlying probability distribution are to be estimated [8] [9]. It is generalized as follows:

Let $y_1, y_2, \cdots, y_N$ be N independent samples drawn from a random variable $\mathbf{Y}$ with m parameters $\theta_1, \theta_2, \cdots, \theta_m$, where $\theta_i \in \theta$, then the likelihood function expressed as a function of θ conditional on $\mathbf{Y}$ is

$$L_N(\mathbf{Y}|\theta) = \prod_{k=1}^{N} f_{Y|\theta}(y_k|\theta_1, \theta_2, \cdots, \theta_m) \qquad (2)$$

The maximum likelihood estimate of $\theta_1, \theta_2, \cdots, \theta_m$ is the set of values $\hat{\theta}_1, \hat{\theta}_2, \cdots, \hat{\theta}_m$ that maximize the likelihood function $L_N(\mathbf{Y}|\theta)$.

As the logarithmic function is monotonically increasing, maximizing $L_N(\mathbf{Y}|\theta)$ is equivalent to maximizing

$\ln(L_N(\mathbf{Y}|\theta))$. Hence, it can be shown that a necessary but not sufficient condition to obtain the ML estimate $\hat{\theta}$ is to solve the likelihood equation

$$\frac{\partial}{\partial\theta}\ln(L_N(\mathbf{Y}|\theta)) = 0 \tag{3}$$

Using the collected clutter radar mentioned above, we apply MLE to obtain $\hat{\mu}$ and $\hat{\sigma}$ for log-logistic, $\hat{\mu}$ and $\hat{\sigma}$ for the log-normal, $\hat{a}$ and $\hat{b}$ for the Weibull, and $\hat{\mu}$ and $\hat{\omega}$ for the Nakagami. The results are shown in Table I. We also explore the standard deviation (STD) error of each parameter. These descriptions are shown in table I in the form of ε_x, where x denotes different parameter for each model. As there are 10 data sets for poor clutter signal, we also calculate the average values of estimated parameters and their STD error.

From Table II, we can see STD error for log-logistic and log-normal parameters are less than 0.02 and their estimated parameters vary little from data to data compared to Weibull and Nakagami. It is obvious that log-logistic model provides the smallest STD error and Nakagami the largest. Therefore, in the view of statistics, log-logistic model fits the collected data best compared to log-normal, Weibull, and Nakagami.

B. Goodness-of-fit in curve and RMSE

We may also observe the extend to which the PDF curve of the statistic model matches that of clutter data by calculating the root mean square error (RMSE). Let i (i=$1, 2, \cdots, n$) be the sample index of clutter amplitude, c_i is the corresponding PDF value whereas $\hat{c}_i$ is the PDF value of the statistical model with estimated parameters by means of MSE. The RMSE is obtained through following equation:

$$\mathsf{RMSE} = \sqrt{\frac{1}{n}\sum_{i=1}^{n}(c_i - \hat{c}_i)^2} \tag{4}$$

Here we apply n=101 for each model.

The goodness-of-fit in curve and the RMSE of each model are illustrated in Fig. 3. The PDF of absolute amplitude of one-time poor data is presented by means of histogram bars. In Fig. 3, it can be seen obviously that log-logistic model with MLE parameters provides the best goodness-of-fit compared to the other models, since it provides the most suitable kurtosis, slope and tail. As for the maximum PDF value, the log-logistic is about 1×10^{-3}, while that of other models are over 1.2×10^{-3}. For the slope part, which connects the kurtosis and the tail and which is in the range from 0.1×10^4 to 0.5×10^4 in view of x axes, the log-logistic provides the smallest skewness whereas Nakagami provides the largest. Examination of the tails show that log-logistic and log-normal provide very close-valued tails, while tails of the Weibull and the Nakagami are lager than the collected data. Meanwhile, we obtain that $\mathsf{RMSE}_{log-logistic} = 2.5425 \times 10^{-5}$, $\mathsf{RMSE}_{log-normal} = 3.2704 \times 10^{-5}$, $\mathsf{RMSE}_{weibull} = 3.7234 \times 10^{-5}$, $\mathsf{RMSE}_{nakagami} = 5.4326 \times 10^{-5}$. This shows that the log-logistic model is more accurate than the other three models.

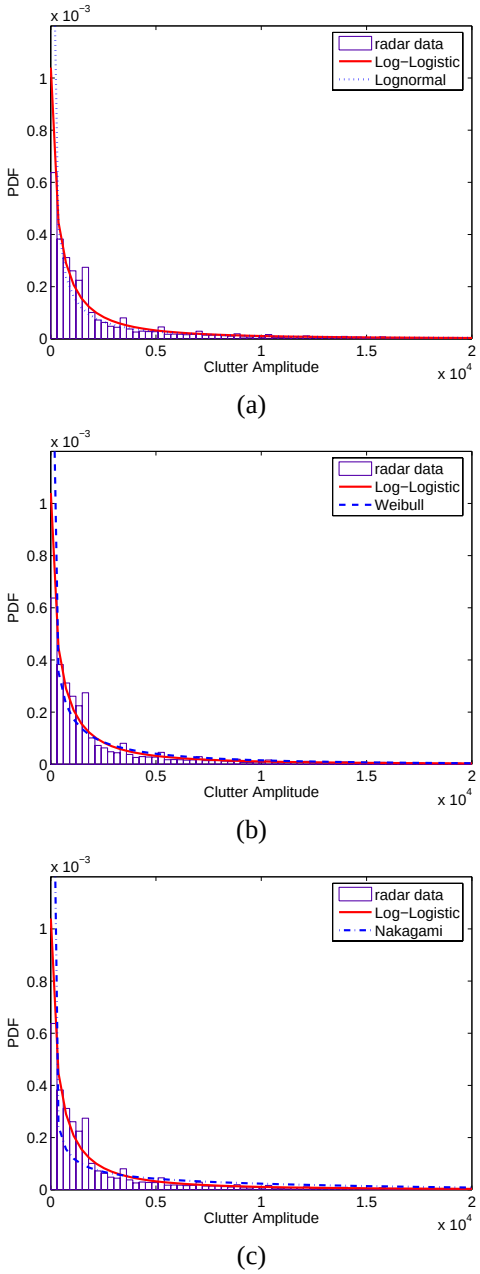

Fig. 3. Clutter model comparison (a) log-logistic vs. log-normal, and (b) log-logistic vs. weibull (c) log-logistic vs. nakagami. $\mathsf{RMSE}_{log-logistic} = 2.5425 \times 10^{-5}$, $\mathsf{RMSE}_{log-normal} = 3.2704 \times 10^{-5}$, $\mathsf{RMSE}_{weibull} = 3.7234 \times 10^{-5}$, $\mathsf{RMSE}_{nakagami} = 5.4326 \times 10^{-5}$.

V. Target Detection Performance

One of the primary goal to be carried out by a radar is target detection. On a basis of the clutter model that have been just studied, we may apply a special case of the Bayesian criterion named Neyman-Person criterion to analyze the target detection performance in the foliage environment.

If the received sample signal to be tested is R, then the two

hypotheses are shown as follows:

$$\begin{aligned} H_0 &: R = C + n \\ H_1 &: R = S + C + n \end{aligned} \tag{5}$$

where C and n represent the random variable of clutter and noise respectively. C follows log-logistic model with both parameters μ and σ, and n is gaussian noise with zero mean and variance ν^2. S is the target signal, which assumes to be a constant for simplicity.

Therefore $f(R|H_0)$ means PDF of R given that a target was not present while $f(R|H_1)$ means PDF of R given that a target was present.

They can be denoted as follows:

$$f(R|H_0) = \int_0^\infty \frac{e^{\frac{lnr-\mu}{\sigma}}}{\sigma r(1+e^{\frac{lnr-\mu}{\sigma}})^2} \times \frac{1}{\sqrt{2\pi}\nu} e^{-\frac{(R-r)^2}{2\nu^2}} dr \tag{6}$$

$$f(R|H_1) = \int_0^\infty \frac{e^{\frac{ln(r-s)-\mu}{\sigma}}}{\sigma(r-s)(1+e^{\frac{ln(r-s)-\mu}{\sigma}})^2} \times \frac{1}{\sqrt{2\pi}\nu} e^{-\frac{(R-s-r)^2}{2\nu^2}} dr \tag{7}$$

If the probability that a target was not present is $P(H_0)$ whereas that of a target was present is $P(H_1)$, then PDF of R is

$$f(R) = P(H_0)f(R|H_0) + P(H_1)f(R|H_1) \tag{8}$$

To decide whether there is a target or not, Neyman-Pearson detection rule is shown as

$$\frac{f(R|H_0)}{f(R|H_1)} \underset{H_1}{\overset{H_0}{\gtrless}} \frac{P(H_1)}{P(H_0)} \tag{9}$$

In case of $P(H_1) = P(H_0)$, (26) is simplified as

$$f(R|H_0) \underset{H_1}{\overset{H_0}{\gtrless}} f(R|H_1) \tag{10}$$

which actually is

$$\frac{e^{[\frac{s^2-2s(R-r)}{2\nu^2} + \frac{ln(\frac{r}{r-s})}{\sigma}]}}{\frac{r}{r-s}[\frac{1+e^{\frac{lnr-\mu}{\sigma}}}{1+e^{\frac{ln(r-s)-\mu}{\sigma}}}]^2} \underset{H_1}{\overset{H_0}{\gtrless}} 1 \tag{11}$$

It is easy to obtain the decision threshold T in terms of the above function

$$T = -\frac{\nu^2}{s} ln[\frac{1+e^{\frac{lnr-\mu}{\sigma}}}{1+e^{\frac{ln(r-s)-\mu}{\sigma}}}]^2 + \frac{\nu^2[ln(\frac{r}{r-s}) - \sigma]}{s\sigma} + \frac{s}{2} + r \tag{12}$$

Under hypothesis H_0, a false alarm occurs anytime $R > T$, therefore the probability of false alarm is

$$\begin{aligned} P_{FA} &= \int_T^\infty f(R|H_0)dR \\ &= \frac{\int_T^\infty \int_0^\infty \frac{e^{[-\frac{(R-r)^2}{2\nu^2} + \frac{lnr-\mu}{\sigma}]}}{(1+e^{\frac{lnr-\mu}{\sigma}})^2 r} drdR}{\sqrt{2\pi}\sigma\nu} \end{aligned} \tag{13}$$

Similarly, Under hypothesis H_1, when $R > T$, the target is detectable. Therefore the probability of detection is

$$\begin{aligned} P_D &= \int_T^\infty f(R|H_1)dR \\ &= \frac{\int_T^\infty \int_0^\infty \frac{e^{[-\frac{(R-r-s)^2}{2\nu^2} + \frac{ln(r-s)-\mu}{\sigma}]}}{(1+e^{\frac{ln(r-s)-\mu}{\sigma}})^2 (r-s)} drdR}{\sqrt{2\pi}\sigma\nu} \end{aligned} \tag{14}$$

As mentioned in section IV, $\mu \approx 7.1$ and $\sigma \approx 1.1$ by means of MLE. If $\nu = 1$, then (13) and (14) become

$$P_{FA} = 0.362675 \int_T^\infty \int_0^\infty \frac{e^{-0.5(R-r)^2 + 0.91(lnr-7.1)}}{[1+e^{0.91(lnr-7.1)}]^2 r} drdR \tag{15}$$

$$P_D = 0.362675 \int_T^\infty \int_0^\infty \frac{e^{-0.5(R-r-s)^2 + 0.91[ln(r-s)-7.1]}}{\{1+e^{0.91[ln(r-s)-7.1]}\}^2 (r-s)} drdR \tag{16}$$

VI. Conclusion

On a basis of foliage clutter data measured by the UWB radar, we show that it is more accurate to describe foliage clutter using log-logistic statistic model rather than log-normal, Weibull, or Nakagami. Future research will investigate the characteristics of target to better achieve the target detection, tracking and imaging.

Acknowledgement

This work was supported in part by Office of Naval Research (ONR) under Grant N00014-07-1-0395, N00014-07-1-1024, and National Science Foundation (NSF) under Grant CNS-0721515.

References

[1] Skolnik, M. I.,*Introduction to Radar Systems*, 3rd ed, New York, McGraw Hill, 2001.

[2] Fleischman, J. G., Ayasli, S., Adams, E. M., and Gosselin, D. R., Foliage penetration experiment: Part I: Foliage attenuation and backscatter analysis of SAR imagery, *IEEE Trans. on Aerosp. Electron. Syst.*, 32, 1, part 1 of 3 (1996), 134-144.

[3] Mccorkle, J. W., "Early results from the ARL UWB Foliage attenuation (FOPEN) SAR", Presented at the SPIE International Symposium on Optical Engineering and Photonics in Aerospace and Remote Sensing, Conference 1942, Underground and Obscured Object Detection, Apr. 1993.

[4] Sheen, D. R., Malinas, N. P., Kletzli, D. W., Lewis, T. B., and Roman, J. F., "Foliage transmission meassurement using a ground-based ultra-wideband (UWB) (300-1300MHz) SAR system", *IEEE Trans. on Geoscience and Remote Sensing*, 32, 1(1994).

[5] Watts, S., "Radar detection prediction in K-distribution sea clutter and thermal noise", *IEEE Trans. on Aerosp. Electron. Syst.*, AES-23, 1, 1987, pp. 40-45.

[6] Dill, C., "Foliage Penetration (Phase II) Field Test: Narrowband versus Wideband Foliage Penetration," Final Report of Contract Number F41624-03-D-7001/04, July 2005 to Feb 2006.

[7] Gupta, R. C., Akman, O. and Lvin, S., "A Study of Log-Logistic Model in Survival Analysis", *Biometrical Journal*, 41, pp. 431-443, 1999

[8] Devore, Probability and Statistics for Engineering and the Sciences. Monterey, CA: BrooksiCole, 1982.

[9] Barkat, M., Signal deteciton and estimation, 2nd, London: Artech house, 2005.

TABLE I

ESTIMATED PARAMETERS AND STD ERROR

PDF	Log-Logistic	Log-normal	Weibull	Nakagami
data 1	$\hat{\mu} = 7.24161$ $\hat{\sigma} = 1.06483$ $\varepsilon_\mu = 0.0141212$ $\varepsilon_\sigma = 0.00724181$	$\hat{\mu} = 7.0455$ $\hat{\sigma} = 2.20761$ $\varepsilon_\mu = 0.0174527$ $\varepsilon_\sigma = 0.0123415$	$\hat{a} = 2975.33$ $\hat{b} = 0.594979$ $\varepsilon_a = 41.6157$ $\varepsilon_b = 0.00356925$	$\hat{\mu} = 0.177062$ $\hat{\omega} = 9.09663e+007$ $\varepsilon_\mu = 0.00150615$ $\varepsilon_\omega = 1.70907e+006$
data 2	$\hat{\mu} = 6.9716$ $\hat{\sigma} = 1.2126$ $\varepsilon_\mu = 0.014747$ $\varepsilon_\sigma = 0.00773723$	$\hat{\mu} = 6.72573$ $\hat{\sigma} = 2.33617$ $\varepsilon_\mu = 0.0184691$ $\varepsilon_\sigma = 0.0130602$	$\hat{a} = 2285.13$ $\hat{b} = 0.563747$ $\varepsilon_a = 33.7127$ $\varepsilon_b = 0.00337485$	$\hat{\mu} = 0.162375$ $\hat{\omega} = 7.4776e+007$ $\varepsilon_\mu = 0.00137422$ $\varepsilon_\omega = 1.46679e+006$
data 3	$\hat{\mu} = 7.00554$ $\hat{\sigma} = 1.10741$ $\varepsilon_\mu = 0.0145728$ $\varepsilon_\sigma = 0.0076303$	$\hat{\mu} = 6.76262$ $\hat{\sigma} = 2.31258$ $\varepsilon_\mu = 0.0182825$ $\varepsilon_\sigma = 0.0129283$	$\hat{a} = 2341.52$ $\hat{b} = 0.57073$ $\varepsilon_a = 34.1207$ $\varepsilon_b = 0.00341448$	$\hat{\mu} = 0.164695$ $\hat{\omega} = 7.46366e+007$ $\varepsilon_\mu = 0.001395$ $\varepsilon_\omega = 1.45459e+006$
data 4	$\hat{\mu} = 7.03055$ $\hat{\sigma} = 1.07858$ $\varepsilon_\mu = 0.0142027$ $\varepsilon_\sigma = 0.00741556$	$\hat{\mu} = 6.80711$ $\hat{\sigma} = 2.25973$ $\varepsilon_\mu = 0.0178647$ $\varepsilon_\sigma = 0.0126329$	$\hat{a} = 2395.85$ $\hat{b} = 0.579381$ $\varepsilon_a = 34.4066$ $\varepsilon_b = 0.00345156$	$\hat{\mu} = 0.167391$ $\hat{\omega} = 7.4926e+007$ $\varepsilon_\mu = 0.0014916$ $\varepsilon_\omega = 1.44727e+006$
data 5	$\hat{\mu} = 7.16226$ $\hat{\sigma} = 1.10132$ $\varepsilon_\mu = 0.014605$ $\varepsilon_\sigma = 0.00750067$	$\hat{\mu} = 6.95712$ $\hat{\sigma} = 2.26592$ $\varepsilon_\mu = 0.0179137$ $\varepsilon_\sigma = 0.0126675$	$\hat{a} = 2806.76$ $\hat{b} = 0.577823$ $\varepsilon_a = 40.4226$ $\varepsilon_b = 0.00347389$	$\hat{\mu} = 0.17112$ $\hat{\omega} = 9.03298e+007$ $\varepsilon_\mu = 0.00145265$ $\varepsilon_\omega = 1.72749e+006$
data 6	$\hat{\mu} = 7.01527$ $\hat{\sigma} = 1.10123$ $\varepsilon_\mu = 0.0144902$ $\varepsilon_\sigma = 0.00758568$	$\hat{\mu} = 6.77515$ $\hat{\sigma} = 2.30286$ $\varepsilon_\mu = 0.0182057$ $\varepsilon_\sigma = 0.012874$	$\hat{a} = 2360.33$ $\hat{b} = 0.572749$ $\varepsilon_a = 34.2753$ $\varepsilon_b = 0.00342376$	$\hat{\mu} = 0.165292$ $\hat{\omega} = 7.50824e+007$ $\varepsilon_\mu = 0.00140035$ $\varepsilon_\omega = 1.46145e+006$
data 7	$\hat{\mu} = 7.14523$ $\hat{\sigma} = 1.09486$ $\varepsilon_\mu = 0.0145132$ $\varepsilon_\sigma = 0.00745994$	$\hat{\mu} = 6.94201$ $\hat{\sigma} = 2.25621$ $\varepsilon_\mu = 0.0178369$ $\varepsilon_\sigma = 0.0126132$	$\hat{a} = 2753.69$ $\hat{b} = 0.578948$ $\varepsilon_a = 39.585$ $\varepsilon_b = 0.00347442$	$\hat{\mu} = 0.170964$ $\hat{\omega} = 8.80474e+007$ $\varepsilon_\mu = 0.00145125$ $\varepsilon_\omega = 1.68382e+006$
data 8	$\hat{\mu} = 6.95411$ $\hat{\sigma} = 1.11486$ $\varepsilon_\mu = 0.0146774$ $\varepsilon_\sigma = 0.00768003$	$\hat{\mu} = 6.71591$ $\hat{\sigma} = 2.31898$ $\varepsilon_\mu = 0.0183331$ $\varepsilon_\sigma = 0.0129641$	$\hat{a} = 2250.66$ $\hat{b} = 0.564989$ $\varepsilon_a = 33.1387$ $\varepsilon_b = 0.0033763$	$\hat{\mu} = 0.162448$ $\hat{\omega} = 7.31436e+007$ $\varepsilon_\mu = 0.00137488$ $\varepsilon_\omega = 1.4338e+006$
data 9	$\hat{\mu} = 7.18561$ $\hat{\sigma} = 1.09854$ $\varepsilon_\mu = 0.0145483$ $\varepsilon_\sigma = 0.00749265$	$\hat{\mu} = 6.9715$ $\hat{\sigma} = 2.27088$ $\varepsilon_\mu = 0.0179529$ $\varepsilon_\sigma = 0.0126952$	$\hat{a} = 2840.72$ $\hat{b} = 0.581219$ $\varepsilon_a = 40.6593$ $\varepsilon_b = 0.0034984$	$\hat{\mu} = 0.172324$ $\hat{\omega} = 8.97304e+007$ $\varepsilon_\mu = 0.00146348$ $\varepsilon_\omega = 1.70923e+006$
data 10	$\hat{\mu} = 7.192$ $\hat{\sigma} = 1.0866$ $\varepsilon_\mu = 0.0144166$ $\varepsilon_\sigma = 0.0073916$	$\hat{\mu} = 6.99196$ $\hat{\sigma} = 2.23975$ $\varepsilon_\mu = 0.0177067$ $\varepsilon_\sigma = 0.0125211$	$\hat{a} = 2869.65$ $\hat{b} = 0.584803$ $\varepsilon_a = 40.837$ $\varepsilon_b = 0.00351294$	$\hat{\mu} = 0.173572$ $\hat{\omega} = 9.01631e+007$ $\varepsilon_\mu = 0.0014747$ $\varepsilon_\omega = 1.71142e+006$

TABLE II

AVERAGED ESTIMATED PARAMETERS

PDF	Log-Logistic	Log-normal	Weibull	Nakagami
average	$\hat{\mu} = 7.0904$ $\hat{\sigma} = 1.1061$ $\varepsilon_\mu = 0.0145$ $\varepsilon_\sigma = 0.0075$	$\hat{\mu} = 6.8695$ $\hat{\sigma} = 2.2771$ $\varepsilon_\mu = 0.0180$ $\varepsilon_\sigma = 0.0127$	$\hat{a} = 2588$ $\hat{b} = 0.5769$ $\varepsilon_a = 37.4316$ $\varepsilon_b = 0.0035$	$\hat{\mu} = 0.1687$ $\hat{\omega} = 8.218e+007$ $\varepsilon_\mu = 0.0014$ $\varepsilon_\omega = 1.4905e+006$

This full text paper was peer reviewed at the direction of IEEE Communications Society subject matter experts for publication in the ICC 2008 proceedings.

A Differential Based Approach for Sense-Through-Foliage Target Detection using UWB Radar Sensor Networks

Jing Liang, Qilian Liang
Department of Electrical Engineering
University of Texas at Arlington
Arlington, TX 76019-0016, USA
Email: jliang@wcn.uta.edu, liang@uta.edu

Sherwood W. Samn
Air Force Research Laboratory/HEX
Brooks City Base
San Antonio, TX 78235, USA
Email: Sherwood.samn@brooks.af.mil

***Abstract*— In this paper, the foliage penetration measurement data is provided by Air Force Office of Scientific Research (AFOSR). When radar echoes are in good quality, the detection of target can be achieved by applying our differential based technology on received single UWB radar waveform. We compared our approach in case of no target as well as with target against the scheme in which 2-D image was created via adding voltages with the appropriate time offset. Results show that our approach can work much better. When radar echoes are in poor condition and single radar is unable to carry out the detection, we employ both Radar Sensor Networks (RSN) and RAKE structure to combine the echoes from different radar members and successfully detect the target.**

I. Introduction

Detection and identification of military equipment in a strong clutter background, such as foliage, soil cover or building leads has been a long-standing subject of intensive study. It is believed that solving the target detection through foliage will significantly benefit sense-through-wall and many other subsurface sensing problems. However, to this date, the detection of foliage-covered military targets, such as artillery, tanks, trucks and other weapons with the required probability of detection and false alarm still remains a challenging issue. This is due to the following facts:

1) Given certain low radar cross section(RCS), scattering from tree trunk and ground reflectivity may overwhelm the returned target signals of interest.
2) Very high multiple fading severely corrupt the amplitude and phase of the echoes.
3) Even if target is stationery, tree leaves and branches are likely to swing in result of gust, which will result in doppler shift of clutter and difficulty of target detection.

Therefore, our main goal is to account for the above effects and better analyze the "defoliated" signal and thus improve the probability of target detection.

Over the past two decades, following 3 types of signals have been mainly studied to examine the performance on target detection in foliage:

1) Traditional sinusoidal waveforms at VHF through UHF bands [1], as the lower the radar frequency, the lower the attenuation and scattering from branches and trees, and thus better penetration through foliage. However, these approaches result in low resolution and low RCS.
2) Millimeter-Wave (MMW) radars are used in [2] [3] and [4]. Results demonstrate the potential for satisfying performance but need further investigation.
3) Relatively low frequency Ultra-wide band (UWB) radars between 100 MHZ and 3 GHz are frequently employed in recent years owning to the characteristics provided by their high resolutions as well as the very good ability of penetration, such as penetrating walls [5] [6]. Despite comparatively short detection range, UWB signal would have advantages over a narrowband signal with limited frequency content.

In this paper, we will apply our expertise in signal processing, data fusion, radar sensor networks (RSN) etc. to achieve effective through-foliage technology using ultra-wideband (UWB) radar and extracting as much information as possible to improve the probability of target detection.

The remainder of this paper is organized as follows. In Section II, we summarize the measurement and collection of data we used in this paper. In Section III, we propose a differential based approach for through-foliage target detection when the signal quality is good. In Section IV, we propose RSN and RAKE structure for through-foliage target detection when the signal quality is poor. We conclude this paper and discuss some future research topics in Section V.

II. Sense-Through-Foliage Data Measurement and Collection

Our work is based on the sense-through-foliage data from Air Force Research Lab [7]. The foliage penetration measurement effort began in August 2005 and continued through December 2005. Working in August through the fall of 2005, the foliage measured included late summer foliage and fall and early winter foliage. Late summer foliage, because of the limited rainfall, involved foliage with decreased water content. Late fall and winter measurements involved largely defoliated but dense forest.

The foliage experiment was constructed on a seven-ton man lift, which had a total lifting capacity of 450 kg. The limit of the lifting capacity was reached during the experiment as essentially the entire measuring apparatus was placed on the lift. The principle pieces of equipment secured on the lift are: Barth pulser, Tektronix model 7704 B oscilloscope, dual antenna mounting stand, two antennas, rack system, IBM laptop, HP signal Generator, Custom RF switch and power supply and Weather shield (small hut). The target is a trihedral reflector (as shown in Fig. 1). Throughout this work, a Barth pulse source (Barth Electronics, Inc. model 732 GL) was used. The pulse generator uses a coaxial reed switch to discharge a charge line for a very fast rise time pulse outputs. The model 732 pulse generator provides pulses of less than 50 picoseconds (ps) rise time, with amplitude from 150 V to greater than 2 KV into any load impedance through a 50 ohm coaxial line. The generator is capable of producing pulses with a minimum width of 750 ps and a maximum of 1 microsecond. This output pulse width is determined by charge line length for rectangular pulses, or by capacitors for 1/e decay pulses.

Fig. 1. The target (a trihedral reflector) is shown on the stand at 300 feet from the lift.

For the data we used in this paper, each sample is spaced at 50 picosecond interval, and 16,000 samples were collected for each collection for a total time duration of 0.8 microseconds at a rate of approximately 20 Hz. We considered two sets of data from this experiment. Initially, the Barth pulse source was operated at low amplitude and 35 pulses reflected signal were averaged for each collection. these collectionsThe scheme for the sense-through-foliage target detection with "poor" signal quality will be presented in Section IV. Later, good signal quality data were collected using higher amplitude pulses and 100 pulses reflected signals were averaged for each collection. The scheme for target detection with "good" signal quality will be presented in Section III.

III. Target Detection with Good Signal Quality: A Differential-Based Approach

In Fig. 2, we plot two collections with good signal quality, one without a target on range (Fig. 2a) and the other one with a target on range (Fig. 2b and target appears at around sample 14,000). To make it more clear to the readers, we provide expanded views of traces (with target) from sample 13,001 to 15,000 for the above two collections in Figs. 3a and 3b. Since there is no target in Fig. 3a, it can be treated as the response of foliage clutter. It's quite straightforward that the target response will be the echo difference between Fig. 3b and Fig. 3a, which is plotted in Fig. 3c. However, in practical situation we either obtain Fig. 3a (clutter echo without target) or Fig. 3b (target on range) without the knowledge about the presence of a target. The challenge is how can certain artificial intelligence make target detection only based on Fig. 3b (with target) or Fig. 3a (no target)?

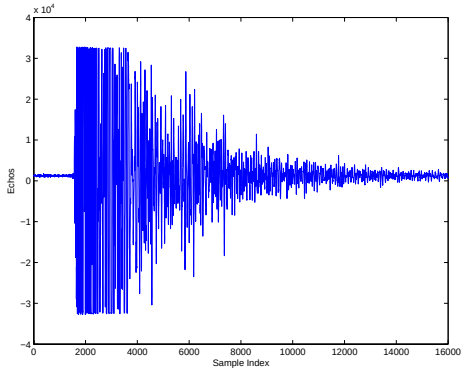

(a)

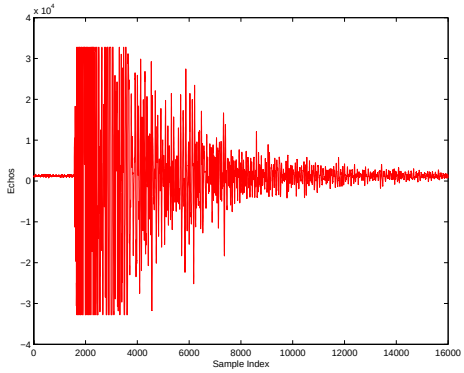

(b)

Fig. 2. Measurement with very good signal quality and 100 pulses average. (a) no target on range (b) with target on range (target appears at around sample 14000)

To solve this problem, a scheme is previously proposed in [8], where 2-D image was created via adding voltages with the appropriate time offset. In Figs. 4(a) and 4(b), we plot the 2-D image created based on the above two data sets (from samples 13,800 to 14,200) using the approach in [8]. However, from these two figures, we can not clearly tell which image shows there is target on range.

The block diagram of our approach is generalized in Fig.5.

Actually, the waveforms in Fig. 2a and 2b result from the synthesized effect of large-scale path loss and small-scale fading. We believe if UWB propagation channel at foliage can be accurately estimated based on transmitted signals and

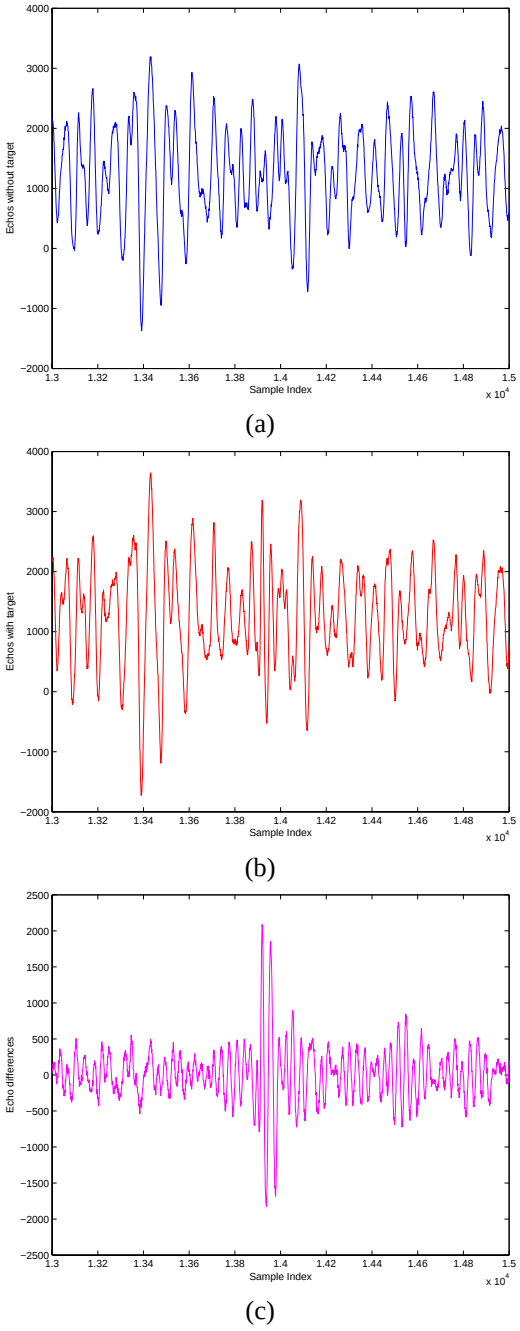

Fig. 3. Measurement with good signal quality and 100 pulses integration (a) Expanded view of traces (no target) from samples 13001 to 15000 (b) Expanded view of traces (with target) from samples 13001 to 15000 (c) Expanded view of traces difference between with and without target

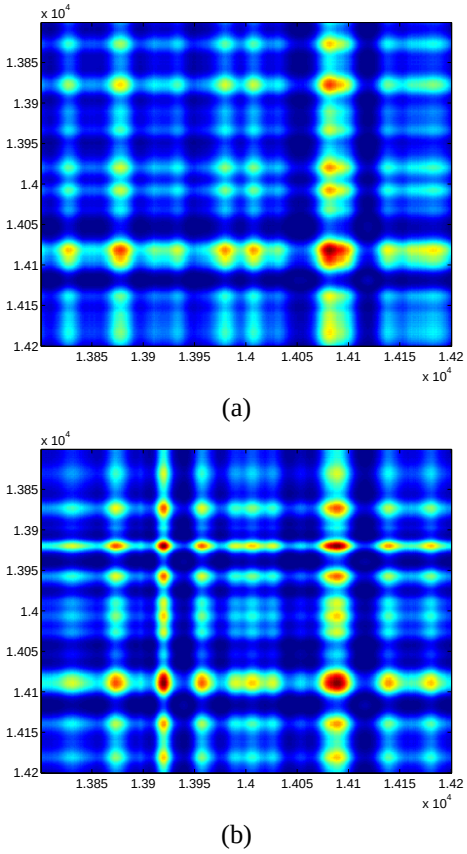

Fig. 4. 2-D image created via adding voltages with the appropriate time offset (a) no target (b) with target in the field

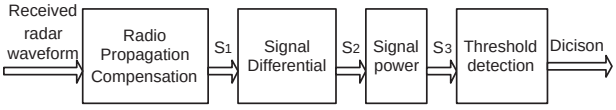

Fig. 5. Block diagram of differential based approach for single radar

received echoes with good quality, we may compensate the "foliage-based" UWB channel effect on received waveforms and the target under foliage will be more detectable. However, to this date, the outdoor channel model for UWB radars is still an open problem.

According to UWB indoor multi-path channel model (IEEE 802.15.SG3a, 2003), the average power delay profile (PDP) is characterized by an exponential decay of the amplitude of the clusters [9]. Therefore, we may roughly consider the foliage channel gain model as

$$\hat{y} = \begin{cases} Ae^{-Bx} & y > 0 \\ -Ae^{-Bx} & \text{otherwise} \end{cases} \quad (1)$$

where $\hat{y}$ is the amplitude of estimated clutter echo, x is sample index and y is the amplitude of original measured data. A and B are constants. These two parameters should be carefully chosen so that $\hat{y}$ is as close to y as possible. Here we use $A = 35000$ and $B = 0.00025$. Although it deserves much

further study on the estimation problem, we shall see later that as the target appears at a tail part, this simple estimation is applicable, therefore we get the processed signal:

$$S_1 = y - \hat{y} \tag{2}$$

Observe Fig. 3b, for samples where target appears (around sample 14,000), the waveform changes much abruptly than that in Fig. 3a. As differential value represents the changing rate of a function, it is quite intuitively that the amplitude of differential value at around sample 14,000 should be large. Apply differentiator and power ordinally,

$$S_2 = \frac{dS_1}{dx} \tag{3}$$

$$S_3 = {S_2}^2 \tag{4}$$

We plot the power of clutter-accounted and differentiated echoes in Fig. 6. It is quite straightforward to see there is no target in Fig. 6a and there is target in Fig. 6b.

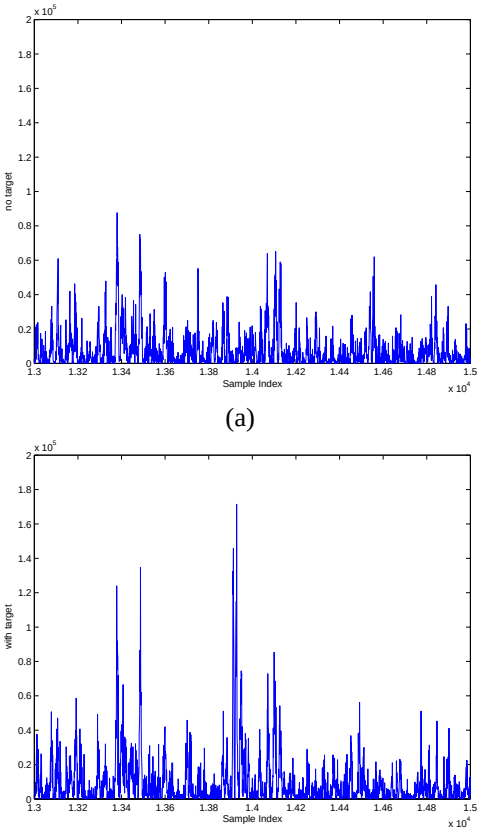

Fig. 6. The power of processed waveforms (a) no target (b) with target in the field

IV. Target Detection with Poor Signal Quality: Radar Sensor Network and Differential-Based Approach

As mentioned in Section II, when the Barth pulse source was operated at low amplitude and the sample values are not obtained based on sufficient pulse response averaging (averaged over 35 pulses for each collection), significant pulse-to-pulse variability was noted and the return signal quality is poor. Fig. 8a illustrate the received echoes in this situation. Even with the application of our proposed differential-based scheme, we can not tell whether there is target or not in the range based on Fig. 8b. Since pulse-to-pulse variability exists in the echos at different time or different site, this motivate us to explore the spatial and time diversity using Radar Sensor Networks (RSN).

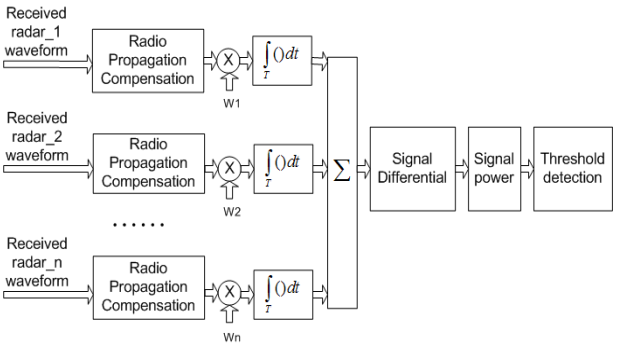

Fig. 7. Block diagram of differential based approach and diversity combination in RSN

In nature, a network of multiple radar sensors can been utilized to combat performance degradation of single radar [10]. These radar sensors are managed by an intelligent clusterhead that combines waveform diversity in order to satisfy the common goals of the network other than each radar operate substantively. As radar sensors are environment dependent [11], it may provide better signal quality if different neighboring radars work collaboratively to perform data fusion. For example, consider a system of two radars. When the signal of either radar unfortunately experience a severe fading, if two radars are spaced sufficiently far apart, it is not likely that both of the radars experience deep fade at the same time. By selecting better waveform from the two radar waveforms, the data is less likely to be lost.

In this paper, we assume the radar sensors are synchronized in RSN and we employed RAKE structure to combine received information for RSN. The detailed process is shown in Fig. 7. The echo, i.e., RF response by the pulse of each cluster-member radar sensor, will be combined by the clusterhead using a weighted average, and the weight w_i is determined by the power of each echo $x_i(m)$ (m is the sample index),

$$w_i = \frac{E_i}{\sum_{i=1}^{n} E_i} \tag{5}$$

and

$$E_i = \text{var}(x_i(m)) + [\text{mean}(x_i(m))]^2 \tag{6}$$

We ran simulations for n = 35 and plot the power of combined signal obtained through differential based approach in Fig. 8c. Compare this figure with Fig. 8a and Fig. 8b, it is quite obvious to see that there is a target around sample 14,000.

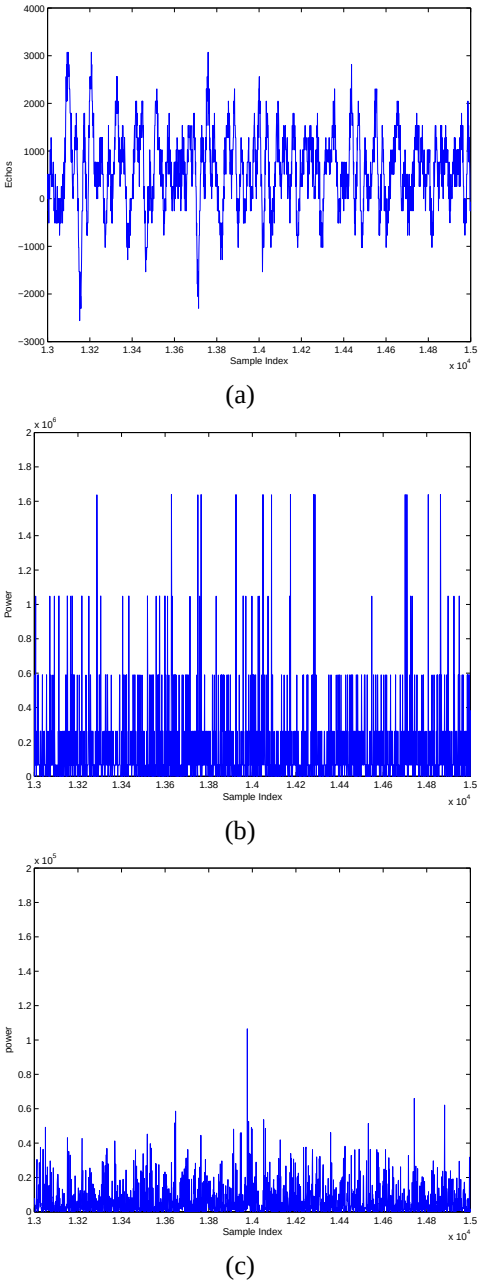

Fig. 8. Measurement with poor signal quality (with target) and 35 pulses integration (a) Expanded view of traces with target from samples 13001 to 15000 (b) Power of single radar after differential based approach (c) Power after both differential based approach and echoes combination in RSN

V. Conclusion and Future Works

In this paper, we propose a differential-based signal processing approach on received UWB Radar waveforms to improve through-foliage target detection. The foliage penetration measurements were taken in Holliston, Massachusetts. When radar echoes are in good quality, the detection of target can be achieved by applying differential-based technology to single radar waveform. We compared our approach in case of no target as well as with target against the scheme in which 2-D image was created via adding voltages with the appropriate time offset. Results show that our approach can work much better. When radar echoes are in poor condition and single radar is unable to carry out detection, we employe both Radar Sensor Networks (RSN) and RAKE structure to combine the echoes from different radar members and finally successfully detect the target. For future works, we will collect more data with different targets and perform automatic target recognition besides target detection.

Acknowledgement

This work was supported in part by Office of Naval Research (ONR) under Grant N00014-07-1-0395, N00014-07-1-1024, and National Science Foundation (NSF) under Grant CNS-0721515.

References

[1] S. Ayasli and L. Bessette, " UHF & VHF SAR phenomenology, presented at the Proc. PIERS, Workshop on Advances in Radar Mathods, Baveno, Italy, July 20-22, 1998"

[2] F. K. Schwering, E. J. Violette and R. H. Espeland, "Millimeter-wave propagation in vegetation: Experiments and theory", *IEEE Trans. Geosci. Remote Sensing*, vol.26, pp. 355-367, May 1988

[3] F. T. Ulaby, T. E. Van Deventer, J. R. East, T. F. Haddock and M. E. Coluzzi, "Millimeter-wave bistatic scaterring from ground and vegetation targets" , *IEEE Trans. Geosci. Remote Sensing*, vol.26, pp. 229-243, May 1988

[4] A. Y. Nashashibi, k. Sarabandi, S. Oveisgharan *et al.*, "Millimeter-Wave Measurement of Foliage Attenuation and Ground Reflectivity of Tree Stands at Nadir Incidence", *IEEE Trans. Antennas Propagat.*, vol.52, pp.1211-2004, May, 2004

[5] B. Ferrell "Ultrawideband foliage penetration measurement", in *Proc. IEEE Nation Radar Conf.*, Mar. 29-31, pp.80-84, 1994

[6] X. Xu; R. M. Narayanan, "FOPEN SAR imaging using UWB step-frequency and random noise waveforms ", *IEEE Trans. Aerospace and Electronic Systems*, vol.37, pp.1287-1300, Oct. 2001

[7] C. Dill, "Foliage Penetration (Phase II) Field Test: Narrowband versus Wideband Foliage Penetration," *Final Report of Contract Number F41624-03-D-7001/04*, July 2005 to Feb 2006.

[8] P. Withington , H. Fluhler, and S. Nag, "Enhancing homeland security with advanced UWB sensors," *IEEE Microwave Magazine*, Sept 2003.

[9] Benedetto M. D and Giancola G., *Understanding Ultra Wide Band Radio Fundamentals*, Person Education, 2004

[10] S. Haykin, "Cognitive radar networks" , *2005 1st IEEE International Workshop on Computational Advances in Multi-Sensor Adaptive Processing*, pp.1-3, Dec 2005.

[11] R. A. Johnson and E. L. Titlebaum, "Range Doppler Uncoupling in the Doppler Tolerant Bat Signal", *Proc. of IEEE Ultrasonics Symposium* , New York, pp.64-67, 1972.

Compressive Sensing for Radar Sensor Networks

Qilian Liang
Department of Electrical Engineering
416 Yates St, Rm 518
University of Texas at Arlington
Arlington, TX 76019-0016
E-mail: liang@uta.edu

***Abstract*— Motivated by recent advances on Compressive Sensing (CS) and high data redundancy among radars in radar sensor networks, we study CS for radar sensor networks. We demonstrate that the sense-through-foliage UWB radar signals are very sparse, which means CS could be applied to radar sensor networks to tremendously reduce the sampling rate. We propose to apply SVD-QR and maximum likelihood algorithms to CS for radar sensor networks. SVD-QR could vastly reduce the number of radar sensors, and CS is applied to the selected radar sensors for data compression. Simulations are performed and our compression ratio could be 192:1 overall.**

Index Terms: Compressive sensing, radar sensor networks, SVD-QR, sense-through-foliage, UWB, sparsity.

I. Introduction

Compressive sensing (CS) is a new method to capture and represent compressible signals at a rate significantly below the Nyquist rate. It employs nonadaptive linear projections that preserve the structure of the signal; the signal is then reconstructed from these projections using an optimization process. This leads immediately to new signal reconstruction methods that are successful with surprisingly few measurements, which in turn leads to signal acquisition methods that effect compression as part of the measurement process (hence "compressive sensing"). These recent realizations (though built upon prior work exploiting signal sparsity) have spawned an explosion of research yielding exciting results in a wide range of topics, encompassing algorithms, theory, and applications.

So far, no work has been reported on CS for radar sensor networks. In CS for radar signals, very few works have been reported. In [1], it shows that matched filter could be eliminated if CS is used for radar. In [2], SAR radar image was processed using wavelets basis. In [13], a stylized compressed sensing radar is proposed in which the time-frequency plane is discretized into an N×N grid. In [15], a joint basis selection and sparse parameter estimation (called fast Bayesian mathcing pursuit) algorithm was proposed. In [17], a heuristic, graph-structured, sparse signal representation algorithm for overcomplete dictionaries that can be decomposed into subdictionaries was proposed and applied to SAR imaging. In [3][4], passive radar using OFDM was applied to target signature detection.

The rest of this paper is organized as follows. In Section II, we give an overview of compressive sensing. In Section III, we study the sparsity of narrowband and UWB radar signals. In Section V, we present our results on compressive sensing for UWB radar signals. Section VI concludes this paper.

II. Compressive Sensing: an Overview

CS provides a framework for integrated sensing and compression of discrete-time signals that are sparse or compressible in a known basis or frame. Let z denote a signal of interest, and Ψ denote a sparsifying basis (or called transform domain), such that $z = \Psi\theta$, with $\theta \in \mathbb{R}^N$ being a K-sparse vector, i.e. $\|\theta\|_0 = K$. Traditional transform coding compression techniques acquire first z in its entirety, and then calculate its sparse representation θ in order to encode its nonzero values and their locations, but CS aims to preclude the full signal acquisition by measuring a set y of linear projections of z into vectors ϕ_i, $1 \leq i \leq M$. By stacking these vectors as rows of a matrix Φ (measurement matrix), we can represent the measurements as $y = \Phi z = \Phi\Psi\theta$. The main result in CS states that when the matrix $\Phi\Psi$ holds the restricted isometry property (RIP) [7][10], then the original sparse representation θ is the unique solution to the linear program

$$\hat{\theta} = \arg\min_{\theta\in\mathbb{R}^N} \|\theta\|_{\ell_1} \quad (1)$$

$$s.t.\ y = \Phi\Psi\theta, \quad (2)$$

known as Basis Pursuit, where ℓ_1–norm is defined as ($\|\theta\|_{\ell_1} \equiv \sum_i |\theta_i|$). Thus, the original signal z can be recovered from the measurement vector y in polynomial time. Furthermore, choosing Φ to be a matrix with independent gaussian-distribtued entries satisfies the RIP for $\Phi\Psi$ when Ψ is a basis or tight frame and $M = O(K\log(N/K))$.

III. Sparsity of Narrowband and UWB Radar Signals

Recently, we studied UWB radar sensor signals in a foliage environment and observed that it is very sparse, which satisfies the requirement for compressive sensing. Our work is based on the data collected by AFRL in radar-based sense-through-foliage experiment in late summer and

fall. Late summer foliage, because of the limited rainfall, involved foliage with decreased water content. Late fall and winter measurements involved largely defoliated but dense forest, providing a rich scattering environment. Because of wind or different temperatures in dense forest, it's also a time-varying environment. The sense-through-foliage experiment was constructed on a seven-ton man lift (as shown in Fig. 1a), which had a total lifting capacity of 450 kg. The limit of the lifting capacity was reached during the experiment as essentially the entire measuring apparatus was placed on the lift. The principle pieces of equipment secured on the lift are: Barth pulser, Tektronix model 7704 B oscilloscope, dual antenna mounting stand, two antennas, rack system, IBM laptop, HP signal Generator, Custom RF switch and power supply and Weather shield (small hut). The target is a trihedral reflector (as shown in Fig. 1b). Throughout this work, a Barth pulse source (Barth Electronics, Inc. model 732 GL) was used. The pulse generator uses a coaxial reed switch to discharge a charge line for a very fast rise time pulse outputs. The model 732 pulse generator provides pulses of less than 50 picoseconds (ps) rise time, with amplitude from 150 V to greater than 2 KV into any load impedance through a 50 ohm coaxial line. The generator is capable of producing pulses with a minimum width of 750 ps and a maximum of 1 microsecond. This output pulse width is determined by charge line length for rectangular pulses, or by capacitors for 1/e decay pulses. For the data we used, each sample is spaced at 50 picosecond interval, and 16,000 samples were collected for each collection for a total time duration of 0.8 microseconds at a rate of approximately 20 Hz. The Barth pulse source was operated at low amplitude and 35 pulses reflected signal were averaged for each collection.

We applied the CLEAN algorithm to obtain the channel model based on the transmitted pulses and received echos. The CLEAN algorithm was first introduced in [14] and has been applied to UWB measurements [8][16] and it assumes that the channel is a series of impulses which is consistent with the tapped-delay line channel model. This algorithm searches the received echos iteratively with the transmit pulse to find the maximum correlation [6]. Based on the CLEAN method, we successfully obtained the channel impulse responses based on transmit pulses and receive echoes. For illustration purposes, in Fig. 2, we plot the channel impulse responses for UWB channels using CLEAN method based on one experiment.

Observe Fig. 2c, the channel impulse response $\theta = [\theta_1, \theta_2, \cdots, \theta_n]$ has very few nonzero taps out of 32,000 sample index). Let $\psi(i)$ denote the transmit pulse, The received echo could be represented as (if no noise)

$$z(i) = \theta * \psi(i) = \sum_{j=1}^{n} \theta_j \psi(i-j) = \Psi\theta \qquad (3)$$

where $*$ stands for convolution, and $\Psi = [\psi_1, \psi_2, \cdots, \psi_n]$ are transform domain functions (different time-shifts of transmit pulse). Since most θ_j's are zeroes under the transform basis Ψ, so the UWB radar signals $z(i)$ are very sparse, which validates that CS could be used to reduce the number of samples to collect.

(a)

(b)

Fig. 1. (a) The lift in the experiment. The antennas are at the far end of the lift from the viewer under the roof that was built to shield the equipment from the elements. (b) The target (a trihedral reflector) is shown on the stand at 300 feet from the lift.

IV. Compressive Sensing for Radar Sensor Networks Using SVD-QR Algorithm

We propose to use SVD-QR algorithm [11] [12] to compressive sensing for radar sensor networks. SVD-QR selects a set of independent data sets that minimize the residual error in a least-squares sense:

- Given $P \in R^{N \times M}$ (assuming $N > M$), and $rank(P) = r \leq M$. Determine a numerical estimate $r^{'}$ of the rank of the data sets matrix P by calculating

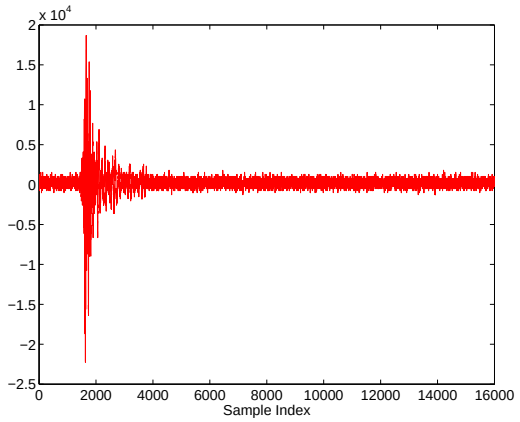

(a)

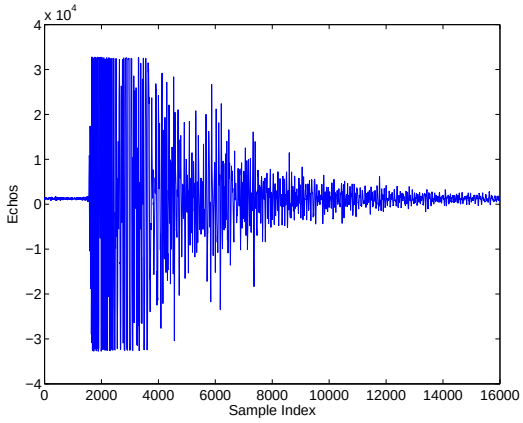

(b)

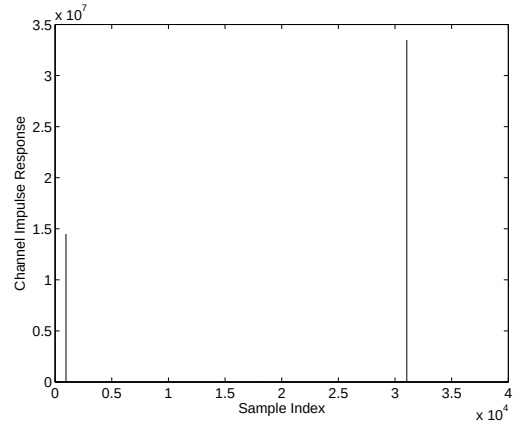

(c)

Fig. 2. UWB radar transmitted pulse, received echo, and channel impulse response in one experiment. (a) Transmitted pulse. (b) Received echo. (c) UWB channel impulse responses using CLEAN method.

the singular value decomposition

$$P = U \begin{bmatrix} \Sigma & 0 \\ 0 & 0 \end{bmatrix} V^T, \tag{4}$$

where, U is an $N \times N$ matrix of orthonormalized eigenvectors of PP^T, V is an $M \times M$ matrix of orthonormalized eigenvectors of $P^T P$, and Σ is the diagonal matrix $\Sigma = diag(\sigma_1, \sigma_2, \ldots, \sigma_r)$, where σ_i denotes the i^{th} singular value of P, and $\sigma_1 \geq \sigma_2 \geq \cdots \geq \sigma_r > 0$. Select $\hat{r} \leq r^{'}$.

- Calculate a permutation matrix Π such that the columns of the matrix $\Gamma_1 \in R^{N \times \hat{r}}$ in

$$P\Pi = [\Gamma_1, \Gamma_2] \tag{5}$$

are independent. The permutation matrix Π is obtained from the QR decomposition of the submatrix comprised of the right singular vectors, which correspond to the $\hat{r}$ ordered *most-significant* singular values.

Our procedures of CS for RSN are as follows:

1) Construct matrix $P \in R^{N \times M}$ (assuming $N > M$) where N is the number of time samples and M is the number of radars.
2) Take SVD-QR to matrix P, and determine the principal radar sensors to be used for CS based on the following steps:
   - Decomposes P, from the SVD of P, save V.
   - Observe Σ. Select an appropriate $\hat{r}$.
   - Partition
   $$V = \begin{bmatrix} V_{11} & V_{12} \\ V_{21} & V_{22} \end{bmatrix} \tag{6}$$
   where $V_{11} \in R^{\hat{r} \times \hat{r}}$, $V_{12} \in R^{\hat{r} \times (M-\hat{r})}$, $V_{21} \in R^{(M-\hat{r}) \times \hat{r}}$, and $V_{22} \in R^{(M-\hat{r}) \times (M-\hat{r})}$. In many practical cases, σ_1 is much larger than $\sigma_{r'}$; thus $\hat{r}$ can be chosen much smaller than the estimate $r^{'}$ of rank(P), even 1.
   - Using QR decomposition with column pivoting, determine Π such that
   $$Q^T [V_{11}^T, V_{21}^T] \Pi = [R_{11}, R_{12}], \tag{7}$$
   where Q is a unitary matrix, and R_{11} and R_{12} form an upper triangular matrix; and Π is the permutation matrix, the column permutation Π is chosen so that $abs(diag(R))$ is decreasing. In short, Π corresponds to the $\hat{r}$ ordered *most-significant* sets, i.e., a sub-set of $\hat{r}$ most important radar sensors are chosen.
3) Perform CS to the $\hat{r}$ most important radar sensors jointly. Explore the redundancy among different sensors in radar sensor network would tremendously reduce the sample sizes. Equation (2) could be extended into matrix format,

$$\hat{\Theta} = \arg \min_{\theta \in \mathbb{R}^N} \|\Theta\|_F \quad s.t. \ \mathbf{y} = \Phi\Psi\Theta, \tag{8}$$

where Θ and $\mathbf{y}$ are matrix, and each column is correpsonding to each sensor; $\|\Theta\|_F$ is Frobenius norm for matrix, which is defined as

$$\|\Theta\|_F = \sqrt{tr(\Theta^H \cdot \Theta)} = \sqrt{tr(\Theta \cdot \Theta^T)} \qquad (9)$$

If AWGN is added, the constraint can be written as

$$\mathbf{y} = \Phi\Psi\Theta + \mathbf{N} \qquad (10)$$

Since $\mathbf{y}$, $\Phi\Psi$ are known, and $\mathbf{N}$ is AWGN matrix, we use maximal likelihood method to determine Θ.

V. Simulations and Performance Analysis

We chose an iid Gaussian random matrix as sensing matrix Φ. $\Phi\Psi$ is also iid Gaussian for various orthonormal bases Ψ such as spikes, sinusoids, wavelets, Gabor functions, curvelets, and so on [10], so we chose $\psi_j(i) = n^{-1/2}\cos(2\pi ji/n), i = 0, 1, \cdots, n-1$. $\Phi\Psi$ is shown to have satisfied RIP with high probability, if $M \geq cK\log(N/K)$, where c is a small constant and hence stable reconstruction is possible with high probability [10]. Note that it is not known in advance which coefficients of Θ are zeroes, or which samples of z are not needed.

We ran simulations based on the above algorithm for a radar sensor networks with 30 radar sensors. Based on the radar sensor network data for 100 collections, we applied SVD-QR to select $\hat{r}$ most important radar sensors, and observed that $\hat{r}$ has mean value 5.23, and std 2.11. For each subset of selected sensors, we performed joint CS, and it turned that we could used only 500 samples to recover the original 16,000 samples, so the compression ratio is 32:1. Combining the spatial reduction (from 30 sensors to around 5 sensors), we could achieved compression ratio about 192:1 overall. For illustration purpose, in Fig. 3(a), we plot 16,000 samples sense-through-foliage signals in one collection of sense-through-foliage UWB radar sensors. In Fig. 3(b), we plot one column of sparse signals Θ (received echo z projected to cosine basis functions $\psi_j(i)$) and the recovered sparse signals (obtained via (2)). Observe that the original signals could be perfectly recovered.

VI. Conclusions

Motivated by recent advances on Compressive Sensing (CS) and high data redundancy among radars in radar sensor networks, we studied CS for radar sensor networks. We demonstrated that the sense-through-foliage UWB radar signals are very sparse, which means CS could be applied to radar sensor networks to tremendously reduce the sampling rate. We proposed to apply SVD-QR and maximum likelihood algorithms to CS for radar sensor networks. SVD-QR could vastly reduce the number of radar sensors, and CS was applied to the selected radar sensors for data compression. Simulations are performed and our compression ratio could be 192:1 overall.

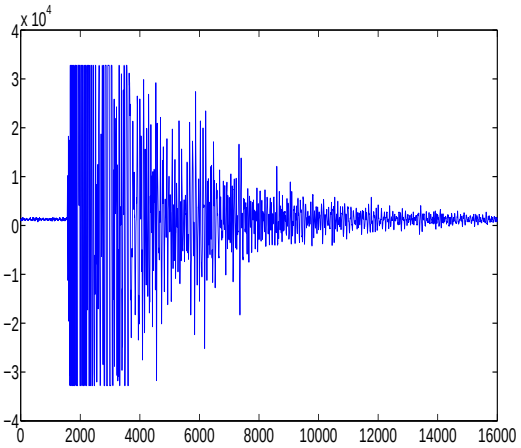

(a)

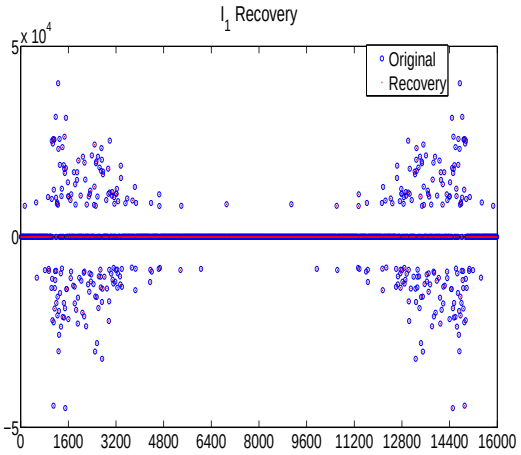

(b)

Fig. 3. (a) Original sense-through-foliage received echos (16,000 samples), and (b) ℓ_1-norm recovered sparse signals and the original sparse signals (origianl 16,000 samples projected to the cosine basis functions).

Acknowledgement

The author would like to thank his PhD student, Mr. Ji Wu, for helping with partial simulations, and Dr. Sherwood W. Samn in Air Force Research Laboratory/RHX for providing the radar data. This work was supported in part by the National Science Foundation under Grants CNS-0964713, CCF-0956438, CNS-1050618, and Office of Naval Research (ONR) under Grant N00014-07-1-0395 and N00014-07-1-1024.

References

[1] R. Baraniuk and P. Steeghs, "Compressive radar imaging," *IEEE Radar Conference*, Waltham, Massachusetts, April 2007.

[2] S. Bhattacharya, T. Blumensath, B. Mulgrew, and M. Davies, "Fast encoding of synthetic aperture radar raw data using compressed sensing," *IEEE Workshop on Statistical Signal Processing*, Madison, Wisconsin, August 2007)

[3] C. R. Berger, S. Zhou, P. Willett, "Signal Extraction Using Compressed Sensing for Passive Radar with OFDM Signals," *Proc. of the 11th Int. Conf. on Information Fusion*, Cologne, Germany, July 2008.

[4] C. R. Berger, S. Zhou, P. Willett, B. Demissie, J. Heckenbach, "Compressed Sensing for OFDM/MIMO Radar," *Proc. of the 42nd Annual Asilomar Conference on Signals, Systems and Computers*, Pacific Grove, CA, Oct. 2008.

[5] D. Bertsimas, J. N.Tsitsiklis " Introduction to Linear Optimization ," *Athena Scientific* , February, 1997.

[6] R. M. Buehrer, et al, "Characterization of the UWB channel," *IEEE Conf on Ultra Wideband Systems and Technologies*, pp. 26-31, Reston, VA, Nov 2003.

[7] E. Candés, "Compressive sampling," *Int. Congress of Mathematics*, vol. 3, pp. 1433-1452, Madrid, Spain, 2006.

[8] R. J.-M. Cramer, *An Evaluation of Ultrawideband Propagation Channels*, Ph.D Dissertation, USC, 2000.

[9] R. J.-M Cramer, R. A. Scholtz, and M. Z. Win, "Evaluation of an ultra-wide-band propagation channel," *IEEE Transactions on Antennas and Propagation*, vol 50, no. 5, May 2002, pp. 561 - 570.

[10] D. Donoho " Compressed Sensing ," *IEEE Trans. on Information Theory*, Vol.52, No.4, pp.1289-1306, April 2006.

[11] Golub, G. H., and C. F. Van Loan, *Matrix Computations*, Johns Hopkins Univ. Press, MD 1983.

[12] Golub, G.H., "Numerical Methods for Solving Least Squares Problems," *Numer. Math*, no. 7, pp. 206-216, 1965.

[13] M. Herman and T. Strohmer, "High-resolution radar via compressed sensing," to appear in *IEEE Trans. on Signal Processing*

[14] J. A. Hogbom, "Aperture synthesis with a non-regular distribution of interferometer baseline," *Atronomy and Astrophysics Supplement Ser.*, vol. 15, 1974.

[15] L. Potter, P. Schniter, and J. Ziniel, "Sparse reconstruction for RADAR," *SPIE Alg. for Syn. Aperture Radar Imagery XV*, 2008.

[16] R. A. Scholtz, M. Z. Win, and J. M. Cramer, "Evaluation of the Characteristics of the ultra-wideband propagation channel," *Proc of Antenna and Propagation Symposium*, vol. 2, no. 626-630, 1998.

[17] K. R. Varshney, M. etin, J. W. Fisher, and A. S. Willsky, "Sparse representation in structured dictionaries with application to synthetic aperture radar," *IEEE Transactions on Signal Processing*, 56(8), pp. 3548 - 3561, August 2008.